

# **Microencapsulation for Next Generation Lubricants**

**Karen Claire Mitchell**

Submitted in accordance with the requirements for the degree of  
Doctor of Philosophy

The University of Leeds  
School of Mechanical Engineering  
School of Chemical and Process Engineering

September 2014

The candidate confirms that the work submitted is her own and that appropriate credit has been given where reference has been made to the work of others.

This copy has been supplied on the understanding that it is copyright material and that no quotation from the thesis may be published without proper acknowledgement.

The candidate confirms that the work submitted is her own and that appropriate credit has been given where reference has been made to the work of others.

This copy has been supplied on the understanding that it is copyright material and that no quotation from this thesis may be published without prior acknowledgement.

## **Acknowledgements**

Firstly, I would like to thank my supervisors, Professor Anne Neville, Dr. Olivier Cayre and Dr. Ardian Morina, for their support and guidance throughout the project. I would also like to thank The Lubrizol Corporation, in particular Dr. Mike Sutton, Dr. Gary Walker and Dr. Chris Friend for keeping the project on track, providing ideas and helping to set goals throughout the work. I would also like to thank The Lubrizol Corporation and the EPSRC for funding for this project.

Thanks greatly to Dr. John Harrington and Mr. Stuart Micklethwaithe for their training, help and technical assistance with SEM, Dr. Adrian Cunliffe and Miss Sara Dona for help in finding, developing and running a range of analytical techniques, Dr. Adrian Eagles for his help with WYKO and Dr. Peiyi Wang for obtaining the TEM images. I would also like to thank all current and former members of both the Biggs research group and particle CIC based in the School of Chemical and Process Engineering department at Leeds University. Special thanks also to the current and former members of the Institute of Functional Surfaces group based in the school of Mechanical Engineering at Leeds University, in particular my colleagues also on the TE77 rig Dr. Hongyuan Zhou, Mr. Luiquan Yang and Mr. Joe Lanigan.

I am grateful to my friends in office G.54b, office 2.47 and those other friends dotted around the university campus that have been able to provide tea, biscuits and smiles. I would also like to thank my friends at Phantom Tiger Taekwondo, particularly in this final month where we have all needed the extra support.

Lastly I would like to thank my parents and relatives for giving support, care and encouragement.

## Abstract

Lubricants within an engine perform the important tasks of increasing engine efficiency and lifetime of parts, dissipating heat and decreasing fuel consumption. To help lubricating engine oils perform to the best of their ability different chemical additives are blended into the oil; the amount of additives added is dictated by the respective solubilities and the nature of any interactions between different additives.

Using a technology already utilised in the pharmaceutical, food and dye industries this work presented in this thesis aims to increase the concentration of one particular additive, a friction modifier (FM), within a model oil. Monodisperse poly(methyl methacrylate) (PMMA) particles have been efficiently produced *via* dispersion polymerisation in a non-aqueous continuous phase and, through the incorporation of a co-solvent within the particle core, the encapsulation of FM inside these particles has been demonstrated.

Work has been carried out to determine the factors which can be used to reproducibly synthesise particles to a desirable size and degree of polydispersity. The storage and release of FM from the particle core when it is required is an important consideration in the action of these particles. The rate of release from the core of particles has been studied to demonstrate the ability of these particles to act as a FM reservoir, replenishing the additive as it is consumed.

An investigation of the action of particles produced, with and without FM encapsulated, on the tribological behaviour of dodecane has been carried out using a TE77 Cameron Plint tribometer. Analysis of the friction and wear results is presented here and a possible mechanism for the action of the particles in the tribological testing has also been suggested.

## Abbreviations

Please note chemical formulae are not including in this list;

a	Semixaxis of the contact ellipse in the transverse direction
A	Exposed shell surface area
AIBN	Azobisisobutyronitrile
AISI	American Iron and Steel Institute
ATR-IR	Attenuated total reflectance – infrared
AW	Antiwear
b	Semixaxis in the direction of motion
C	Active concentration
d	Shell thickness
D	Diffusion coefficient
DLS	Dynamic light scattering
DPF	Diesel particulate filters
E'	Reduced Young's modulus
EGR	Exhaust gas recirculation
EHL	Elastohydrodynamic lubrication
ELSD	Evaporative light scattering detector
EP	Extreme pressure
FM	Friction modifier
GC-MS	Gas chromatography - mass spectrometry
GMO	Glycerol mono-oleate
GPa	Gigapascals

GPC	Gel permeation chromatography
H	Partition coefficient
HL	Hydrodynamic lubrication
$h_{\min}$	Minimum film thickness
HPLC	High performance liquid chromatography
HRC	Hardness
Hz	Hertz
IR	Infrared
k	Ellipticity parameter
LC-MS	Liquid chromatography – mass spectroscopy
$\mu\text{m}$	Micrometer
MeOH	Methanol
mm	Millimetre
MMA	Methyl methacrylate
MoDTC	Molybdenum dialkyldithiocarbamate
N	Newton
nm	Nanometre
OFM	Organic friction modifier
PDI	Polydispersity index
PDMS	Poly(dimethyl siloxane)
PDMS-MA	Methacrylate terminated poly(dimethyl siloxane)
PMMA	Poly(methyl methacrylate)
PS	Polystyrene
N.B.	Nota bene
R'	Reduced radius of curvature
$R_a$	Surface roughness

RI	Refractive index
rpm	Revolutions per minute
SAPS	Sulphated ash, phosphorus, sulphur
SCR	Selective catalytic reduction
SEM	Scanning electron microscopy
TEM	Transmission electron microscopy
THF	Tetrahydrofuran
U	Entraining surface velocity
UV	Ultraviolet
VI	Viscosity Index
W	Contact load
w.r.t.	With respect to
wt%	Weight percent
ZDDP	Zinc dialkyldithiophosphate
$\alpha$	Pressure viscosity coefficient
$\eta_0$	Viscosity at atmospheric pressure of the lubricant
$\emptyset$	Diameter
$\mu$	Coefficient of friction

## Contents

<b>Acknowledgements</b> .....	<b>3</b>
<b>Abstract</b> .....	<b>4</b>
<b>Abbreviations</b> .....	<b>5</b>
<b>Contents</b> .....	<b>8</b>
<b>Figures</b> .....	<b>12</b>
<b>Tables</b> .....	<b>23</b>
<b>Conferences Presentations</b> .....	<b>24</b>
Papers from This Thesis.....	25
<b>Chapter 1. Introduction</b> .....	<b>26</b>
1.1 Engine tribology and lubricant additives .....	26
1.2 Microencapsulation as an additive reservoir in engines .....	27
1.3 Aims and objectives of the study .....	29
1.4 Thesis chapter outline .....	30
<b>Chapter 2. Background Literature</b> .....	<b>32</b>
2.1 Introduction .....	32
2.2 Tribology.....	32
2.2.1 Lubrication and lubricant additives.....	34
2.2.1.1 Additive types and uses.....	35
2.2.2 Lubrication regimes .....	36
2.2.3 Friction modifiers.....	41
2.2.3.1 Organic friction modifiers.....	42
2.2.4 Additive–additive interactions .....	46
2.2.5 Technological drivers for a change to organic FMs.....	48

2.3 Heterogeneous polymerisation.....	49
2.3.1 Polymerisation of methyl methacrylate .....	49
2.3.2 Types of heterogeneous polymerisation.....	54
2.3.2.1 Suspension polymerisation.....	54
2.3.2.2 Emulsion and miniemulsion polymerisation.....	56
2.3.2.3 Dispersion polymerisation .....	58
2.3.2.4 Heterogeneous polymerisation summary.....	60
2.4 Microencapsulation .....	61
2.4.1 Microencapsulation <i>via</i> dispersion polymerisation.....	62
2.5 Use of microencapsulation for lubrication applications.....	63
2.5.1. Use of nanoparticles and microparticles in lubrication.....	65
<b>Chapter 3. Characterisation Techniques .....</b>	<b>68</b>
3.1 Introduction .....	68
3.2 Particle analysis techniques.....	68
3.2.1 Dynamic light scattering .....	68
3.2.2 Scanning electron microscopy .....	70
3.2.3 Transmission electron microscopy.....	73
3.2.4 Attenuated total reflectance-infrared.....	74
3.2.5 High performance liquid chromatography.....	75
3.3 Plate analysis techniques.....	77
3.3.1 TE77 .....	77
3.3.2 Interferometry .....	80
3.4 Summary .....	82
<b>Chapter 4. Investigation into the Effect of Changing the Initial Polymerisation Recipe of Final PMMA Particle Size .....</b>	<b>83</b>
4.1 Introduction .....	83
4.2 Synthesis of solid PMMA particles .....	84

4.2.1 Effect of changing monomer concentration.....	85
4.2.2 Effect of changing stabiliser concentration.....	88
4.2.3 Effect of changing initiator concentration.....	93
4.2.4 Increasing the stabiliser concentration and decreasing monomer concentration.....	97
4.3 Synthesis of PMMA particles with a methanol core.....	100
4.3.1 Effect of changing the ratio of continuous phase:co-solvent.....	101
4.4. Summary .....	104

**Chapter 5. Investigation into the release rate of friction modifier from  
intact core shell particles ..... 106**

5.1 Introduction .....	106
5.2 Synthesis of PMMA particles containing encapsulated FM for release rate testing. ....	108
5.3 Determination of particle morphology.....	109
5.4 Identification of the friction modifier supplied by Lubrizol .....	113
5.5. Identification of the friction modifier within PMMA particles .....	116
5.6 Determination of FM release rate by high performance liquid chromatography.....	117
5.6.1 Development of HPLC method.....	117
5.6.2 FM release testing .....	120
5.6.3 Release rate of FM into fresh dodecane.....	121
5.7 Summary .....	123

**Chapter 6. Investigation into the tribological effect of PMMA particles in  
a model oil ..... 125**

6.1 Introduction .....	125
6.2 Effect of adding particles of different morphologies to dodecane.....	128
6.2.1 Friction .....	128
6.2.2 Wear .....	130

6.3 Effect of particle size .....	134
6.3.1 Friction .....	134
6.4 Effect of changing FM concentration encapsulated in particles .....	136
6.4.1 Friction .....	136
6.4.2 Wear .....	140
<b>Chapter 7. Discussion .....</b>	<b>142</b>
7.1 Introduction .....	142
7.2 Particle optimisation.....	142
7.3 Proposed mechanism of friction reduction .....	144
7.3.1 Scanning electron microscopy of the used steel plates .....	145
7.3.2 Formation of polymer tribofilm .....	151
<b>Chapter 8. Conclusions.....</b>	<b>154</b>
8.1 Concluding remarks .....	154
8.2 Suggestions for future work .....	156
<b>Appendix A .....</b>	<b>160</b>
<b>Appendix B .....</b>	<b>165</b>
<b>Appendix C .....</b>	<b>167</b>

## Figures

<b>Figure 1-1. Breakdown of energy losses within a passenger car as reported by Holmberg <i>et al.</i> [3].....</b>	<b>26</b>
<b>Figure 1-2. Proposed mechanism of FM release from unbroken particles.....</b>	<b>28</b>
<b>Figure 2-1. The moving parts and basic cycle of a four-stroke engine [37].....</b>	<b>34</b>
<b>Figure 2-2. The Stribeck curve (red), showing the coefficient of friction (<math>\mu</math>) as a function of lubricant viscosity multiplied by shear velocity divided by the applied load. Also shown here by the blue line is the corresponding film thickness (h) found in each of the lubrication regimes [39].....</b>	<b>36</b>
<b>Figure 2-3. In the hydrodynamic lubrication regime, both surfaces are separated by a complete fluid layer. Direction of surface movement is shown by the arrows.....</b>	<b>37</b>
<b>Figure 2-4. Mixed lubrication regime where surfaces are separated by a lubricant film and there are few asperity contacts. Direction of surface movement indicated by the arrows. ....</b>	<b>38</b>
<b>Figure 2-5. Asperity–asperity contact under boundary lubrication. Direction of surface movement indicated by arrows. ....</b>	<b>39</b>
<b>Figure 2-6. The lubrication regimes (boundary, mixed, elastohydrodynamic and hydrodynamic) formed under different film thicknesses [1]. ....</b>	<b>39</b>
<b>Figure 2-7. Examples of organic friction modifiers for use in engine oils. ....</b>	<b>41</b>
<b>Figure 2-8. An example of an inorganic friction modifier, molybdenum disulphide, and the layered structure it forms [47].....</b>	<b>42</b>
<b>Figure 2-9. Nature of the bonding at the substrate surface between molecules of stearamide (left) and the organic multilayer formation (right).....</b>	<b>43</b>

<b>Figure 2-10. Effect of increasing hydrocarbon chain length on the boundary friction coefficient of a FM [50].</b>	<b>44</b>
<b>Figure 2-11. Coefficient of friction of reference oil RL 179/2 containing different organic FMs (GMO, ‘OFM A’ and oleylamide) at different temperatures [52].</b>	<b>45</b>
<b>Figure 2-12. Formation of nitrogen gas and water vapour in selective catalytic reduction.</b>	<b>48</b>
<b>Figure 2-13. Basic polymerisation scheme. ‘n’ number of monomer units ‘M’ polymerises to form a polymer of repeating ‘M’ units of chain length ‘n’.</b>	<b>49</b>
<b>Figure 2-14. Generation of free radical species by breakdown of AIBN.</b>	<b>50</b>
<b>Figure 2-15. Initiation of methyl methacrylate polymerisation by the free radical.</b>	<b>51</b>
<b>Figure 2-16. Propagation step where the chain continues to grow.</b>	<b>51</b>
<b>Figure 2-17. Termination via combination.</b>	<b>52</b>
<b>Figure 2-18. Termination via disproportionation.</b>	<b>53</b>
<b>Figure 2-19. A. Monomer (orange) is insoluble in the continuous phase (blue). Initiator (green) which is only soluble in the monomer phase is added. B. Upon stirring monomer droplets are formed and are prevented from coalescing by the use of stabiliser (black). C. When heated initiation and polymerisation occur within the droplets resulting in the final polymer particles (red) the same size as the initial monomer droplets.</b>	<b>55</b>
<b>Figure 2-20. A. Initiator (green) and monomer (orange), which is slightly soluble, are dissolved in the continuous phase (blue). Unsolubilised monomer is held in droplets by stabiliser (black). B. Upon heating and stirring stabilised polymer seeds form (red). Monomer moves from droplets into the continuous phase. C. All monomer has been polymerized and final particles are formed.</b>	<b>57</b>
<b>Figure 2-21. The droplet nucleation process typical of miniemulsion polymerisation (adapted from Bechthold and Landfester [75]).</b>	<b>57</b>

<b>Figure 2-22. A – Stabiliser (black), initiator (green) and monomer (orange) are dissolved in a continuous phase (light blue). B – Upon stirring and heating primary particles form and grow in solution. C – When all of the monomer has reacted polymerisation is complete. Polymer particles (red) are prevented from aggregating by surface stabiliser. ....</b>	<b>59</b>
<b>Figure 2-23. D – Continuous phase (containing stabiliser (black), initiator (green) and monomer (orange)) and a co-solvent (dark blue) are stirred and heated. E - Primary particles are produced in solution. F - Co-solvent dissolves inside the growing polymer particles. G – Polymer particles (red) are formed which contain co-solvent encapsulated within. Stabilisers prevent aggregation. ....</b>	<b>63</b>
<b>Figure 2-24. The end section of a cast material with microencapsulated lubricant particles adhered to the surface of the cast [98]. ....</b>	<b>64</b>
<b>Figure 2-25. Process of lubricant release and debris entrapment. ....</b>	<b>65</b>
<b>Figure 2-26. Microcapsules, containing lubricant, fully embedded within a surface which is released as wear occurs [101]. ....</b>	<b>65</b>
<b>Figure 3-1. Apparatus used for dynamic light scattering (DLS) [127]. ....</b>	<b>69</b>
<b>Figure 3-2. Hydrodynamic diameter (nm) versus particle concentration (wt%) for a dodecane sample containing solid, monodisperse PMMA particles measuring ~ 280nm diameter. ....</b>	<b>70</b>
<b>Figure 3-3. Scanning electron microscopy apparatus [131]. ....</b>	<b>71</b>
<b>Figure 3-4. SEM stubs inside the ultra high vacuum chamber. ....</b>	<b>72</b>
<b>Figure 3-5. Scanning electron micrograph of poly(methyl methacrylate) particles measuring ~ 1.5µm (measured by DLS). It should be noted that size of particles when measured by DLS is carried out while the sample is in the dodecane continuous phase while SEM is carried out on samples which have had all solvent removed. ....</b>	<b>73</b>
<b>Figure 3-6. Basic transmission electron microscopy apparatus [142]. ....</b>	<b>74</b>
<b>Figure 3-7. Basic principle of attenuated total reflectance – infrared [144]. ....</b>	<b>75</b>

<b>Figure 3-8. A common high performance liquid chromatography system [147].</b> .....	<b>76</b>
<b>Figure 3-9. TE77 test apparatus [148].</b> .....	<b>78</b>
<b>Figure 3-10. TE77 testing apparatus used in this project.</b> .....	<b>79</b>
<b>Figure 3-11. Schematic of the apparatus and beam pathways in a white light interferometer [149]. N.B. Mirau interferometer refers to the position of the reference surface in relation to the sample surface. In a Michelson interferometer this reference would be positioned 90° to the sample [150].</b> .....	<b>81</b>
<b>Figure 3-12. Schematic showing the build up of a surface structure by vertical scanning interferometry [150].</b> .....	<b>81</b>
<b>Figure 4-1. Effect of changing monomer concentration on particle size. Error bars are included in all data.</b> .....	<b>85</b>
<b>Figure 4-2. Effect of changing monomer concentration on polydispersity index. Error bars are included in all data.</b> .....	<b>86</b>
<b>Figure 4-3. Scanning electron micrograph of smaller PMMA particles produced using a lower concentration (5.5 wt% w.r.t continuous) of monomer [490nm, PDI = 0.04]. N.B. Sizes quoted in the caption have been measured by DLS.</b> .....	<b>87</b>
<b>Figure 4-4. Scanning electron micrograph of larger, more polydisperse particles produced using a higher concentration (21.9 wt% w.r.t. continuous) of monomer [2900nm, PDI = 0.7]. N.B. Sizes quoted in the caption have been measured by DLS.</b> .....	<b>88</b>
<b>Figure 4-5. Steric repulsion between two particles caused by the polymeric chains protruding from the surface of the dispersed particles.</b> .....	<b>89</b>
<b>Figure 4-6. Effect of changing stabiliser concentration on particle size. Error bars are included in all data.</b> .....	<b>89</b>
<b>Figure 4-7. Effect of changing stabiliser concentration on polydispersity index.</b> .....	<b>90</b>

<b>Figure 4-8. Scanning electron micrograph of larger PPMA particles produced using a lower concentration (7.4wt % w.r.t monomer) of stabiliser [1660nm, PDI = 0.15]. N.B. Sizes quoted in the caption have been measured by DLS. ....</b>	<b>91</b>
<b>Figure 4-9. Scanning electron micrograph of smaller particles produced using a higher concentration (108.9wt % w.r.t. monomer) of stabiliser [310nm, PDI = 0.06]. N.B. Sizes quoted in the caption have been measured by DLS. ....</b>	<b>92</b>
<b>Figure 4-10. Scanning electron micrograph of smaller particles produced using a higher concentration (108.9wt % w.r.t. monomer) of stabiliser [310nm, PDI = 0.06]. N.B. Sizes quoted in the caption have been measured by DLS. ....</b>	<b>92</b>
<b>Figure 4-11. Generation of two free radical species by breakdown of AIBN. ....</b>	<b>93</b>
<b>Figure 4-12. Effect of changing initiator concentration on particle size. Error bars are included in all data. ....</b>	<b>94</b>
<b>Figure 4-13. Effect of changing initiator concentration on polydispersity index. Error bars are included in all data. ....</b>	<b>94</b>
<b>Figure 4-14. Effect of changing initiator concentration on polymer chain molecular weight. ....</b>	<b>96</b>
<b>Image 4-15. Scanning electron micrograph of larger PMMA particles produced using a higher concentration (5.17wt % w.r.t monomer) of initiator [1180nm, PDI = 0.14]. N.B. Sizes quoted in the caption have been measured by DLS. ....</b>	<b>96</b>
<b>Figure 4-16. Scanning electron micrograph of smaller PMMA particles produced using a lower concentration (0.72wt % w.r.t. monomer) of initiator [930nm, PDI = 0.19]. N.B. Sizes quoted in the caption have been measured by DLS. ....</b>	<b>97</b>
<b>Image 4-17. Scanning electron micrographs of PMMA particles measuring [180nm, PDI = 0.04]. N.B. Sizes quoted in the caption have been measured by DLS. ....</b>	<b>99</b>

<b>Figure 4-18. Scanning electron micrographs of PMMA particles measuring [150nm, PDI = 0.11]. N.B. Sizes quoted in the caption have been measured by DLS. ....</b>	<b>99</b>
<b>Figure 4-19. Scanning electron micrographs of the smallest PMMA particles produced so far [130nm, PDI = 0.10]. N.B. Sizes quoted in the caption have been measured by DLS .....</b>	<b>100</b>
<b>Figure 4-20. Effect of changing the volume of co-solvent (total volume was kept constant) on particle size. Error bars are included in all data.....</b>	<b>102</b>
<b>Figure 4-21. Effect of changing the volume of co-solvent (total volume was kept constant) on polydispersity index. Error bars are included in all data. ....</b>	<b>102</b>
<b>Figure 4-22. Cryo-transmission electron micrograph of a PMMA particle produced using a 5:1 continuous phase:co-solvent ratio [430nm, PDI = 0.07]. ....</b>	<b>103</b>
<b>Figure 5-1. Proposal for FM release from unbroken particles. ....</b>	<b>106</b>
<b>Figure 5-2. The regular hole structure of the Quantifoil® R2/2 holey carbon grids. ....</b>	<b>109</b>
<b>Figure 5-3. Cryo-transmission electron micrograph of a PMMA particle with a methanol liquid core. ....</b>	<b>110</b>
<b>Figure 5-4. Movement of the darker region of the particle imaged at different tilt angles. If the darker region is due to the contact of the particle at the surface it will appear to move within the particle when tilted. If the darker region is due to a true core-shell morphology it will stay central to the particle when tilted.....</b>	<b>111</b>
<b>Figure 5-5. Cryo-transmission electron micrograph of PMMA shell – methanol core particles the image was taken with the samples at 0° sample insertion.....</b>	<b>112</b>
<b>Figure 5-6. Cryo-transmission electron micrograph of PMMA shell – methanol core particles the image was taken with the sample at 25° insertion.....</b>	<b>113</b>

<b>Figure 5-7. ATR-FTIR spectra for FM (“Lubrizol additive”) and the structure it indicates. ....</b>	<b>114</b>
<b>Figure 5-8. Stearamide.....</b>	<b>115</b>
<b>Figure 5-9. IR spectra for PMMA particles containing increasing amount of FM. ....</b>	<b>116</b>
<b>Figure 5-10. High performance liquid chromatogram of FM (10wt%) in methanol. FM = 8 minutes, methanol = 9.5 – 10 minutes.....</b>	<b>118</b>
<b>Figure 5-11. High performance liquid chromatogram of dodecane saturated with FM, in a THF mobile phase. FM = 8 minutes, dodecane = 9 minutes. ....</b>	<b>118</b>
<b>Figure 5-12. High performance liquid chromatogram of FM in THF. FM = 8 minutes, THF = 10 minutes.....</b>	<b>119</b>
<b>Figure 5-13. Calibration curve for the detection of FM in methanol, using a THF mobile phase. “Peak area” is the measured area underneath the peak and corresponds to “amount” of FM added to the standard solutions.....</b>	<b>120</b>
<b>Figure 5-14. Each centrifugation and redispersion will be referred to as one cycle. ....</b>	<b>121</b>
<b>Figure 5-15. Cumulative FM released (wt%) with each cycle. “Cycle” refers to the amount of time the particles were dispersed in each aliquot of fresh dodecane.....</b>	<b>122</b>
<b>Figure 6-1. Friction coefficient (<math>\mu</math>) over a time period of two hours. Pure dodecane (red <math>\blacklozenge</math>), dodecane containing solid PMMA particles (14wt% particles) (purple x), dodecane containing methanol core, no FM, PMMA particles (14wt% particles) (black <math>\bullet</math>), dodecane saturated with FM (green <math>\blacksquare</math>) and dodecane containing particles with encapsulated FM (14wt% particles) (blue <math>\blacktriangle</math>). Each plot is the average of three separate tests, carried out under identical conditions, error bars are the standard deviation of the three tests. ....</b>	<b>129</b>

**Figure 6-2. Wear volume ( $\mu\text{m}^3$ ) of the steel plates after the two-hour test period. Pure dodecane (red horizontal line [ $\sim 9.7 \times 10^6$ ]), dodecane containing solid particles (purple x), dodecane saturated with FM (green horizontal line [ $\sim 5.9 \times 10^6$ ]) and dodecane containing particles with encapsulated FM (blue  $\blacktriangle$ ) (14wt% particles is equivalent to 3wt% FM. 7wt% particles = 1.5wt% FM. 4wt% particles = 0.8wt% FM and 1wt% particles = 0.3wt% FM). Each plot is the average wear volume measured of three separate test plates, carried out under identical conditions. It should be noted that the concentration of friction modifier as the concentration of particles changes. .... 130**

**Figure 6-3. [Top image] Depth of wear scar on a steel plate tested when dodecane is used as a lubricating oil and [Bottom image] when dodecane fully saturated with FM (0.004wt%) is used as a lubricating oil in TE77 testing..... 131**

**Figure 6-4. 2D and 3D interferometry images of the wear scar of a plate tested when dodecane with solid particles (14wt% particles) is used as a lubricating oil..... 132**

**Figure 6-5. 2D and 3D interferometry images of the wear scar of a plate tested when FM containing particles (14wt% particles; 3wt% FM) is used as a lubricating oil in TE77 testing..... 133**

**Figure 6-6. Friction coefficient ( $\mu$ ) during the last 30 minutes of the two hour tests, error bars coloured for clarity. Pure dodecane (red (upper horizontal) line, friction coefficient = 0.139, line is for comparison only, there are no particles in this sample), dodecane containing 1600nm solid PMMA particles (purple  $\blacksquare$ ), dodecane containing 850nm solid PMMA particles (orange x), dodecane containing 150nm solid PMMA particles (blue  $\bullet$ ) and dodecane saturated with FM (green (lower horizontal) line, friction coefficient = 0.084, line is for comparison only, there are no particles in this sample). .... 135**

**Figure 6-7. Friction coefficient ( $\mu$ ) during the last 30 minutes of the two hour tests versus number of particles in the sample. Pure dodecane (red (upper horizontal) line, friction coefficient = 0.139, line is for comparison only, there are no particles in this sample), dodecane containing 1600nm solid PMMA particles (purple ■), dodecane containing 850nm solid PMMA particles (orange x), dodecane containing 150nm solid PMMA particles (blue ●) and dodecane saturated with FM (green (lower horizontal) line, friction coefficient = 0.084, line is for comparison only, there are no particles in this sample). ..... 136**

**Figure 6-8. Friction coefficient ( $\mu$ ) during the last 30 minutes of the two hour tests, error bars coloured for clarity. Pure dodecane (red (upper horizontal) line, friction coefficient = 0.139, line is for comparison only, there are no particles in this sample), dodecane containing 1100nm ‘low’ FM loaded particles (orange ●) (1wt% particles is equivalent to 0.1wt% FM. 3wt% particles = 0.2wt% FM. 7wt% particles = 0.4wt% FM and 14wt% = 0.7wt% FM), dodecane containing 900nm ‘medium’ FM containing particles (purple x) (1wt% particles = 0.1wt% FM. 3wt% particles = 0.4wt% FM. 7wt% particles = 0.7wt% FM and 14wt% particles = 1.5wt% FM), dodecane containing 1100nm ‘high’ FM containing particles (blue ▲) (1wt% particles = 0.3wt% FM. 3wt% particles = 0.8wt% FM. 7wt% particles = 1.5wt% FM and 14wt% particles = 3.1wt% FM) and dodecane saturated with FM (green (lower horizontal) line, friction coefficient = 0.084, line is for comparison only, there are no particles in this sample). ..... 138**

**Figure 6-9. Friction coefficient ( $\mu$ ) during the last 30 minutes of the two hour tests, error bars coloured for clarity. Dodecane containing particles with encapsulated FM. Particle concentrations correspond to the samples shown in Figure 6-8..... 139**

**Figure 6-10. Wear volume ( $\mu\text{m}^3$ ) of the steel plates after the two-hour test period. Pure dodecane (red horizontal line [ $\sim 9.7 \times 10^6$ ] (off y-axis scale), dodecane containing ‘low’ FM particles (orange ●), dodecane containing ‘medium’ FM particles (purple x) and dodecane containing ‘high’ FM particles (blue ▲). Each plot is the average wear volume measured of three separate test plates, carried out under identical conditions. It should be noted that the concentration of friction modifier as the concentration of particles changes. FM concentrations for each sample are as stated for Figure 6-8..... 141**

**Figure 7-1. Demonstration of refractive index matching monitored with the use of gridlines. A. Showing a polymer tube in air, with high distortion of the gridlines, B. Polymer tube in a fluid which is a close refractive index match, showing some distortion of the gridlines and C. Polymer tube in a refractive index matched liquid, where no distortion of the gridlines is seen. Note: distortion at the branch point in all samples is intentional in order to show the position of the tube in the various liquids [179]..... 143**

**Figure 7-2. Scanning electron micrograph of outside the wear scar of steel plates after tribological testing using pure dodecane (0wt% particles) as a lubricating oil..... 146**

**Figure 7-3. Scanning electron micrograph of inside the wear scar of steel plates after tribological testing using pure dodecane (0wt% particles) as a lubricating oil..... 147**

**Figure 7-4. Scanning electron micrographs of inside the wear scar after tribological testing using dodecane containing 1.5wt% solid PMMA particles..... 147**

**Figure 7-5. Scanning electron micrographs of outside the wear scar after tribological testing using dodecane containing 1.5wt% solid PMMA particles..... 148**

**Figure 7-6. Scanning electron micrographs of steel plates used in tribological testing inside the wear scar (14wt% solid particles), polymer tribofilm can be damaged by the electron beam..... 149**

<b>Figure 7-7. Scanning electron micrographs of steel plates used in tribological testing outside of the wear scar (14wt% particles), some particles remain on the surface but no polymer tribofilm can be seen. Plates are rinsed with hexane and dried at 40°C for one week before testing by SEM.....</b>	<b>150</b>
<b>Figure 7-8. Scanning electron micrograph of steel plates after tribological testing. Intact PMMA particles and wear debris found outside the wear scar. ....</b>	<b>151</b>
<b>Figure 7-9. Proposed mechanism of friction and wear reduction in samples containing solid particles. ....</b>	<b>152</b>
<b>Figure 7-10. Proposed mechanism of friction and wear reduction in samples containing FM-loaded particles. It should be noted that polymer tribofilm is likely to form on both surfaces as is the FM layer. ....</b>	<b>152</b>
<b>Figure A-1. Common examples of antioxidant additives used in engine oil formations. ....</b>	<b>160</b>
<b>Figure A-2. Example antiwear/extreme pressure additives. ....</b>	<b>162</b>
<b>Figure A-3. Micellular action of detergents to suspend unwanted chemical species found in oil [196].....</b>	<b>163</b>
<b>Figure A-4. Generic structures of detergents molecules [196].....</b>	<b>163</b>
<b>Figure A-5. Examples of viscosity index improvers.....</b>	<b>164</b>
<b>Figure C-1. Steady state viscosity at different shear stresses (Pa) at 80°C. Pure dodecane (blue ♦), dodecane containing 1600nm particles with a methanol core (red ■).....</b>	<b>168</b>

## Tables

<b>Table 2-1. Antagonistic and synergetic additive-additive interactions. Red = antagonistic effect. Blue = synergic effect [10].</b>	<b>46</b>
<b>Table 3-1. Cameron Plint TE77 test conditions.</b>	<b>80</b>
<b>Table 4-1. Initial polymerisation mixture.</b>	<b>84</b>
<b>Table 4-2. Changing monomer concentration, keeping ratios unchanged.</b>	<b>98</b>
<b>Table 5-1. Initial polymerisation mixture.</b>	<b>108</b>
<b>Table 5-2. Assignment of the main IR peaks in the FM spectra.</b>	<b>114</b>
<b>Table 5-3. MSDS data for stearamide [165].</b>	<b>115</b>
<b>Table 5-4. Elution time for analytes in HPLC testing.</b>	<b>119</b>
<b>Table 6-1. Testing matrix for comparison of particles of solid PMMA particles, containing no FM, in dodecane at different concentrations and different hydrodynamic diameter. Each x signifies each two hour test carried out, for that particular particle type.</b>	<b>126</b>
<b>Table 6-2. Testing matrix for comparison of particles of solid PMMA particles, PMMA particles with a liquid core containing no FM and PMMA particles with a liquid core containing FM, all in dodecane at different particle concentration. Note particle size remains constant within error. Each x signifies each two hour test carried out, for that particular particle type.</b>	<b>126</b>
<b>Table 6-3. Testing matrix for comparison of PMMA particles with a liquid core containing FM at the same particle size within error and different particles loading. Note changing particle concentration also changes overall FM concentration in the system. Each x signifies each two hour test carried out, for that particular particle type.</b>	<b>127</b>
<b>Table 6-4. Cameron Plint TE77 test conditions.</b>	<b>127</b>

## **Conferences Presentations**

Mitchell, K.C., Morina, A., Neville, A., Cayre, O.J. and Friend, C., PMMA Microcapsules for Next Generation Lubricants (Poster), Tribo UK 2012

Mitchell, K.C., Cayre, O.C., Morina, A., Neville, A., Friend, C. and Sutton, M., Microencapsulation for Next Generation Lubricants (Poster), Institute of Physics Tribology Meeting 2012

Mitchell, K.C., Cayre, O.C., Morina, A., Neville, A., Walker, G. and Sutton, M., Microencapsulation of Additives for Next Generation Lubricants (Poster), Tribo UK 2013

Mitchell, K.C., Cayre, O.C., Morina, A., Neville, A., Walker, G. and Sutton, M., Microencapsulation for Next Generation Lubricants (Poster), Leeds-Lyon 2013

Mitchell, K.C., Cayre, O.C., Morina, A., Neville, A., Walker, G. and Sutton, M., Microcapsules for use in Next Generation Lubricants, World Tribology Congress 2013

Mitchell, K.C., Neville, A., Morina, A., Cayre, O., Walker, G. and Sutton, M., Synthesis and Tribological Testing of Poly (Methyl Methacrylate) Particles Containing Encapsulated Organic Friction Modifier: Effect of Friction Modifier Loading, Leeds-Lyon 2014

## **Papers from This Thesis**

Mitchell, K.C., Cayre, O.C., Morina, A., Neville, A., Walker, G. and Sutton, M., Synthesis and Tribological Testing of Poly (Methyl Methacrylate) Particles Containing Encapsulated Organic Friction Modifier, [SUBMITTED to Journal of Physics D: Applied Physics]

## Chapter 1. Introduction

### 1.1 Engine tribology and lubricant additives

In a passenger car as much as 33% of the fuel is used in overcoming the frictional forces within an engine, with as little as 12% of the total energy being used to drive the wheels, with the exact breakdowns of these figures being proposed by different authors [1-4]. The main energy losses in a passenger car were detailed by Holmberg *et al.* in 2012 are shown below in **Figure 1-1**.

Pressure to increase the fuel economy of passenger vehicles, lower the emissions and increase the lifetime of engine parts has been growing over recent years and has driven the development of new engine technologies and lubricants [5].

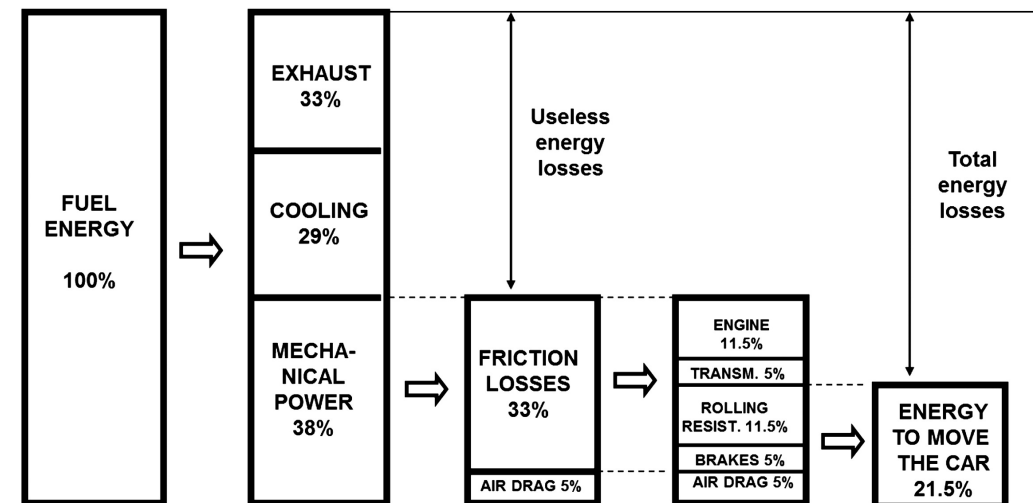


**Figure 1-1.** Breakdown of energy losses within a passenger car as reported by Holmberg *et al.* [3].

To help engine oils and engines perform to the best of their ability different chemical compounds are blended into the oil. There are many different types of additives which are used, these can function either to enhance the lubricating

performance of the base oil being used or to protect the metallic surfaces of the engine from chemical, thermal or mechanical degradation [6-9]. At present the amount of each additive which can be blended into an engine oil is dictated by the solubility of each individual additive into that oil and desire to balance and control additive-additive interactions [10-14]. As stricter regulations regarding engine exhaust emissions (including, but not limited to, CO<sub>2</sub> mass (mg/Km), NO<sub>x</sub> mass (mg/Km) and particulate mass (mg/Km)) are laid down [15], new technologies are being developed to help meet these regulations. In order to do this and to help new technologies perform correctly new additives and lubricant packages must be developed [16, 17]. One such consideration is the move towards lubricant additive packages with contain less sulphated ash (for example Zn, Mo, Mg containing additives), phosphorus and sulphur (SAPS), all of which have a negative impact on the operation of new components designed to reduce greenhouse gas emissions.

Here, the use of microencapsulation to increase the concentration of one engine oil additive, in this case the organic friction modifier (FM) stearamide, which can be blended into an engine oil is described. The FM used, as well as the particles synthesised, all meet with low SAPS requirements making them suitable for incorporation into future additive packages.

## **1.2 Microencapsulation as an additive reservoir in engines**

The use of microencapsulation has been detailed in a wide variety of industries including the pharmaceutical, food and dye industries among many others and as such has been widely studied [18-20]. Reasons for microencapsulation can therefore be quite varied and include; protection of the core from chemical reaction, oxidation or degradation, protection from harsh environments or to allow the targeted and controlled release of a substance from the core of a particle over a given time period or under specific conditions (i.e. temperature, pH etc.) [21]. The particles prepared here are designed to act as an 'additive reservoir' which will replenish the additive concentration in the oil as it is consumed.

Currently, formulated engine oils contain about 0.3wt% of FM; this figure was provided by Lubrizol and is based on their current, typical, fully formulated engine

oil. Using microencapsulation, the aim of this project has been to increase this amount to at least 1wt% FM. Microencapsulated FM would ideally be used as an ‘additive reservoir’, complementary to the amount of FM conventionally blended into the finished engine oil which is being used. **Figure 1-2** shows schematically the proposed mechanism of the FM release from within the core of the particles into the surrounding oil.

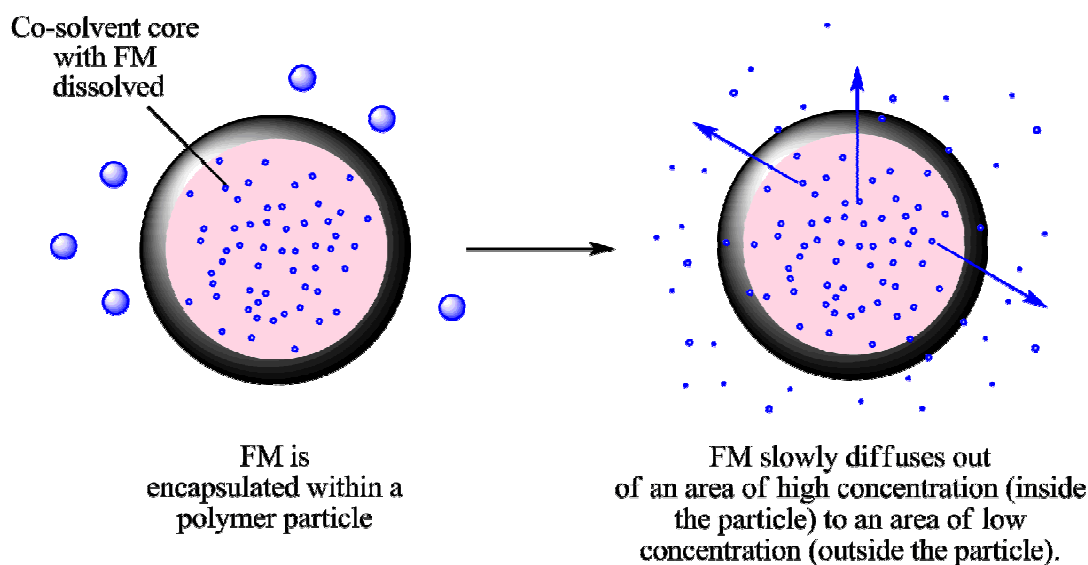


**Figure 1-2.** Proposed mechanism of FM release from unbroken particles.

Particles have a core shell morphology; being comprised of a poly(methyl methacrylate) (PMMA) shell and a methanol liquid core. FM is dissolved in methanol before synthesis and incorporated into the core of the final particle as it has preferential solubility in the methanol co-solvent rather than the dodecane continuous phase.

As FM dissolved conventionally in the oil is depleted, FM from inside the polymer particle will diffuse out of the particle and maintain an equilibrium between the two environments.

The PMMA shell of these microcapsules will also serve to protect the FM from possible additive-additive interactions that may occur. While in this project only one type of additive, the FM, is present in the model oil, dodecane, this will be

an important consideration when using this technology in fully formulated engine oils in the future.

### 1.3 Aims and objectives of the study

In this study microencapsulation has been used with the overall aim of increasing the amount of organic FM which can be blended into an engine oil. The work focuses on the following objectives (in italics):

- *Development of an efficient method of synthesising monodisperse PMMA particles.* The method used should ideally be suitable for eventual scale up and be applicable to use in fully formulated engine oil. This will be achieved *via* a dispersion polymerisation in a non-aqueous continuous phase.
- *The development of particles containing encapsulated FM within the core of the particle* with the eventual aim of increasing the amount of FM which can be blended into a finished, fully formulated engine oil. Encapsulation of FM in particles *via* dispersion polymerisation using a suitable co-solvent will be shown.
- *Reproducible particle synthesis to a desirable size and degree of polydispersity.* Ideally particles should be capable of containing a large amount of FM while not changing the final appearance of the oil. One of the criteria stipulated by Lubrizol was that any particles used should not be noticeable to the customer and the final appearance of any oil containing these particles should not differ from those currently available. While larger particles will be capable of carrying large amounts of FM they may however be visible to the naked eye. Reduction of particle size towards 100nm reduces the visibility of particles thus making the final product more desirable to the customer. It will be the role of the formulator to choose the optimum particle size and concentration when blending fully formulated engine oils containing these particles. To make this process easier an investigation has been carried out to determine the factors which can be used to control the final particle size and polydispersity.
- *To facilitate within the particle the storage of FM and release the FM from the particle core* when it is required. The rate of release of FM from within the

particles will be studied to demonstrate the capability of particles to act as a FM reservoir, replenishing the additive as it is consumed within a model tribological system.

- *Determination of the effect of the particles produced on the lubricating action of a model oil.* Using dodecane as a model oil the effect of particle size (between 130nm – 1.6µm), composition (solid PMMA particles, PMMA particles with a methanol core and PMMA particles with a methanol core which contain encapsulated FM), particle concentration (between 1wt% and 14wt%) and FM loading (0.1wt% in the total system to 3.1wt% in the total system) on the friction and wear measured when dodecane is used as the lubricating oil in tribological testing.

## 1.4 Thesis chapter outline

The chapters in this thesis will firstly look at the polymerisation of PMMA and the analysis of the polymer particles synthesised, before moving onto the testing of these particles tribologically.

**Chapter two** covers the background literature regarding tribology with particular focus on the action of organic friction modifiers as engine oil additives. The second half of this chapter is concerned with heterogeneous polymerisation techniques which can be used to encapsulate active species with a suitable polymer particle. This goes on to be discussed in detail in relation to microencapsulation *via* dispersion polymerisation in a non-aqueous solvent.

Particle characterisation techniques which are relative to this thesis will be discussed in **Chapter three**. This includes a brief overview of the methodology of the techniques used to image and characterise the particles produced, testing the tribological effect of particles synthesised on the friction reducing action of dodecane and the analysis of the steel plates used in this tribological testing.

**Chapter four** details the synthesis of PMMA particles which have been stabilised with a PDMS-MA steric stabiliser *via* a dispersion polymerisation in a dodecane continuous phase. This goes on to look at a particle size study which investigates the possibility of controlling final particle size and polydispersity by

varying the concentration of monomer, stabiliser, initiator and co-solvent used in the initial polymerisation mixture.

Presented in **Chapter five** is a FM release study which aims to investigate the rate of diffusion of FM from within the core of unbroken particles into fresh dodecane occurring due to the concentration gradient in the system. This will show the potential of particles to replenish an oil as FM outside of the particles, which is dissolved in the oil, is depleted. It will also demonstrate that an oil containing these particles will be stable whilst in storage and that FM will not be released into the oil as a function of time, i.e. once the oil is saturated FM will preferentially remain in the core of the particle rather than in the surrounding phase.

**Chapter six** investigates the effect of particles on the tribological properties of dodecane. This work compares the friction reducing and wear reduction properties of pure dodecane and dodecane which has been traditionally blended with FM to samples of dodecane containing solid PMMA particles, PMMA particles with methanol liquid cores, and PMMA particles with methanol liquid cores which contain the encapsulated FM. This work will also look at the effect of changing particle concentration, changing particle size, particle composition, and FM loading of the particles on the friction coefficient and wear measured.

A discussion of the main results obtained is given in **Chapter seven**. This will include a mechanism for the action of the polymer particles in tribological testing based upon literature available and presents SEM analysis of the steel plates used in tribological testing in order to support this.

The main conclusions of the work are given in **Chapter eight** as well as suggesting feasibility and possible future work.

## **Chapter 2. Background Literature**

### **2.1 Introduction**

This chapter will give an overview of literature relevant to this project. This will initially focus on engine tribology, the use of lubricants and details of the various types of lubricant additives which can be found within a fully formulated engine oil. The literature will then focus on a particular type of additive, the organic friction modifier (FM), as this is the class of additive which is used in this project.

In the second part of this literature review the polymerisation of poly(methyl methacrylate) (PMMA) is detailed and the main methods of heterogeneous polymerisation are presented.

Lastly the use of nanoparticles, microparticles and microencapsulation in lubrication applications is discussed.

### **2.2 Tribology**

The word 'tribology' is derived from the Greek root words 'tribos', meaning 'to rub', and 'logia', meaning 'to study' and can literally be defined as the study of friction, lubrication and wear between interacting surfaces in relative motion. In 1966 the word tribology was first used in a report which was written by a committee headed by Professor H. Peter Jost, given to the United Kingdom government, detailing the importance of education and research into lubrication and the impact this would have upon industry. The 'Jost Report' estimated that, in the United Kingdom alone, the potential savings that could be made from a better understanding of tribological principles would total £515 million *per annum* (£8.1 billion, adjusted for inflation) and more recently has been estimated at over \$40 billion *per annum* scaling up to become \$1 trillion *per annum* worldwide [1, 3, 22].

This calculation was based on the losses in passenger cars only and does not take into account frictional losses found in other types of engine or mechanical systems. It should also be noted that these calculations were based on a total of 850 million passenger cars worldwide, while in 2011 the actual number was estimated to have increased to 1.015 billion passenger vehicles [23].

Today tribology is applied to many areas of science and engineering, can be studied in relation to a broad range of topics and, due to the interdisciplinary nature of tribology, can have many overlaps between the areas of interest [24, 25]. There are also many instances in everyday life where tribology is encountered. In the 2009 paper “A Tribological Day” Dowson [26] details the tribological processes encountered by people each day; from waking up and getting dressed through to travelling to work and the interactions occurring between surfaces which allow life to continue as normal.

Examples of industries where tribology is of interest include,

- Computing – inside a modern day computer the interface between the head and disk in a hard drive must remain narrow enough (<5nm) to enable the disk to be read and recorded on by the head, allow the high speed of the disk while in operation and to reduce the possibility of contamination [27, 28]. While outside the computer casing the user interface can be studied by tribologists in the form of contacts between the computer and its user, an example of this would be the contact between skin and touch pad [29].
- Health – heart valves [30], contact lenses [31] and synovial joints, both ‘real’ and artificial [32], are all topics that are covered by biotribology which is concerned with friction, lubrication and wear within biological systems.
- Beauty – teeth brushing, hair combing and shaving can all be studied with the aim of better understanding the interactions of humans and their surroundings [26, 33].
- Sport – once again this may have overlaps with other industries, the interactions between a tennis ball and racket, snow and a ski and a swimmer and the surrounding water can all be encompassed by the field of tribology [34, 35].
- Space – the components within spacecrafts must be able to operate for long time periods between servicing. These parts and the lubricants used must be able to withstand a wide range of conditions as they operate on earth, through launch, in space and, if necessary upon re-entry [36].

- Automotive – a four stroke internal combustion engine, shown in **Figure 2-1**, has many moving components each of which have associated frictional losses within an engine, for example, from the bearings found in the gearbox, between cams and followers and between cylinder liners and piston rings.

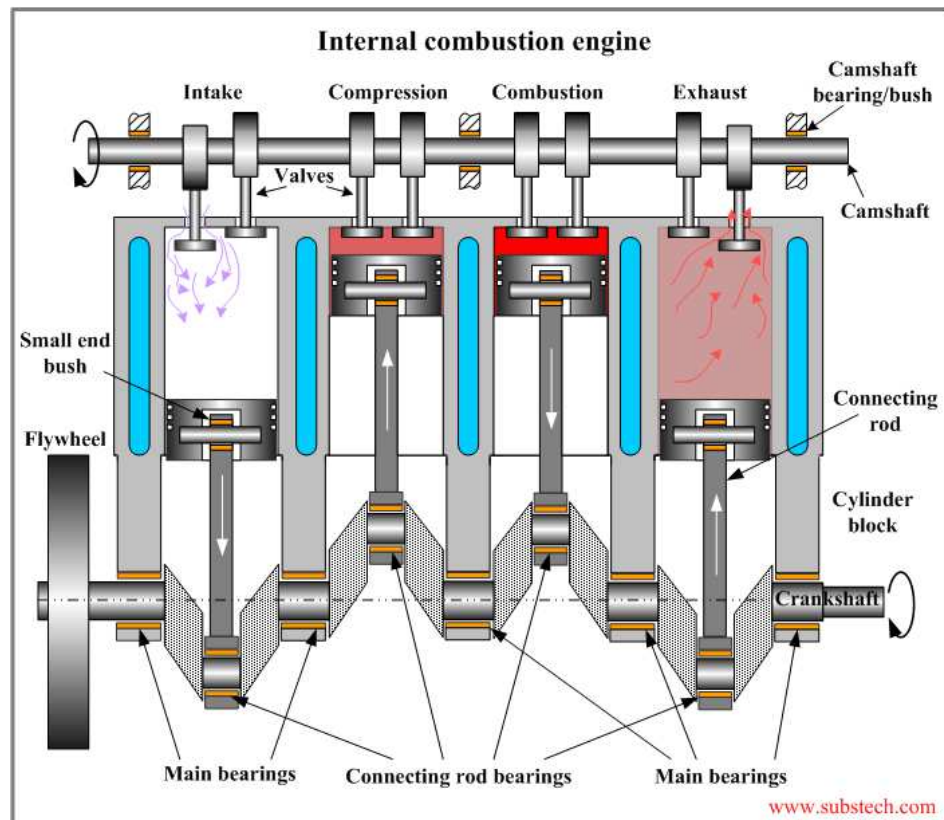


**Figure 2-1.** The moving parts and basic cycle of a four-stroke engine [37].

Tribological losses within a car engine are of particular interest within the work presented here where the overall aim is to develop a method of increasing the concentration of a FM in a fully formulated engine oil [5]. In this project the action of the piston moving within the cylinder will be modelled.

### 2.2.1 Lubrication and lubricant additives

In an engine the large number of moving parts and the many contacts between surfaces mean that a large amount of friction is generated. This friction may be beneficial or detrimental depending on the situation where it occurs. For example in

the brakes of a car it is beneficial to increase the amount of friction between the brake pads and the brake discs in order to slow the car. However in other working parts of an automotive engine, such as inside the engines cylinders, the desired effect is to decrease the friction between the moving parts thus reducing the energy used up and lost in overcoming that friction. When friction occurs here, it decreases the efficiency of the engine through the loss of kinetic energy as heat and it can also cause catastrophic wear of the rubbing parts, again leading to a loss of efficiency and may lead to the ultimate failure of the engine parts. Lowering friction and wear by the use of the correct lubrication increases the efficiency of the engine, increases the lifetime of engine parts and decreases fuel consumption [38] and each of these factors in turn leads to an economic saving to the user.

The many bearings and other moving parts within the engine all generate friction which needs to be lowered in order to prevent energy being wasted as heat and to stop wear of the parts. To prevent the generation of friction coatings can be applied to the surfaces of the engine, or lubricant can be added to the engine in the form of oils or greases. The addition of lubricants reduces wear between parts and allows the heat generated to be dissipated through the bulk of the oil. Due to the fact that different parts of the engine operate under different loads, and as such operate under different lubrication regimes (detailed in **Section 2.2.2**), any lubricant used must be able to operate under many different conditions. The design of a lubricant which can satisfy the demands of each moving part involves some compromise over the properties of that lubricant, and this is what the addition of lubricant additives aims to tackle.

To help the lubricating oils and engines perform to the best of their ability, different chemical compounds are blended into the oil. These chemical additives can function either to enhance the lubricating performance of the base oil used or they can protect the metallic surfaces of the engine.

#### **2.2.1.1 Additive types and uses**

There are many different classes of additives, all of which act to improve lubrication, each additive achieving this in different ways. Some of the main

additive categories, the applications and mode of operation of these additives, as well as some examples of their structure can be found in **Appendix A**.

### 2.2.2 Lubrication regimes

The lubrication regime of an oil describes the thickness of the fluid film found between the moving components of a system. The Stribeck curve plots the relationship between the coefficient of friction ( $\mu$ ) and the thickness of the lubricant film formed ( $\lambda$ ). This is demonstrated in **Figure 2-2**.

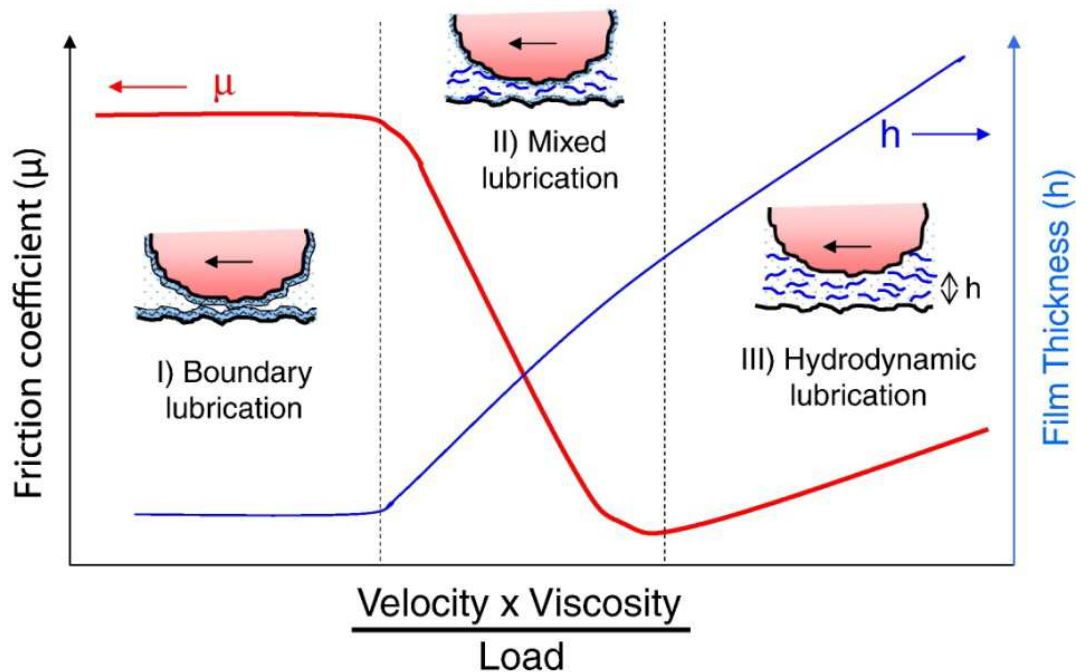


**Figure 2-2.** The Stribeck curve (red), showing the coefficient of friction ( $\mu$ ) as a function of lubricant viscosity multiplied by shear velocity divided by the applied load. Also shown here by the blue line is the corresponding film thickness ( $h$ ) found in each of the lubrication regimes [39].

In the hydrodynamic (HL) or full film lubrication regime a complete layer of lubricant is present between the two surfaces due to viscous entrainment. The asperities on the surfaces are completely separated; while friction coefficient may be expected to drop in this situation this is not the case due to shear stresses arising

between the surfaces and the liquid itself, and so instead friction increases. This complete separation of surfaces is shown in **Figure 2-3** where the lubricant compressed between the surfaces is sufficient to support a load due to the amount of pressure created. In some versions of the Stribeck curve the elastohydrodynamic lubrication (EHL) regime is also included, here surfaces are separated but other physical phenomena such as elastic deformation of the surfaces can be found, this makes characterisation of the film and the properties of the film much more complex. Under these conditions where there is a full lubricant film formation  $\lambda > 3$ . Friction coefficients measured in systems operating in this lubrication regime can be reduced below 0.002 [40].

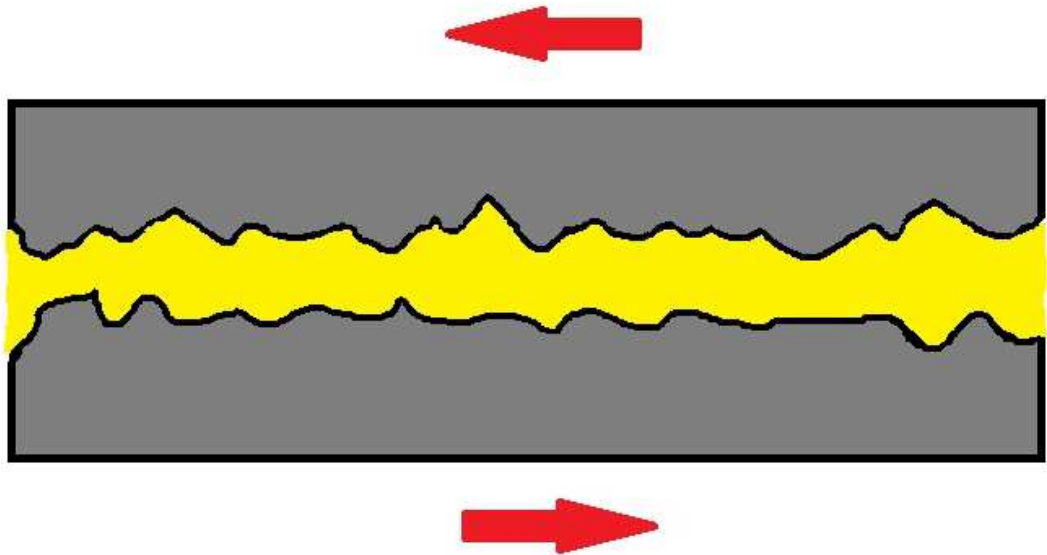


**Figure 2-3.** In the hydrodynamic lubrication regime, both surfaces are separated by a complete fluid layer. Direction of surface movement is shown by the arrows.

The mixed lubrication regime occurs between EHL/HL and boundary lubrication regimes. During mixed lubrication the surfaces are separated by a fluid film and there is negligible contact between asperities on opposing surfaces ( $1.2 > \lambda > 3$ ), as shown in **Figure 2-4**. This regime tends to be found in low speed, high load conditions.

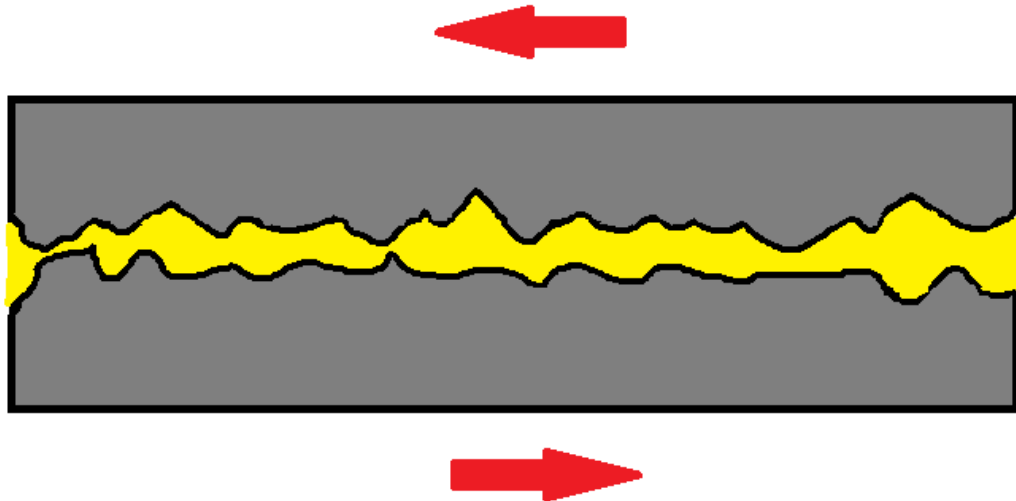


**Figure 2-4.** Mixed lubrication regime where surfaces are separated by a lubricant film and there are few asperity contacts. Direction of surface movement indicated by the arrows.

Boundary lubrication forms under high load, low viscosity and low velocity conditions and leads to a large amount of friction being generated due to the high number of asperity-asperity contacts ( $\lambda < 1.2$ ). This condition is true when the roughness of the surface asperities is greater than the thickness of the lubricant film formed. This is shown below in **Figure 2-5**. These points of contact cause some of the asperities to break off as stick-slip mechanisms occur [41-43]. Boundary lubrication also encompasses the study of chemical reactions at the surface, such as those cited by Gates and Hsu [44] detailing the effects of sulphonate, phenate and salicylate based compounds upon the tribofilms formed at the surface under boundary conditions. The formation of tribofilms upon the surface is caused by the high temperatures found at the asperities when they come into contact and can be controlled by regulating the formulation of the base oil or the chemical additives which are blended into it. The generation of tribofilms at the surface for the purpose of friction modification tend to be sacrificial in nature, designed to protect the surface from the shear stresses caused by the movement of the components [45].

The different lubrication regimes and where they can be found in different components of an internal combustion engine are shown in a modified Stribeck curve in **Figure 2-6**.

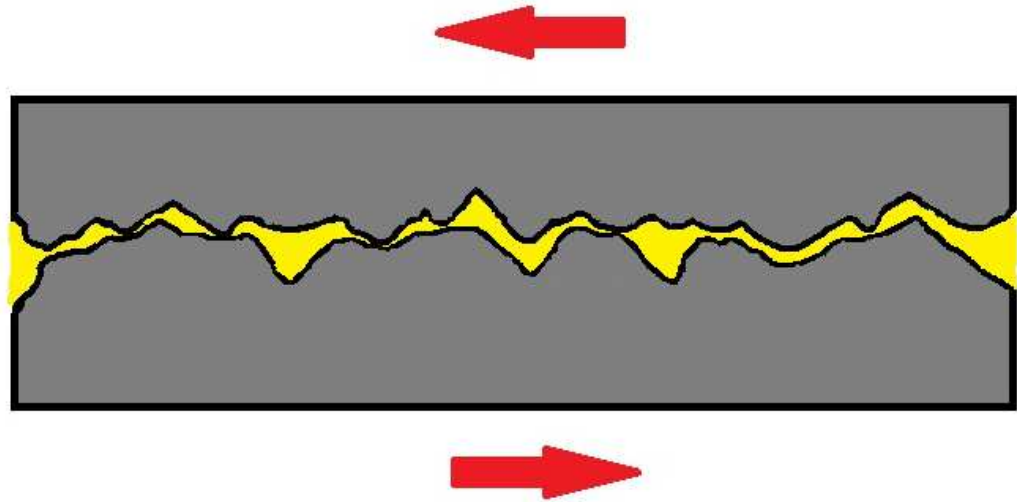


**Figure 2-5.** Asperity–asperity contact under boundary lubrication. Direction of surface movement indicated by arrows.

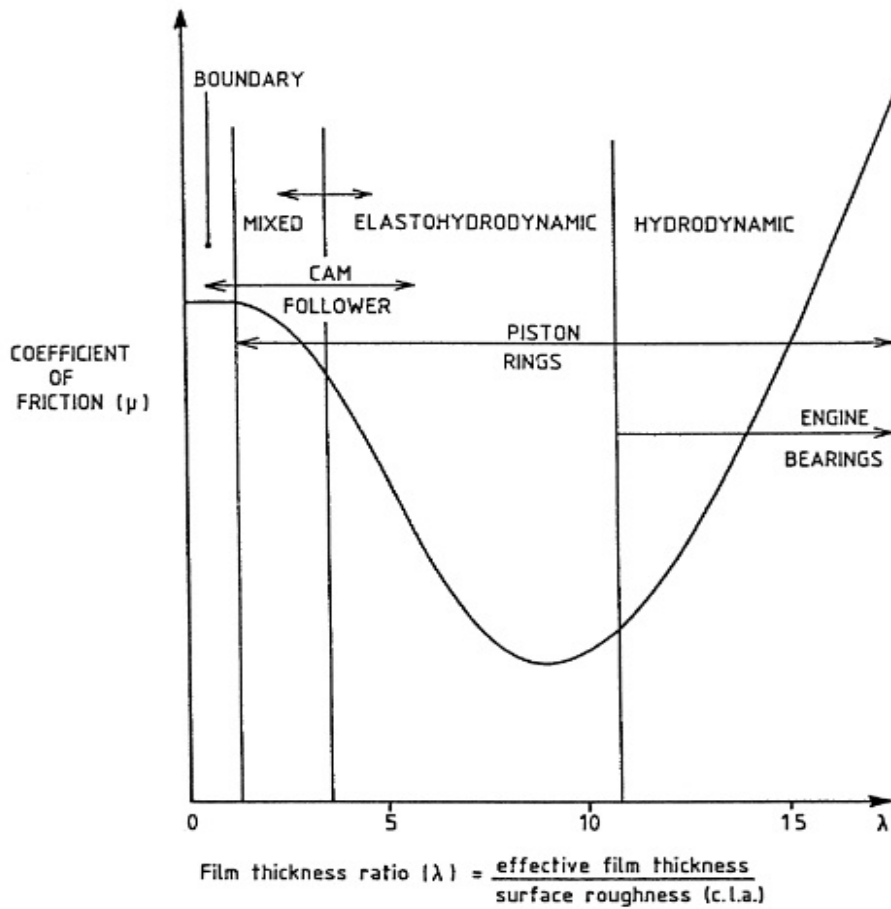


**Figure 2-6.** The lubrication regimes (boundary, mixed, elastrohydrodynamic and hydrodynamic) formed under different film thicknesses [1].

Film thickness ratio is expressed as follows:

$$\lambda = \frac{h_{\min}}{((Rms_1)^2(Rms_2)^2)^{0.5}}$$

Where,

$\lambda$  = film thickness ratio

$h_{\min}$  = minimum film thickness

Rms = Root mean squared surface roughness (of each surface respectively)

The minimum film thickness,  $h_{\min}$ , is calculated as follows:

$$\frac{h_{\min}}{R'} = 3.63 \left( \frac{U\eta_0}{E'R'} \right)^{0.68} (\alpha E')^{0.49} \left( \frac{W}{E'R'^2} \right)^{-0.073} (1 - e^{-0.68k})$$

Where,

$h_{\min}$  = minimum film thickness

$R'$  = reduced radius of curvature (m)

$U$  = entraining surface velocity (m/s)

$\eta_0$  = viscosity at atmospheric pressure of the lubricant (Pa)

$E'$  = reduced Young's modulus (Pa)

$\alpha$  = pressure ~ viscosity coefficient ( $m^2/N$ )

$W$  = contact load (N)

$k$  = ellipticity parameter defined as:

( $k = a/b$  where;  $a$  = semiaxis of the contact ellipse in the transverse direction (m) and  $b$  = the semiaxis in the direction of motion (m))

### 2.2.3 Friction modifiers

FMs are a class of additive which are blended into fully formulated engine oils and act by forming a protective layer over the surface of the substrate. The function of adding a friction modifier (FM) is to reduce friction between two surfaces when they are under conditions where a full liquid film has not formed between the sliding surfaces, these conditions are known as boundary lubrication conditions. These FMs can be inorganic species, such as molybdenum disulphide, which react directly with the surface atoms, or organic molecules species, such as oleylamide or glycerol mono-oleate (GMO) (**Figure 2-7**), which form adsorbed layers upon the surface.

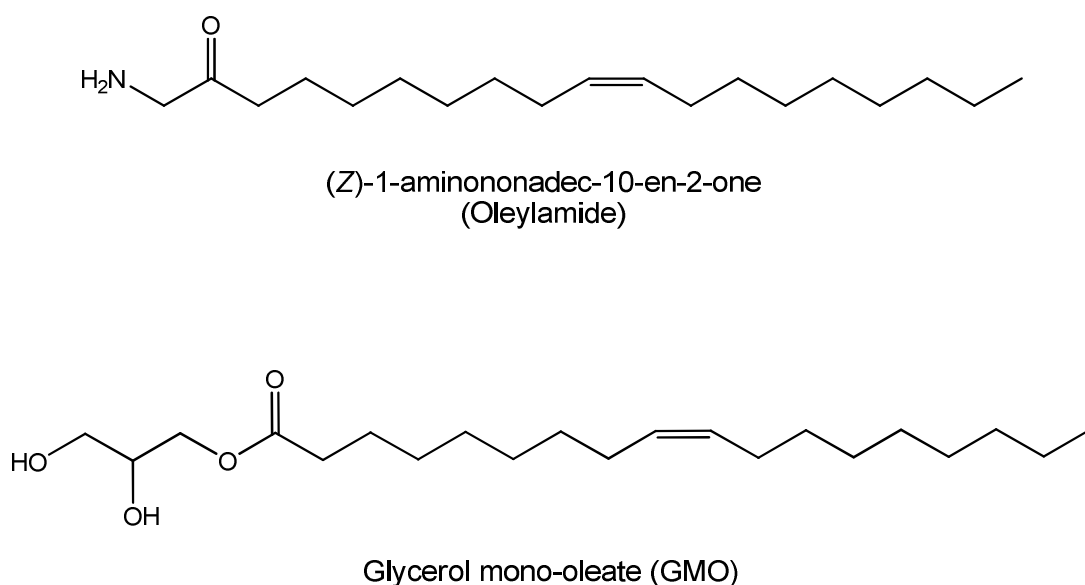


**Figure 2-7.** Examples of organic friction modifiers for use in engine oils.

Organic friction modifiers, such as the one used in this project, were discussed further in **Section 2.2.3.1**.

In molybdenum disulphide, an inorganic friction modifier, a protective layer is formed over a metallic surface, lubricity is due to the crystalline nature of the structure. Strong covalent bonds form within each layer of the MoS<sub>2</sub> however the bonds between the layers are weak with Van der Waals forces being present between the sulphur atoms of each layer. These weaker bonds allow the layers to be sheared apart leading to a reduction in friction [46]. This formation of a sacrificial

layer is common amongst inorganic friction modifiers. The bond lengths of MoS<sub>2</sub> are shown in **Figure 2-8**.

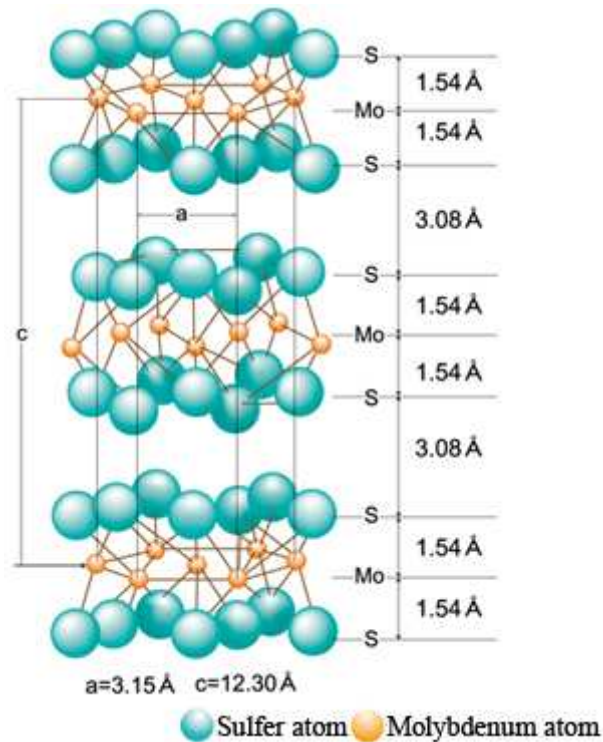


**Figure 2-8.** An example of an inorganic friction modifier, molybdenum disulphide, and the layered structure it forms [47].

The FM supplied by Lubrizol is an organic type FM, which the following literature review will now focus on. Analysis of the FM provided by Lubrizol is detailed in **Chapter 4**.

### 2.2.3.1 Organic friction modifiers

Organic FM molecules, such as those shown in **Figure 2-7**, contain a polar head group region and a non-polar tail region [48]. The polar head group is attracted to the surface of metallic substrates through hydrogen bonding. The polar head groups become anchored to the surface creating a monolayer while the non-polar tail of each molecule remains solubilised in the lubricating oil and aligns perpendicular to the surface. These tail portions are held in place next to each other by weak Van der Waals forces, and the head groups remain held close by dipole-dipole

interactions, combined these forces provide the stabilisation required to form a thin film on the metal surface, the forces involved and molecular orientation are shown in **Figure 2-9**.

Many layers are then formed on top of this initial layer in a head-head tail-tail arrangement as shown in **Figure 2-9**. It should also be noted that this is the ideal stacking situation and in reality there may also be some entanglement between the non-polar chains the degree of which will be dependent on the length of the chain itself. The alignment of the chains in these FM layers makes compression difficult while the ease at which the bonds between these layers are broken makes shearing of the chains occur when surfaces move parallel to the layer. The layers are also easily reformed meaning that there is always a protective, sacrificial FM layer upon the surface of the metal which can provide lower friction and prevent wear [45, 49].

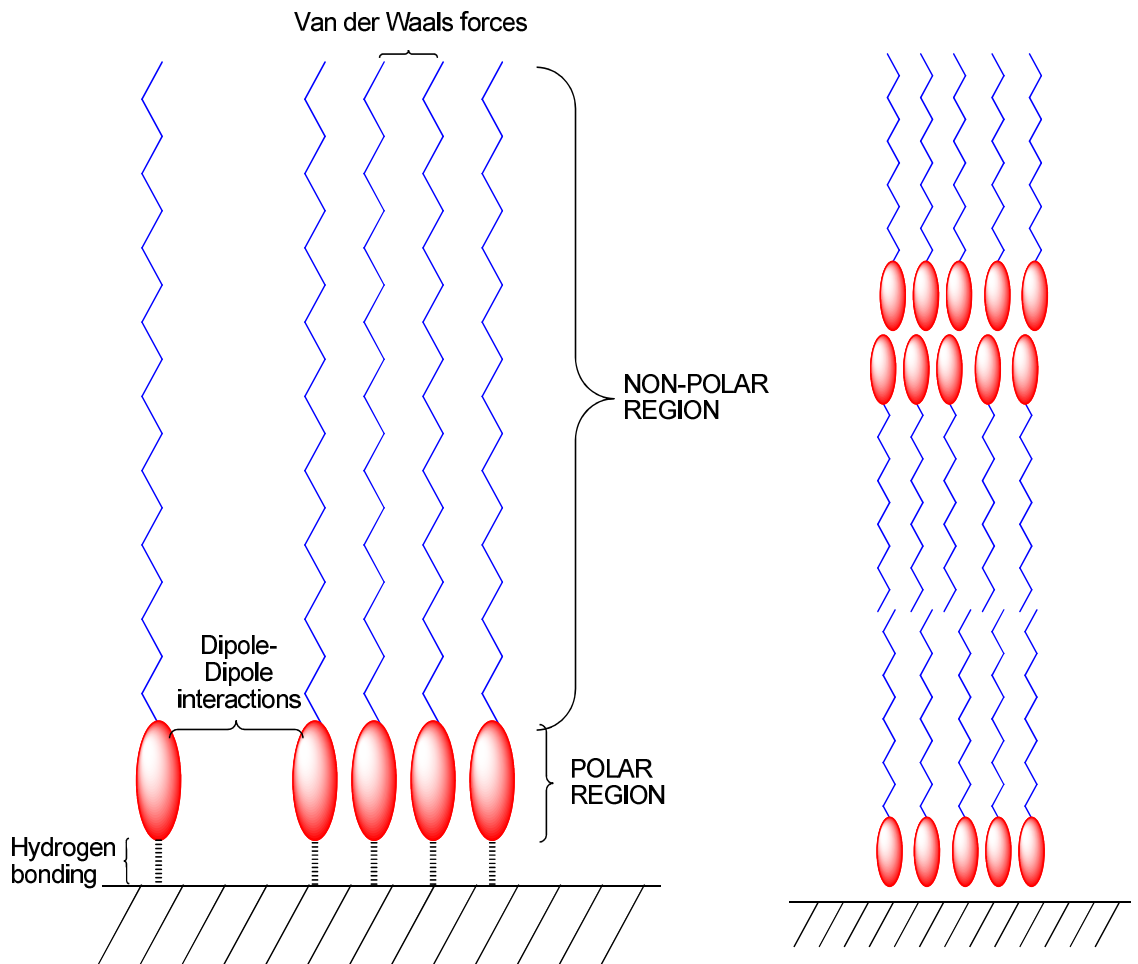


**Figure 2-9.** Nature of the bonding at the substrate surface between molecules of stearamide (left) and the organic multilayer formation (right).

A study by Castle and Bovington [50], where carboxylic acid based FMs with saturated, straight chain hydrocarbons are to be used to lubricate surfaces, it was found that the length of the hydrocarbon chain has a direct effect on the molecules friction reducing properties. Increasing the length of the hydrocarbon chain portion of the friction modifier being used decreased the friction coefficient, which is shown in **Figure 2-10**. Straight, fully saturated chains were found to be superior to unsaturated chains in terms of friction reduction. This is most likely due to the double bonds in unsaturated species hindering free movements of the chain. They are also less stable than fully saturated chains and can react with other additives or contaminants in the oil. A patent by Landry-Coltrain *et al.* [51] similarly describes the formation of stearamide coatings in lubricating layers. In it they state that the ideal length of the non-polar chain portion, of FMs with the general formula R-CONH<sub>2</sub>, is between 16 to 22 carbons in length.

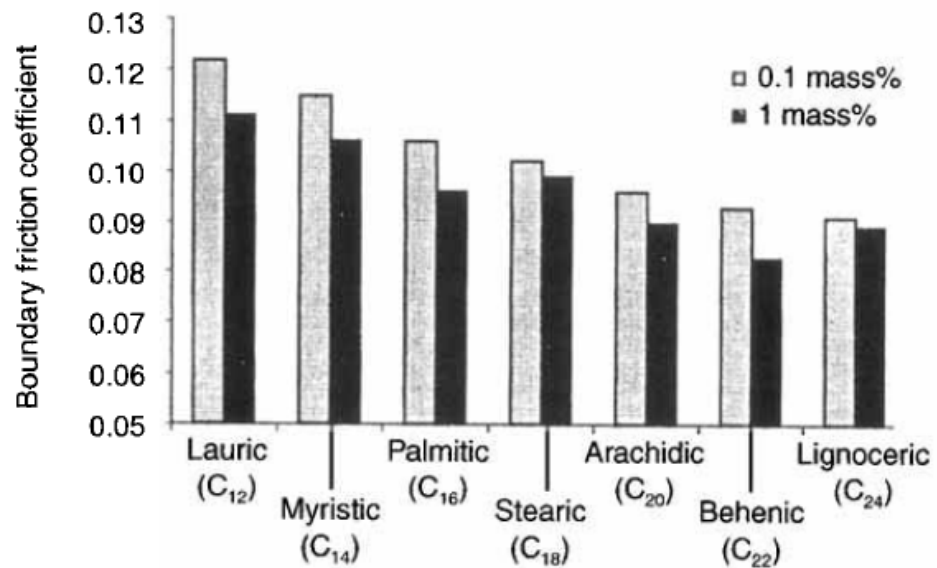


**Figure 2-10.** Effect of increasing hydrocarbon chain length on the boundary friction coefficient of a FM [50].

In an engine, the lubricant is repeatedly exposed to high temperature and so additives in the lubricant need to be stable enough to not lose functionality under these conditions. Temperature is an important consideration in the testing of the

effectiveness of an FM, for example desorption of the FM from the metal surface occurs at higher temperatures destroying the layers which have been created. The process of FM decomposition is an exothermic process this again defines the need for strict temperature control in the testing carried out in this project. However the breakdown of the molecule is not a factor in how effective the additive is at friction reduction. This characteristic is useful as it shows that the activity of the FM will not be destroyed by the polymerisation processes that will be used in this project during the encapsulation of FM. In the book *Lubricant Additives Chemistry and Applications*, Kenbeck and Bunemann [52] present a figure showing how the friction coefficient of different organic friction modifiers is effected by changing the operating temperatures during testing. Optimum working temperatures for FM action during a low speed (0.03 m/s) pin-on-disc tribometer test are shown in **Figure 2-11**. The increase in friction coefficient with increasing temperature is linked to the viscosity of the lubricant; at higher temperatures the viscosity of the oil decreases and the oil becomes less able to support the applied load i.e. the film thickness decreases. As seen earlier in this section, the decrease in film thickness leads to a greater number of asperity-asperity contacts and therefore an increase in friction.

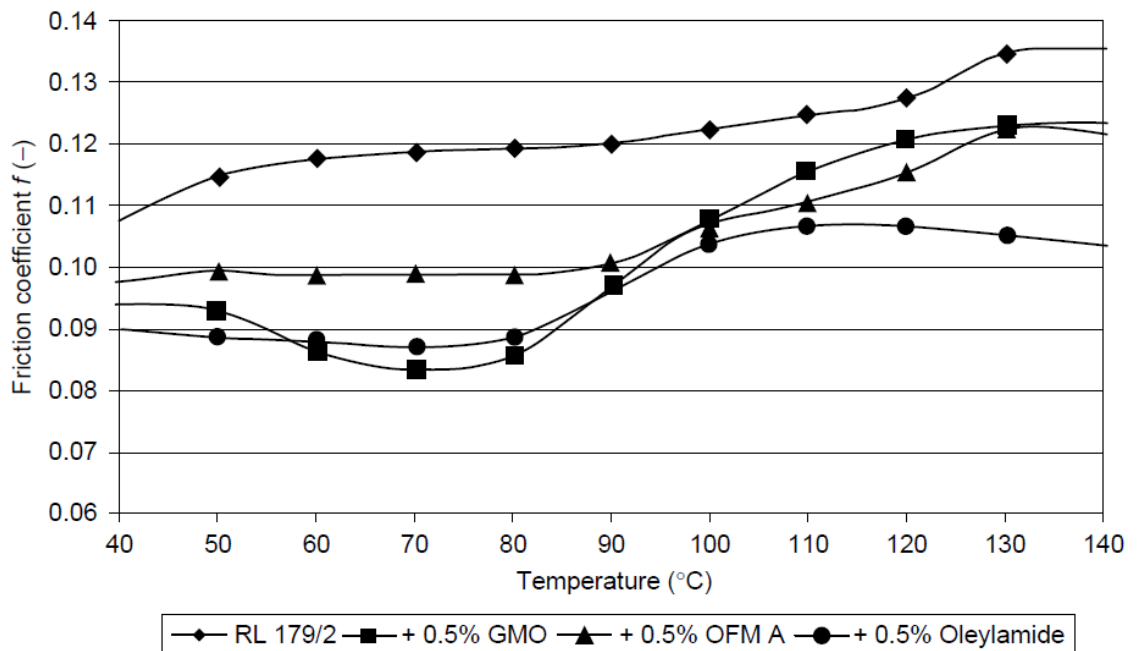


**Figure 2-11.** Coefficient of friction of reference oil RL 179/2 containing different organic FMs (GMO, ‘OFM A’ and oleylamide) at different temperatures [52].

Testing conditions used in this project in **Chapter 6** were chosen with this in mind. TE77 tests were carried out at 80°C in order to optimise the performance of the FM while keeping below the glass transition temperature of the chosen PMMA polymer, which is 105°C for atactic PMMA [53].

### 2.2.4 Additive-additive interactions

Chemical additives are incorporated into an engine oil in order to try and overcome all the problems associated with formulating a lubricating oil for different conditions. However adding additives provides another area for formulators to consider in the form of additive-additive interactions, which may be antagonistic or synergetic. One review of additive-additive interactions by Spikes [10] summarised known interactions at the time, the results of this are reproduced in **Table 2-1**.

**Table 2-1.** Antagonistic and synergetic additive-additive interactions. Red = antagonistic effect. Blue = synergetic effect [10].

	VI improver	Pour point depressant	Detergent/ dispersant	Oxidation inhibitor	Corrosion inhibitor	Antiwear	Extreme pressure	Antifoam
VI improver		Blue				Blue		Red
Pour point depressant	Blue							
Detergent/ dispersant				Blue	Blue	Red	Red	Red
Oxidation inhibitor			Blue		Blue	Blue		
Corrosion inhibitor			Blue	Blue		Red	Red	
Antiwear	Blue		Red	Blue	Red		Blue	
Extreme pressure			Red		Red	Blue		
Antifoam	Red		Red					

This article is now over 20 years old and many new additives have since been developed. For every new additive developed new studies on the additive-additive interactions need to be carried out.

The majority of literature looking at the additive-additive interactions of FMs has focused on interactions involving inorganic FM, such as the interaction between molybdenum dialkyldithiocarbamate (MoDTC) [54], a well known FM, and zinc dialkyldithiophosphate (ZDDP) [11, 55], a common AW additive.

There are few examples of additive-additive interactions concentrating on organic FM. One of the reasons for encapsulating the FM is to minimise the potential of negative additive-additive interactions occurring as well as to ensure that the concentration of FM in the oil is great enough to overcome competition from other surface active species. As previously mentioned organic FMs function by forming a protective, sacrificial layer on the surface of substrates but in some cases there is a competition for the surface between the FM and other additives which function *via* a similar mechanism.

- Extreme pressure – friction modifier

EP additives also function by forming a surface layer, or tribolayer, on asperities, leading to a competition between the two additives. The formation of this tribolayer is governed by the polarities of both additives and whichever of the two is most polar will be the one which forms a layer on the surface. EP and FM additives protect the surface under different conditions so it is detrimental to have one additive form a surface layer in conditions for which the other additive is designed [10].

- Antiwear – friction modifier

Antiwear additives are also considered as surface active additives and both AW and FM operate under similar conditions. These additives can also undergo competition to form a tribolayer on a surface. Due to their polar nature these additives may also interact with each other in solution [12].

### 2.2.5 Technological drivers for a change to organic FMs

As stricter regulations have come into place regarding the levels of exhaust emissions new technologies have been developed to help meet these regulations. New technologies include exhaust gas recirculation (EGR), selective catalytic reduction (SCR) and diesel particulate filters (DPF).

EGR redirects a proportion, typically 5-15%, of warm exhaust gases back towards the air intake where it combines with fresh air and enters the cylinders. This method reduces the heat released by the engine due to the decreased availability of oxygen during the combustion stage of the cylinder cycle. The lower temperature reduces the formation of NO<sub>x</sub> species during combustion however this method does increase the formation of diesel particulates [17, 56].

SCR converts NO<sub>x</sub>, by the injection of automotive grade urea into the stream of exhaust gases, into less harmful N<sub>2</sub> and H<sub>2</sub>O. This process is shown in **Figure 2-12** [57, 58].



**Figure 2-12.** Formation of nitrogen gas and water vapour in selective catalytic reduction.

DPFs work to remove soot and other particular matter from exhaust gases. As trapped particulates will eventually block the DPF it is important that the filters are cleaned regularly. DPFs continually regenerate by raising their operating temperature to burn off particles that are trapped in the filter. Hydrocarbons are easily burnt off but any metallic ash particles cannot be removed and will eventually build up leading to clogging of the filter [16, 59].

Each of these new technologies changes the operating conditions of the engine and this has led to the rise of lubricant additive packages which can be termed low SAPS (low sulphated ash, phosphorus and sulphur). Ash is mainly present due to the use of metal containing compounds in lubricants, with inorganic FMs being one of the additives which are currently a source of metallic atoms. Switching from inorganic FMs to organic FMs, such as the stearamide used in this project may be

the solution to formulating oils which are more compatible with the new technologies.

## 2.3 Heterogeneous polymerisation

Polymerisation is the chemical process of linking small molecules, monomers, to form a larger molecule, a polymer, made up 'n' number of repeating units [60]. Polymers may be made up of the same repeating monomer units or a mixture of different monomer units, these are termed copolymers, and the degree of regularity of these copolymers can be controlled during synthesis. The basic process of polymerisation is often represented as shown in **Figure 2-13**.

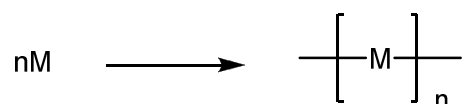


**Figure 2-13.** Basic polymerisation scheme. 'n' number of monomer units 'M' polymerises to form a polymer of repeating 'M' units of chain length 'n'.

Polymerisation can be initiated in many ways including free radical reactions, cationic reactions and anionic reactions. Of these initiation methods free radical initiation is the one which corresponds to the method used in this project to prepare suitable polymer particles [61].

### 2.3.1 Polymerisation of methyl methacrylate

Below is an example of a free radical polymerisation reaction (bond angles distorted for clarity) using the methyl methacrylate (MMA) monomer and azobisisobutyronitrile (AIBN) initiator, both of which have been used in the production of polymer particles in this project. The first stage of the reaction is the

decomposition of AIBN by addition of heat or radiation to form  $N_{2(g)}$  and two identical free radical species (**Figure 2-14**).

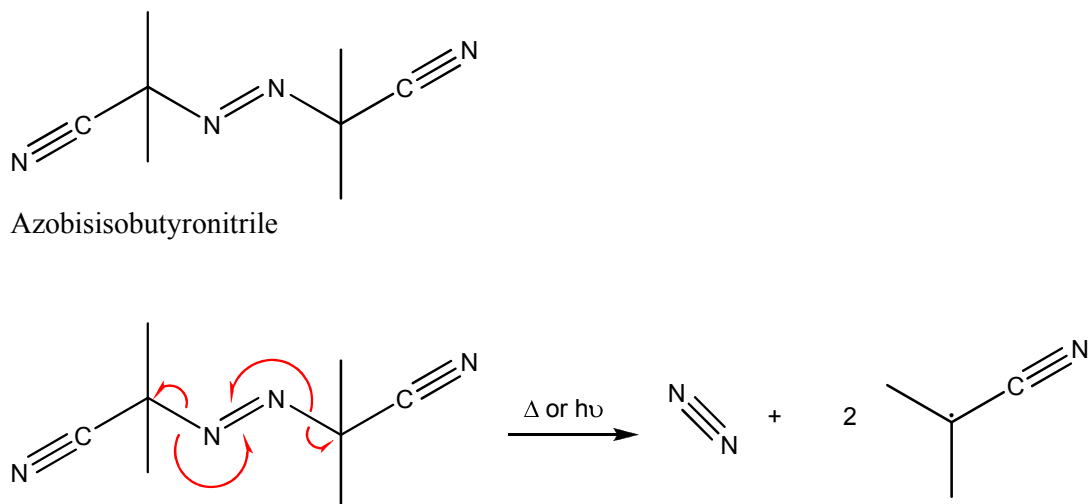
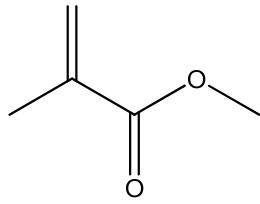


**Figure 2-14.** Generation of free radical species by breakdown of AIBN.

The free radical species generated can then be used to initiate the polymerisation of the MMA. The free radical combines with one electron from the double bond of the MMA while the other electron moves onto the alpha carbon. This produces an active radical centre on the methyl methacrylate group which can then continue growing. It should be noted that initiation may occur from the other side of the alkene, in this case the radical would be located on the  $CH_2$  group (**Figure 2-15**).



Methyl methacrylate monomer

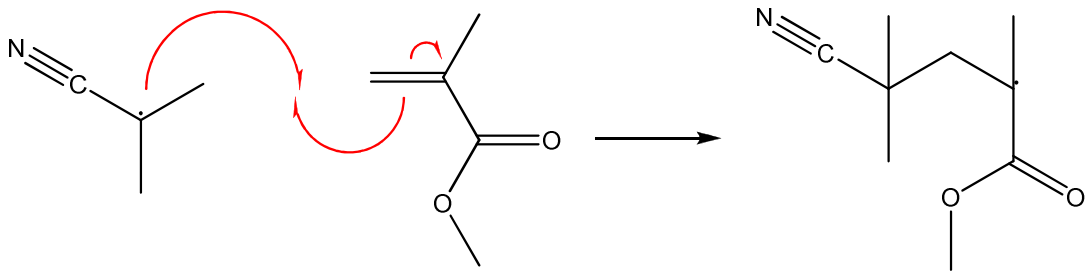


**Figure 2-15.** Initiation of methyl methacrylate polymerisation by the free radical.

This active radical can attack other methyl methacrylate monomers producing a growing polymer chain. This is termed the propagation step (**Figure 2-16**).

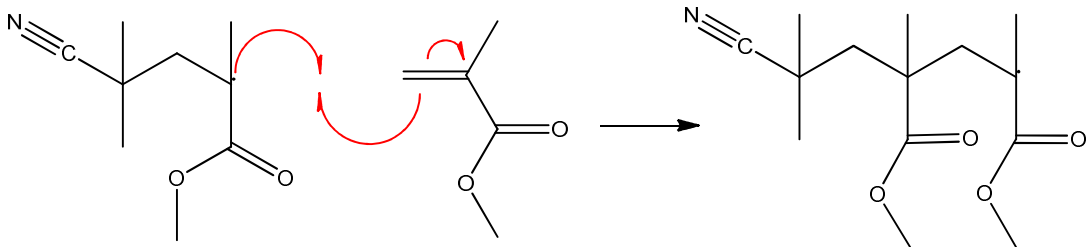


**Figure 2-16.** Propagation step where the chain continues to grow.

The final stage of polymer synthesis is the termination step. Termination can typically occur in two ways; the combination of chains or the disproportionation of chains. In a combination termination the free radical species of two growing polymer chains come within close proximity of each other forming a new bond between the two chains. Combination can also occur between the radical on a growing chain and the radical of an initiator species (**Figure 2-17**).

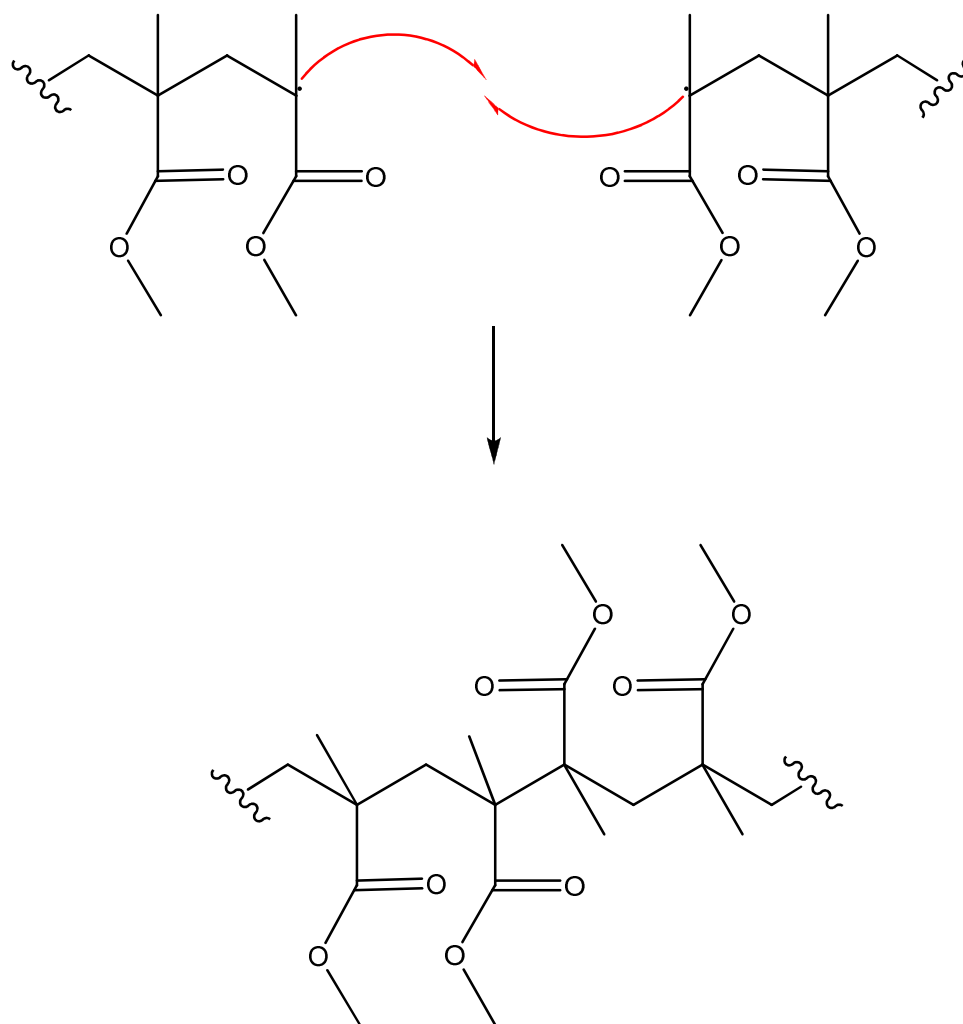


**Figure 2-17.** Termination via combination.

In a disproportionation termination the free radical of one polymer chain removes an atom, most likely hydrogen, from another growing chain. This produces two polymer chains; one of which is saturated and the other which has an unsaturated terminal group (**Figure 2-18**).

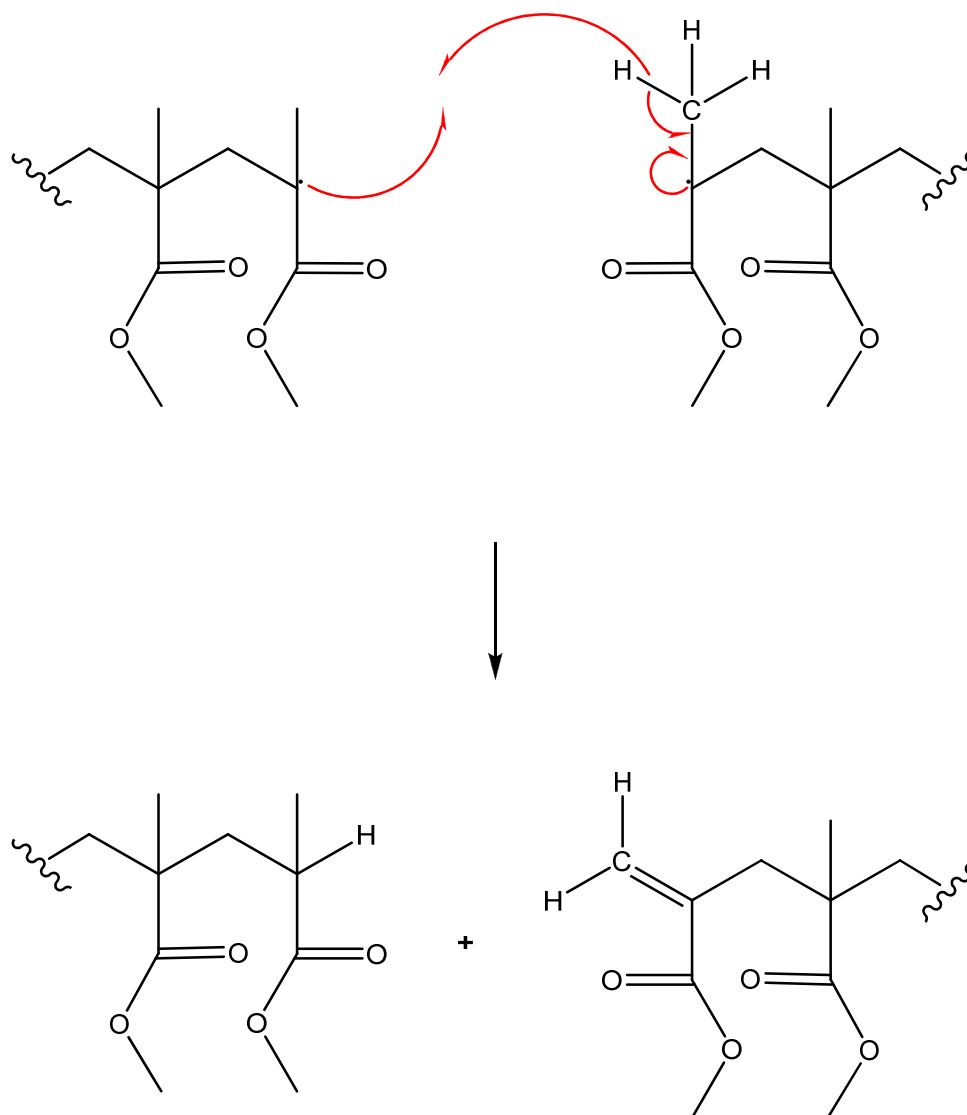


**Figure 2-18.** Termination via disproportionation.

In most polymerisation processes a combination of both termination steps can occur within the same system. While polymerisation can occur until all monomer has been consumed it is normally the case that growing chains will reach the termination step before this happens. The exception to this is in the case of living polymerisations where chains are prevented from terminating and the sequential addition of more monomer allows polymerisation to continue at a controlled pace.

### 2.3.2 Types of heterogeneous polymerisation

There are four common types of polymerisation which use free radical initiation; bulk, emulsion, suspension and dispersion. Each of these four general types can be further broken down into more specific classifications of polymerisation. Bulk polymerisation is used in the creation of polymer monolith, for example that used in molecular imprinted polymers [62], and will therefore not be discussed further here. The other three types, which are classed as heterogeneous polymerisations, will be described in detail in the following paragraphs.

#### 2.3.2.1 Suspension polymerisation

Suspension polymerisation typically produces spherical polymer particles greater than 1µm in diameter [60]. A thermo-sensitive initiator is solubilised in a monomer and this monomer is then dispersed in an immiscible liquid continuous phase. The droplets of monomer are mixed into a suspension by the use of agitation and stabilisers and upon the addition of heat to this mixture, the polymerisation is initiated. Droplet size in the monomer form is influenced by the dynamic equilibrium between droplets coalescing and being broken apart again by the action of the stirrer. The size of the final particles produced is dependent on the size of the monomer droplets, therefore final particle size can be controlled by changing the speed of agitation and the concentration of stabiliser [63]. The process of suspension polymerisation is shown in **Figure 2-19**. This form of polymerisation is often likened to a small scale bulk polymerisation occurring in each droplet and as such kinetics of this polymerisation are often treated as bulk polymerisations.

Mass, or semi, suspension polymerisation is similar to suspension polymerisation but involves two steps. In the first step a slow stirring speed is used and polymerisation proceeds as it would in a bulk polymerisation reaction. Once a pre-determined concentration of polymer has been reached agitation is increased and the system undergoes suspension polymerisation as detailed previously. These two steps can either be carried out in two separate reaction vessels, where monomer and initiator used in step one are added to continuous phase and stabiliser in step two, or can be carried out *in situ* in a single reactor. The latter was demonstrated by

Jahanzad *et al.* [64], who investigated what effect changing the timing of the switch between the steps had on MMA polymerisation in an aqueous system. It was found that polymer size was dependent on the ratio of polymer to monomer upon entering the suspension stage; higher ratios led to larger particles. In the same work it was noted that in systems where the monomer concentration was low, the droplets would be broken by the action of the stirrer creating even smaller, monodisperse droplets while at higher concentrations it is still possible to burst these droplets but there is also the possibility that the particles will deform and remain their original size leading to a wide distribution of final particle sizes.

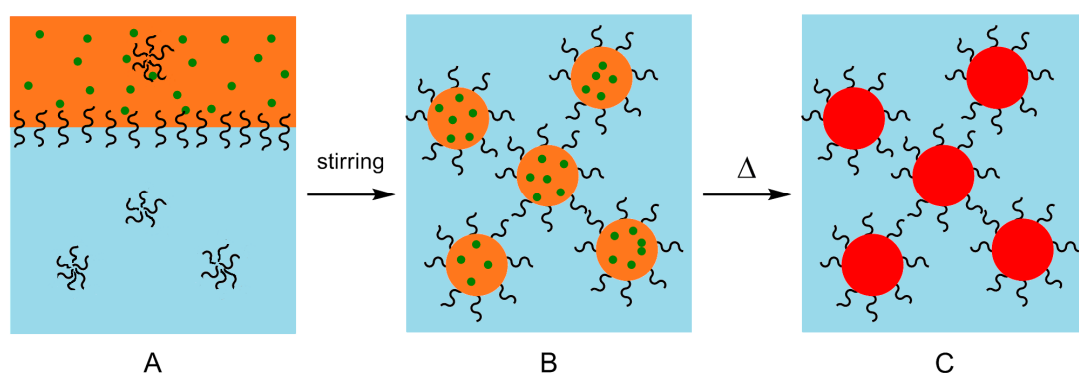


**Figure 2-19.** A. Monomer (orange) is insoluble in the continuous phase (blue). Initiator (green) which is only soluble in the monomer phase is added. B. Upon stirring monomer droplets are formed and are prevented from coalescing by the use of stabiliser (black). C. When heated initiation and polymerisation occur within the droplets resulting in the final polymer particles (red) the same size as the initial monomer droplets.

Encapsulation by suspension polymerisation can be achieved by dissolving the active to be encapsulated in the monomer. The active may be either dissolved directly in the monomer or more typically the active will contain some degree of functionalisation to aid solubility. The polymerisation progresses as shown in **Figure 2-19** with the final polymer product having the active encapsulated within it [65-67]. This process was demonstrated in PMMA by Duguet *et al.* [68] who demonstrated the encapsulation of alumina particles by functionalising the surface of

the the alumina using 3-(trimethoxysilyl)propylmethacrylate. The functionalised alumina was blended with the MMA which then underwent suspension polymerisation to produce PMMA particles with an alumina core.

Creation of a core shell morphology is achieved by the use of an initiator which, due to polarity of that initiator, breaks down and generates free radicals at the interface between the monomer and the continuous phase [67] and is also dependent on the minimum total free energy change [69-71]. In order to control particle size distribution and prevent secondary nucleation a polymerisation inhibitor may be added to the continuous phase [72], thus ensuring that polymerisation only occurs within the monomer droplet.

### **2.3.2.2 Emulsion and miniemulsion polymerisation**

Emulsion polymerisation generally results in particles less than 1 $\mu$ m and is able to produce highly monodisperse spherical polymer particles. For emulsion polymerisation a monomer is chosen which is only sparingly soluble in the continuous phase. Any monomer which does not solubilise is held in emulsion droplets surrounded by a stabiliser. The initiator, which is soluble in the continuous phase, initiates the reaction by polymerising the small amount of monomer dissolved in the continuous phase. Primary particles form within the micelles created by the stabiliser, here they act as seed particles and continue to grow as monomer is released from the droplets into the continuous phase. Due to the polymerisation being initiated in the continuous phase the size of the particles produced is dependent on the ratio between monomer and stabiliser. As with all the other free radical polymerisation methods, the final particle size is also affected and can be controlled by the temperature of the system, choice of reagents and concentration of reagents [60, 63]. The emulsion polymerisation process is shown in **Figure 2-20**.

The use of non-aqueous solvents allows water sensitive reactions, oxidations and catalytic processes to occur within the polymer mixture. Completely non-aqueous (oil in oil) emulsion polymerisations appear to have had little research focus due to the difficulty of forming stable emulsions and finding two immiscible, non-aqueous solvents [73, 74].

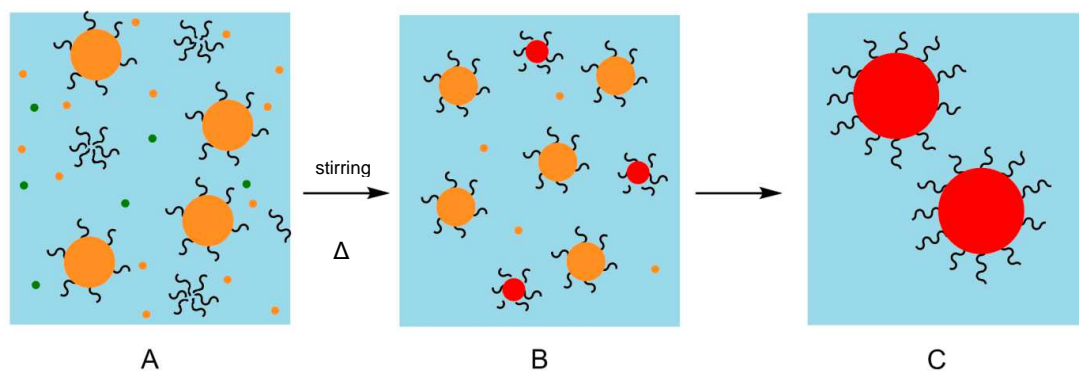


**Figure 2-20.** A. Initiator (green) and monomer (orange), which is slightly soluble, are dissolved in the continuous phase (blue). Unsolubilised monomer is held in droplets by stabiliser (black). B. Upon heating and stirring stabilised polymer seeds form (red). Monomer moves from droplets into the continuous phase. C. All monomer has been polymerized and final particles are formed.

Miniemulsions are so called because the emulsion droplets formed are much smaller than those formed in emulsion polymerisations (1-10 $\mu\text{m}$  for emulsion polymerisation compared to 0.01-0.5 $\mu\text{m}$  for miniemulsion). Typically the initiation step takes place within the emulsion droplets rather than in the continuous phase as is the case in emulsion polymerisation. The kinetics of this process, as well as other possible initiation processes, were presented by Bechthold and Landfester [75], the initiation process demonstrated in this study is shown **Figure 2-21**.

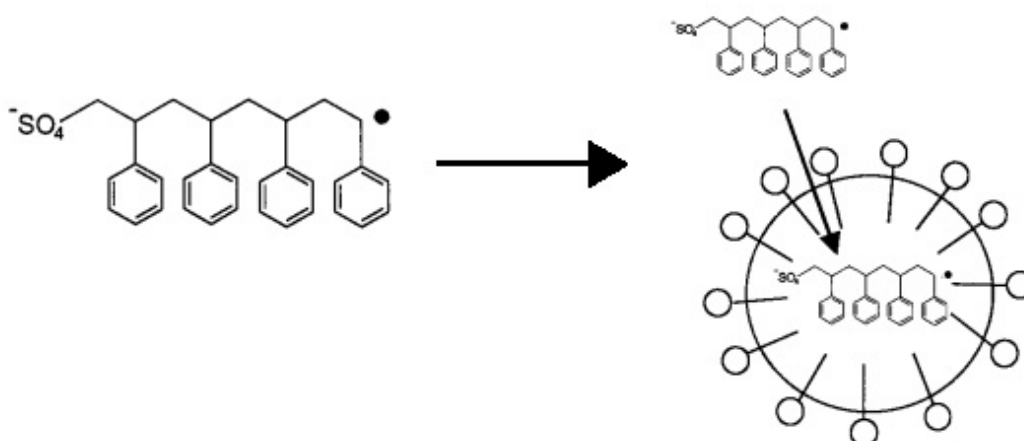


**Figure 2-21.** The droplet nucleation process typical of miniemulsion polymerisation (adapted from Bechthold and Landfester [75]).

For a given volume of monomer, smaller droplets have a larger surface area and therefore need more stabiliser at their surface to create a stable emulsion. Since there is no free stabiliser in the continuous phase there will be no micellar formation. Seed particles which form in the solution must enter the monomer droplets in order for polymerisation to take place. This process has been used successfully in the preparation of biodegradable nanoparticles suitable for future drug development [76-78].

Encapsulation by miniemulsion and is the subject of a number of reviews by Landefester [79-81] and has been well documented for the encapsulation of both organic and inorganic materials [80]. The active to be encapsulated is dissolved within the monomer, leading to the formation of highly monodisperse particles. The main advantage of miniemulsion over emulsion or dispersion polymerisation is the great degree of control over the composition and size of the final polymer particles formed. If the active is insoluble in the monomer, such as  $\text{TiO}_2$  in MMA detailed by Haga *et al.* [82] or silver in styrene detailed by Quaroni and Chumanov [83], functionalisation of the surface may be required. This however tends to result in secondary nucleation of particles and aggregation and so encapsulation by emulsion polymerisation tends to be the preferred method.

Given that the final application of the particles in this project is the incorporation of particles into a fully formulated engine oil, emulsion polymerisation has not been considered to be an appropriate technique to use in particle production. Ideally, particles would be synthesised in base oil before blending to produce a final, fully formulated engine oil. However the lack of literature on oil in oil emulsion polymerisation, due in part to the difficulty of synthesis, made this an undesirable approach. Despite the high degree of control and the ability to produce particles within the desired size range miniemulsion in non-aqueous continuous phases does not appear to have been reported in the literature.

### **2.3.2.3 Dispersion polymerisation**

Dispersion polymerisation results in the production of highly monodisperse spherical polymer particles. Spherical particles have a higher elasticity than irregular particles and are less likely to interact with surface asperities, making them highly

suitable for tribological applications. The general principle behind dispersion polymerisation is that the monomer used is soluble in the reaction medium but the corresponding polymer is insoluble and thus precipitates during the polymerisation process to form a particle seed. This seed then continues to grow until all monomer is consumed [63, 84]. The use of polymeric stabilisers prevents particle aggregation throughout the process. The presence of these polymers on the surface of the final particles provides colloidal stability in the continuous phase [85-90]. This process is described schematically in **Figure 2-22**.

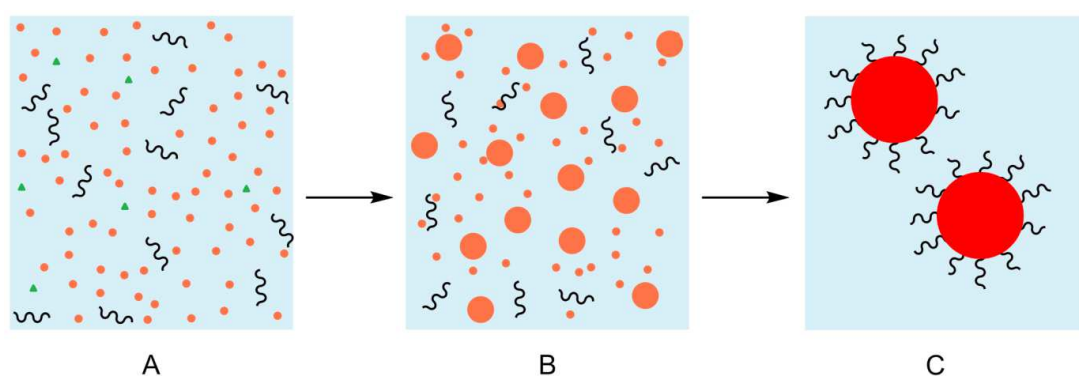


**Figure 2-22.** A – Stabiliser (black), initiator (green) and monomer (orange) are dissolved in a continuous phase (light blue). B – Upon stirring and heating primary particles form and grow in solution. C – When all of the monomer has reacted polymerisation is complete. Polymer particles (red) are prevented from aggregating by surface stabiliser.

Although there appears to be much less literature reporting the production of polymer particles by dispersion polymerisation in non-aqueous solvent than in aqueous solvents it is not a recent invention [91]. This type of procedure is routinely used to produce polymer particles typically incorporated in coatings and paints and thus has a history of being used in large scale synthesis [63, 71] of the type which would be required in producing particles suitable for use in lubrication formulation in the future. In 1979 Dawkins and Taylor [92] detailed the polymerisation of polystyrene (PS) in alkanes. The success of the redispersion in different alkanes was found to be dependent on the solubility of the poly(dimethyl siloxane) (PDMS) stabiliser used in that alkane. In particular, if the PDMS stabiliser was not soluble in the continuous phase, it would lead to flocculation of particles. This will be an

important consideration when transferring particles produced in this project to the final engine oil for tribology applications [93, 94].

The dispersion polymerisation of PMMA in hexane using a methacryloxypropyl terminated poly(dimethyl siloxane) stabiliser was reported by Klein *et al.* [85]. The use of a PDMS based stabiliser and an alkane continuous phase in the polymerisation of MMA is a system similar to the one used in this project. The effects of changing various factors of the polymerisation were then investigated. The first variable investigated was the time allowed for the polymerisation. It was found that the longer the reaction time the greater the yield of particles produced however after a certain amount of time, in their case two hours, the increase in yield was negligible. This is due to the abundance of monomer at the start of polymerisation compared to the concentration of unreacted monomer at the end. The amount of time a polymerisation will reach completion is dependent on the concentration of initiator used to start the reaction and the concentration of monomer. This same pattern was seen in the size of the particles produced. Particle diameter increased quickly within the first two hours of the reaction and remained almost unchanged subsequently.

#### **2.3.2.4 Heterogeneous polymerisation summary**

While examples of other encapsulation methods can be found in literature, for example interfacial polymerisation [95], coacervation [96] or spray drying [97], these methods do not allow for fine control over final particle size or polydispersity. For this reason heterogeneous polymerisation was chosen as a more suitable method of encapsulation.

Each of the methods of heterogeneous polymerisation detailed here, suspension, emulsion and dispersion polymerisations, can be used in encapsulation of active species. All of the methods described in this section are capable of producing spherical particles suitable for tribological applications. One of the desired criteria when choosing a polymerisation method was the ability to reproducibly synthesise particles below 100nm. The careful control of particle size, alongside particle concentration, by the formulator of the final engine oil will be used to control the visibility of particles used in fully formulated oil. Particles below 100nm diameter will have reduced visibility to the naked eye making any fully

formulated engine oil containing those particles more desirable to the customer. The control of particles in this size range by suspension polymerisation is not possible therefore this synthesis method was not used.

Emulsion polymerisation is dependent on both the presence of stabiliser micelles and limited solubility of the monomer in the continuous phase and is therefore less commonly achieved in non-aqueous systems. Additionally, only a few examples of emulsion polymerisation for use in encapsulation exist in literature with none of these examples being found in non-aquous environments.

Dispersion polymerisation has been chosen due to the ability to have great control over the final particle size and polydispersity, which is advantageous in producing particles down to 100nm in size which is discussed further in **Chapter 4**. Dispersion polymerisation can be carried out in non-aqueous environments with the possibility to easily transfer particles synthesised into a different non-aqueous solvent if required. While not unique to dispersion polymerisation, this method of synthesis also has the ability to scale up such polymerisations in order to increase the volume of particles produced so as to be suitable for industrial applications.

## **2.4 Microencapsulation**

The main advantages of microencapsulation can be summarized as such;

1. Transportation - this may mean making a chemical safe for its user to handle or the transportation of a chemical to where it is needed, for example, transportation of a drug active to exactly where it is needed within the human body. In the case of engine oil additives this means delivering the FM to the vicinity of the tribocontact where it is needed in a larger concentration within the engine and allowing for its release into the precise area it is needed.
2. Protection - chemical reaction, oxidation and degradation can all be limited by the use of encapsulation. As previously mentioned, additive-additive interactions may take place under certain conditions and at certain additive concentrations. Encapsulation of the FM within a core shell structure will

protect the FM from any unwanted reactions which affect its friction reducing action in an engine.

3. Allow for a controlled release - the method of release from a microcapsule can be quite varied; there may be degradation of the polymer, diffusion of the core through the shell into the outside environment or via a dialysis reaction. Each of these may, in turn, be triggered by a number of different stimuli, for example the external temperature, environmental pH, chemical reaction or solubilisation. In this project the microcapsules aim to release the FM into the engine oil as the FM which has been traditionally blended into the oil itself is depleted. The microcapsules will therefore act as a 'FM reservoir' to ensure that the concentration of FM is always present in the oil to the maximum of the solubility of that FM without any human intervention.

#### **2.4.1 Microencapsulation *via* dispersion polymerisation**

To achieve the synthesis of microcapsules *via* dispersion polymerisation, an immiscible co-solvent can be incorporated into the particle core. For this purpose, the same system as detailed in **Section 2.3.2.3** can be used, with the addition of a co-solvent which is immiscible with the continuous phase and, upon precipitation of the polymer during the reaction process and growing of the particle seeds, will phase separate into the particle core.

The co-solvent is added at the start of the synthesis alongside the polymerisation mixture consisting of monomer, initiator, stabiliser and continuous phase. This is then stirred and heated to initiate the polymerisation in the continuous phase. Primary particles form in the continuous phase, the co-solvent is then included within the particles where it resides preferentially than in the bulk. The particle seeds, swollen with monomer and co-solvent, continue growing until all monomer in the continuous phase is consumed. The microencapsulation process *via* dispersion polymerisation is show in **Figure 2-23**.

When using this method of encapsulation to incorporate the FM into a liquid core the following criteria must be met:

1. Co-solvent and continuous phase must be immiscible.

2. FM must be soluble in the co-solvent but not soluble in the continuous phase.

This will ensure that there is minimal mixing between the co-solvent and the continuous phase and that all of the FM is encapsulated along with the co-solvent.

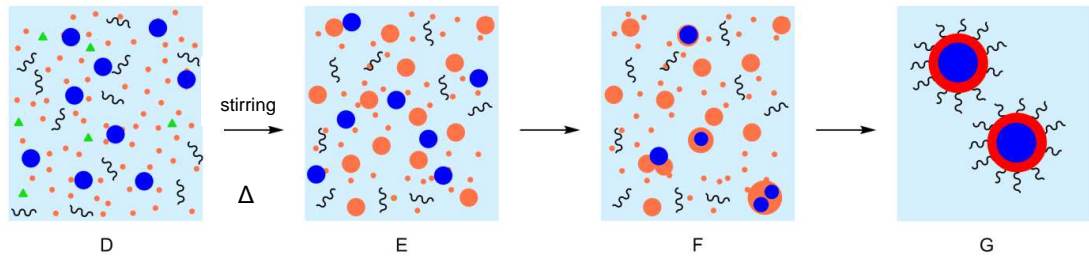


**Figure 2-23.** D – Continuous phase (containing stabiliser (black), initiator (green) and monomer (orange)) and a co-solvent (dark blue) are stirred and heated. E - Primary particles are produced in solution. F - Co-solvent dissolves inside the growing polymer particles. G – Polymer particles (red) are formed which contain co-solvent encapsulated within. Stabilisers prevent aggregation.

Solubility testing has been carried out and it has been established that the FM used in this project is highly soluble in methanol but has limited solubility in dodecane, two solvents which are immiscible. For this reason dodecane continuous phase and methanol co-solvent were chosen for the encapsulation process used in the work presented here.

## 2.5 Use of microencapsulation for lubrication applications

The use of microcapsules in lubrication has been mainly focused on encapsulation of the lubricating oil rather than separate components as is the objective of this work. The microcapsules that have been detailed in literature thus far can be classified as three types; firstly those which are resting upon the surface, secondly those partially embedded in a surface and thirdly those fully embedded in a surface.

A patent by Williamson *et al.* [98] details the use of microcapsules, containing lubricant, which sit on the surface of an orthopaedic cast material which is used in repairing broken bones, this is shown below in **Figure 2-24**. Chemicals mixed into the material allow the adhesion of poly(vinyl alcohol) microcapsules to the surface, typically nylon or rayon. The use of microencapsulation here prevents the surface becoming too slippery to handle but, after rupturing the particles with light pressure the cast can be kept pliable for long enough to mold tightly to the limb. A downside to this approach however is that the microcapsules at the surface can be easily ruptured in transit thus making the material unusable.

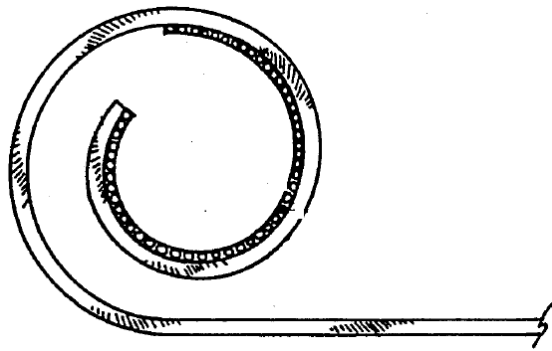


**Figure 2-24.** The end section of a cast material with microencapsulated lubricant particles adhered to the surface of the cast [98].

Partially embedding the microcapsules into a surface may offer the protection of the particles missing from the patent above however due to the particles protrusion from the surface they are still easy to rupture. Guo *et al.* [99, 100] followed this approach and reported a 53% decrease in specific wear rate with only a 1wt% addition of poly(melanine formaldehyde) particles to the surface of a polymer composite. As the number of microcapsules incorporated into the surface was increased wear continued to decrease but the incorporation of further particles was found to be at the detriment of the strength of the surface itself. Investigation under scanning electron microscope (SEM) showed that wear debris created upon rupturing the particles became trapped in the cavities the microcapsules created in the surface. This process is seen in **Figure 2-25**.

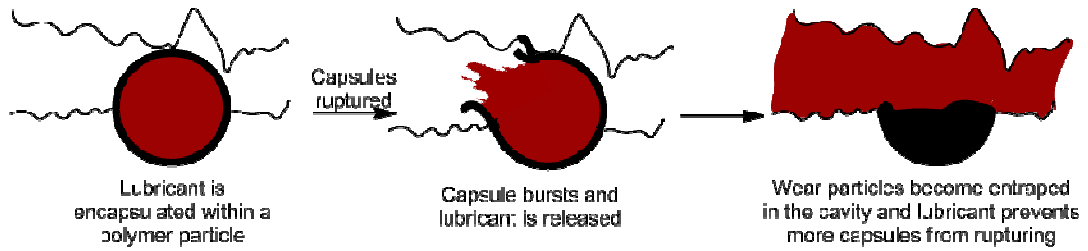


**Figure 2-25.** Process of lubricant release and debris entrapment.

Fully embedding microcapsules into a metal substrate works on a similar principle as that detailed in the case of partial embedment, the structure of this is shown in **Figure 2-26**. As the two surfaces come into contact and wear starts to occur the particles are no longer buried inside the substrate but are now closer to the surface. Once the particles are at the surface they encounter shear stress from the rubbing of the surfaces and the particles rupture thus preventing further wear of the surfaces [101]. Once again wear debris becomes trapped in the cavities produced by the loss of lubricant from the core of the microcapsules. Such a technology is only really suitable for applications where the components will go a very long time between services, such as in aerospace technologies. In systems where it is possible to add lubricant externally these microcapsules would not be the preferred method of lubrication as it requires wear which can be catastrophically damaging to the component.



**Figure 2-26.** Microcapsules, containing lubricant, fully embedded within a surface which is released as wear occurs [101].

### 2.5.1. Use of nanoparticles and microparticles in lubrication

The majority of the literature concerning nanoparticles in lubricants focuses on the use of particles, measuring between 10nm - 200nm, as solid lubricants or the use of inorganic nanoparticles, such as SiO<sub>2</sub>, as the additive. Nanoparticles used in

engine oils often require surface modification in order to increase the solubility of those nanoparticles in the base oil [102-105]. Testing of these particles is typically reported in EHL rather than boundary lubrication conditions such as those used in the work presented here.

Titanium dioxide particles, studied by Kao and Lin [106], were shown to provide the lowest friction coefficient measurements in paraffin oil at between 60°C and 95°C. This is a similar temperature range as the one used in this project. As previously stated the temperature used during TE77 tribology testing in the work presented in this thesis was designed to be below the glass transition temperature of PMMA (105°C) and is also the optimum operating temperature of organic friction modifiers.

Nanoparticles have also been reported to have the ability to have a ‘mending effect’ on surfaces [107-109]. Luo *et al.* reported this phenomena in Al<sub>2</sub>O<sub>3</sub>/TiO<sub>2</sub> nanocomposites where particles were deposited into the wear scar during four ball testing repairing the surfaces damaged during the tribological testing [110].

The effect of adding different concentrations of fullerene nanoparticles was reported by Lee *et al.* [111]. They found that, in disc-on-disc testing, the addition of fullene reduced the friction coefficient below that measured in base oil at particle concentrations as low as 0.01 volume %. This was achieved by to the reduction of surface contacts due to the action of the fullerene.

Fullerene-like MoS<sub>2</sub> particles have been the studied by Rabaso *et al.* [112] to determine the effects of particle size and particle morphology on the wear produced. They hypothesised that particles containing structural defects would be able to penetrate breaks in a surface and more easily be broken down to produce a protective tribofilm at the surface. However they found that spherical, nanoparticles, measuring between 150nm and 300nm performed best when measuring friction and wear generated in tribotesting due to the structure of these particles providing less opportunity for interactions with other additives present in the oil or the surface outside of the contact.

While many of the nanoparticles commonly reported in tribological applications, such as SiO<sub>2</sub>, Ni and MoS<sub>2</sub>, are commonly reported to be in the range of 10nm to 200nm it is often the case that aggregation of the particles occurs above 1.0wt% producing species much larger than reported [113-115]. Aggregation of

PMMA particles in this project is prevented by the use of PDMS-MA stabiliser which sterically stabilises the particles.

Much of the previous work carried out concludes that only low percentages of nanoparticles need to be incorporated into an oil in order to produce lower friction and antiwear effects. The exact concentration of particles required varies with type, size and shape used. Their effect, whether positive or negative, is also strongly dependent on the system used, i.e. the substrates, their surface roughness and factors including load and testing speed [41, 42, 93, 102, 105, 111, 114, 116-124]. The mechanism of friction and wear reduction will be discussed in **Chapter 7**.

## **Chapter 3. Characterisation Techniques**

### **3.1 Introduction**

In this chapter a basic background to the particle analysis and tribological equipment will be provided. This will also include detail on the particle structure and the identification of the structure and location of the FM used, all of which can be considered essential primary analysis upon which further characterisation is based.

### **3.2 Particle analysis techniques**

Particle analysis techniques has been focused upon the study of both solid and liquid core particles. Analysis techniques were carried out both in and out of the dodecane continuous phase.

#### **3.2.1 Dynamic light scattering**

Dynamic light scattering (DLS) is a popular techniques which can be used to measure the size and size distribution of particles in colloidal suspensions in both chemical and biological systems. This method employs the measurement of light scattered by particles due to Brownian motion.

A Malvern Zetasizer™ Nano ZS was used to measure the hydrodynamic diameter and polydispersity of the samples tested in this thesis. Samples to be analysed by DLS are first shaken and sonicated in order to break apart any aggregates that may have formed due to sample storage and to resuspend the PMMA particles in the dodecane continuous phase; this ensures that particles are evenly

dispersed throughout the continuous phase. A laser light source is directed into the sample, light which does not encounter any particles passes through the sample and light which hits a particle undergoes Rayleigh scattering. Particles in solution undergo Brownian motion, defined as the random movement of the particles in the fluid cause by collisions between the particles and the medium they are in [125, 126], with smaller particles moving more than larger particles. Brownian motion causes fluctuations in the intensity of the scattered light, this light will undergo constructive or destructive interference, which once recorded by the Zetasizer can then be used to determine the size and polydispersity of the PMMA particles present. The refractive indices and densities of the polymer and the continuous phase are used within the calculation to allow for effects of the materials used upon the particle motion observed. The basic apparatus used for DLS is shown in **Figure 3-1**.

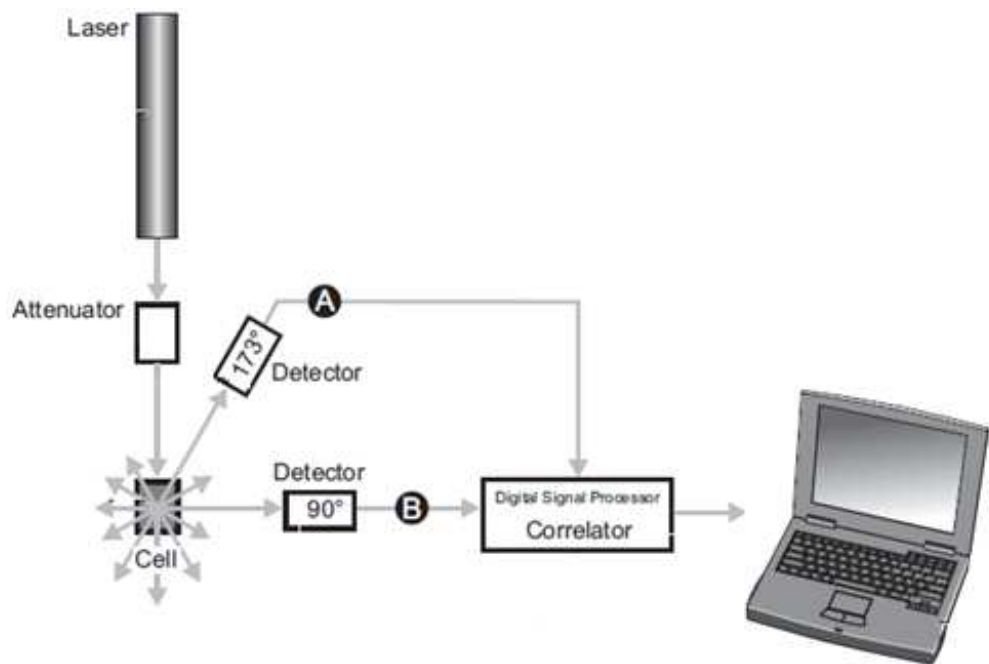


**Figure 3-1.** Apparatus used for dynamic light scattering (DLS) [127].

Ideally each photon measured by the detector will only undergo a single scattering event, in reality this is rarely the case and instead multiple scattering events occur. Samples are tested using different concentrations of particles in dispersant to overcome the effect concentration has on the size measured due to

increased likelihood of multiple scatterings at higher concentrations. To combat this effect a plot of particle concentration in weight percent (wt%) versus measured hydrodynamic particle diameter in nanometers (nm) has been produced for each sample. This produces a straight line in monodisperse samples which, when extrapolated to  $x = 0$ , gives an approximation of the particle size at infinite dilution[128], a theoretical condition where only a single light scattering event is recorded. An example of this is shown in **Figure 3-2**.

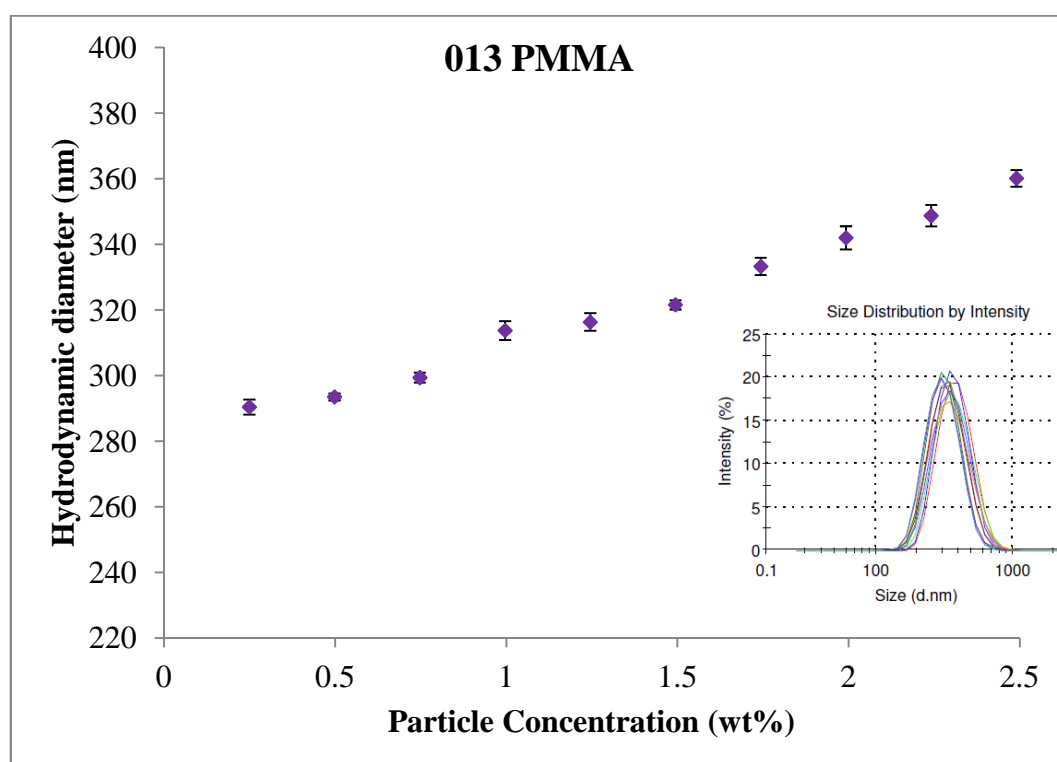


**Figure 3-2.** Hydrodynamic diameter (nm) versus particle concentration (wt%) for a dodecane sample containing solid, monodisperse PMMA particles measuring ~ 280nm diameter.

### 3.2.2 Scanning electron microscopy

Scanning electron microscopy (SEM) is a high resolution imaging technique which in this thesis has been used to image both particle samples and the surface of steel samples after tribological testing. Samples are tested under ultra high vacuum and for this reason are in a dry environment. A beam of primary electrons is

generated by an electron gun and focused, with the use of lenses, onto the surface of the sample. When these primary electrons hit the surface of the sample they are either absorbed or reflected. The primary electrons which are reflected do so in a distinctive pattern and are then received by a backscatter detector. Those electrons which are absorbed excite the electrons at the sample surface, if these electrons gain enough energy they are emitted from the sample. The intensity and pattern of these secondary electrons is picked up by a secondary detector. When the signals from both detectors are combined it produces an image of the point at which the beam was initially focused. To produce an image of the entire surface area of the sample the electron beam does not remain stationary but instead scans across the surface. To magnify the image seen the electron beam scans across a smaller area [129, 130]. **Figure 3-3** shows the apparatus used in SEM imaging.

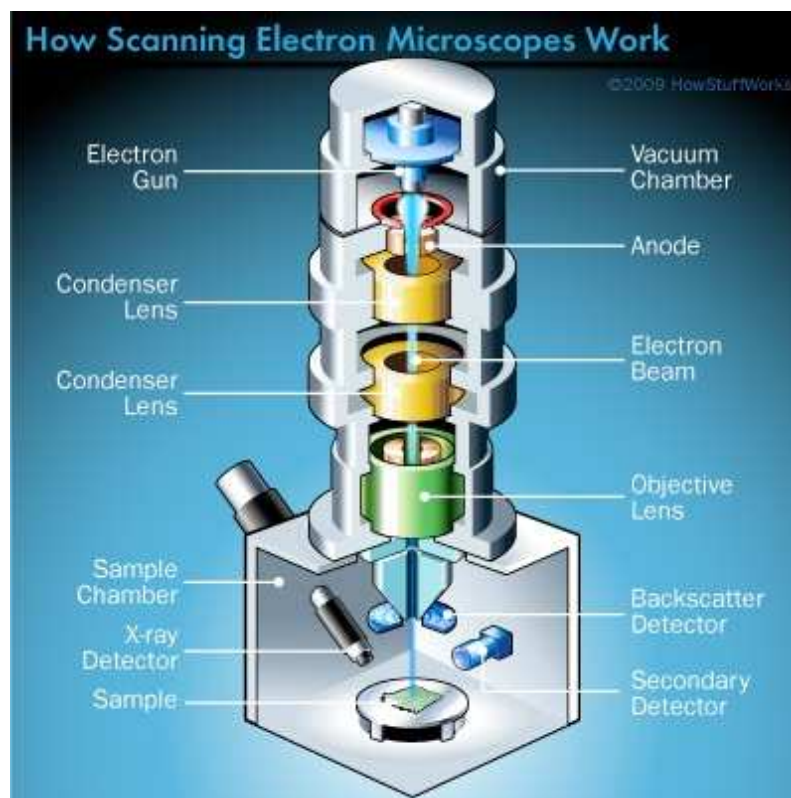


**Figure 3-3.** Scanning electron microscopy apparatus [131].

Samples to be tested by SEM must first be mounted on a clean metallic stub or onto a small glass, or silicone, slide attached to the top of a metal stub. Samples mounted upon a glass slide are shown in **Figure 3-4**. Both of these mounting

techniques have advantages and disadvantages. Mounting directly onto the stub allows good conductance though the sample however if the surface of the stub is not completely smooth the surface of the stub itself may be seen in the image produced. Mounting onto glass provides a smoother background but doesn't allow conductance. To overcome this a thin layer of metal is painted between the stub and the sample before a thin conductive layer is vapour deposited onto the sample surface, this is particularly relevant when analyzing non-conductive samples such as polymers [132].



**Figure 3-4.** SEM stubs inside the ultra high vacuum chamber.

When preparing the slide care should be taken not to scratch its surface. Slides were cut on a clean surface and were only handled with tweezers. Once cut they were rinsed with deionized water, decon and ethanol before being dried with a  $N_{2(g)}$  gun. Once the slide had been attached to the stub using double sided tape one drop of the sample to be analysed was pipetted onto the slide. To avoid contamination by dust the prepared stub was then attached into a stub holder before being placed into a vacuum oven for 5 days to remove solvent from the sample. When the sample was dry it was sputter coated with a thin layer of platinum measuring 3nm thick.

SEM is a common technique used in polymer analysis however it should be noted that the electron beam can cause damage to the polymer. To overcome this the electron beam was focused away from the area of interest and quickly moved to the area to be imaged, thus allowing a true image to be seen [64, 133-136]. An example of the images obtained from SEM can be seen in **Figure 3-5**. Particles pack in a hexagonal fashion but are in fact spherical. This slight shape change is due to the effect of the drying process.

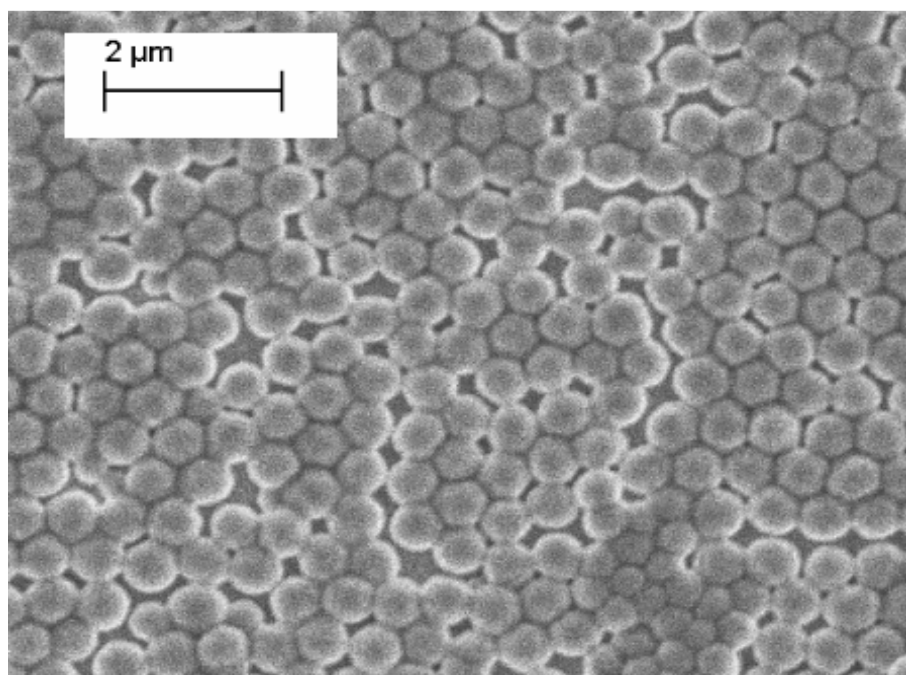


**Figure 3-5.** Scanning electron micrograph of poly(methyl methacrylate) particles measuring  $\sim 1.5\mu\text{m}$  (measured by DLS). It should be noted that size of particles when measured by DLS is carried out while the sample is in the dodecane continuous phase while SEM is carried out on samples which have had all solvent removed.

### 3.2.3 Transmission electron microscopy

Transmission electron microscopy (TEM) is another analytical imaging technique using an electron beam and can provide images of the internal structure of the polymer particles being analysed. Unlike SEM, where the electrons are either absorbed or reflected off the sample, in TEM the electrons are targeted through the

sample under ultra high vacuum. Electrons targeted at the sample can either pass through the sample, become retarded by the sample or may be scattered by the sample. Whichever of these processes the electron undergoes effects the energy the electron has as it continues on through the TEM towards a fluorescent film where the image is formed. Denser areas of the sample allow fewer electrons to pass through and therefore appear darker in the final image and sparser areas allow a greater number of electrons to pass through and thus appear lighter in the final image. The image produced is then recorded by a camera [137-141]. The apparatus used in TEM is shown in **Figure 3-6**.

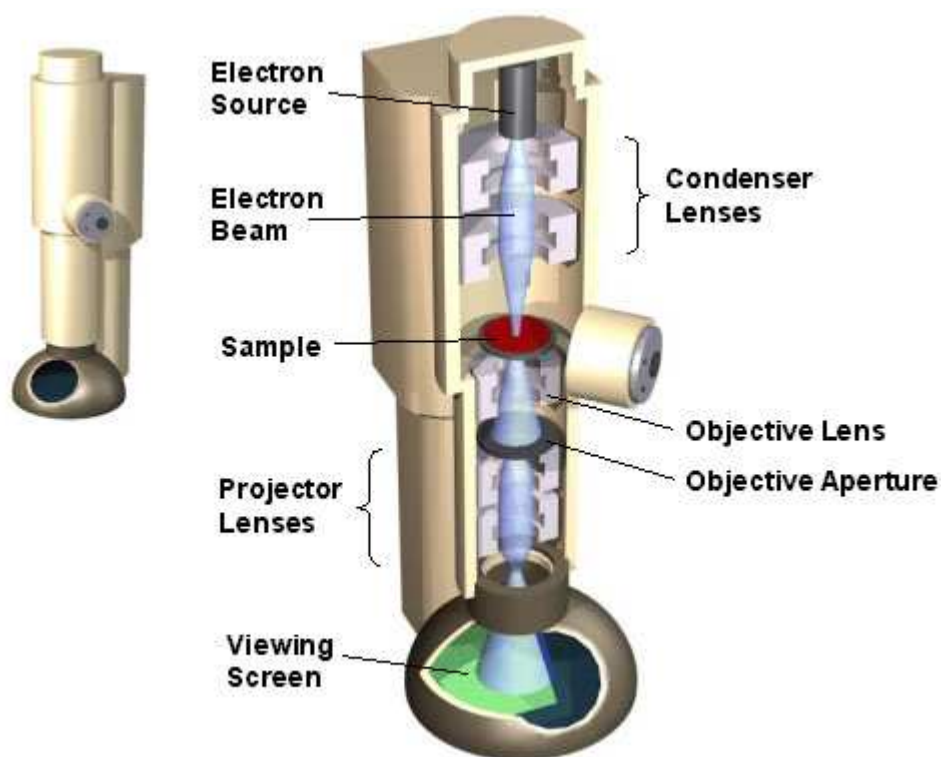


**Figure 3-6.** Basic transmission electron microscopy apparatus [142].

### 3.2.4 Attenuated total reflectance-infrared

Infrared (IR) is used as a fingerprinting technique meaning that each sample produces a characteristic spectra which can be compared to a library for easy identification. Traditional IR requires the preparation of a nujol mull containing the sample which is then sandwiched between two salt lenses. Attenuated total

reflectance-infrared (ATR-IR) requires no, or very little sample preparation and gives a very quick result.

The sample is placed upon a crystal and is held by an arm which is screwed down to ensure complete contact. The IR beam is passed through the ATR crystal and as the beam hits the inner surfaces it is reflected until it eventually passes out of the crystal. At each point of reflectance some of the IR beam continues in a straight line into the sample. This beam will be absorbed at certain wavelengths and the beam becomes altered, or attenuated. The attenuated energy passes back into the crystal and combines with the unaltered IR beam. The spectra produced by the detector will show where the IR was absorbed by the sample [143]. This process is shown briefly in **Figure 3-7**.

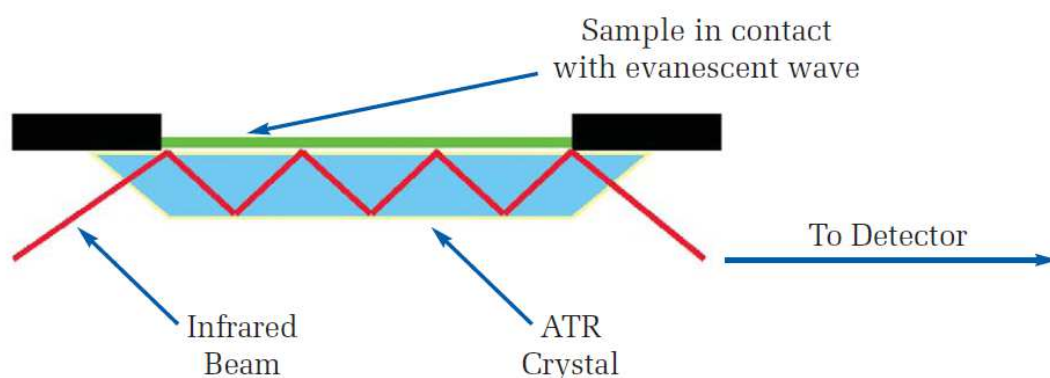


**Figure 3-7.** Basic principle of attenuated total reflectance – infrared [144].

The characterisation and location of FM used were studied using ATR-IR and is detailed in **Chapter 5**. However when using ATR-IR in this project limitations have been found when attempting to quantify the amount of FM in a sample.

### 3.2.5 High performance liquid chromatography

High performance liquid chromatography (HPLC) has instead been used to determine the presence of FM and quantify the amount of FM in samples. This process is detailed further in **Chapter 5**.

Fresh solvent, termed the mobile phase, is pumped through the HPLC system, a few microlitres of liquid sample is injected into this mobile phase and is carried towards a HPLC column packed with chromatographic material, this is termed the stationary phase. This column separates the sample into its various chemical compounds, the mobile phase continues with ease through the column while the different compounds are eluted from the column at different rates. The mobile phase containing the, now separated, compounds continues to flow towards a detector. The signal produced by the different compounds will differ from the mobile phase and this will produce a corresponding peak on the computer data system. This computer records the signal received by the detector over time. The separated chemicals will reach the detector at different times depending on how well they were retained by the column. Each peak is compared to a standard, which can either be internal or external, containing a known amount of each compound to enable a quantification of the chemical of interest in a sample of unknown concentration. Mobile phase which has passed through the detector then travels towards a waste container for disposal [62, 128, 145, 146]. The basic HPLC apparatus is shown in **Figure 3-8**.

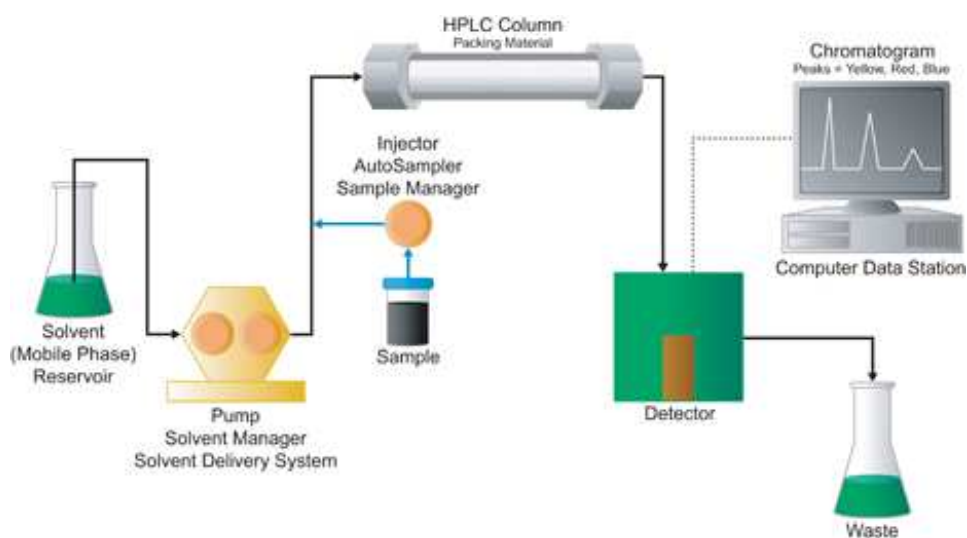


**Figure 3-8.** A common high performance liquid chromatography system [147].

Each component of a HPLC system can be adapted to meet the needs of the user. Some common variations are as follows:

- Sample injection may be manual, which more common in older machines, or automatic sample injection, which is much more likely today.
- Pre-columns may be used to filter the sample before it reaches the column. This ensures that the column does not become clogged with species which would not be easily eluted.
- Different columns with different packing materials and lengths can be employed dependent on the properties of the sample to be tested.
- A column heater may be used to aid the elution of the sample from the column.
- Different types of detector may be used, for example ultraviolet (UV), refractive index (RI) or evaporative light scattering detector (ELSD).
- HPLCs can also be coupled with other analytical techniques, most commonly with mass spectroscopy (LC-MS).

### **3.3 Plate analysis techniques**

Analysis of the steel plates includes the measurement of the friction coefficient of dodecane, and how this is affected by the addition of PMMA particles, as well as the measurement of the wear caused by the tribological testing.

#### **3.3.1 TE77**

Tribological testing in this project was designed to replicate the contact between a piston ring and the cylinder liner. The different areas of an engine have different types of surfaces coming into contact and each of these contacts can be modelled using the wide variety of tribometers available. The relevant tribometer is chosen for its ability to accurately simulate the type of materials, lubrication regime and contact in the particular area of interest.

Tribological testing in this was carried out using a Cameron Plint TE77 low speed reciprocating test machine. The low speed Cameron Plint TE77 tribometer comprises a pin, or ball bearing, attached to a reciprocating arm which moves across a stationary plate. This stationary plate is positioned within a heated oil bath.

TE77 testing allows for the study of friction and wear under dry sliding or lubricated conditions at a range of temperatures and can be operated with different loads and reciprocation frequency in order to simulate a wide variety of test conditions. In the work presented here the pin held by the reciprocating arm represents the piston ring and the stationary plate represents the cylinder liner. In an engine the piston ring rubs against the unmoving cylinder liner during four stroke cycle of the cylinder in an engine. The TE77 apparatus is show in **Figure 3-9**.

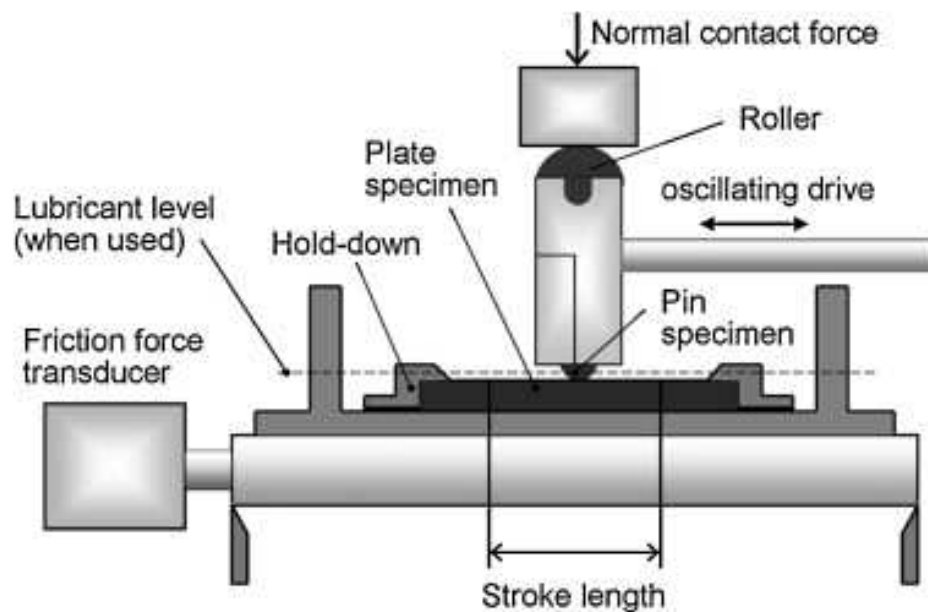


**Figure 3-9.** TE77 test apparatus [148].

Prior to testing the removable components of the TE77 are placed into beaker of acetone, sonicated for 15 minutes and are then allowed to dry. This removes any oil, debris or polymer build up which may have been left behind by previous tests. Pins and plates to be used in the testing are placed in separate beakers and undergo the same cleaning procedure. The plate for testing is clamped into position inside a stainless steel oil bath and this unit is then bolted onto a heating block. The heating block is controlled *via* a thermocouple which is placed into the oil bath. The test pin is clamped onto the reciprocating arm and is positioned using a spirit level to ensure even contact across the centre of the plate. Once all components have been aligned the desired lubricant is added to the oil bath. Load is applied using a cradle fixed across the reciprocating arm this holds weights which are hung, using springs,

directly underneath the rig. The frictional force transducer measures the frictional force generated horizontally while testing is underway. The entire system is monitored and results are processed by LabView and Microsoft Excel.

In this thesis coefficients of friction reported are the average of 1000 data points recorded over five minute intervals for a two hour test period. Once testing is complete the pin and plate are removed from their respective holders and are rinsed with heptane to remove excess lubricant and stored in aluminium foil. This ensures that any film formed is not removed and that the possibility of atmospheric reactions during storage is minimised. A photograph of the TE77 apparatus used in this project is shown in **Figure 3-10**.

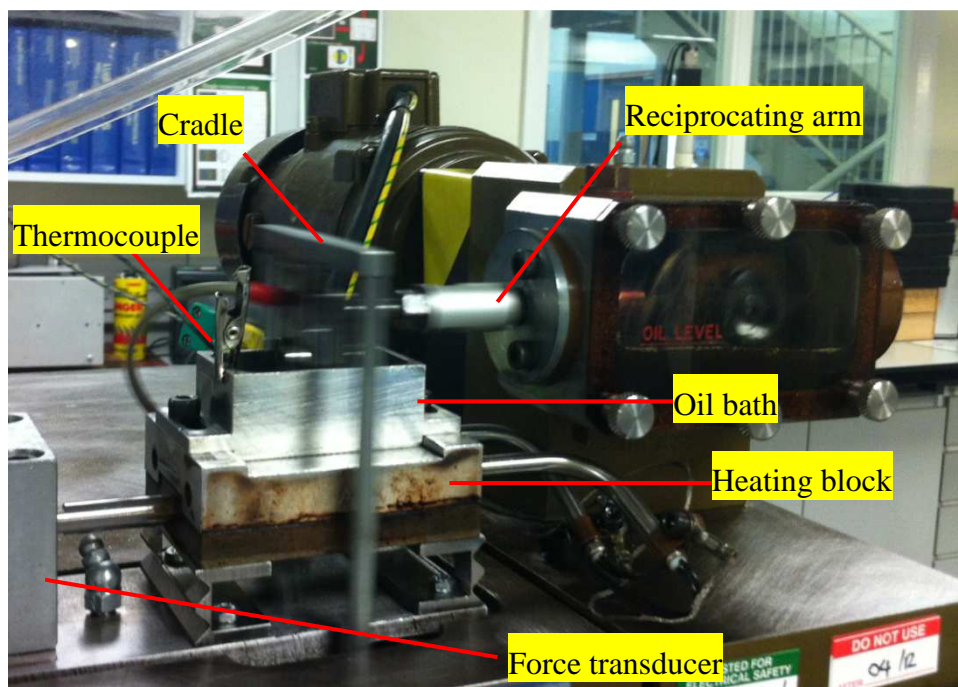


**Figure 3-10.** TE77 testing apparatus used in this project.

Testing conditions were chosen to stimulate the running conditions of the piston ring and cylinder liner system working within the boundary lubrication regime. The load, frequency and applied force were chosen to replicate boundary lubrication conditions. The radius of the pin, the materials of the pin and plate and the roughness of both were also chosen to achieve boundary lubrication and to mimic the materials used in the engine. The operating temperature of testing carried out was chosen to be within the working range of organic friction modifiers while

being below the glass transition temperature of the PMMA used. Operating conditions are detailed in **Table 3-1**

**Table 3-1.** Cameron Plint TE77 test conditions.

Pins	Cast iron ( $\varnothing$ 6mm, radius 10mm, 43-47 HRC)
Plates	AISI 52100 Steel (58-60 HRC)
Run Conditions	80°C, 25Hz, 24.5N, 0.78GPa, 5mm stroke length

The software used in TE77 tribotesting analyses the friction generated in real time but wear of the plates must be analysed once this testing is complete.

### 3.3.2 Interferometry

Wear analysis was conducted using scanning white light interferometry on a Bruker NP FLEX<sup>TM</sup> interferometer. Interferometry is a non-contact, high precision technique which can be used to analyze surface topography.

A light source is directed towards a beam splitter which produces two waves of equal frequency, one of these waves will travel towards the surface of the sample to be analysed, the other will travel towards an internal reference mirror. Upon meeting the surface both of the beams are reflected, then become recombined and are sent towards a detector (**Figure 3-11**). The detector measures the intensity of the light at different points of the sample as it undergoes vertical scanning; the highest points on the sample surface will be the first to cause interference (**Figure 3-12**). When the waves are recombined they will either undergo constructive interference, which happens when the waves are in phase, or destructive interference, which occurs when the waves are out of phase. The intensity of the light is measured by the

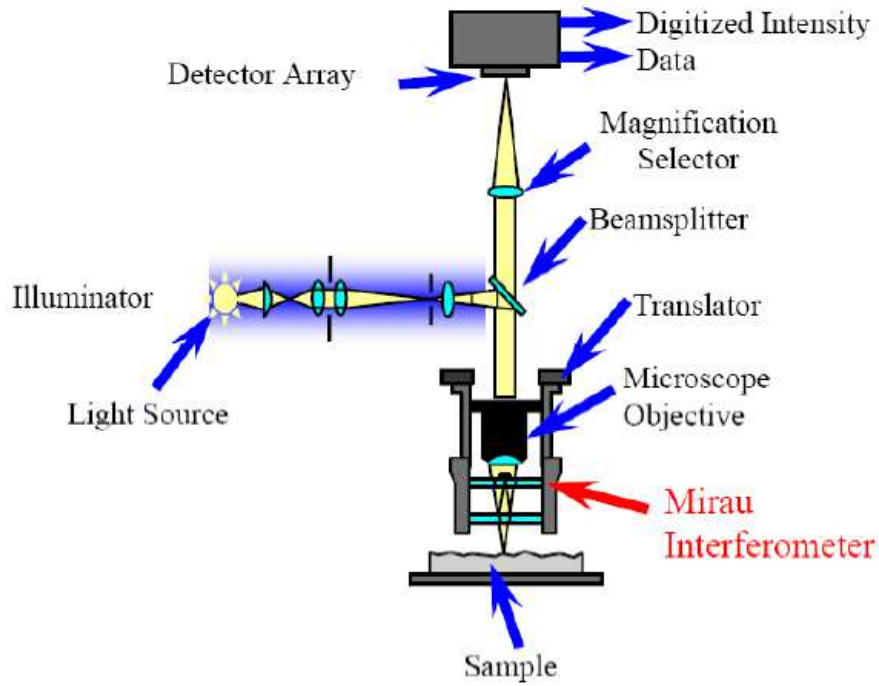


**Figure 3-11.** Schematic of the apparatus and beam pathways in a white light interferometer [149]. N.B. Mirau interferometer refers to the position of the reference surface in relation to the sample surface. In a Michelson interferometer this reference would be positioned  $90^\circ$  to the sample [150].

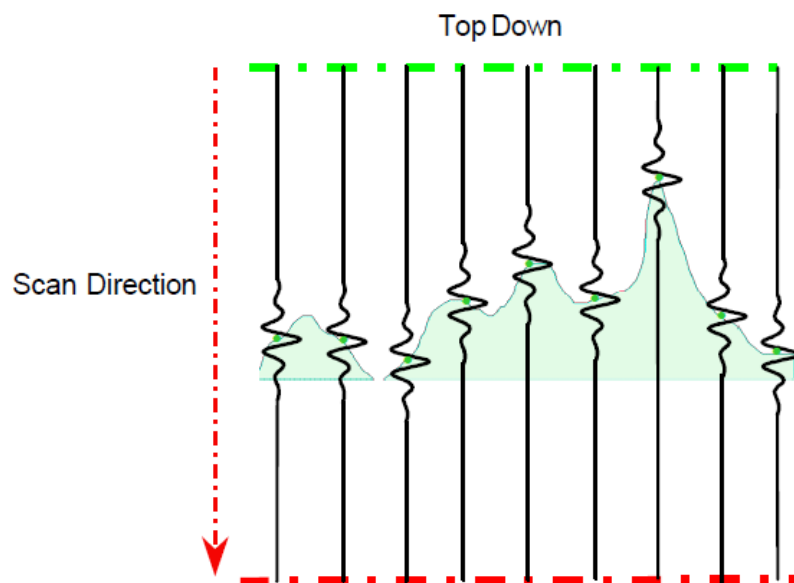


**Figure 3-12.** Schematic showing the build up of a surface structure by vertical scanning interferometry [150].

detector as a function of time, this determines at what point the beams met the respective surfaces, and corresponds to the sample height. When combined this is used to produce a three-dimensional image of the surface [149-152].

The software used in analysis corrects for the influence of surface bias (eg. curvature or tilt) and can also give information on wear volume and surface roughness.

### **3.4 Summary**

This chapter has provided an overview and a basic background to the main analytical techniques used in this project. Attenuated total reflectance – infrared has been used to determine the structure of the FM used in this project as that of stearamide, this is discussed further in **Section 5.4**, and was also used to confirm the presence of the FM inside particles. Through SEM and TEM analysis the particles were shown to have a polymer shell – liquid core morphology, and is shown in **Section 5.3**. All particles produced were spherical and the size of particles in each sample and the polydispersity of each sample was confirmed using DLS. Monodispersity is important as it allows for direct comparison of all particles in the sample and ensures that all particles have an equal effect on the friction and wear recorded. The release of encapsulated FM from within the core of particles was recorded using HPLC and is further detailed in **Chapter 5**.

Plates were analysed by SEM to identify where the particles could be found on unrinsed samples after TE77 testing and WYKO white light interferometry was carried out on plates after testing to measure the surface topography and volume of wear, results of this work are given in **Chapter 6**.

## **Chapter 4. Investigation into the Effect of Changing the Initial Polymerisation Recipe of Final PMMA Particle Size**

### **4.1 Introduction**

The technology developed in this project has the potential to improve the performance of lubricating oils, however in order for it to be suitable for use in a commercially available fully formulated engine oil certain key features of the lubricating oil should remain unchanged from present specifications. One such desired characteristic specified by Lubrizol is the the final appearance of the lubricating oil should not change upon the addition of particles. Although this is unlikely to affect the performance of the oil itself, it will affect the confidence of customers in the product they are buying.

In data tables PMMA particles have a quoted refractive index of about 1.49, this is different to that of the dodecane continuous phase which is 1.421 [153]. Particles which have a refractive index different to that of the continuous phase they are in will scatter light very effectively thus causing suspensions to appear opaque. One possible method of making the particles less visible in an oil would be to chose a polymer which has the same, or very similar, refractive index as the oil it is blended into.

Another possible method, and the one which will be investigated further in this chapter is through careful control of the final particle size. Larger particles, above 100nm in size, will be visible when added to an engine oil but have the potential to carry a large amount of FM within the particle core. Reducing the concentration of particles required in an oil may also lead to a lowering in particle visibility. Smaller particles, below 100nm diameter, can be less visible or even invisible, to the human eye. However this may require a larger number of particles to be blended into the oil to achieve the same overall increase in FM concentration. For this reason the choice between particle size and particle concentration is essential; the ideal system is

considered to have small (<100nm) particles that are barely visible which carry a large concentration of FM in the particle core.

The investigation into factors which can be altered during synthesis with the aim of controlling final particle size and polydispersity is therefore essential. This has been carried out by altering the concentrations of the various components in the initial polymerisation mixture, as shown in **Table 4-1**, or changing the physical process involved in the particle production.

This chapter presents work carried out to synthesise solid PMMA particles, containing no co-solvent or additive, with controllable final particle size and polydispersities. This chapter thus describes the influence of a range of parameters on the final particle size and demonstrates the ability of the dispersion polymerisation process to enable good control of particle size down to diameters approaching sub-100nm. The chapter then goes on to show the influence of adding a co-solvent to the initial polymerisation mixture and the effect on the particle size and polydispersity measured.

## 4.2 Synthesis of solid PMMA particles

The initial polymerisation mixture used to produce particles in this thesis is detailed below in **Table 4-1**.

**Table 4-1.** Initial polymerisation mixture.

Monomer	Methyl methacrylate (MMA) (2.5 – 22.0wt% w.r.t. continuous phase)
Initiator	Azobisisobutyronitrile (AIBN) (0.72-5.2wt% w.r.t. monomer)
Stabiliser	Methacrylate terminated poly(dimethyl siloxane) (PDMS-MA) (7.4-109.0wt% w.r.t monomer)
Continuous phase	Dodecane

PDMS-MA, dodecane, AIBN and MMA were added, in this order, to a round bottom flask which was then fitted to a refluxer. The whole system was then purged

with  $N_{2(g)}$ , in an ice bath, while stirring at 300 revolutions per minute for 30 minutes. Subsequently the nitrogen source was removed and polymerisation was carried out at  $80^{\circ}C$ , 300rpm for 4 hours. Once polymerisation was complete the warm particle suspension was filtered through a plug of glass wool to remove any aggregates that may have formed. At the point of opening the reaction vessel, air enters the system degrading the free radicals present and stopping the reaction. Unreacted monomer and excess stabiliser were removed from the suspension through a cycle of centrifugation, removal of dodecane from the supernatant and resuspension of the particles in fresh dodecane.

A Malvern Zetasizer Nano ZS was used to measure the hydrodynamic diameter and polydispersity of the resulting particle suspension.

#### 4.2.1 Effect of changing monomer concentration

The amount of monomer used in the initial polymerisation mixture directly changes the size and polydispersity of the polymer particles which are produced and this is shown in **Figures 4-1** and **Figure 4-2**.

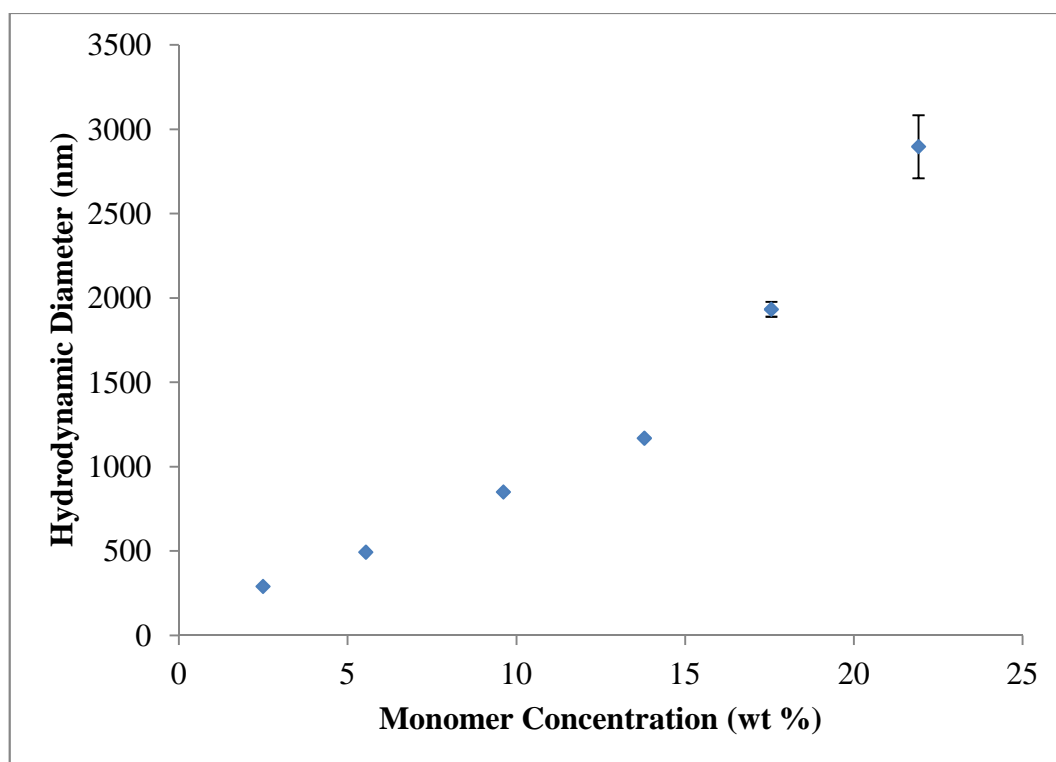


**Figure 4-1.** Effect of changing monomer concentration on particle size. Error bars are included in all data.

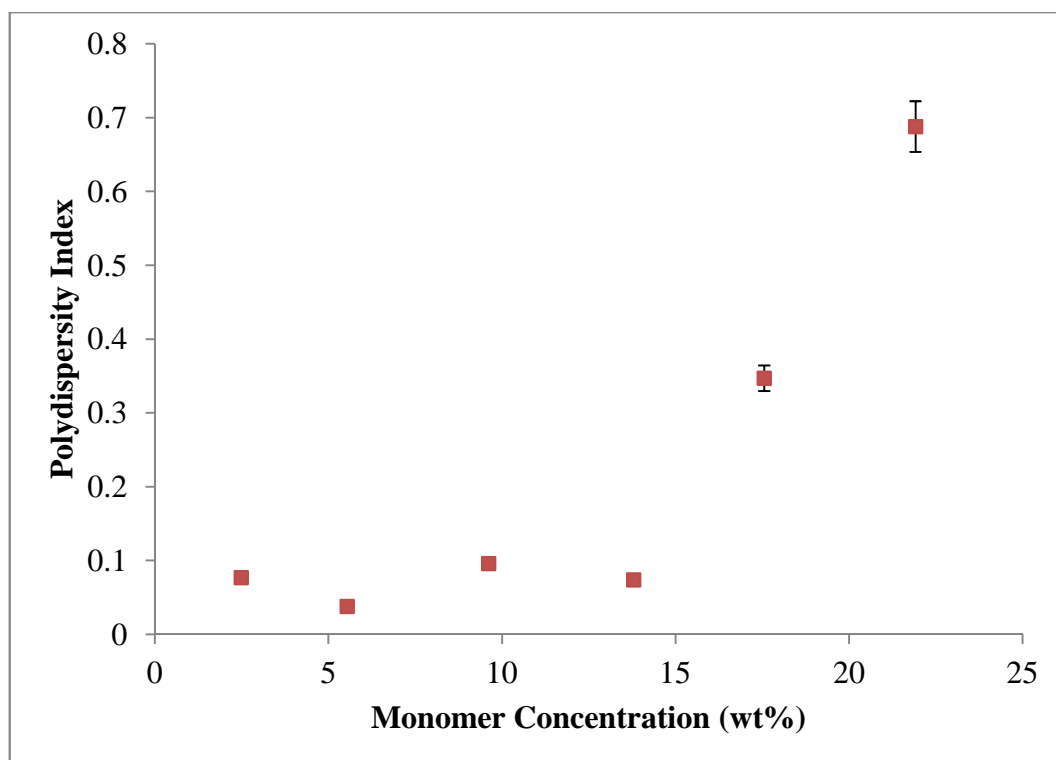


**Figure 4-2.** Effect of changing monomer concentration on polydispersity index. Error bars are included in all data.

Particle seeds are formed within the first few minutes of the initiation step during polymerisation and the resulting particles grow from these seeds. Polymerisation is considered complete once all of the monomer in the reaction vessel has been consumed, however in reality this is never truly the case as reactions rarely achieve 100% conversion of monomer to polymer. The reaction here was stopped after four hours, at this point the conversion rate was 83%. Using higher concentrations of monomer in the initial polymerisation mixture results in larger particles and the use of lower monomer concentrations in the initial polymerisation mixture results in smaller particles. It can therefore be said that the amount of monomer used in the polymerisation mixture has a direct effect on the size of polymer particles which can be produced.

Monomers tend to be a good solvent for their own polymer, so higher monomer concentrations also have the added effect of increasing the solvency of the growing polymer in the continuous phase. This retards the precipitation of the polymer meaning that the particle seeds created during the initiation process contain

polymers of longer chain length. The solvency changes throughout polymerisation as the monomer is converted to polymer and these growing polymer chains precipitate, this also has an effect on final particle size and polydispersity of those particles. The dramatic increase in polydispersity with increasing monomer concentration, which can be seen above 14wt% monomer concentration, is due to this changing solvency. The increase in polydispersity with increasing monomer concentrations can also be explained by the fact that size differences amongst particles become more obvious when the particles have larger diameters [63, 154-156].

All particles synthesized were spherical, ranging in size from 290nm to 2.9 $\mu$ m, and, up to 13.8wt% monomer concentration, were highly monodisperse.

The expected increase in measured particle size and polydispersity with increasing initial MMA concentration has been seen for this system. The particle samples produced were imaged using SEM and are shown in **Figures 4-3** and **4-4**.

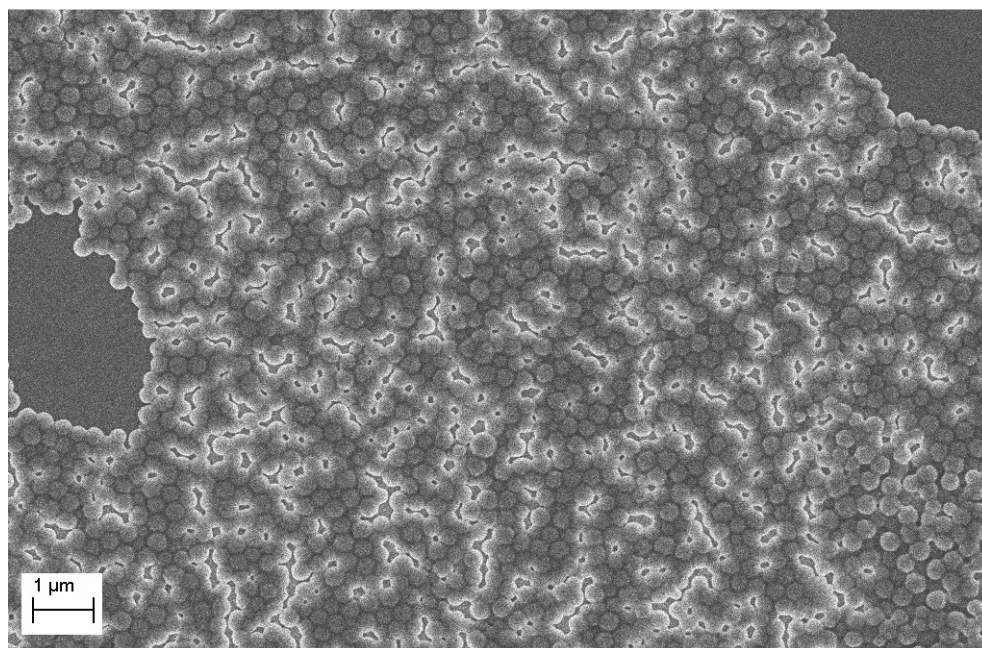


**Figure 4-3.** Scanning electron micrograph of smaller PMMA particles produced using a lower concentration (5.5 wt% w.r.t continuous) of monomer [490nm, PDI = 0.04]. N.B. Sizes quoted in the caption have been measured by DLS.

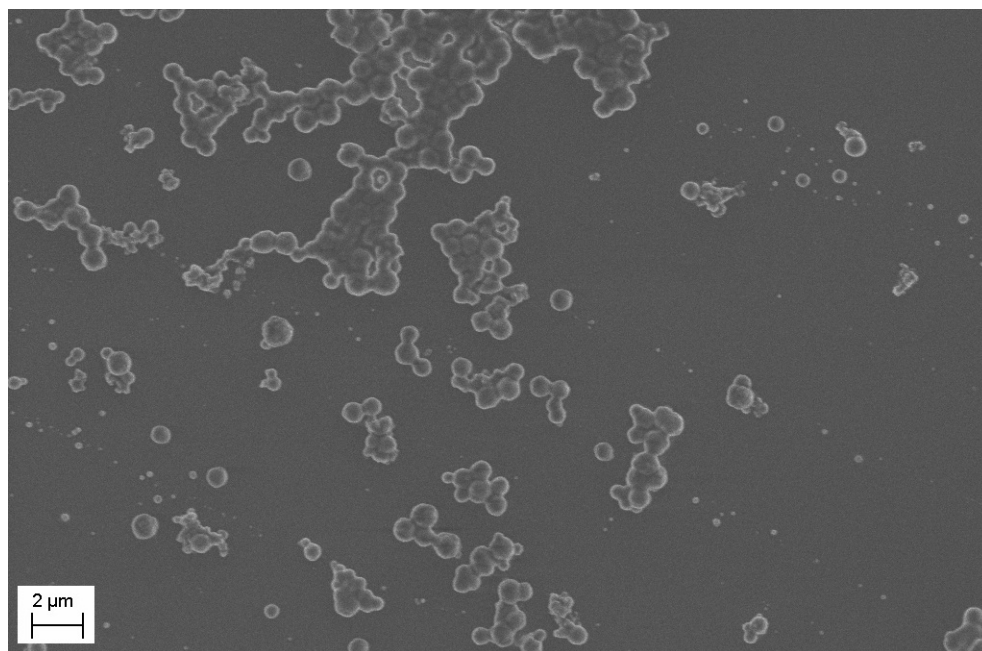


**Figure 4-4.** Scanning electron micrograph of larger, more polydisperse particles produced using a higher concentration (21.9 wt% w.r.t. continuous) of monomer [2900nm, PDI = 0.7]. N.B. Sizes quoted in the caption have been measured by DLS.

#### **4.2.2 Effect of changing stabiliser concentration**

The stabiliser used in the initial polymerisation mixture is a copolymer with a poly(dimethyl siloxane) chain at one end of the molecule and a methacrylate group at the other end. The methacrylate group is capable of incorporation by the growing PMMA chains within the particle itself, this causes the PDMS portion of the polymer to protrude from the surface of the polymer particle into the surrounding dodecane [91]. The PDMS chain sterically stabilises the particles preventing the aggregation of the polymer particles, which is a common problem when metallic nanoparticles, such as  $\text{TiO}_2$  or  $\text{WS}_2$ , are used as lubricant additives. The use of steric stabilisers rather than using electrostatic stabilisation will allow the particles which are created in dodecane to be transferred to other alkanes with no alteration to the particles themselves. The mechanism of action of steric stabilisation is shown in **Figure 4-5**.

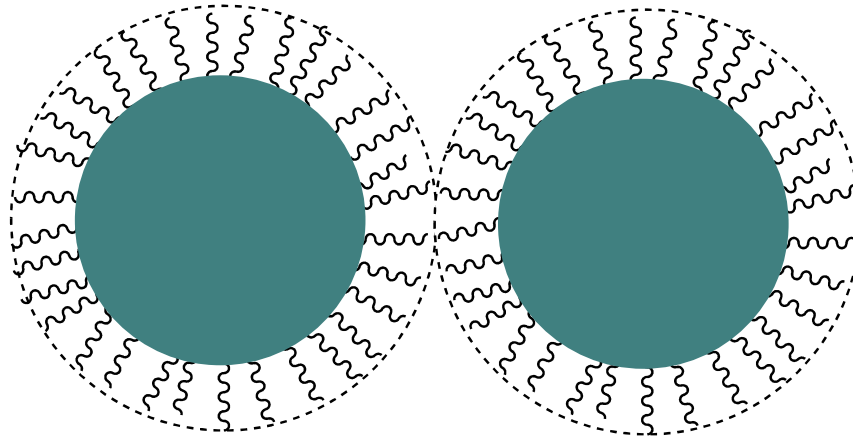


**Figure 4-5.** Steric repulsion between two particles caused by the polymeric chains protruding from the surface of the dispersed particles.

Particles were synthesised using initial polymerisation mixtures containing different amounts of stabiliser. The effect of this on the final particle size and polydispersity is shown in **Figure 4-6** and **Figure 4-7**.

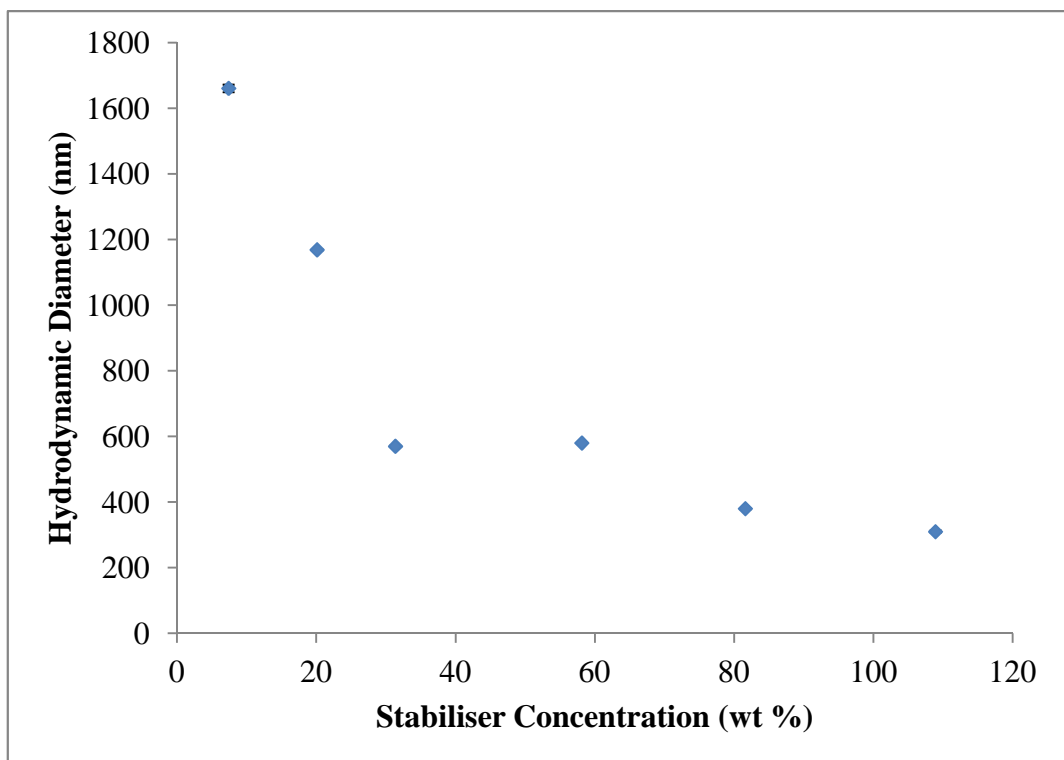


**Figure 4-6.** Effect of changing stabiliser concentration on particle size. Error bars are included in all data.

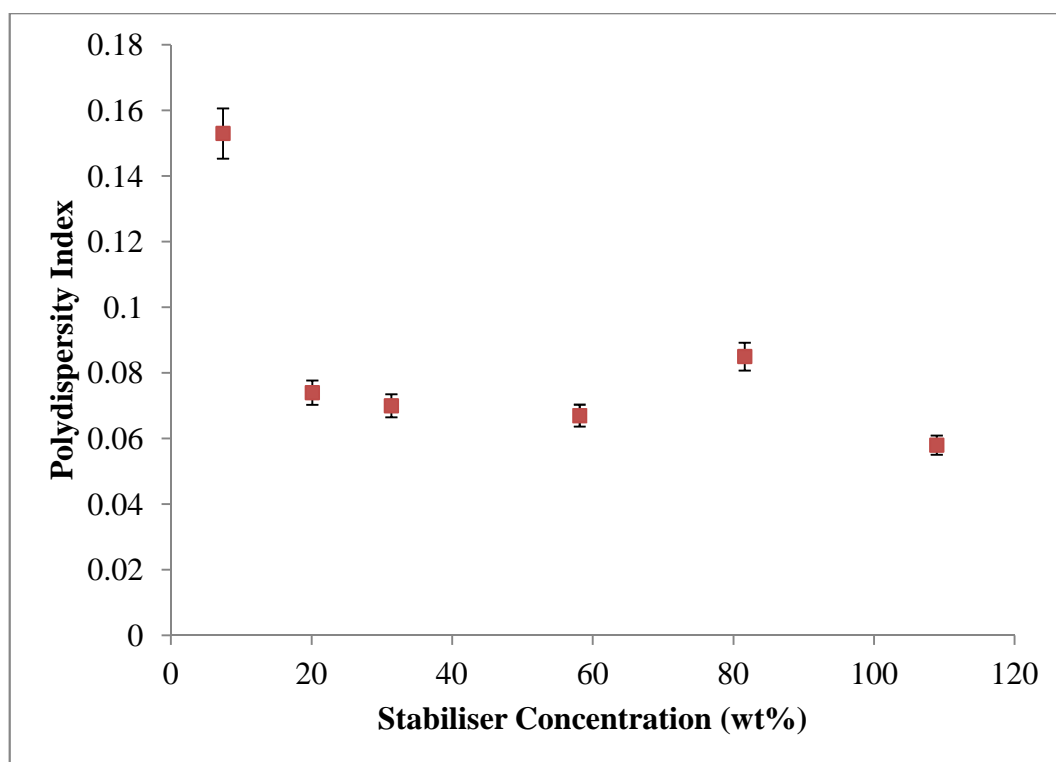


**Figure 4-7.** Effect of changing stabiliser concentration on polydispersity index.

Steric stabilisers of the type used here form a layer on the outer surface of the PMMA particles which physically separates particles providing colloidal stability, this prevents aggregation and flocculation of the particles. As the stabiliser is physically bound to the surface the amount used in the polymerisation will have a direct effect on the surface area of the particles and therefore on the size of the final particles produced.

The amount of PDMS-MA stabiliser used in polymerisation has a direct effect on the final size of the polymer particle produced. For a given volume of polymer, smaller particles will have a larger surface area than larger particles. Smaller particles therefore have a greater surface area which needs to be stabilised. If an inadequate amount of PDMS-MA is available to the growing particle seeds these seeds will aggregate, coming together to form larger particles. Aggregation is effected by PDMS-MA concentration, low amounts of stabiliser may lead to increased aggregation and an increase in the polydispersity of particle sizes seen in the final product [157, 158]. It should be noted that while the change in polydispersity here (**Figure 4-7**) may seem large it is in fact a much smaller variation than can be seen when changing the monomer concentration (**Figure 4-2**).

Examples of the particles produced during these synthesis are shown in **Figure 4-8**, **Figure 4-9** and **Figure 4-10**.

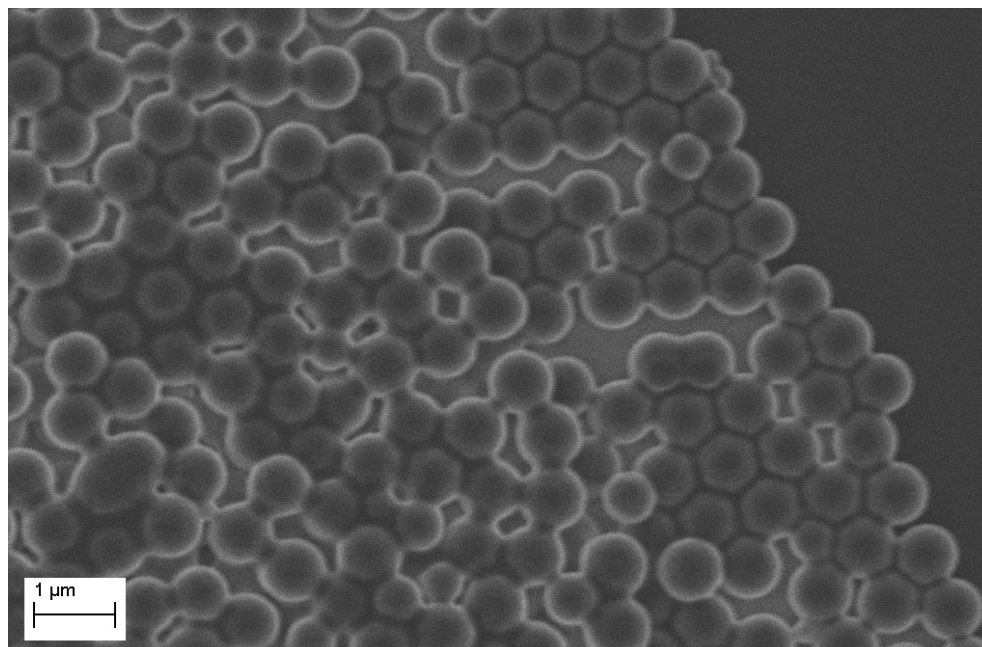


**Figure 4-8.** Scanning electron micrograph of larger PPMA particles produced using a lower concentration (7.4wt % w.r.t monomer) of stabiliser [1660nm, PDI = 0.15]. N.B. Sizes quoted in the caption have been measured by DLS.

More important than the concentration of stabiliser used is the ratio of stabiliser to monomer in the initial polymerisation system. If the amount of PDMS-MA stabiliser is kept constant and the concentration of MMA monomer is increased, the ratio between the surface area created during the initiation step and the total surface area that can be occupied by the stabiliser will decrease and this will once again lead to the possibility of inducing aggregation of particle seeds. There are currently very few studies in literature which explore the very large stabiliser to monomer ratio and so this will be investigated further in **Section 4.2.4**.

The expected decrease in measured particles size and polydispersity with increased PDMS-MA concentration has been seen in this system. All of the particles synthesized were spherical and the particle morphology was unaffected by altering the amount of stabiliser in the polymerisation mixture.

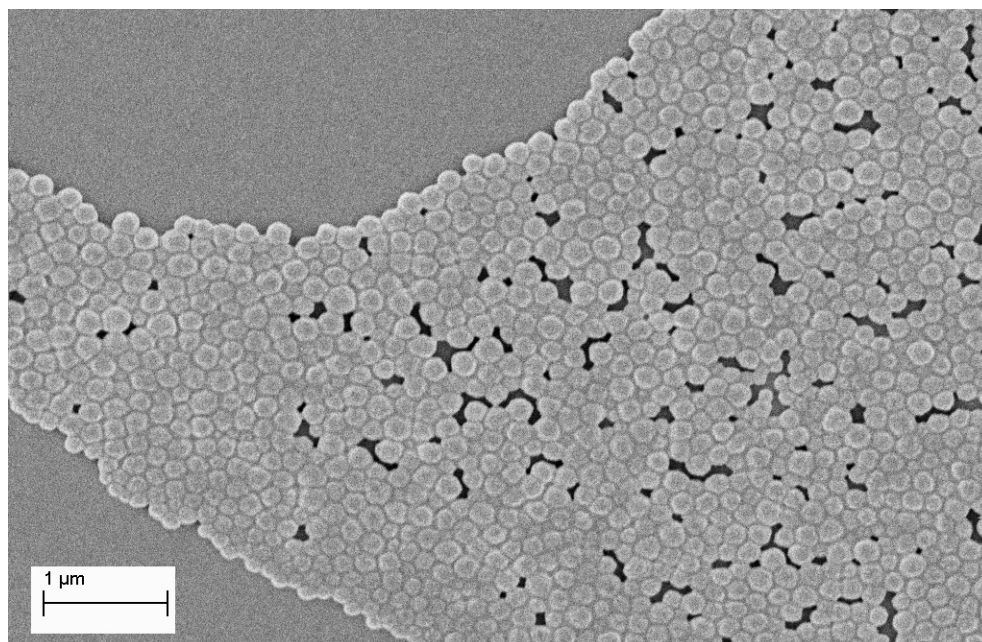


**Figure 4-9.** Scanning electron micrograph of smaller particles produced using a higher concentration (108.9wt % w.r.t. monomer) of stabiliser [310nm, PDI = 0.06]. N.B. Sizes quoted in the caption have been measured by DLS.

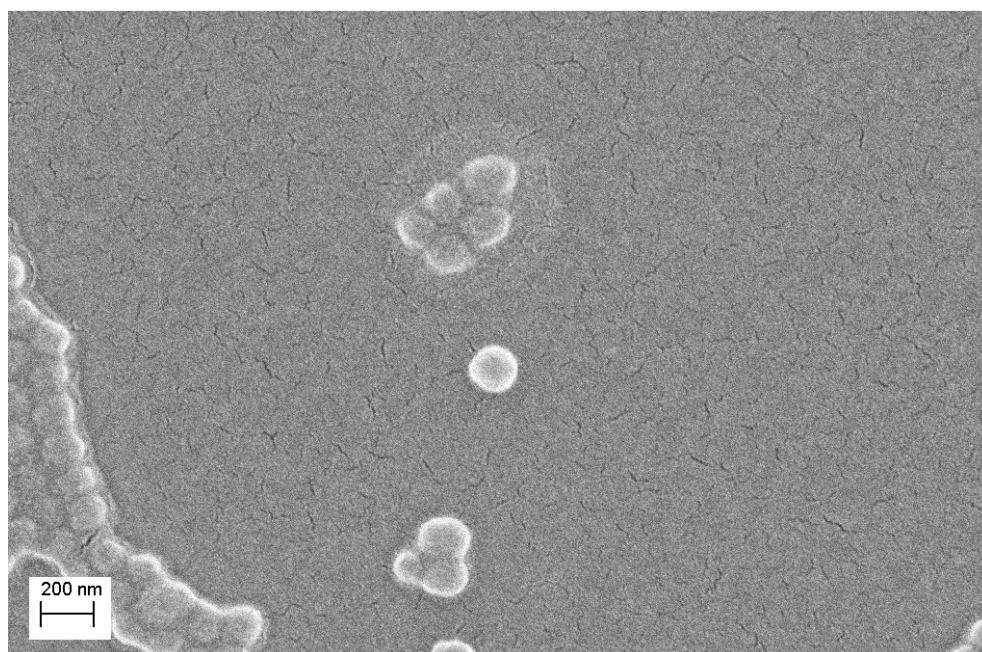


**Figure 4-10.** Scanning electron micrograph of smaller particles produced using a higher concentration (108.9wt % w.r.t. monomer) of stabiliser [310nm, PDI = 0.06]. N.B. Sizes quoted in the caption have been measured by DLS.

Jiang *et al.* [157] reported that the rate of the the dispersion polymerisation in in MMA when using a polymeric stabiliser was independent of the amount of stabiliser in the system and that kinetics were in fact greater affected by the number of free radicals, from the breakdown of AIBN, present in the system. The effect of AIBN on the final particle size is investigated in the next section.

#### 4.2.3 Effect of changing initiator concentration

The initiation step of the work presented here begins with the breakdown of AIBN which can occur by either thermal decomposition or photoinitiation. AIBN is an explosive compound which decomposes at temperatures above 65°C. The initiation process used in the work presented here is *via* the thermal decomposition of an AIBN molecule to generate two free radical containing 2-cyanoprop-2-yl species, shown below in **Figure 4-11**, which can then go on to react with the C=C portion of the MMA molecule, as detailed in **Section 2.3.1**.

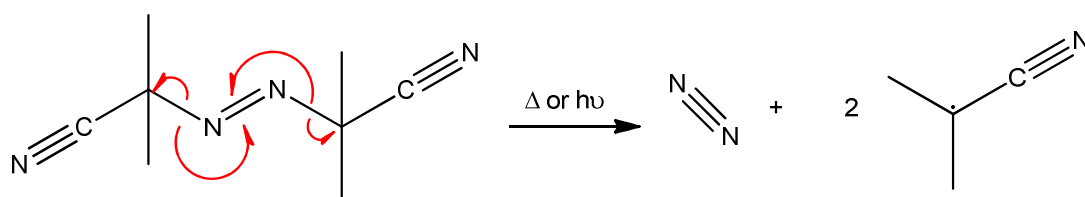


**Figure 4-11.** Generation of two free radical species by breakdown of AIBN.

One molecule of AIBN initiator breaks down to produce two free radical species, and thus using a higher concentration of AIBN will lead to the formation of more free radicals in the system. Free radicals produced can undergo either initiate the polymerisation of MMA or they be used in the termination of a growing PMMA chain. Moad *et al.* [159] monitored the final location of the AIBN species in the polymerisation of styrene by <sup>13</sup>C labelling of the AIBN. They reported that only 5% of the 2-cyanoprop-2-yl free radical species became involved in the termination of polymer chains in solution this therefore means the majority of free radicals produced go on to initiate the polymerisation in this case.

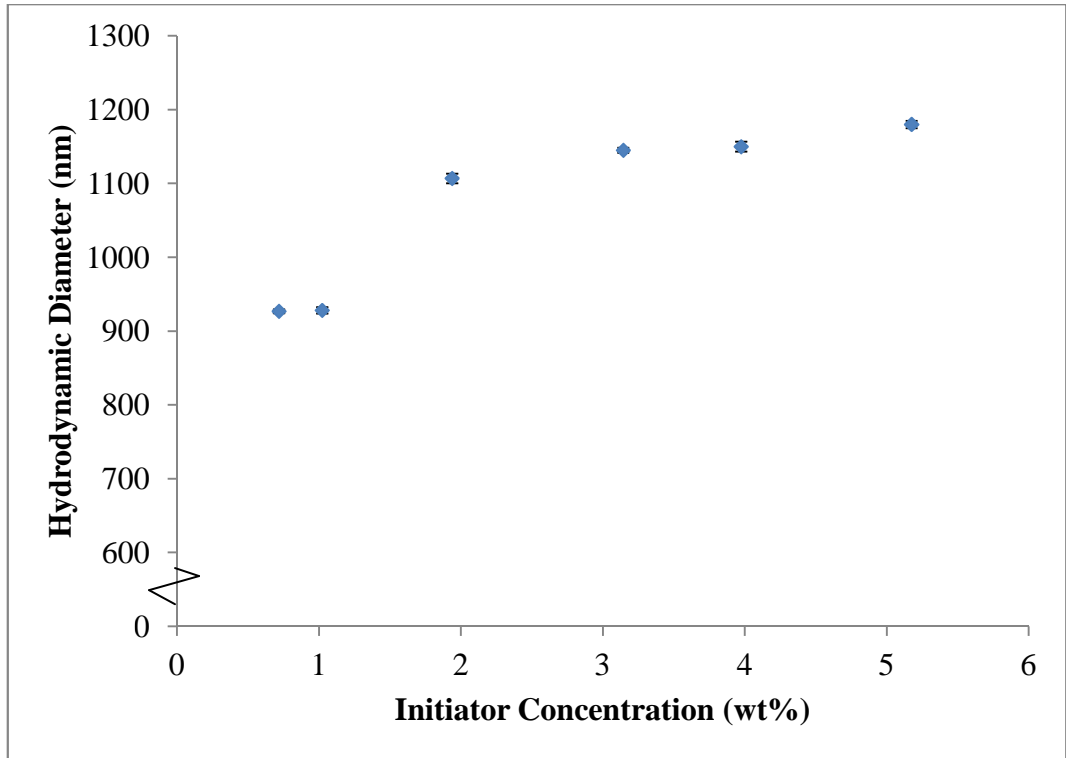


**Figure 4-12.** Effect of changing initiator concentration on particle size. Error bars are included in all data.

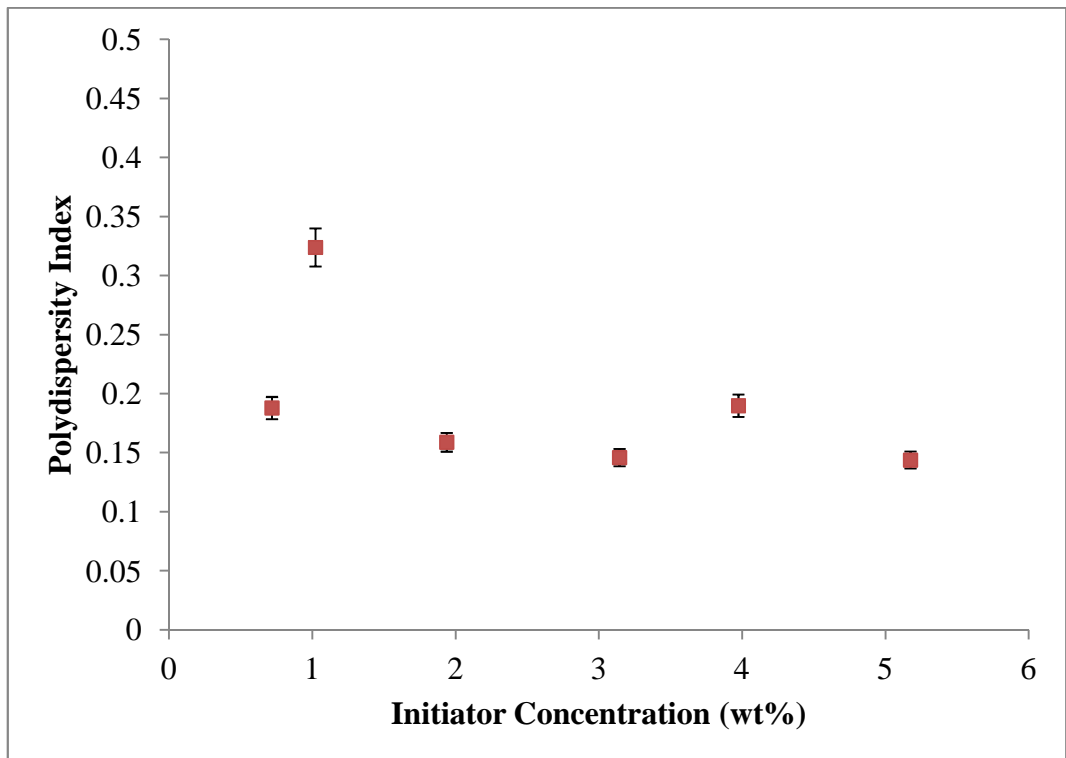


**Figure 4-13.** Effect of changing initiator concentration on polydispersity index. Error bars are included in all data.

Increasing the amount of AIBN increases the number of free radical species generated, having a greater number of free radicals in the reaction vessel will produce a greater number of initiation events. Each initiation event can facilitate the growth of a new polymer chain so, for a given amount of MMA monomer, increasing the amount of AIBN will increase the number of low molecular weight polymer chains in the polymerisation system. These chains will take a greater period of time to become large enough to precipitate which delays the formation of particle seeds. At the same time the stabiliser takes longer to become an active di-block species and the number of growing chains present in the continuous phase increases the likelihood of termination events occurring between the growing chains. The rate of aggregation under these conditions is greater than the rate of stabiliser adsorption so increasing the concentration of initiator produces larger particles containing low molecular weight polymer chains [160, 161]. The broader particle size distribution is due to the gradual change in solvency as the polymer chains become incorporated into the growing particles.

The molecular weight of the final polymer produced was measured by gel permeation chromatography (GPC), a form of HPLC where separation occurs due to particle size. Testing was carried out using a Perkin Elmer, HPLC system with a RI detector at 40°C. A 4 PL gel 300 x 7.5 mm GPC column was heated to 40°C was used and all testing was carried out in a THF mobile phase under a 1.0mL/min flow rate. High and low molecular weight polystyrene standards were used for comparison. Samples were taken using an autoinjector fitted with a 300µL injection loop. The testing was carried out by Emma Haywood at the Lubrizol test laboratories in Hazelwood, UK. A plot of the molecular weight of the polymer chains versus initiator concentration is presented in **Figure 4-14**.

The expected increase in measured particle size and polydispersity with increased AIBN concentration has been seen for this system. Morphology of the particles, as expected, is unaffected by the change in initiator concentration. Examples of particles produced during these synthesis are shown in **Figure 4-15** and **Figure 4-16**.

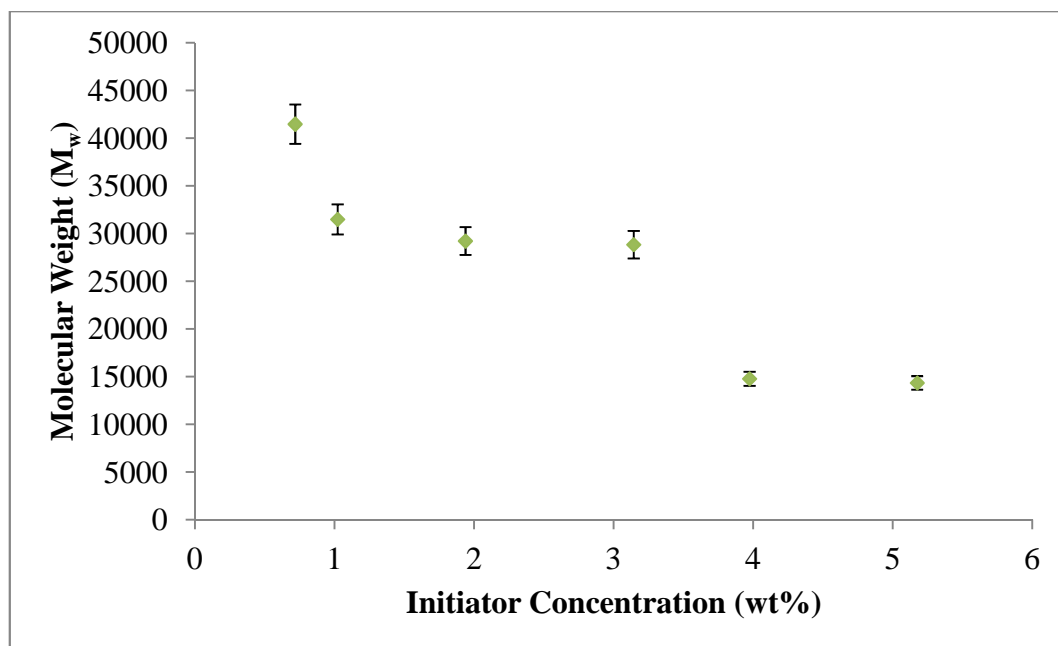


**Figure 4-14.** Effect of changing initiator concentration on polymer chain molecular weight.

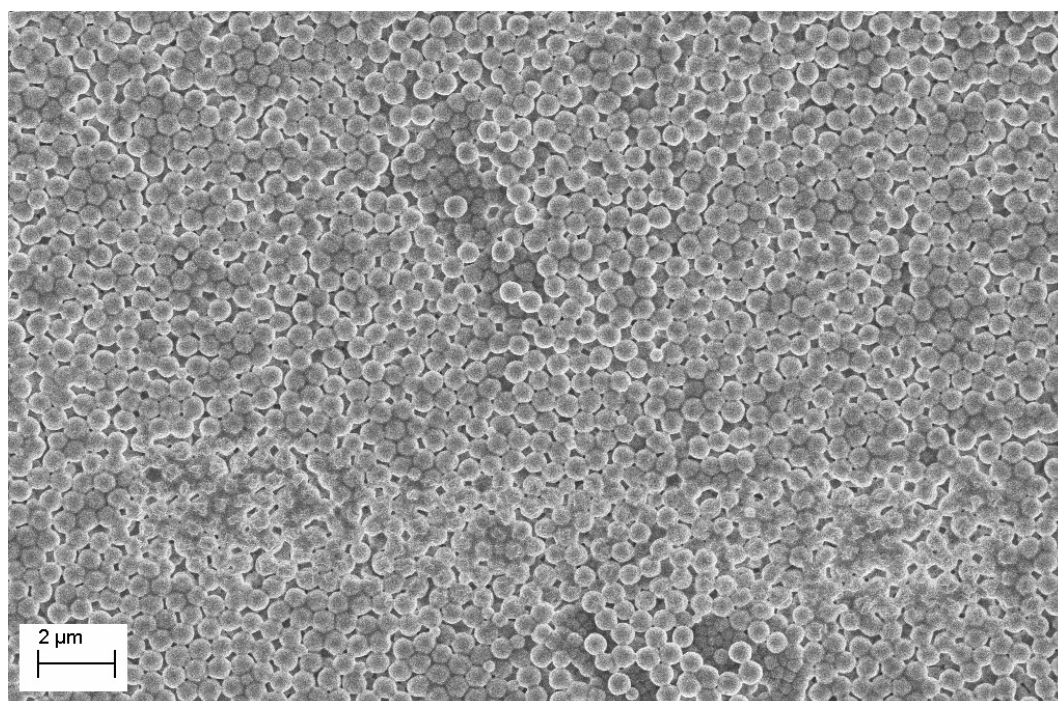


**Image 4-15.** Scanning electron micrograph of larger PMMA particles produced using a higher concentration (5.17wt % w.r.t monomer) of initiator [1180nm, PDI = 0.14]. N.B. Sizes quoted in the caption have been measured by DLS.

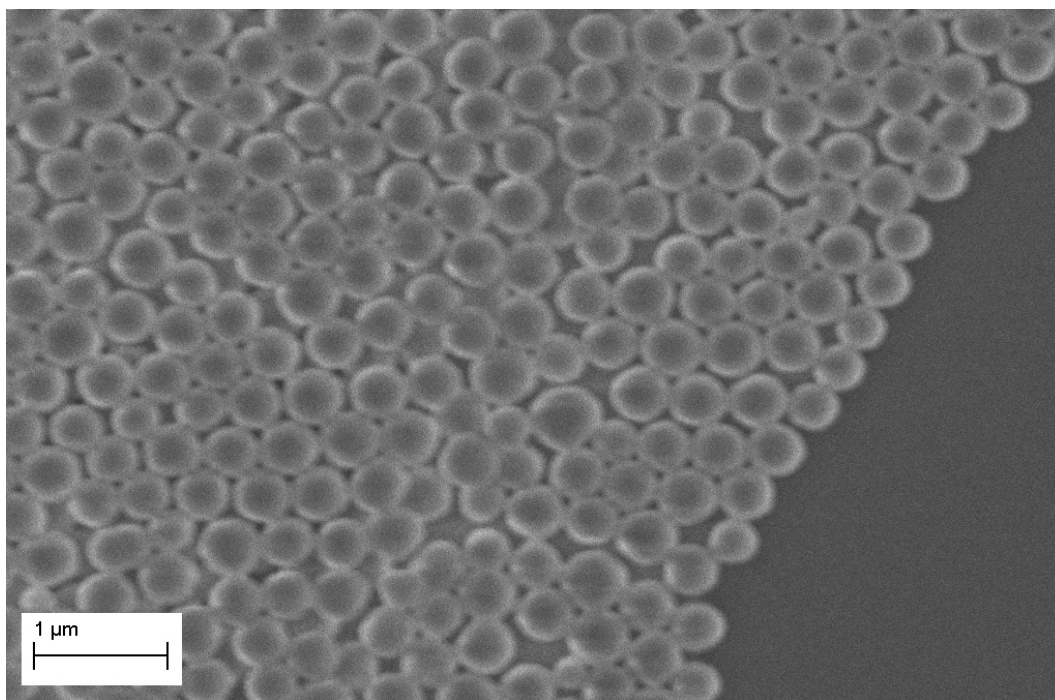


**Figure 4-16.** Scanning electron micrograph of smaller PMMA particles produced using a lower concentration (0.72wt % w.r.t. monomer) of initiator [930nm, PDI = 0.19]. N.B. Sizes quoted in the caption have been measured by DLS.

In the next section the effect of combining the above variables is investigated.

#### **4.2.4 Increasing the stabiliser concentration and decreasing monomer concentration**

Investigating the effect of sequentially changing a single polymerisation variable has found that smaller particles can be synthesised by:

- Decreasing monomer concentration,
- Increasing the stabiliser concentration or,
- Decreasing the initiator concentration.

As these factors were shown to all lead to a decrease in the final particle size produced some of these parameters were then combined with the aim of reducing particle size further and if possible approach a target of 100nm. In order to achieve this particle size the effect of decreasing monomer concentration while increasing

stabiliser concentration was investigated. Initiator concentration showed only a slight effect on particle size and therefore was not tested incorporated into this testing.

**Table 4-2.** Changing monomer concentration, keeping ratios unchanged.

Monomer concentration (wt %)*	Stabiliser concentration (wt %)†	Initiator concentration (wt %)†	Hydrodynamic diameter (nm)	Polydispersity Index
7.2	322.6	5.7	180	0.04
5.0	322.3	5.7	130	0.10
2.5	321.5	5.8	150	0.11

\* wt % w.r.t. continuous phase

† wt % w.r.t. monomer

The effect of changing the monomer concentration while keeping the same ratios of monomer to stabiliser and monomer to initiator have been looked at. Having a high concentration of stabiliser increases the stability of particles with larger surface areas. For a given amount of monomer, increasing the amount of PDMS-MA stabiliser in the initial polymerisation mixture produces smaller final particles. This effect has been pushed further by limiting the amount of monomer in the mixture producing particles approaching 100nm in size. At this size particles will be barely visible in an oil therefore making any fully formulated engine oil containing those particles more desirable to customers.

An important consideration when choosing the polymerisation system in this project and for choosing to synthesise particles *via* dispersion polymerisation was the ability to scale up production of particles for use in industrial applications. With this in mind testing was carried out which increased the amount of monomer in the initial polymerisation mixture while keeping the monomer to stabiliser ratio constant. This allowed for a greater yield of particles to be synthesised while maintaining the desired low particle size. Particles produced in this testing are shown in the following figures.

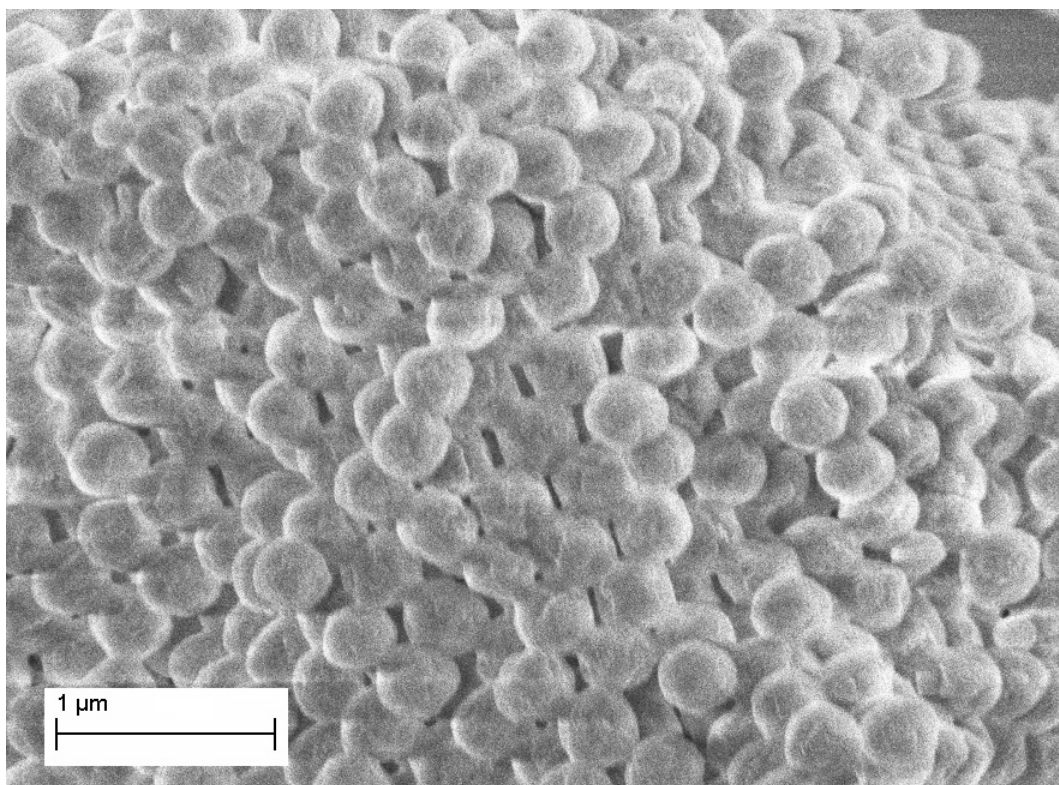


**Image 4-17.** Scanning electron micrographs of PMMA particles measuring [180nm, PDI = 0.04]. N.B. Sizes quoted in the caption have been measured by DLS.

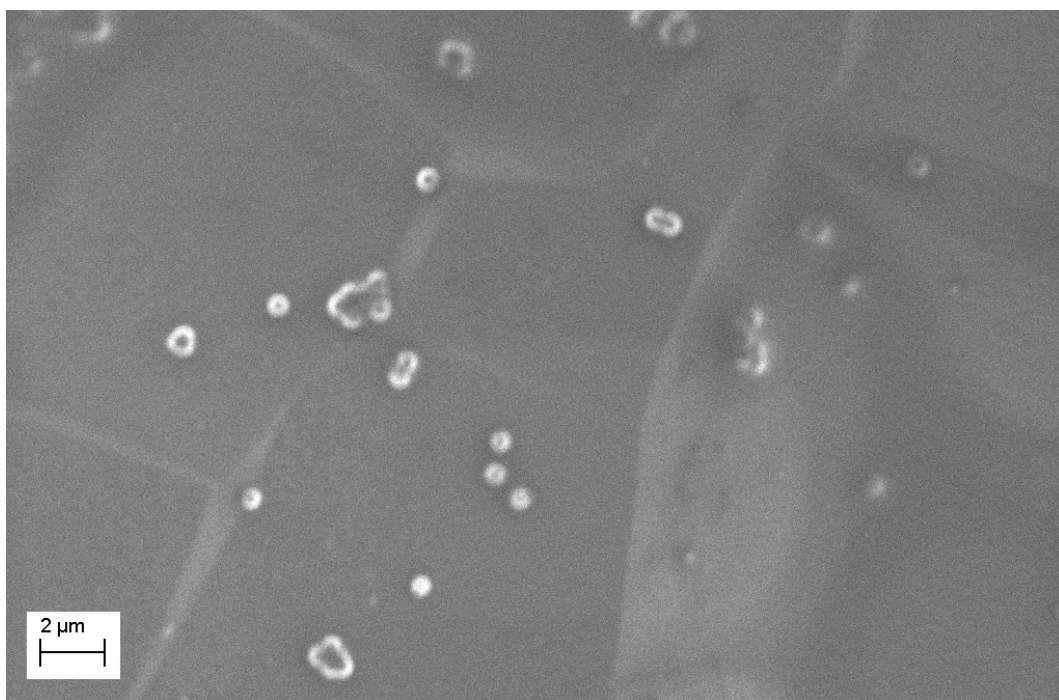


**Figure 4-18.** Scanning electron micrographs of PMMA particles measuring [150nm, PDI = 0.11]. N.B. Sizes quoted in the caption have been measured by DLS.

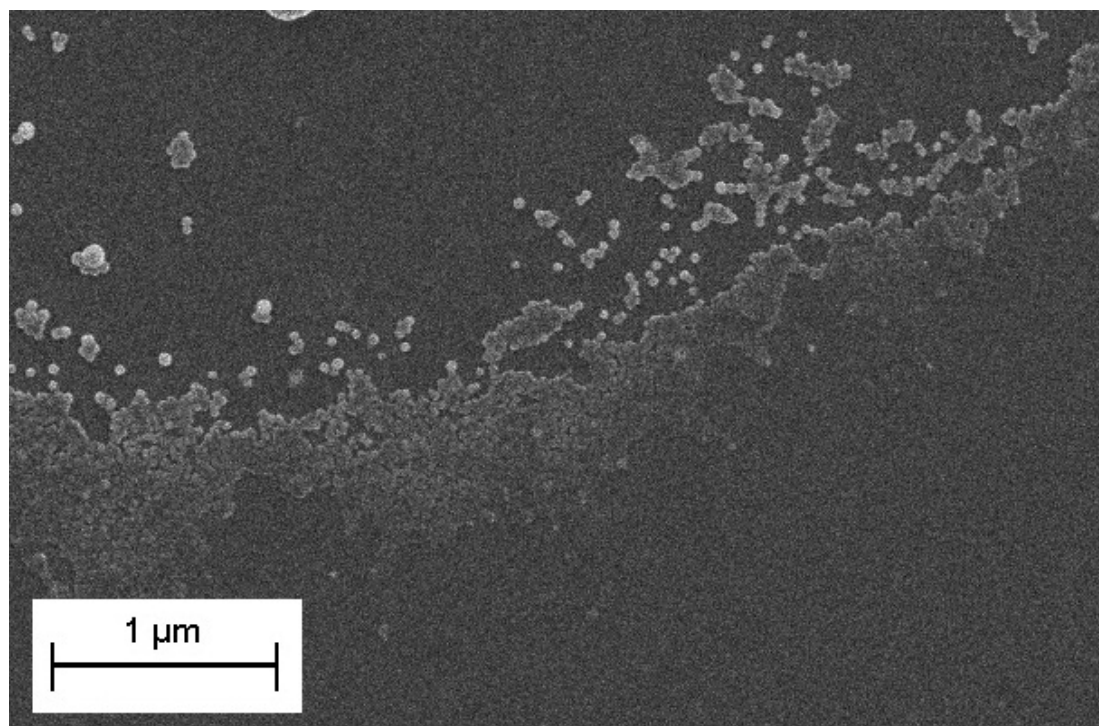


**Figure 4-19.** Scanning electron micrographs of the smallest PMMA particles produced so far [130nm, PDI = 0.10]. N.B. Sizes quoted in the caption have been measured by DLS

### **4.3 Synthesis of PMMA particles with a methanol core.**

Synthesis of the PMMA particles with a methanol core was carried out as detailed in **Section 4.2** with the addition of a co-solvent in the initial polymerisation mixture. This co-solvent was required to be immiscible with the continuous phase and once primary particles form this co-solvent is included within the particles where it resides preferentially to the bulk. Polymerisation continues as before with the final product being polymer particles with the co-solvent encapsulated. As before, unreacted monomer and excess stabiliser were removed via the centrifugation and redispersion steps. The details of this process are explained further in **Chapter 5**.

When using this method of encapsulation to incorporate the FM into the liquid core the following criteria must be met:

1. Co-solvent and continuous phase must be immiscible.
2. The FM must be soluble in the co-solvent but not soluble in the continuous phase.

This ensures that there is minimal mixing between the co-solvent and the continuous phase and that all of the FM is encapsulated along with the co-solvent.

Solubility testing was carried out establishing that FM is highly soluble in methanol but has limited solubility in dodecane, these are two solvents which are immiscible. For this reason dodecane continuous phase and methanol co-solvent were chosen for the encapsulation process used in the work presented here.

Particles with a liquid core- polymer shell morphology were prepared by dispersion polymerisation of MMA where dodecane was used as a continuous phase and methanol was used as a co-solvent at various ratios. Particles prepared were highly monodisperse and were controllably synthesised.

#### **4.3.1 Effect of changing the ratio of continuous phase:co-solvent**

A co-solvent is used in order to produce a core shell particle with a liquid core, the morphology is which will be discussed further in **Chapter 5**. This co-solvent is immiscible with the continuous phase and eventually becomes encapsulated in the final polymer particle. Provided all co-solvent is encapsulated, changing the amount of co-solvent used should change the size of the microcapsules produced. This also alters the thickness of the particle wall, which can have further effects on the rate of release of the FM through the particle shell. This release rate is examined in **Chapter 5**. It is envisaged that the greater the volume of co-solvent used the thinner the wall of the subsequent particle.

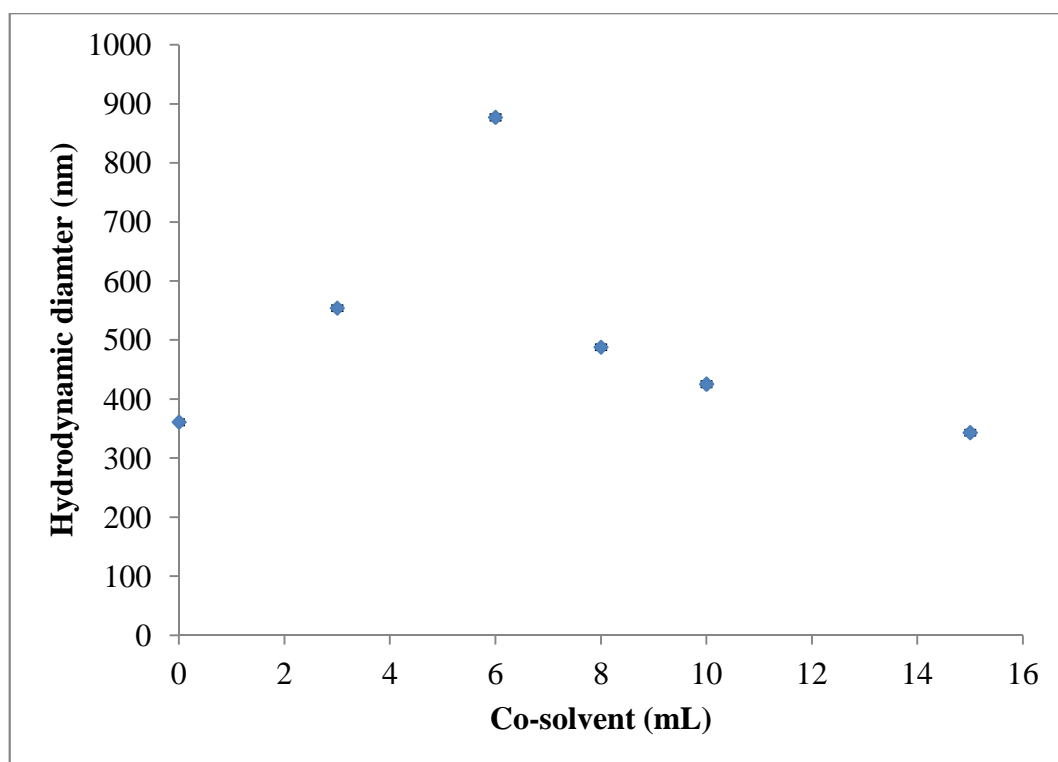


**Figure 4-20.** Effect of changing the volume of co-solvent (total volume was kept constant) on particle size. Error bars are included in all data.

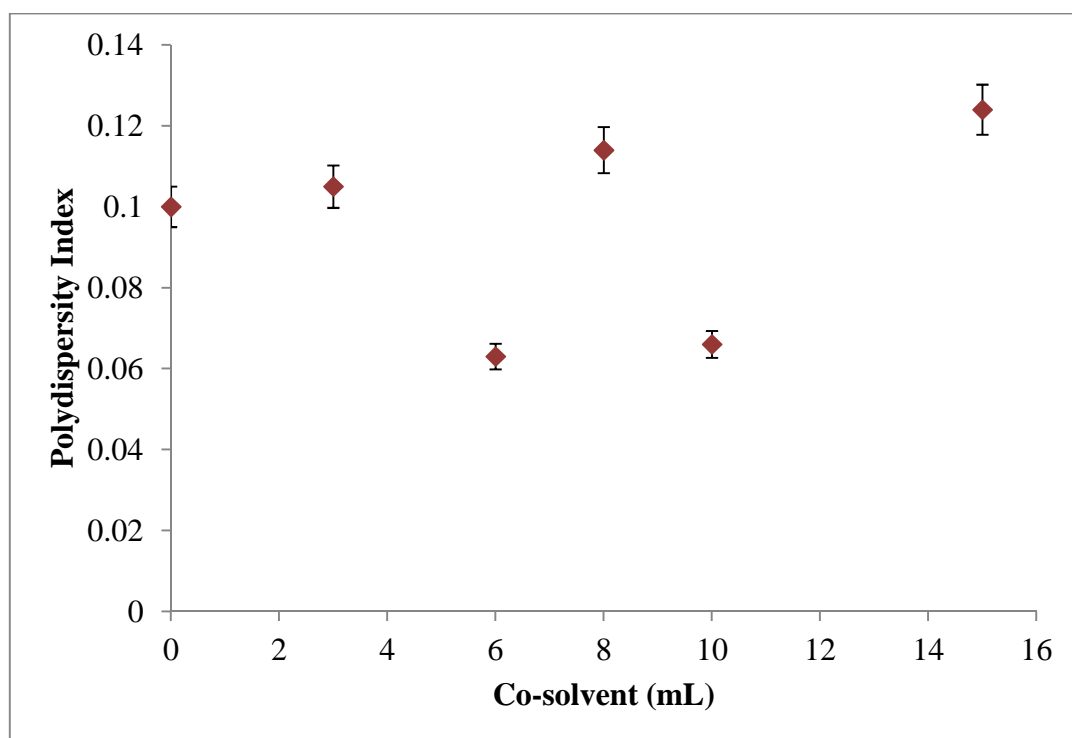


**Figure 4-21.** Effect of changing the volume of co-solvent (total volume was kept constant) on polydispersity index. Error bars are included in all data.

This expected trend continued up to a 9:1 ratio of solvent: co-solvent. Particles produced in this system, and which follow this trend, measure 877nm in diameter, large enough to be used in the TE77 comparison testing. TEM testing showed that the calculated theoretical wall thickness agreed with the measured wall thickness. The theoretical wall thickness was calculated from the volumes of MMA and methanol added at the start of the synthesis and the measured diameter (by DLS) of the particles produced. The working for this calculation is found in **Appendix B**. An example of the largest particles produced here is shown below in **Figure 4-22** where the darker methanol core of the particle can be seen surrounded by the PMMA shell.

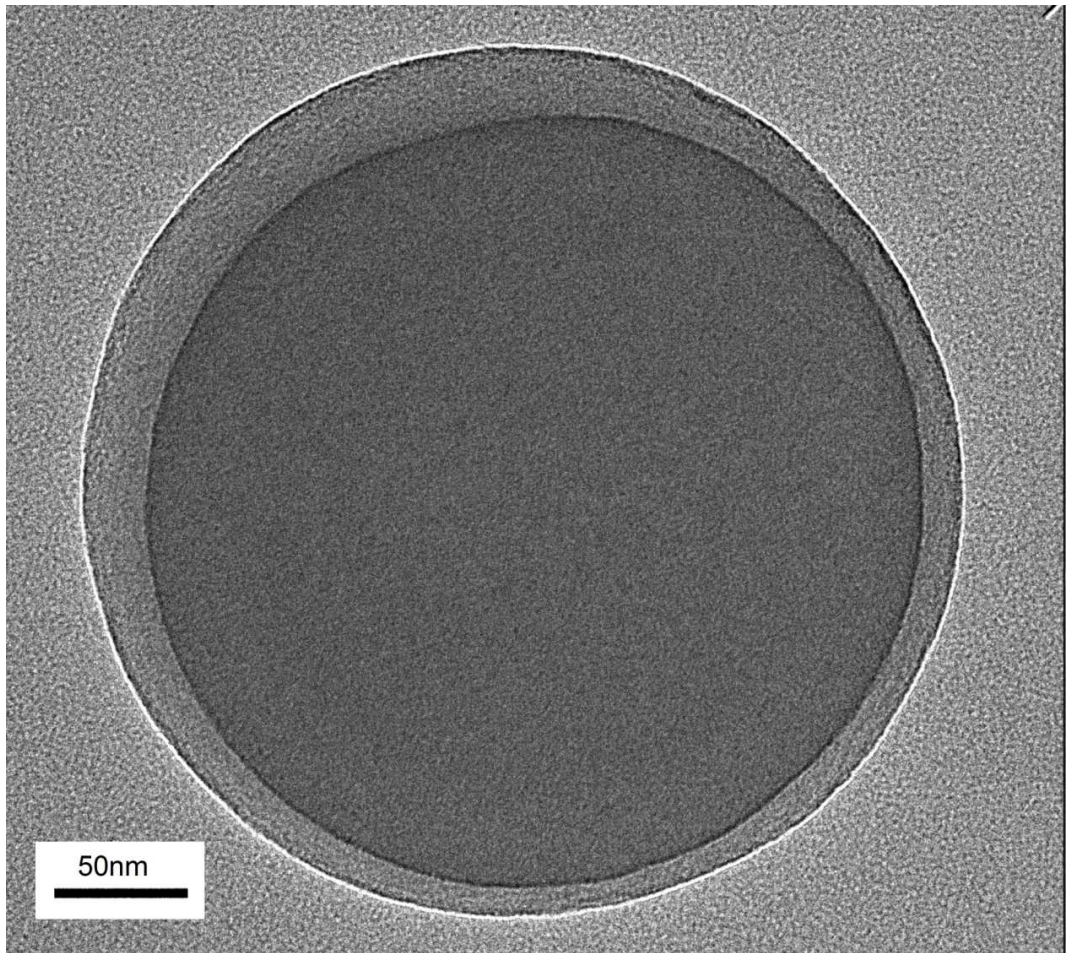


**Figure 4-22.** Cryo-transmission electron micrograph of a PMMA particle produced using a 5:1 continuous phase:co-solvent ratio [430nm, PdI = 0.07].

Above this ratio particle size decreases down towards 340nm while the polydispersity of the particles produced remains constant measuring around 0.1, suggesting that the particle morphology has changed and solid particles are being produced. This may be due to the particle walls becoming too thin to support this structure; or possibly due to a change in solvency in the system with the addition of methanol. In these particles not all co-solvent is encapsulated within the PMMA particles produced. The reason for the reduction in particle size above a continuous phase:co-solvent ratio of 6.5:1 was not examined here as it was outside the scope of the project however could be investigated in future work. In this case these particles were not chosen for testing by TE77 as the presence of methanol in the system could be identified but not quantified. This would further lead to quantification problems in particles which were synthesized using FM in the initial polymerisation mixture.

#### **4.4. Summary**

This study shows that it is possible to produce monodisperse, solid PMMA particles in the size range 130nm to 2.8 $\mu$ m. This has been achieved by systematically changing the concentrations of the various components used, while keeping other variables constant, during the polymerisation. The greatest amount of control over final particle size was seen when altering the amount of monomer used. Lower monomer concentrations can be used to limit the growth of the particles by starving the growing particle seeds of additional monomer needed to continue growing. These studies also showed a significant influence of the concentration of stabiliser used, which changed the amount of surface area that could be stabilised during the initiation process. For a given monomer concentration the addition of larger amounts of stabiliser enables the synthesis of a greater number of particles all of which have smaller particle diameters than those created using lower concentrations of stabiliser. When these two parameters were altered at the same time it was possible to reduce particle size down to 134nm, close to the size limits set by Lubrizol. Particles at this size become more difficult to be seen by the human eye and therefore will aid the work of formulators aiming to incorporate particles into a final engine oil without changing the appearance of the oil from those

currently available which may adversely affect customers confidence in the product. All of the particles shown here can be reproduced easily and reliably.

It has been shown that the yield of particles synthesized can be increased by increasing the concentration of monomer and keeping the monomer to stabiliser ratio at a constant. Producing particles *via* a dispersion polymerisation means this system will have the ability to be scaled up with ease and therefore also have the potential to produce a large volume of particles in a single synthesis which would clearly be beneficial when producing these particles in industry.

It is also possible to control particle size by changing the ratio of continuous phase to co-solvent however this has some limitations due to wall thickness. While this was not investigated here, as particles of the desired size for tribological testing were produced before this point, this could be an area of further investigation to determine why particle size doesn't continue to grow above a 9:1 solvent to co-solvent ratio.

## Chapter 5. Investigation into the release rate of friction modifier from intact core shell particles

### 5.1 Introduction

In order for the particles produced in this project to act as a reservoir for friction modifier into a fully formulated oil, the particles should remain unbroken and slowly leach out FM over the lifetime of the oil. This process is schematically shown in **Figure 5-1**.

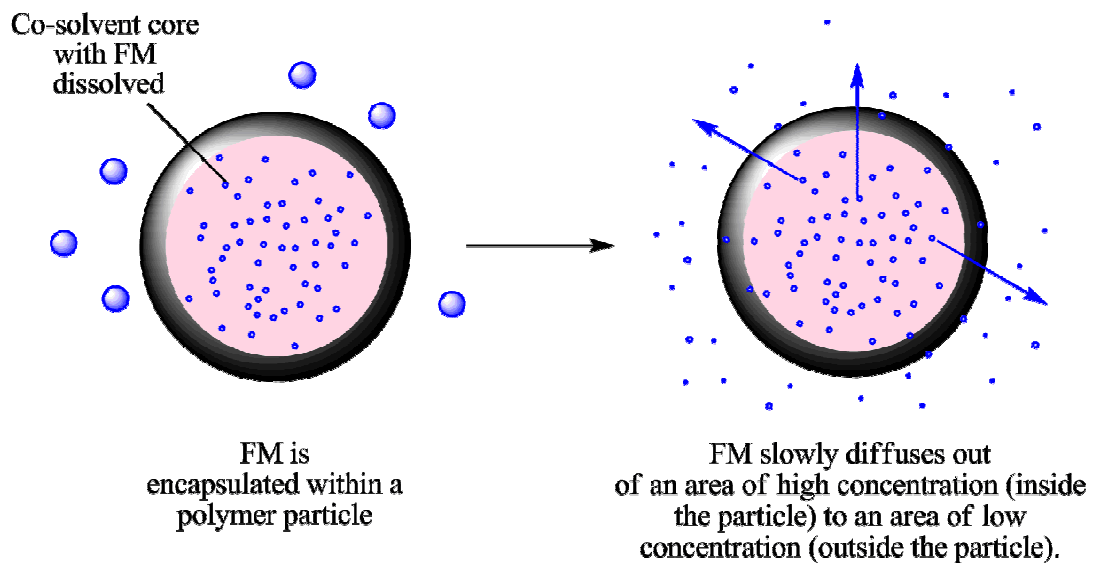


**Figure 5-1.** Proposal for FM release from unbroken particles.

In the majority of cases, slow release of an active ingredient from a particle or capsule would occur at a rate driven by a range of factors including porosity of the capsule shell, solubility of the active in the continuous phase and the concentration difference between the core or the capsules and the continuous phase.

The typical relationship that describes such a process is referred to by Fick's Laws of diffusion [162] and can be expressed as follows:

$$\frac{dC}{dt} = A \times H \times D \frac{(C_{in} - C_{ext})}{d}$$

where

C is the concentration of the active

A is the exposed surface area of the shell

H is the partition coefficient

D is the diffusion coefficient

d is the thickness of the shell

In this case, the surface area exposed for release of the active, the diffusion coefficient and the shell thickness are likely to remain constant throughout the procedure. Thus the most likely source of slow release will be the difference in concentration of the active between the core of the particle and the outside continuous phase. As FM is consumed from the continuous phase by the action of the tribological contact the difference in concentration between the continuous phase and the particle core will increase thus driving an increase in the release rate of the FM.

To achieve a polymer particle with a liquid core, in which the FM is encapsulated, a co-solvent is added to the initial polymerisation mixture (**Figure 2-23**). This co-solvent is incorporated within the particle core as it preferentially wets the precipitating polymer and is insoluble in the continuous phase [21, 133, 163].

To encapsulate the FM in the core of a particle the following criteria must be met:

- Continuous phase and co-solvent must be immiscible.
- The FM should be soluble in the co-solvent but not in the continuous phase.

This should ensure that all co-solvent is encapsulated within the polymer particles and all FM will be dissolved in that co-solvent rather than in the continuous phase.

## 5.2 Synthesis of PMMA particles containing encapsulated FM for release rate testing.

To produce particles with a PMMA shell and methanol core the initial polymerisation mixture is changed slightly from that used to produce solid particles. The components of this mixture are detailed in **Table 5-1**.

**Table 5-1.** Initial polymerisation mixture.

Monomer	Methyl methacrylate (MMA)
Initiator	Azobisisobutyronitrile (AIBN)
Stabiliser	Methacrylate terminated poly(dimethyl siloxane) (PDMS-MA)
Continuous phase	Dodecane
Co-solvent	Methanol
Additive	Stearamide (FM)

Liquid core - polymer shell particles loaded with FM were prepared by dispersion polymerisation of MMA where dodecane was used as the continuous phase and methanol was used as the co-solvent in a 9:1 ratio. Synthesis was carried out as detailed in **Chapter 4** with the FM initially dissolved in the methanol co-solvent used in the polymerisation process. As described previously, unreacted monomer and excess stabiliser were removed *via* a centrifugation and redispersion step, the dodecane removed in this process was then tested as the first cycle in the following release study.

The samples used contained a total of 3.1wt% FM, encapsulated within the particle core, in the system. Particles were highly monodisperse and were

controllably synthesised to the size of 760 - 890nm. This particle size was chosen as they were neither the largest ( $\sim 2.6\mu\text{m}$ , not presented here) or the smallest ( $\sim 340\text{nm}$ , **Section 4.3.1**) and were comparable to the particles to be used in the TE77 tribological testing (detailed in **Chapter 6**).

### 5.3 Determination of particle morphology

The structure of the particles produced was analysed by cryo-TEM. In this project samples to be tested were added to holey carbon grid, stained using 1% uranyl acetate and excess liquid was then wicked away. The holey carbon grids were S173-2 Quantifoil® R2/2, 300 mesh Cu supplied by Agar Scientific. These grids have a regular hole structure which can be seen in **Figure 5-2**. This structure allows for better wetting of the surface which can be hydrophilic or hydrophobic dependent on the pre-treatment of the grids.

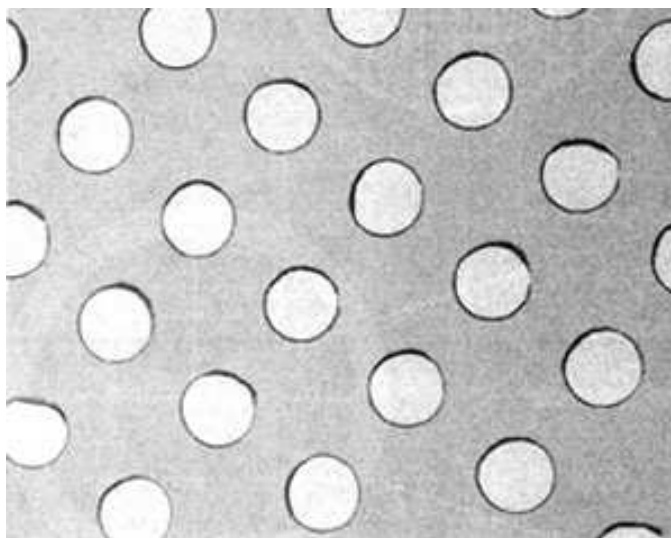


**Figure 5-2.** The regular hole structure of the Quantifoil® R2/2 holey carbon grids.

When imaged the majority of the particles added could be found within the holes of the grid. As the system operates under a vacuum samples could not contain liquid when they are analysed; this prevents a problem when imaging samples with a liquid core. To overcome this and to image the internal structure of the particles which have a liquid core (synthesis detailed in **Chapter 4**) samples can either be

fixed within a resin or can be frozen using liquid nitrogen. When using a resin the liquid core of the particles is first replaced with a resin and then the particles are suspended in that same resin. The resin containing the particles is then thinly sliced, allowing that samples to be viewed under the TEM producing a cross section of those particles. In cryo-TEM particles are flash frozen preventing the liquid in the sample from forming large crystals which may distort the observed particle shape. This allowed for the observation of the samples hydrated in their nature state and not distorted by any drying processes as is possible with imaging techniques such as SEM. This is a large advantage in biological systems where this TEM method of imaging is commonly used [141].

Dodecane containing PMMA particles with a methanol core (without FM) were analysed by cryo-TEM as detailed above. The image in **Figure 5-3** shows a particle with a PMMA shell – methanol core morphology.

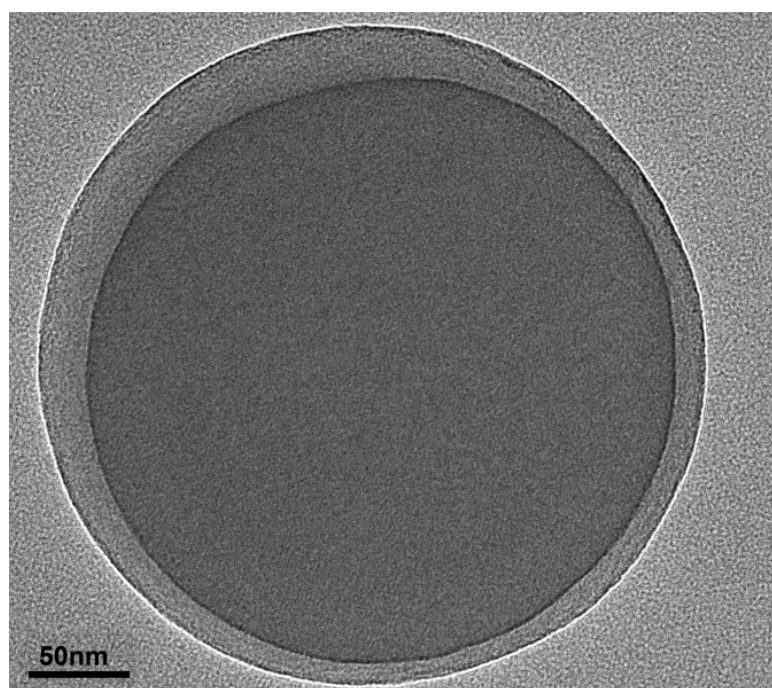
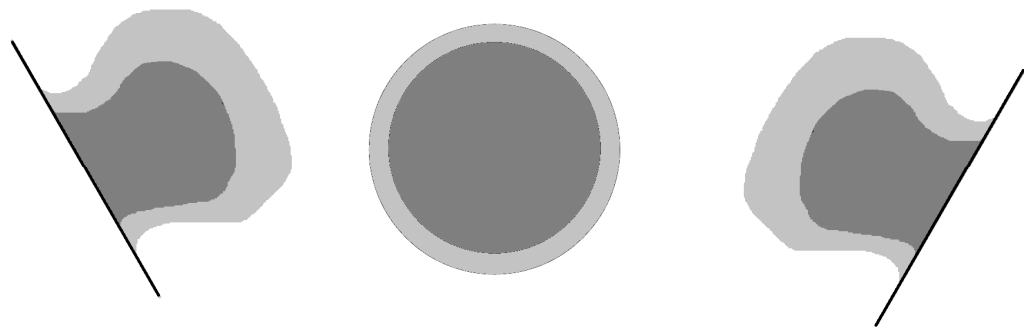


**Figure 5-3.** Cryo-transmission electron micrograph of a PMMA particle with a methanol liquid core.

When carrying out TEM it is important to understand what is being seen may actually be an optical illusion [164]. **Figure 5-3** may be showing a core-shell structure where the darker centre is the methanol core and the surrounding outline

being the PMMA shell or the dark centre may be caused by the settling of the particle onto the carbon grid itself. To overcome this possibility, particles were viewed at a  $0^\circ$  sample tilt and  $25^\circ$  tilt. A  $25^\circ$  tilt angle was chosen due to the thickness of the ice obscuring the images at higher tilt angles. If the darker area in the centre of the particle is due to the particle coming into contact with the surface of the film then tilting the sample would result in the darker area appearing to move to the side of the particle. If the particle has a true core-shell morphology the darker region would remain in the centre of the particle once the sample is tilted. This is shown in **Figure 5-4**.

If darker areas are due to contact of the particle on the holey carbon film:

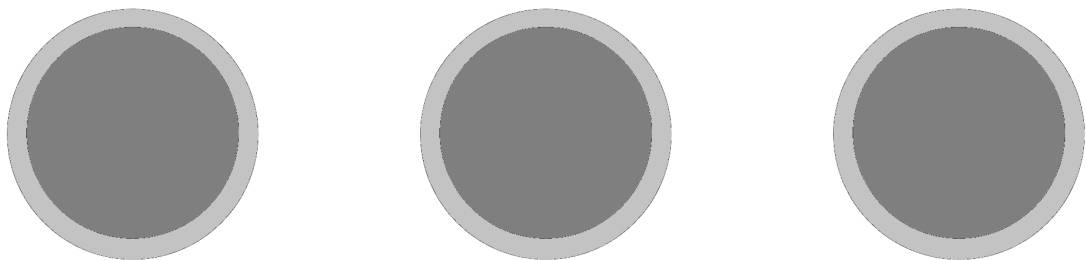


25 degree tilt

0 degree tilt

25 degree tilt

If darker areas are due to a true core-shell morphology:



25 degree tilt

0 degree tilt

25 degree tilt

**Figure 5-4.** Movement of the darker region of the particle imaged at different tilt angles. If the darker region is due to the contact of the particle at the surface it will appear to move within the particle when tilted. If the darker region is due to a true core-shell morphology it will stay central to the particle when tilted.

It is worth noting that the image seen in **Figure 5-3** appears much clearer as here the particle was not obscured by a thick droplet of frozen dodecane. In the preparation of the sample in **Figure 5-3** excess dodecane was wicked away to allow clear imaging of the particles. However this means that the possibility of the particles settling on the grid surface had now arisen but this was overcome by tilting the surfaces. The lower amount of dodecane present means that this image is much more suitable for measuring particle shell thickness than those shown below. Images were taken at a  $0^\circ$  tilt angle (**Figure 5-5**) and at  $25^\circ$  tilt angle (**Figure 5-6**). Analysing the sample at different tilt angles confirmed that the structure was that of a polymer shell with a liquid core. The images here appear less clear as these particles are suspended within a droplet of frozen dodecane. The effect of this droplet affects the clarity of the image however the polymer shell, here seen as the darker region, is clearly visible with the lighter area in the middle being the methanol core of the particle. The polymer shell allows fewer electrons to pass through the sample and therefore appears darker in the final image. Which areas appear darker can also be an effect of the staining method used which may explain the difference in darkness between the core and the shell in the image above to those below. Due to the thickness of the ice in the images below they are suitable for the determination of particle morphology but not for use in the measurement of shell thickness.

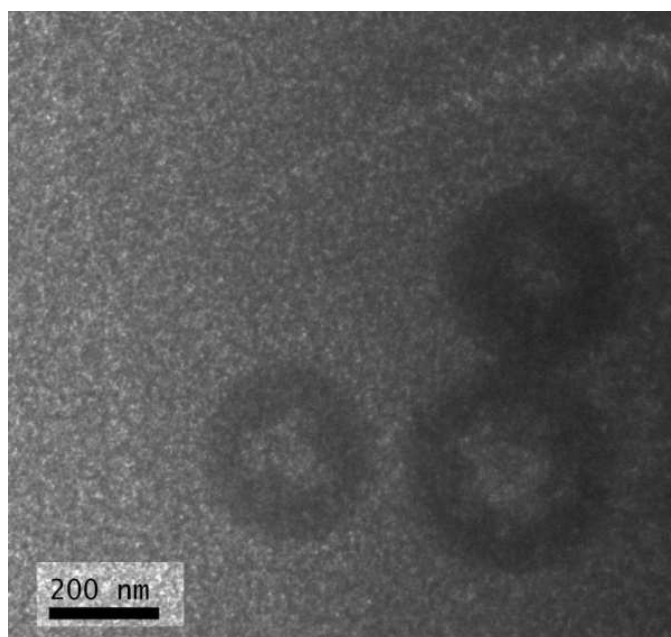


**Figure 5-5.** Cryo-transmission electron micrograph of PMMA shell – methanol core particles the image was taken with the samples at  $0^\circ$  sample insertion

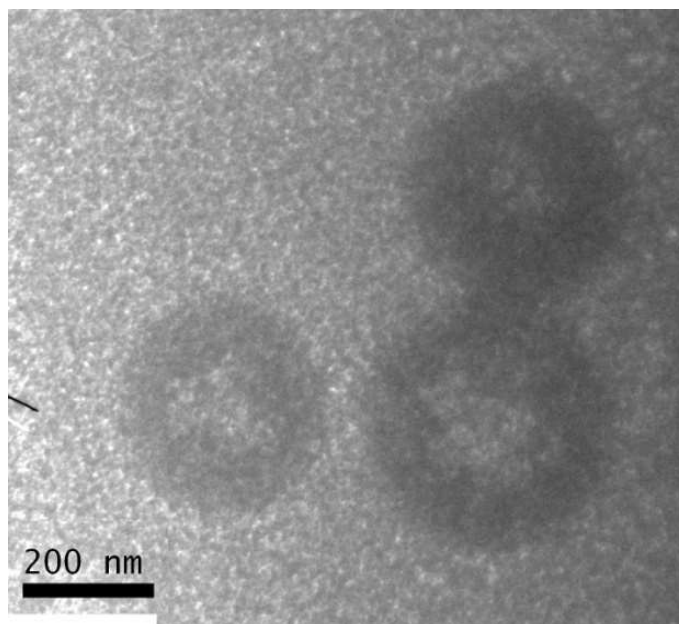


**Figure 5-6.** Cryo-transmission electron micrograph of PMMA shell – methanol core particles the image was taken with the sample at 25° insertion.

#### **5.4 Identification of the friction modifier supplied by Lubrizol**

A sample of the FM to be used in this project was supplied by The Lubrizol Corporation. Due to corporate confidentiality the data sheets provided with the FM supplied show only the general chemical classification and safety data of the sample but not the actual identification of the FM provided. The general chemical classification given indicates that the FM is an alkenyl amide. This eliminates the possibility of the FM being an inorganic species. Identifying the FM supplied is important as it may allow for identification and possibly quantification of the FM within the particle core and may also allow the FM to be measured in the oil or possibly at the surface of the tribocontacts during or after tribological testing.

ATR-FTIR was used to determine the structure of the FM being used in this project. This is shown below in **Figure 5-7** and the assignment of the peaks seen in this spectra is detailed in **Table 5-2**.

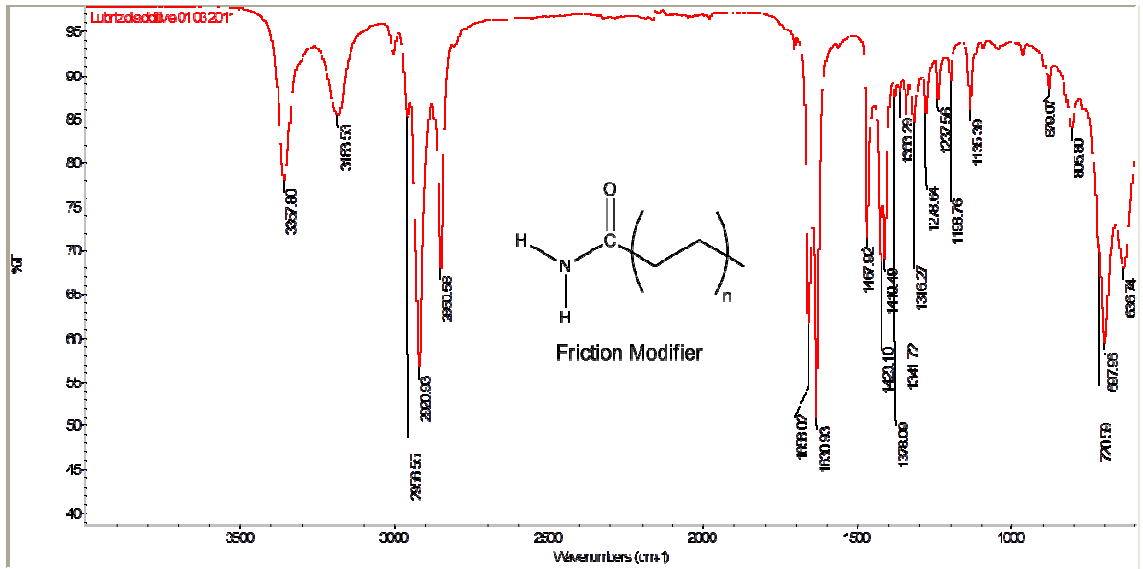


**Figure 5-7.** ATR-FTIR spectra for FM (“Lubrizol additive”) and the structure it indicates.

**Table 5-2.** Assignment of the main IR peaks in the FM spectra.

3357.80	-N-H	Stretch	Amide	3100-3500	Unsubstituted have 2 bands
3183.53					
2956.55	-C-H	Stretch	Alkane	2850-3000	Strong
2920.93					
2850.58					
1658.02	C=O	Stretch	Amide	1640-1690	Strong
1630.93	-N-H	Bend	Amide	1550-1640	
1363-1467	-C-H	Band	Alkane	1350-1480	Variable

Infrared analysis of the FM shows a large peak in the carbonyl region of its spectra. This was confirmed as a peak used for identification by Lubrizol and from the spectra it could be concluded that the structure of the FM was a hydrocarbon chain with a polar amide group at one end.

The spectrum shows that the FM is an amide structure with a straight chain alkane portion. Lubrizol have confirmed that the FM contains an amide group and

that the FM structure contained 18 carbon atoms. Using this information a number of possible structures, both branched chain and straight chain, were generated. Only one of the possible structures, stearamide, is produced and sold by Lubrizol for use in lubricants as a friction modifier. Further testing of the sample by gas chromatography– mass spectroscopy (GC-MS) and melting point analysis has shown that the FM sample is highly likely to be stearamide. FTIR is considered a fingerprinting analysis technique meaning that spectra generated can be compared to spectra of known chemicals. Comparison of the FM spectra and the spectra of stearamide confirmed that they were the same chemical species. Details of stearamide are given in **Table 5-3** and the structure is shown in **Figure 5-8**.

**Table 5-3.** MSDS data for stearamide [165].

Generic Name:	Stearamide
IUPAC Name:	Octadecanamide
Formula:	$\text{CH}_3(\text{CH}_2)_{16}\text{CONH}_2$
CAS Number:	124-26-5
Appearance:	Creamy solid
Melting Point:	102-104°C
Solubility:	Soluble in organic compounds. Insoluble in water
Stability:	Stable. Incompatible with strong acids, bases and oxidizing agents

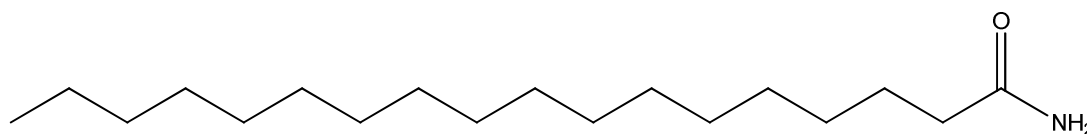


**Figure 5-8.** Stearamide.

The structure of the stearamide molecule allows for the amide region to become anchored to the metallic, or polymeric, surfaces through hydrogen bonding while the non-polar, straight chain hydrocarbon portion remains solubilised in the lubricating oil. The hydrocarbon chain aligns perpendicular to the surface and the chain sections of separate molecules are held in close proximity by Van der Waals

forces. This allows for the molecule to form a sacrificial multilayer protecting the surface from the rubbing action of the two opposing surfaces.

### 5.5. Identification of the friction modifier within PMMA particles

In order to determine whether the FM had become encapsulated within the core of the PMMA particles synthesised (synthesis detailed in **Chapter 4**), the IR spectra of PMMA, and methanol were obtained. These could then be compared to the spectra of the FM shown in **Figure 5-7**.

There were two regions which were identified as possible fingerprint regions which could be used to identify the presence of FM. The FM shows a split double peak between  $3000\text{cm}^{-1}$  and  $3500\text{cm}^{-1}$ , and a split peak at  $1600\text{cm}^{-1}$  which are unique to the sample. **Figure 5-9** shows the combination of spectra for PMMA, methanol and FM. All of the samples tested were in the dodecane continuous phase in which they had been stored. Each type of particle produced (solid, methanol core without FM and methanol core with FM) was tested.

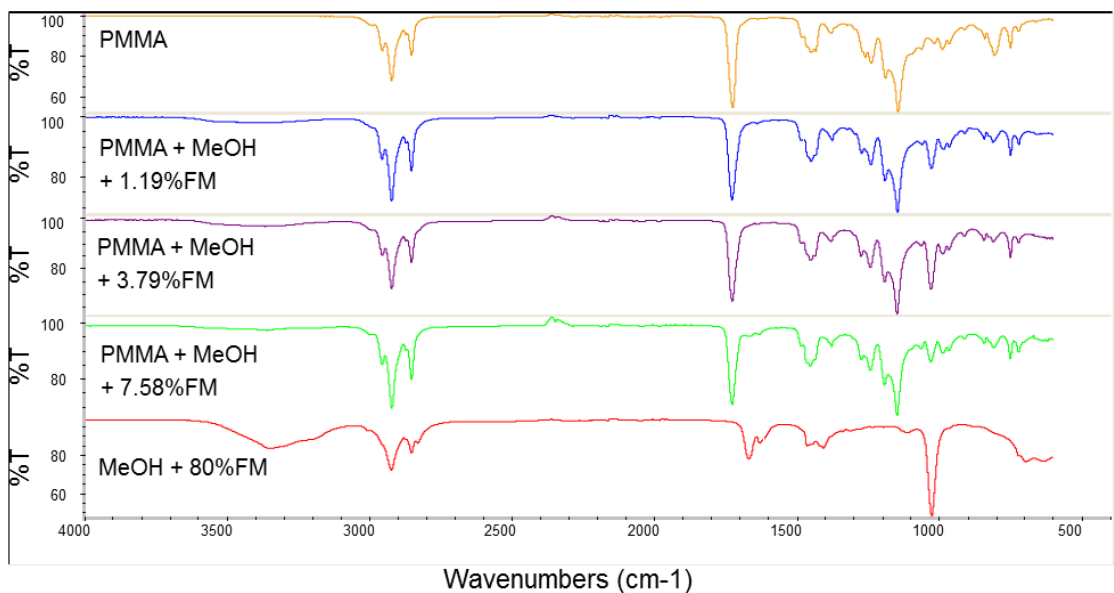


**Figure 5-9.** IR spectra for PMMA particles containing increasing amount of FM.

In the top spectra, coloured orange, the PMMA in dodecane sample showed a peak due to dodecane at  $1700\text{cm}^{-1}$  which would affect the identification of the amide peak of the FM (at  $\sim 1600\text{cm}^{-1}$ ). As methanol, seen in the blue spectra, is introduced to the matrix a large broad peak begins to appear between  $3000\text{-}3600\text{cm}^{-1}$ . This overlaps the double peak of the FM (at  $3000\text{-}3500\text{cm}^{-1}$ ) and now makes this peak unsuitable for FM identification. As the concentration of FM increases, seen in the green spectra containing 7.58wt% FM, a shoulder develops on the dodecane peak ( $\sim 1700\text{cm}^{-1}$ ) which is due to the amide group of the FM. These spectra show that it is possible to detect the presence of FM and that the FM has been encapsulated successfully using IR techniques, however the complexity of the matrix comprising of dodecane, PMMA, methanol and FM makes quantification of the FM encapsulated difficult.

## **5.6 Determination of FM release rate by high performance liquid chromatography**

### **5.6.1 Development of HPLC method**

Testing was carried out using a Perkin Elmer, high performance liquid chromatography (HPLC), normal phase system with refractive index detector. A Varian PLGel  $3\mu\text{m}$  100A 300 x 7.5mm GPC column (stationary phase) heated to  $30^\circ\text{C}$  was used in all testing with tetrahydrofuran (THF) as the mobile phase and samples were taken using an autoinjector fitted with a  $20\mu\text{L}$  injection loop. THF was used as all components were soluble in this solvent.

The following samples were also tested to determine retention times of the various possible components;

- FM (10wt%) in methanol
- FM at saturation in dodecane
- FM in THF

The chromatograms for these are shown in **Figure 5-10**, **Figure 5-11** and **Figure 5-12**. Retention times for all analytes are given in **Table 5-4**.

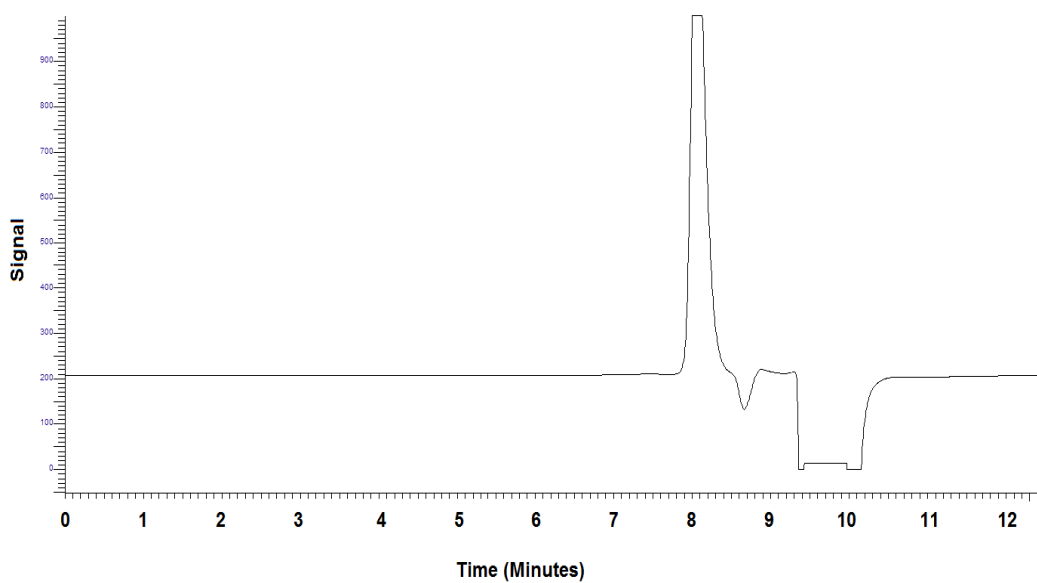


**Figure 5-10.** High performance liquid chromatogram of FM (10wt%) in methanol.  
FM = 8 minutes, methanol = 9.5 – 10 minutes.

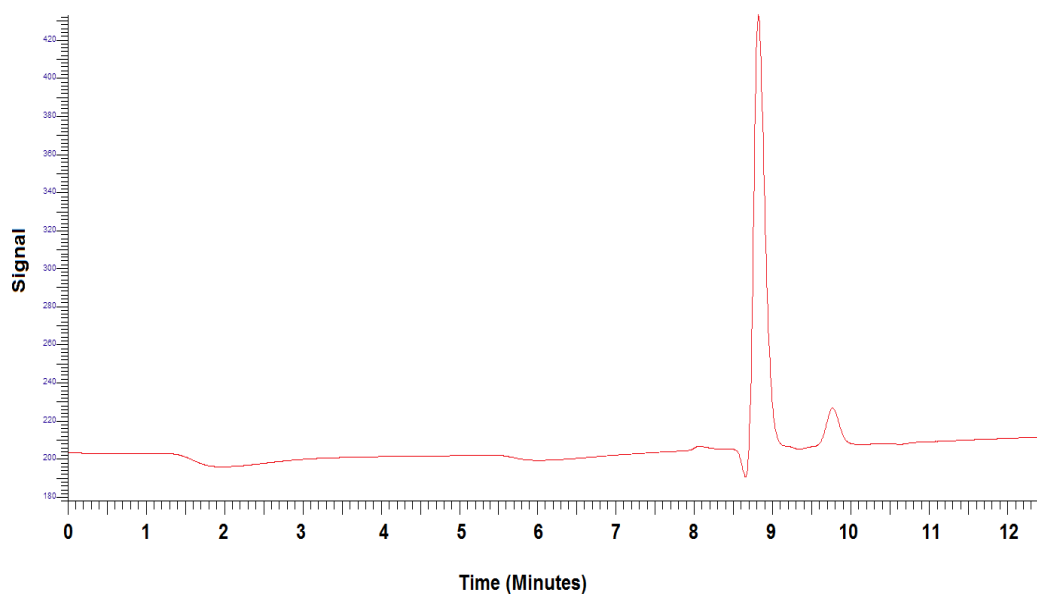


**Figure 5-11.** High performance liquid chromatogram of dodecane saturated with FM, in a THF mobile phase. FM = 8 minutes, dodecane = 9 minutes.

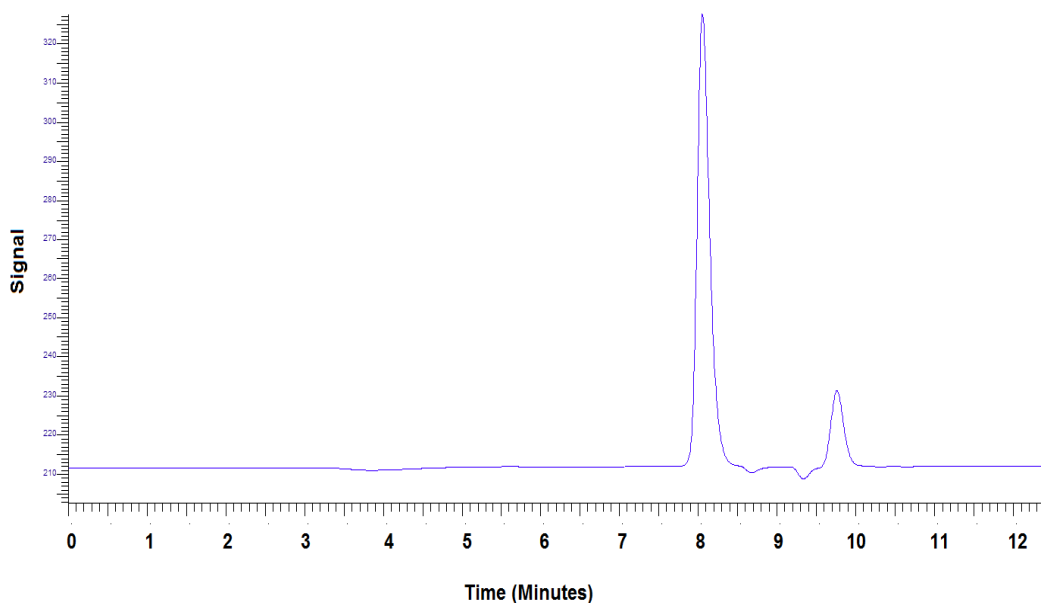


**Figure 5-12.** High performance liquid chromatogram of FM in THF. FM = 8 minutes, THF = 10 minutes.

**Table 5-4.** Elution time for analytes in HPLC testing.

Analyte	Retention time
FM	8 minutes (positive peak)
Methanol	9.5 – 10 minutes (negative peak)
Dodecane	9 minutes (positive peak)
THF	10 minutes (positive peak)

Calibration standards were prepared of varying amounts (0.0001wt% – 10wt%) of FM in methanol. These were tested *via* HPLC using THF as a mobile phase. The calibration curve produced is shown in **Figure 5-13**.

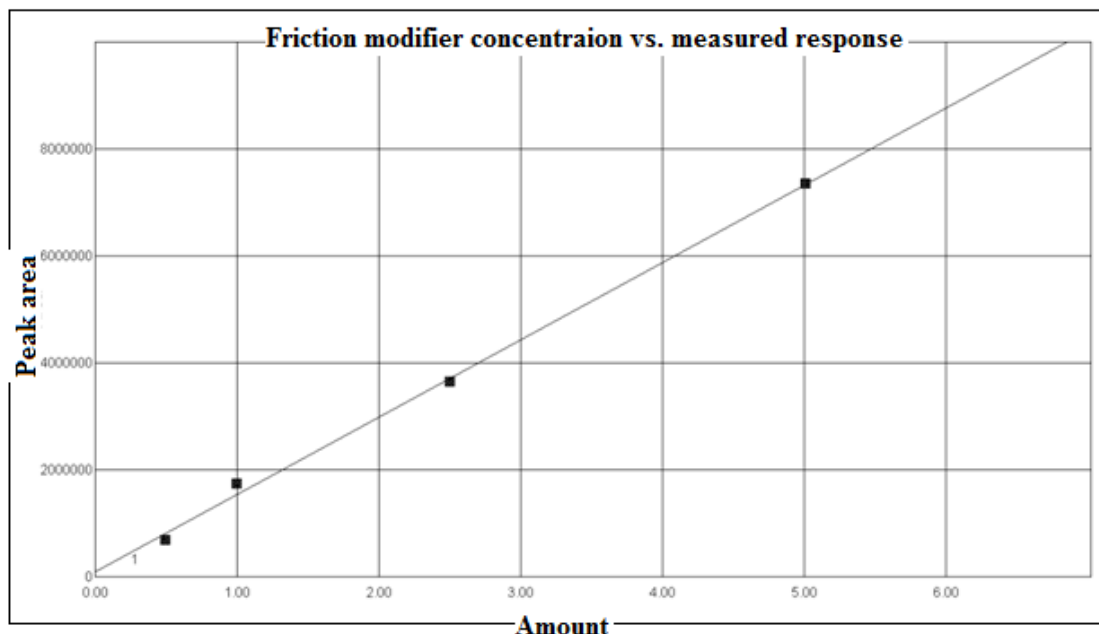


**Figure 5-13.** Calibration curve for the detection of FM in methanol, using a THF mobile phase. “Peak area” is the measured area underneath the peak and corresponds to “amount” of FM added to the standard solutions.

The area underneath the peak, measured from the baseline to the top of the peak is recorded and this corresponds to the amount of FM within a sample. A smaller peak area therefore indicates a sample containing lower quantities of FM. The area measured in each sample, of unknown FM concentration, is compared to the calibration curve, produced using known concentrations of FM, giving the amount of FM found in each sample being tested.

### 5.6.2 FM release testing

Once synthesised particles were centrifuged, supernatant dodecane was removed and fresh dodecane was added to the particles which were then resuspended and gently shaken for one hour exactly. The FM in the supernatant dodecane was then extracted using large aliquots of warm methanol to ensure full partitioning of the FM into the solvent. These were then tested by HPLC to determine the concentration of FM released from the particles, into the continuous phase, in one cycle. This process is shown in **Figure 5-14**.

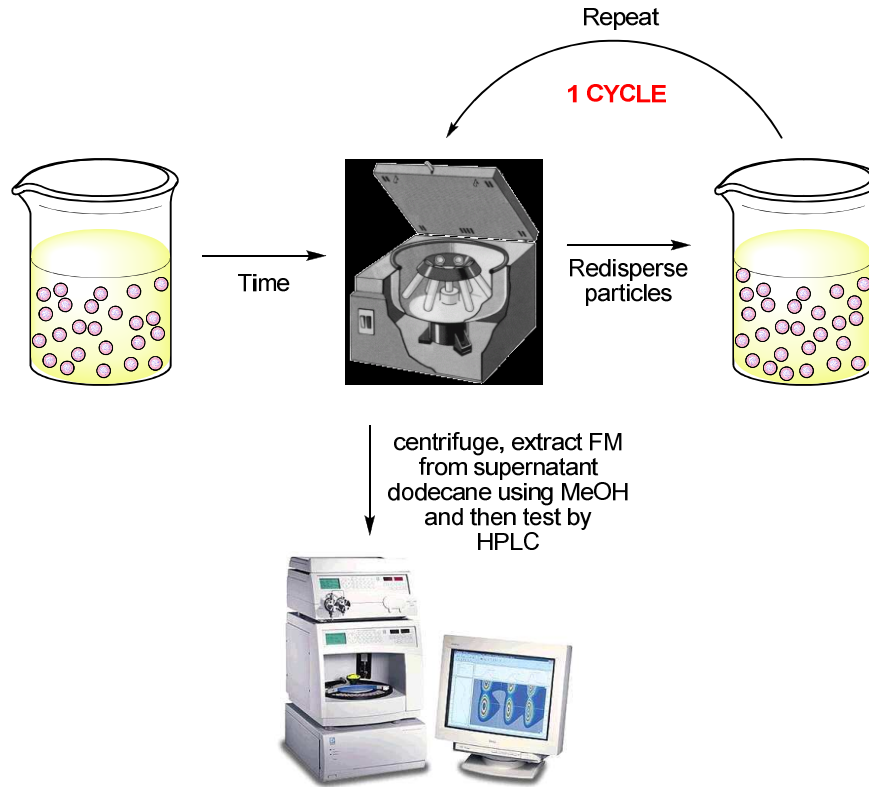


**Figure 5-14.** Each centrifugation and redispersion will be referred to as one cycle.

Testing was continued until a constant release amount was reached for each cycle. Systems of this type typically show an initial ‘burst release’ followed by a constant release rate until there is full depletion of the active. This experiment was designed to test this behaviour.

### 5.6.3 Release rate of FM into fresh dodecane

Two cycle times were tested. The first set of tests had cycles of one hour in duration, this was to ensure that the greatest amount of FM possible was being released in each cycle. The second set of testing used cycles of 15 minutes duration, this was the shortest time period possible due to the time taken to centrifuge the sample, remove the supernatant and redisperse the sample. The shorter cycle time was designed to determine how quickly the FM could be released from within the core of the particle.

The cumulative total of FM released over the testing periods is shown in **Figure 5-15.**

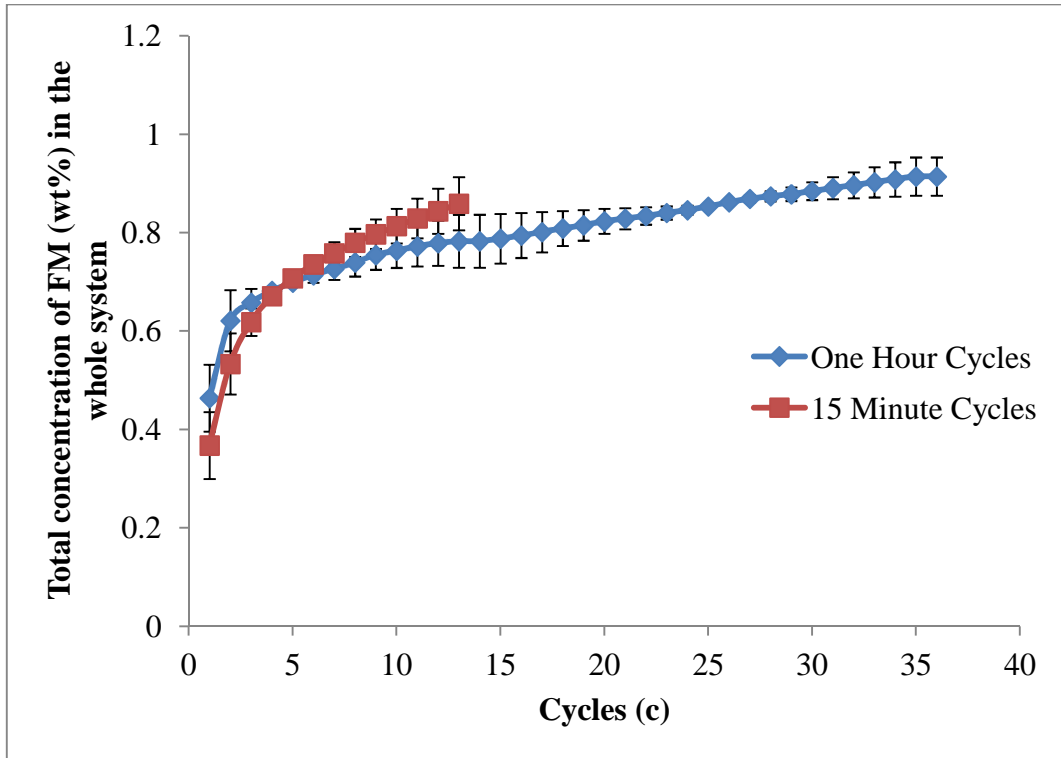


**Figure 5-15.** Cumulative FM released (wt%) with each cycle. “Cycle” refers to the amount of time the particles were dispersed in each aliquot of fresh dodecane.

Measurements found that the first cycle of testing contained between 12% and 15% of the FM which was added to the system in the initial polymerisation mixture was removed during the first cycle. This amount of FM is equivalent to about 0.4wt% of FM in the continuous phase. When  $c = 0$  this would correspond to the synthesis of the particles when it is assumed that all FM in the system is being encapsulated and concentration of the FM in the dodecane should equal zero.

All particles produced and subsequently tested for their tribological characteristics undergo one cycle ( $c = 1$ ) of centrifugation and redispersion after synthesis to remove excess stabiliser and unreacted monomer. This means that in the synthesis phase 85-88% of the FM added is actually encapsulated within the particles. This may be due to the slight solubility of the FM in dodecane as well as FM becoming associated with the excess stabiliser or unreacted monomer. The amount of encapsulated FM is still high enough to dramatically raise the concentration of FM above that which can be traditionally blended into dodecane (0.004wt%).

The amount of FM being released from the particles in each cycle was found to be 0.007-0.014wt%. This is true for both the 15 minute tests and the one hour tests respectively. This shows that 15 minutes is a sufficient amount of time to allow the maximum concentration of FM to be released from within the particles.

The amount of FM released in each cycle is greater than the amount of FM which can be solubilised in dodecane but is still within experimental error. Testing and literature searches found that methanol and dodecane are immiscible and no data or testing protocols could be found in order to test the solubility of methanol in dodecane. Release of FM from the core is driven by the concentration gradient between the core of the particles and the continuous phase. As the methanol and dodecane are immiscible it should not be the case that the methanol is aiding the transport of the FM into the dodecane by the methanol leaving the core of the particle. It may be the case that some particles rupture during the centrifuge and redispersion process, which may account for some increase in the FM measurement.

Assuming the maximum amount of FM possible is released at every cycle it would take 160 cycles before all FM, added at the time of synthesis, was accounted for.

## **5.7 Summary**

It has been shown that particles are capable of releasing FM from their core into fresh dodecane on the basis of slow diffusion through the polymer particle matrix. This demonstrates that slow release into the oily continuous phase of the formulated lubricant could occur without the need for the particles to rupture. This appears to be dependent on the concentration of FM in the dodecane, into the environment outside of the particles. Saturation of FM in dodecane was found to be higher (by up to 130%) in samples which had been exposed to centrifugal force than were measured for dodecane saturated by traditional blending methods. The cause of this needs further clarification but, due to issues surrounding the miscibility of methanol and dodecane, was determined to be outside the scope of this project.

The release properties of FM from the core of the PMMA particles is comparable with the release curves seen in the literature. This is due to the particles

obeying Fick's Law whereby the addition of fresh dodecane to the system creates a non-equilibrium in concentration of FM between the outside dodecane and the inner methanol [166-170]. An example of the typical cumulative release profile over time can be found in the analysis of peppermint oil released into hot water from gelatine-gum Arabic microcapsules reported by Dong *et al.* [167]. While the release profiles found in literature are not carried out *via* the same procedure as the centrifugation – HPLC method used in this work the results do appear to be comparable with other studies of concentration driven active release. Qiu *et al.* [171] studied the release rate of ibuprofen from polyelectrolyte multilayer capsules and stated that the driving factor in the rate of release was the solubility of the ibuprofen into the continuous phase. This has also been found in this work where the limiting factors of the release of FM into the fresh dodecane were found to be the solubility of FM into dodecane with the possible aid of the limited solubility of methanol into the dodecane.

A high proportion (85-88%) of the FM in the initial polymerisation mixture is encapsulated in the methanol core of the particles produced. This is sufficient to increase the total amount of FM in the system beyond the current capabilities. Traditionally blended engine oils contain about 0.3wt% of FM at present, if particles containing encapsulated FM were used alongside this the amount of FM inside the particles would be sufficient to sustain this level in the oil, keeping it topped up as the FM is depleted.

Within an engine, or indeed in the tribometer testing, a different release mechanism needs to be considered, that of particle breakage. This phenomenon is tested in the following chapters.

## **Chapter 6. Investigation into the tribological effect of PMMA particles in a model oil**

### **6.1 Introduction**

Polymer particles have been produced which incorporate FM within a liquid core and the rate of FM release from unbroken particles has been investigated. The action of organic FM in model oils and fully formulated oils is well documented [93, 94, 102, 115, 120, 172]. It is now important to investigate the actions of the particles themselves in a model oil dodecane and whether the particles improve friction and wear seen in the system. A testing matrix was devised in order to investigate the friction and wear reduction properties of;

- 1) Dodecane, here used as a model oil, containing no engine oil additives or particles.
- 2) Dodecane fully saturated with FM. This represents the maximum concentration of FM which can be blended into the model oil through traditional blending methods.
- 3) Solid PMMA particles, which contain no FM, in dodecane. These have been used to determine the effect of particle size. Particles measuring 150nm (small), 850nm (medium) and 1600nm (large) have been tested.
- 4) Particles with a methanol core, which contain no FM, in dodecane.
- 5) Particles with a methanol core containing FM in dodecane. Here particles measuring ~ 1000nm have been tested which contain different concentrations of FM within their cores.

This is shown on the next page in **Tables 6-1, 6-2 and 6-3**.

**Table 6-1.** Testing matrix for comparison of particles of solid PMMA particles, containing no FM, in dodecane at different concentrations and different hydrodynamic diameter. Each x signifies each two hour test carried out, for that particular particle type.

SOLID PARTICLES		Particle size		
		1600nm	850nm	150nm
Particle concentration	14wt%	xxx	xxx	xxx
	7wt%	xxx	xxx	xxx
	3wt%	xxx	xxx	xxx
	1wt%	xxx	xxx	xxx
FM concentration		-	-	-

**Table 6-2.** Testing matrix for comparison of particles of solid PMMA particles, PMMA particles with a liquid core containing no FM and PMMA particles with a liquid core containing FM, all in dodecane at different particle concentration. Note particle size remains constant within error. Each x signifies each two hour test carried out, for that particular particle type.

CHANGING PARTICLE COMPOSITION		Particle size		
		Solid PMMA particles	PMMA particles with a methanol core	PMMA particles with a methanol core containing FM
		1600nm	1600nm	1600nm
Particle concentration	14wt%	xxx	xxx	xxx
	7wt%	xxx	xxx	xxx
	3wt%	xxx	xxx	xxx
	1wt%	xxx	xxx	xxx
FM concentration		-	-	7.7wt%

**Table 6-3.** Testing matrix for comparison of PMMA particles with a liquid core containing FM at the same particle size within error and different particles loading. Note changing particle concentration also changes overall FM concentration in the system. Each x signifies each two hour test carried out, for that particular particle type.

PARTICLES WITH A METHANOL CORE CONTAINING ENCAPSULATED FM		Particle size		
		1600nm	900nm	1100nm
Particle concentration	14wt%	xxx	xxx	xxx
	7wt%	xxx	xxx	xxx
	3wt%	xxx	xxx	xxx
	1wt%	xxx	xxx	xxx
FM concentration		7.7wt%	15.3wt%	32.2wt%

Tribological testing was carried out using a Cameron Plint TE77 low speed reciprocating test machine. The TE77 tribometer comprises of a pin attached to a reciprocating arm which moves across a stationary plate positioned within a heated oil bath. Details and a schematic of the TE77 apparatus used in this project are given in **Chapter 3**.

The materials and test conditions used are detailed below in **Table 6-4**.

**Table 6-4.** Cameron Plint TE77 test conditions.

Pins	Cast iron (Ø 6mm, radius 10mm, 43-47 HRC)
Plates	AISI 52100 Steel (58-60 HRC)
Run Conditions	80°C, 25Hz, 24.5N, 0.78GPa, 5mm stroke length

Particles were synthesised as detailed in **Chapter 4**. All particle samples are compared to pure dodecane (0wt% particles), which was used as a model oil, and also dodecane fully saturated with FM (0wt% particles).

To produce dodecane fully saturated with FM (0wt% particles) incremental amounts of FM were weighed into the dodecane, at room temperature, until no more would dissolve. This is the traditional method of blending additives into an engine oil and represents the amount of FM which can be blended into an oil currently; a concentration which this work aims to improve upon. The maximum amount of FM soluble in dodecane is about 0.004wt%.

Wear analysis was conducted using scanning white light interferometry on a Bruker NP FLEX interferometer. All measurements were taken under vertical scanning interferometry mode, scan speed 1, magnification 2.5x.

## **6.2 Effect of adding particles of different morphologies to dodecane**

### **6.2.1 Friction**

Here the tribological behaviour of dodecane which contains solid PMMA particles, PMMA particles with a liquid methanol core or PMMA particles with a liquid methanol core containing encapsulated FM are compared. Each sample is also compared to pure dodecane and dodecane which is fully saturated with FM through traditional blending methods. This has been carried out in order to determine the effects of the PMMA particles themselves, what effect methanol has and also, whether the presence of FM produces the desired decrease in friction over the duration of the test (2 hours). Each of the tests has been carried out using the same test parameters as described in **Section 6.1** and was repeated at least 3 times. It should be noted that, in the case of the FM loaded particles, the concentration of FM changes as the concentration of particles changes.

Over the two-hour measurement, presented in **Figure 6-1**, the coefficient of friction for the case of pure dodecane as the lubricant was consistently higher than for any other sample. It also showed the largest fluctuation of any of the samples

tested. As expected, when dodecane is fully saturated with FM the friction coefficient measured is reduced and appears to reach a steady state within the first 30 minutes of the test.

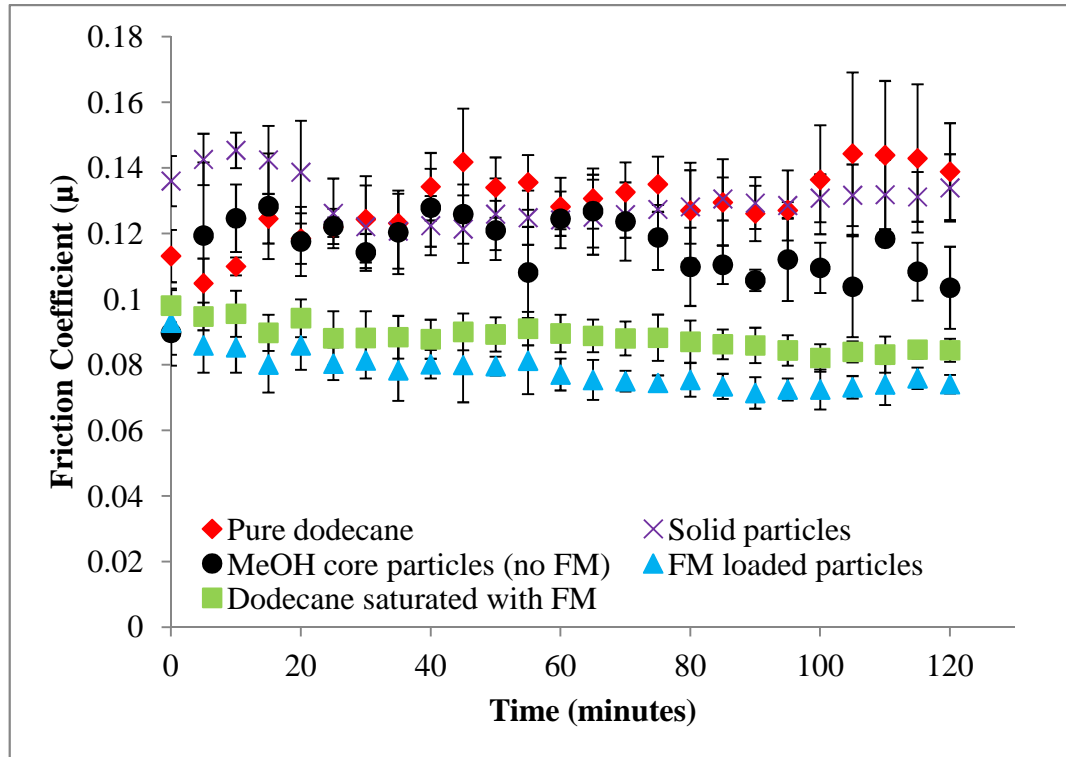


**Figure 6-1.** Friction coefficient ( $\mu$ ) over a time period of two hours. Pure dodecane (red  $\blacklozenge$ ), dodecane containing solid PMMA particles (14wt% particles) (purple  $\times$ ), dodecane containing methanol core, no FM, PMMA particles (14wt% particles) (black  $\bullet$ ), dodecane saturated with FM (green  $\blacksquare$ ) and dodecane containing particles with encapsulated FM (14wt% particles) (blue  $\blacktriangle$ ). Each plot is the average of three separate tests, carried out under identical conditions, error bars are the standard deviation of the three tests.

All of the samples containing the PMMA particles recorded lower friction coefficients than in the case of pure dodecane. The dodecane/ solid particle and the dodecane/ methanol core particle samples contained no FM yet still reduced the friction below that measured for pure dodecane. These results do not show any significant effect of solid particles on friction reduction. This is not surprising as the polymer used for the particles does not have any friction reducing properties itself.

The addition of FM containing particles to dodecane measured the lowest friction coefficient of all samples and this will be explored further later in this chapter.

### 6.2.2 Wear

In **Figure 6-2** wear results obtained from testing dodecane with solid and FM containing particles are shown. Each result is the average wear volume measured of three separate plates, carried out under identical conditions.

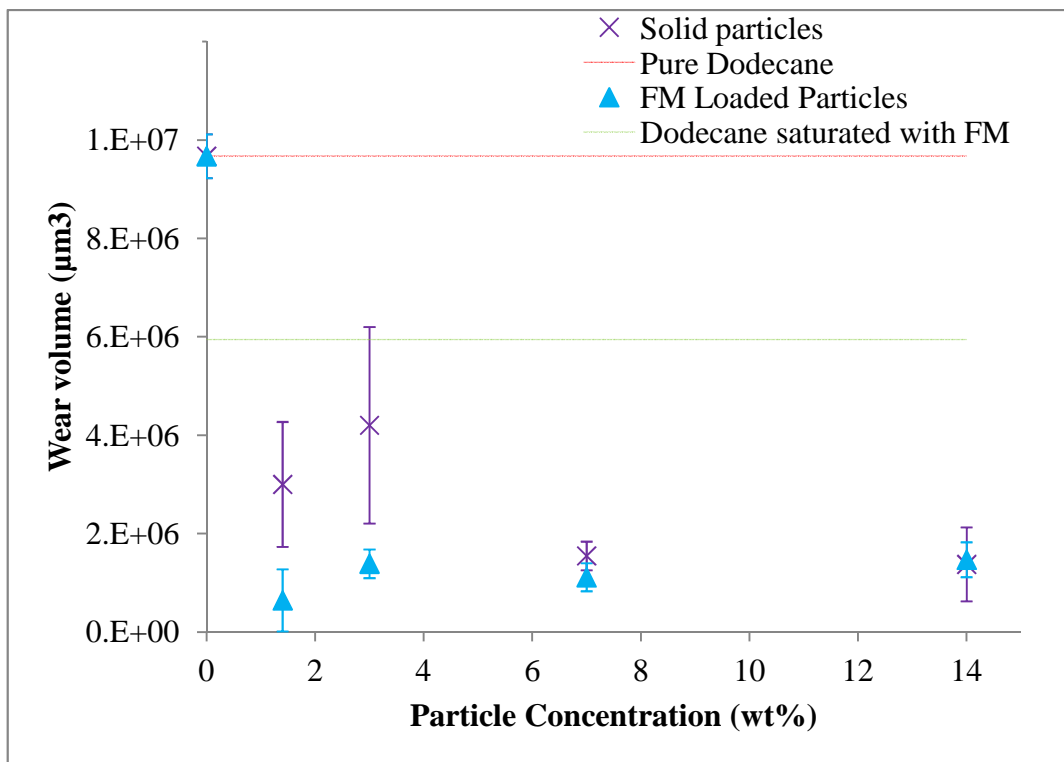


**Figure 6-2.** Wear volume ( $\mu\text{m}^3$ ) of the steel plates after the two-hour test period. Pure dodecane (red horizontal line [ $\sim 9.7 \times 10^6$ ]), dodecane containing solid particles (purple x), dodecane saturated with FM (green horizontal line [ $\sim 5.9 \times 10^6$ ]) and dodecane containing particles with encapsulated FM (blue  $\blacktriangle$ ) (14wt% particles is equivalent to 3wt% FM. 7wt% particles = 1.5wt% FM. 4wt% particles = 0.8wt% FM and 1wt% particles = 0.3wt% FM). Each plot is the average wear volume measured of three separate test plates, carried out under identical conditions. It should be noted that the concentration of friction modifier as the concentration of particles changes.

At all particle concentrations measured the volume of wear was lower than those measured in pure dodecane ( $\sim 9.7 \times 10^6 \pm 4 \times 10^5 \mu\text{m}^3$ ). The effect of changing the concentration of solid particles follows no systematic trend. It can be seen that only a small amount of the solid PMMA particles needs to be blended into dodecane in order to produce a dramatic reduction in wear volume. However, the largest drop in measured wear volume can be seen in the samples containing the highest concentration of particles.

The addition of FM (at saturation) to dodecane produces a lower wear volume ( $\sim 5.9 \times 10^6 \pm 7 \times 10^5 \mu\text{m}^3$ ) than measured for pure dodecane. A comparison of the wear scar generated when pure dodecane is used compared and wear scar generated when dodecane fully saturated with FM are used as lubricating oils is given below in **Figure 6-3**. The wear scar of the sample containing FM ( $\sim 1.1 \mu\text{m}$ ) is much shallower than the sample which didn't contain FM ( $\sim 4.7 \mu\text{m}$ ).

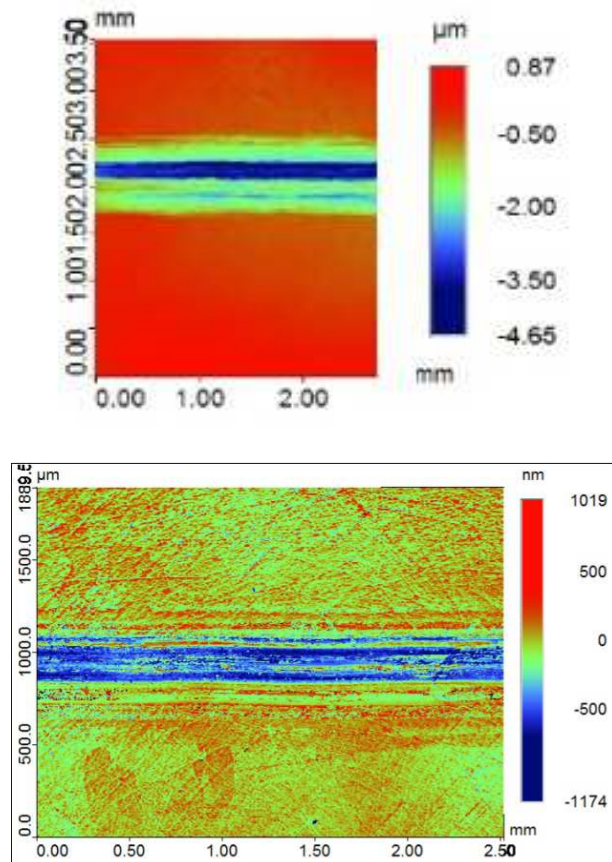


**Figure 6-3.** [Top image] Depth of wear scar on a steel plate tested when dodecane is used as a lubricating oil and [Bottom image] when dodecane fully saturated with FM (0.004wt%) is used as a lubricating oil in TE77 testing.

The use of particles containing encapsulated FM significantly reduces the wear recorded in all other samples, including for the case of a dodecane solution saturated with FM. Samples containing these particles showed an 84% reduction in wear when compared to dodecane fully saturated with FM and an 89% reduction in wear compared to plates tested in pure dodecane. There appears to be very little variance between samples of different particle concentration. This again shows that only a small percentage of particles need be incorporated into dodecane to produce the desired reduction in wear.

Examples of the wear scars seen for dodecane containing solid particles (14wt%) and those generated for dodecane containing particles with encapsulated FM (14wt% particles, equivalent to 3wt% FM) are shown in **Figures 6-4** and **Figure 6-5**. The wear scars here can be seen to be much shallower than when pure dodecane ( $\sim 4.7\mu\text{m}$ ) can be used as a lubricating oil. The wear scar generated when dodecane with solid particles appears deeper ( $\sim 0.45\mu\text{m}$ ) and better defined than the wear scar imaged when dodecane with particles containing FM ( $\sim 0.10\mu\text{m}$ ) have been used.

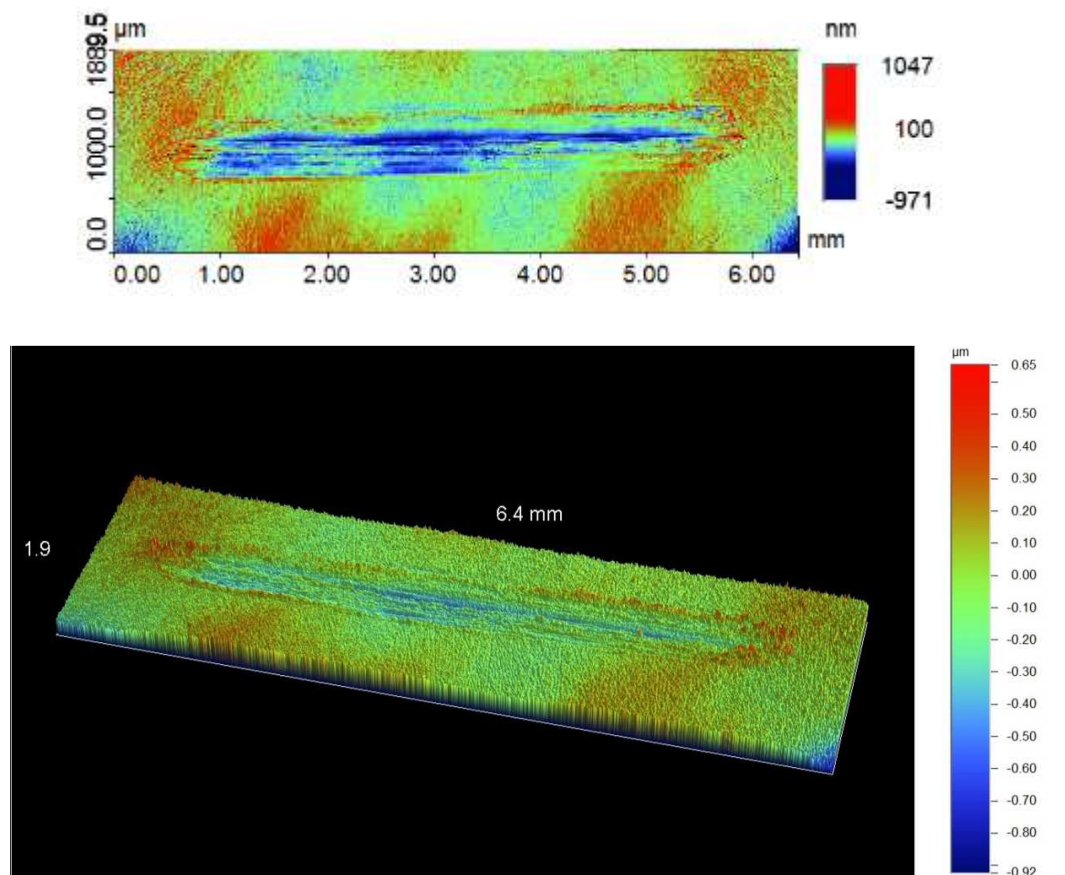


**Figure 6-4.** 2D and 3D interferometry images of the wear scar of a plate tested when dodecane with solid particles (14wt% particles) is used as a lubricating oil.

The black areas in **Figure 6-5** are areas which have been masked from the scanned image when measured the wear volume. Here the wear scar created during testing was slightly off centre of the steel plate, meaning that the edge of the plate could be seen in the interferometry scan. If these were not masked they would lead to artificially high wear volumes being measured.

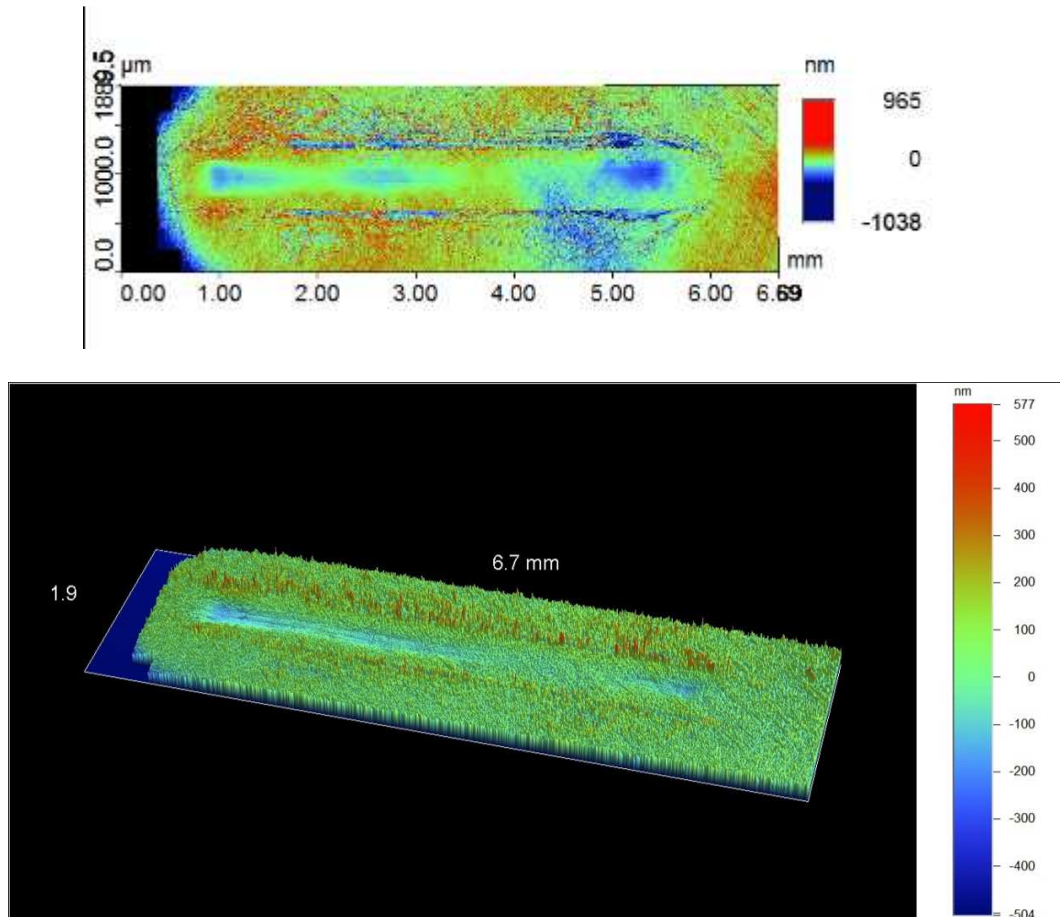


**Figure 6-5.** 2D and 3D interferometry images of the wear scar of a plate tested when FM containing particles (14wt% particles; 3wt% FM) is used as a lubricating oil in TE77 testing.

Organic friction modifiers and antiwear additives are both considered surface active additives and operate under similar conditions. It may therefore be possible that the organic friction modifier used in this study has some mild antiwear properties [12].

At most particle concentrations the encapsulated FM particles produced lower wear during testing than solid particles. This suggests that there is a synergy between FM and PMMA used to form the particle shell which results in wear reducing properties. This will be discussed further in the next chapter.

## **6.3 Effect of particle size**

### **6.3.1 Friction**

The two hour tests are considered to have reached a steady state during the last 30 minutes of the test. The friction coefficients during this steady state period are averaged out for each sample and given in **Figure 6-6**. Each result is the average of the last 30 minutes of the three separate tests and the error bar for each point is the standard deviation of these 3 tests. Particle samples which were used to determine the effect of particle size were all solid PMMA particles which contained no FM. The solid particles tested measure 1600nm, 850nm and 150nm. It should be noted that the stated friction coefficients for pure dodecane and dodecane saturated with FM are for comparison only and contain no particles.

As expected, blending the FM into dodecane produces a friction coefficient ( $0.0084 \pm 0.003$ ) lower than measured for the dodecane itself ( $0.139 \pm 0.015$ ).

At all particle concentrations tested the measured coefficient of friction is higher than those measured for dodecane saturated with FM. The effect of changing the concentration of solid particles used appears to follow no systematic trend. There is little evidence in these samples that changing the concentration of particles used has a significant effect on the friction measured. Particle size has a greater effect on friction coefficient at higher particle concentrations and at the lowest particle concentration (1wt%), in all samples, the friction coefficient measured is similar for all three particle sizes, indicating that only a low concentration is necessary to improve reliability and particle friction reduction regardless of particle size. As stated previously, one of the desired characteristics for the synthesised particles in this project was to produce particles as small as 100nm in order to make the particles

less visible within an engine oil. As such this may be the driving factor when deciding which particle size to incorporate.

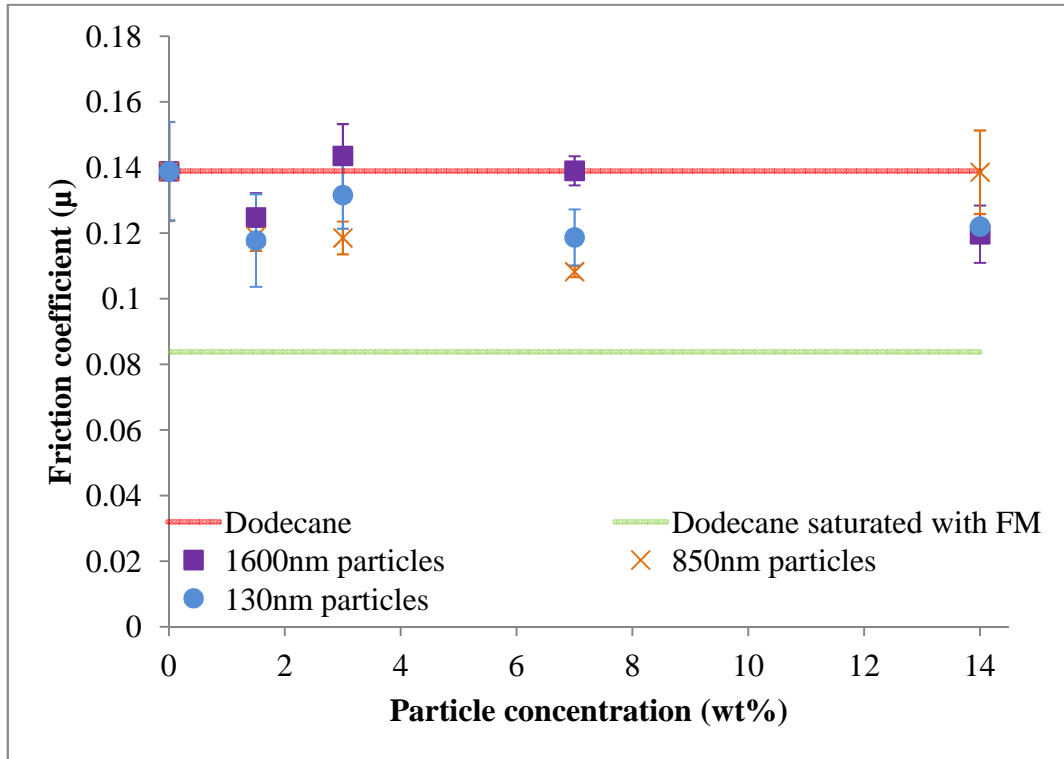


**Figure 6-6.** Friction coefficient ( $\mu$ ) during the last 30 minutes of the two hour tests, error bars coloured for clarity. Pure dodecane (red (upper horizontal) line, friction coefficient = 0.139, line is for comparison only, there are no particles in this sample), dodecane containing 1600nm solid PMMA particles (purple ■), dodecane containing 850nm solid PMMA particles (orange x), dodecane containing 150nm solid PMMA particles (blue ●) and dodecane saturated with FM (green (lower horizontal) line, friction coefficient = 0.084, line is for comparison only, there are no particles in this sample).

Each sample was tested at the same particle concentrations but due to the differing particles sizes each sample also contains a different number of particles. Over the range studied, it seems that the number of particles in the system does not have a direct effect on the friction coefficient measured, shown in **Figure 6-7**.

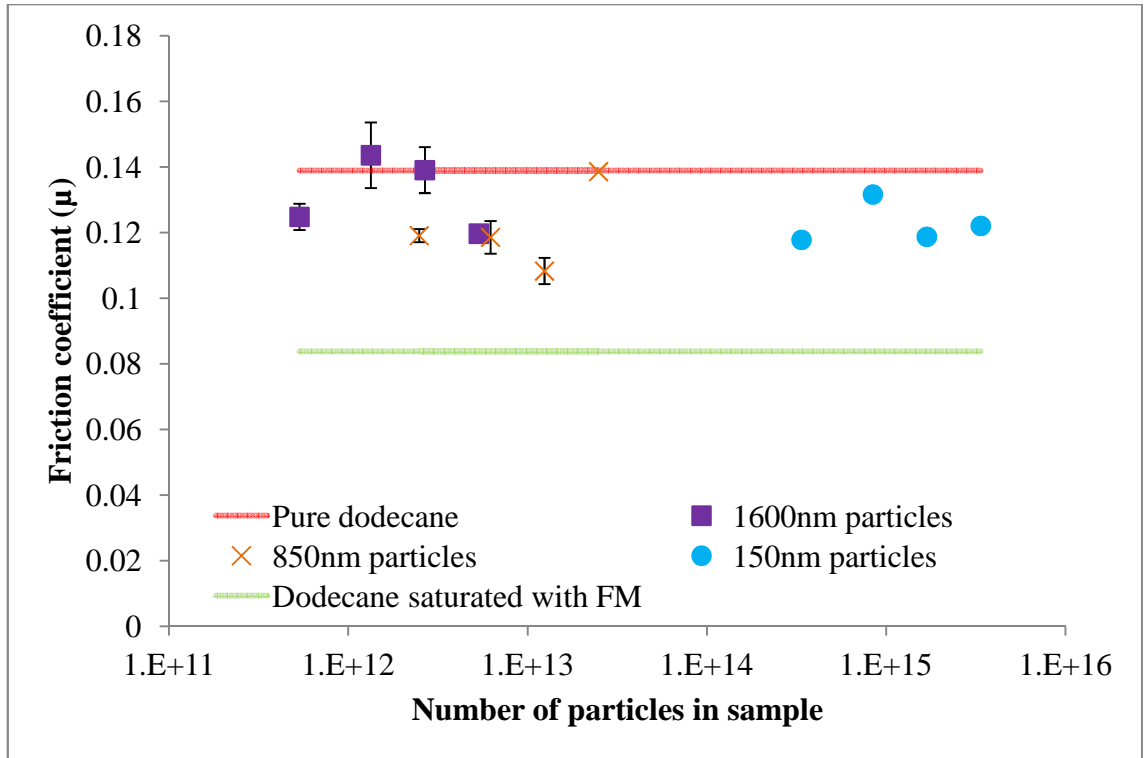


**Figure 6-7.** Friction coefficient ( $\mu$ ) during the last 30 minutes of the two hour tests versus number of particles in the sample. Pure dodecane (red (upper horizontal) line, friction coefficient = 0.139, line is for comparison only, there are no particles in this sample), dodecane containing 1600nm solid PMMA particles (purple ■), dodecane containing 850nm solid PMMA particles (orange x), dodecane containing 150nm solid PMMA particles (blue ●) and dodecane saturated with FM (green (lower horizontal) line, friction coefficient = 0.084, line is for comparison only, there are no particles in this sample).

## 6.4 Effect of changing FM concentration encapsulated in particles

### 6.4.1 Friction

As seen in **Figure 6-8** particles containing encapsulated FM have the potential to reduce the measured coefficient of friction below that of dodecane fully saturated with FM, which here represents the amount of FM which can be blended traditionally. This suggests that a greater concentration of FM can be incorporated into an oil when it is encapsulated within PMMA particles. The next stage of this

chapter is designed to study whether encapsulated greater amounts of FM can lead to a corresponding decrease in friction coefficient. Particles were synthesized as detailed in Chapter 4 using varying amounts of FM. It should be noted that the concentration of FM changes as the concentration of particles changes.

For all samples containing particles with encapsulated FM tested the measured coefficient of friction is lower than those measured for pure dodecane ( $0.139 \pm 0.015$ ). The effect of changing the concentration of particles used appears to follow no systematic trend and once again there is little evidence in these samples that changing the concentration of particles used has a significant effect on the friction measured. For each particle sample the error is seen to decrease as the concentration of particles decreases indicating that only a low concentration is necessary to improve reliability and particle friction reduction.

The particles which contain the highest concentrations of FM encapsulated within their core measured the lowest friction coefficients and in some cases reduced the friction coefficient measured below those measured for dodecane fully saturated with dodecane by traditional blending methods ( $0.0084 \pm 0.003$ ). It should be noted that altering the particle concentration also alters the FM concentration within the system directly. All of these samples have a FM concentration much higher than can be blended by conventional means. When comparing the 3.5wt% and 14wt% particle samples it can be seen that there has only been a small change in friction meaning that only a relatively small concentration of particles is needed to reduce friction. This is advantageous in terms of blending particles into a fully formulated oil, as a lower concentration of particles will reduce the visibility of those particles within the oil.

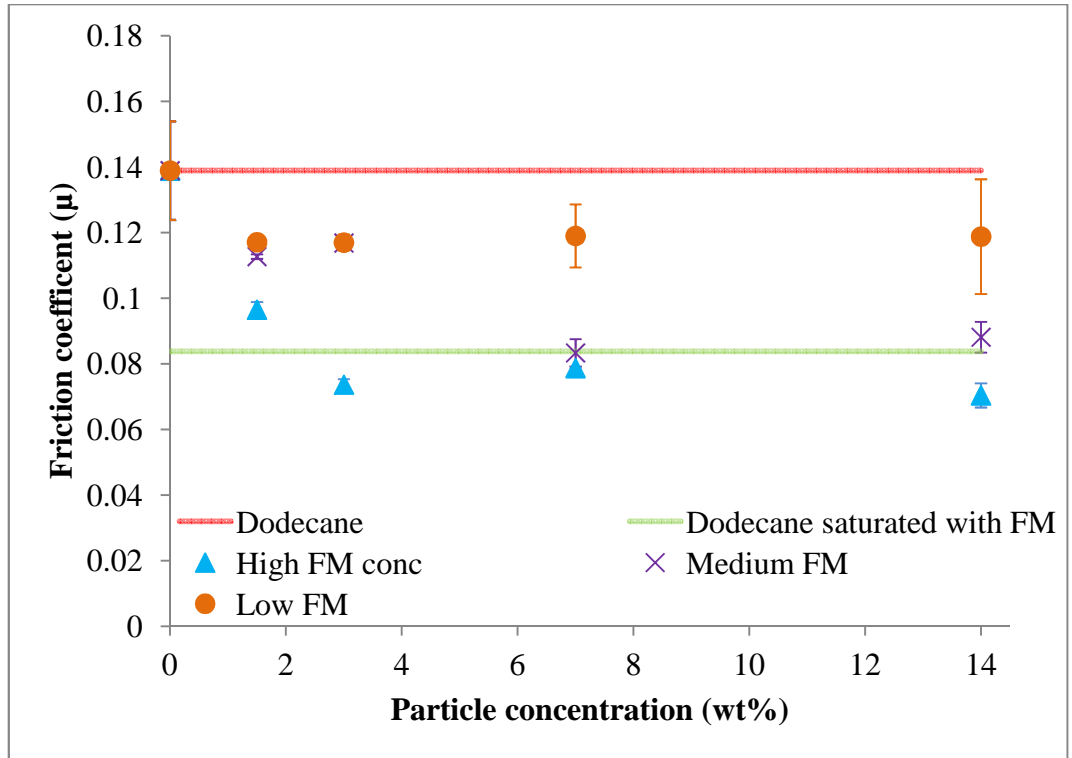


**Figure 6-8.** Friction coefficient ( $\mu$ ) during the last 30 minutes of the two hour tests, error bars coloured for clarity. Pure dodecane (red (upper horizontal) line, friction coefficient = 0.139, line is for comparison only, there are no particles in this sample), dodecane containing 1100nm ‘low’ FM loaded particles (orange ●) (1wt% particles is equivalent to 0.1wt% FM. 3wt% particles = 0.2wt% FM. 7wt% particles = 0.4wt% FM and 14wt% = 0.7wt% FM), dodecane containing 900nm ‘medium’ FM containing particles (purple x) (1wt% particles = 0.1wt% FM. 3wt% particles = 0.4wt% FM. 7wt% particles = 0.7wt% FM and 14wt% particles = 1.5wt% FM), dodecane containing 1100nm ‘high’ FM containing particles (blue ▲) (1wt% particles = 0.3wt% FM. 3wt% particles = 0.8wt% FM. 7wt% particles = 1.5wt% FM and 14wt% particles = 3.1wt% FM) and dodecane saturated with FM (green (lower horizontal) line, friction coefficient = 0.084, line is for comparison only, there are no particles in this sample).

The amount of FM encapsulated appears to have an influence on the friction coefficient measured. Changing the concentration of particles produces a change in the concentration of FM in the system being tested. As a consequence of this some of the different samples tested in fact contained the same overall FM concentration.

**Figure 6-9** shows the effect FM concentration has on the measured coefficient of friction.

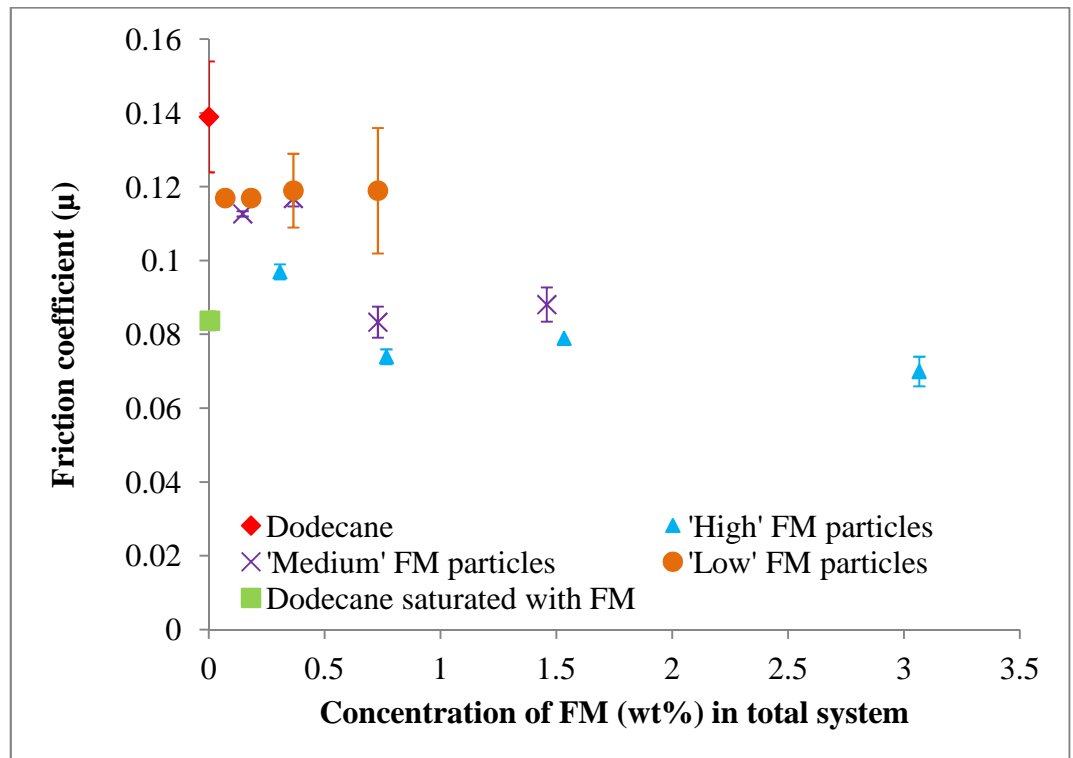


**Figure 6-9.** Friction coefficient ( $\mu$ ) during the last 30 minutes of the two hour tests, error bars coloured for clarity. Dodecane containing particles with encapsulated FM. Particle concentrations correspond to the samples shown in **Figure 6-8**.

The amount of FM encapsulated appears to have an influence on the friction coefficient measured. Changing the concentration of particles produces a change in the concentration of FM in the system being tested. As a consequence of this some of the different samples tested contained the same overall FM concentration. Despite these systems containing the same amount of FM those particles which contain the most FM within their cores still measure the lowest friction coefficients. This again shows that the number of particles does not have a direct effect on the friction coefficient measured.

This shows that the inclusion of a low concentration of particles which contain a high amount of encapsulated FM can produce lower coefficient of friction than a

high concentration of particles which contain very low amount of FM. This is independent of the concentration of FM there is in the overall system. This suggests that the delivery method of the FM may be dominated by the bursting of particles and the quick delivery of FM where and when it is needed rather than the slow leeching of FM from the particles over time as was the initial hypothesis.

#### **6.4.2 Wear**

**Figure 6-10**, shows the wear results obtained from particles containing different concentration of FM encapsulated within their cores. Each result is the average wear volume measured of three separate plates, carried out under identical conditions.

At all particle concentrations measured the volume of wear was lower than those measured in pure dodecane ( $\sim 9.7 \times 10^6 \pm 4 \times 10^5 \mu\text{m}^3$ ) and those of dodecane fully saturated with FM ( $\sim 5.9 \times 10^6 \pm 7 \times 10^5 \mu\text{m}^3$ ). The effect of changing the concentration of particles, and thus the concentration of FM in the system, follows no systematic trend. There appears to be little difference between particles containing the various concentrations of FM and also little variance between samples of different particle concentration. This suggests that while the organic friction modifier being used may exhibit some mild antiwear properties, this has reached a saturation point where the addition of further FM provides no advantage to the wear reduction seen. Once again it can be seen that only a small amount of these FM containing particles are needed in order to dramatically reduce the wear volume.

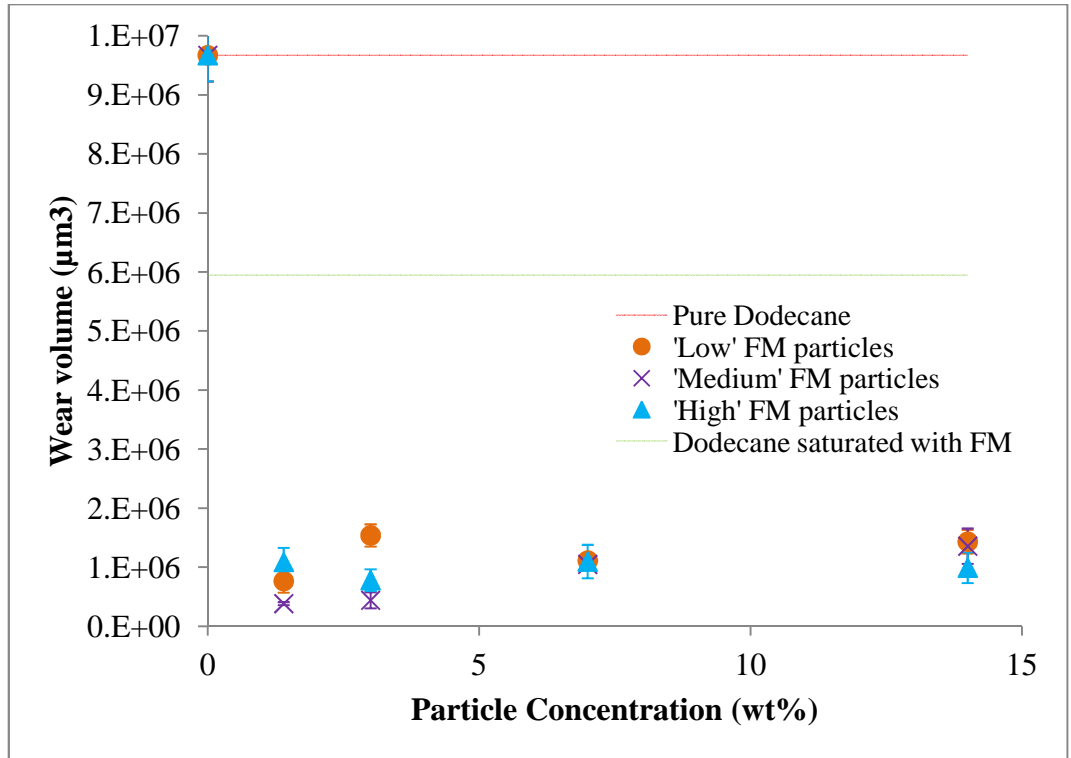


**Figure 6-10.** Wear volume ( $\mu\text{m}^3$ ) of the steel plates after the two-hour test period. Pure dodecane (red horizontal line [ $\sim 9.7 \times 10^6$ ]) (off y-axis scale), dodecane containing 'low' FM particles (orange ●), dodecane containing 'medium' FM particles (purple x) and dodecane containing 'high' FM particles (blue ▲). Each plot is the average wear volume measured of three separate test plates, carried out under identical conditions. It should be noted that the concentration of friction modifier as the concentration of particles changes. FM concentrations for each sample are as stated for **Figure 6-8**.

## **Chapter 7. Discussion**

### **7.1 Introduction**

Particles have been produced which can reduce the friction coefficient and recorded wear associated with using a model oil, in this case dodecane, than is possible through traditional blending techniques. This chapter will propose a possible mechanism for the action of these particles and the release of FM from within the core of these particles.

### **7.2 Particle optimisation**

PMMA were synthesised controllably in a non-aqueous continuous phase *via* a dispersion polymerisation. Solid PMMA particles were produced by the systematic altering of the initial polymerisation mixture. This included changing the concentration of monomer (MMA), stabiliser (PDMS-MA), initiator (AIBN) respectively and then altering both the monomer and stabiliser together. With the incorporation of a co-solvent into the initial polymerisation mixture PMMA particles were created which had a polymer shell – liquid core morphology. Size control of these particles was also investigated by changing the ratio of co-solvent to continuous phase in the initial polymerisation mixture. In doing this control over particle size and polydispersity allowed for the synthesis of particles below 100nm, which will be barely visible to the naked eye, and enable the synthesis of larger particles ( $>1\mu\text{m}$ ) capable of carrying large quantities of FM within their cores and thus requiring fewer particles to be added to be blended into the oil used. In addition to controlling the final particle size and concentration blended into the final engine oil, particle visibility could be further improved by matching the refractive indices of the polymer being used and the oil. This would

allow the particles to ‘disappear’ in the oil [173-178], this process is shown simply in **Figure 7-1**.

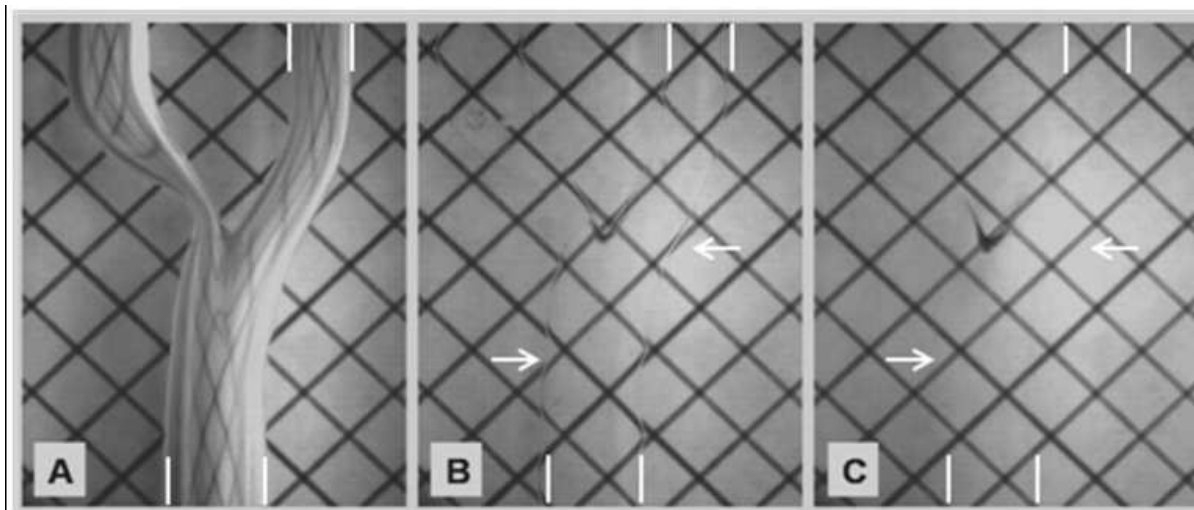


**Figure 7-1.** Demonstration of refractive index matching monitored with the use of gridlines. A. Showing a polymer tube in air, with high distortion of the gridlines, B. Polymer tube in a fluid which is a close refractive index match, showing some distortion of the gridlines and C. Polymer tube in a refractive index matched liquid, where no distortion of the gridlines is seen. Note: distortion at the branch point in all samples is intentional in order to show the position of the tube in the various liquids [179].

Particles produced were tested and optimised for the particular model system and polymerisation method used in this project. Each part of the polymerisation process and initial polymerisation mixture can be altered in order to produce particles which may be suitable for incorporation into a base oil and eventually into a fully formulated engine oil. Encapsulation of different additives, either inorganic FMs (such as  $\text{MoS}_2$ ) or other additive types (for example antiwear) should be possible *via* dispersion polymerisation as long as the co-solvent and continuous phase used are immiscible and the additive is preferentially soluble in the co-solvent rather than the continuous phase.

Dodecane samples which contained particles used in this project were shaken and sonicated before TE77 testing in order to break apart and aggregates which may have formed while in storage and to resuspend particles into the dodecane.

Aggregation in the particles synthesised here was unlikely as polymeric steric stabilisers were used to prevent this from occurring. Settling may occur at certain particle sizes due to the density of the particle compared to the density of the dodecane it is in. To overcome the possibility of particles settling too quickly a co-solvent which has a similar density to the outer continuous phase could also be considered. This would allow the particles to remain suspended in the oil for longer without the need for shaking or stirring.

While the particles produced, oil used and additive encapsulated may all be altered in order to optimise the final oil for the desired system, in this case the piston ring and cylinder liner in an internal combustion engine, it should also be considered that the FM-oil system presented here may be suitable for a different application, for example in tribocontacts where one or more of the substrates is itself is a polymer. This would eliminate any potential problems which may arise from polymer particle debris collecting in the engine. Literature has shown that the incorporation of polymer particles can be used in self healing systems to strengthen surfaces and repair microscopic cracks in the substrate [98-101, 180-183].

Undisturbed particles will act as an FM reservoir, working in addition to the FM blended into the continuous phase *via* traditional blending methods, releasing FM from within their cores to replenish depleted FM from the continuous phase. It has been determined that this leeching process can saturate fresh dodecane with FM in 15 minutes or less. This indicated that the particles are capable of keeping the additive concentration topped up efficiently.

### **7.3 Proposed mechanism of friction reduction**

Literature suggests that when inorganic particles are used, either as an additive or as a solid lubricant, a tribofilm is formed at the surface of the contacts or that the particles can act as rolling bearings in order to physically separate the surfaces [42, 93, 102, 104, 105, 113-116, 184-188]. While a number of mechanisms of friction reduction and wear reduction are proposed in these same works, care must be taken in applying these to the particle system tested in this thesis. Mechanisms proposed in literature are focused on metallic based nanoparticles with the majority working in

the EHL regime [116, 189]. Particles in these studies were generally measured at particle concentrations [189, 190] lower than 0.1wt% to overcome the problem of particle aggregation. A problem which is overcome in this study by the use of steric stabilisers incorporated onto the particles surface.

In **Chapter 6**, it was shown that the addition of a relatively small concentration of PMMA particles to dodecane is enough to dramatically reduce the friction coefficient measured. Tribological test conditions chosen in this thesis were designed to produce boundary lubrication. Particles were prevented from aggregating by the incorporation of a polymeric based stabiliser (PDMS-MA) during the synthesis of particles.

### **7.3.1 Scanning electron microscopy of the used steel plates**

SEM testing of the steel plates, used during tribological testing, has been carried out to determine the existence of a polymer film within the wear scar. When exposed to the beam of electrons in electron microscopy PMMA will cross link and become damaged, changing the appearance of the polymer. This phenomenon can be advantageous in confirming the presence of a PMMA film; focusing the electron beam in one area long enough for damage to occur to the polymer produces an area which appears darker when compared to the area surrounding it. SEM analysis of the plate showed the formation of these darker areas was possible inside the wear scar all along the length of the scar but was not possible at any point outside of the wear scar thus making it clear that a PMMA tribofilm is formed in the wear scar, but not outside of it, during testing. The PMMA tribofilm only forms in the area of the contact suggesting that the formation of this tribofilm is due to the action of the contact. Formation of the PMMA tribofilm may account also for the wear reduction seen in samples containing particles when compared to samples without particles.

Plots of friction coefficient versus particle concentration, both of solid particles and those loaded with FM (**Chapter 6**), appeared to show a drop in friction coefficient at two different particle concentrations (3.5wt% and 14wt%). This suggests that there may be different friction reduction mechanisms taking place dependent on the concentration of particles that are present in the dodecane.

Through comparison of the wear scar in the samples tested, a mechanism for the formation of the tribofilm can be proposed. In the plates tested using pure dodecane (0wt% particles) the direction of rubbing can be clearly seen. The plates supplied have a known roughness which means that before testing is carried out some scratches due to polishing can be seen on the surface of the plates. The scratches present on the surface of the material before tribological testing can be seen outside the wear scar but have been removed by the reciprocating action of the pin moving across the surface of the plate creating the wear scar (**Figure 7-2** and **Figure 7-3**). Wear particles, characterised by their irregular shape and size, can be seen across the plate. The majority of these wear particles are found near to the wear scar.

At 1.5wt% solid particle concentration the film formed inside the wear scar is not complete and intact particles can be seen outside the wear scar trapped in scratches on the surface. This can be seen in **Figure 7-4** and **Figure 7-5** respectively. This process was also reported by Kao and Lin when using titanium dioxide particles [106].

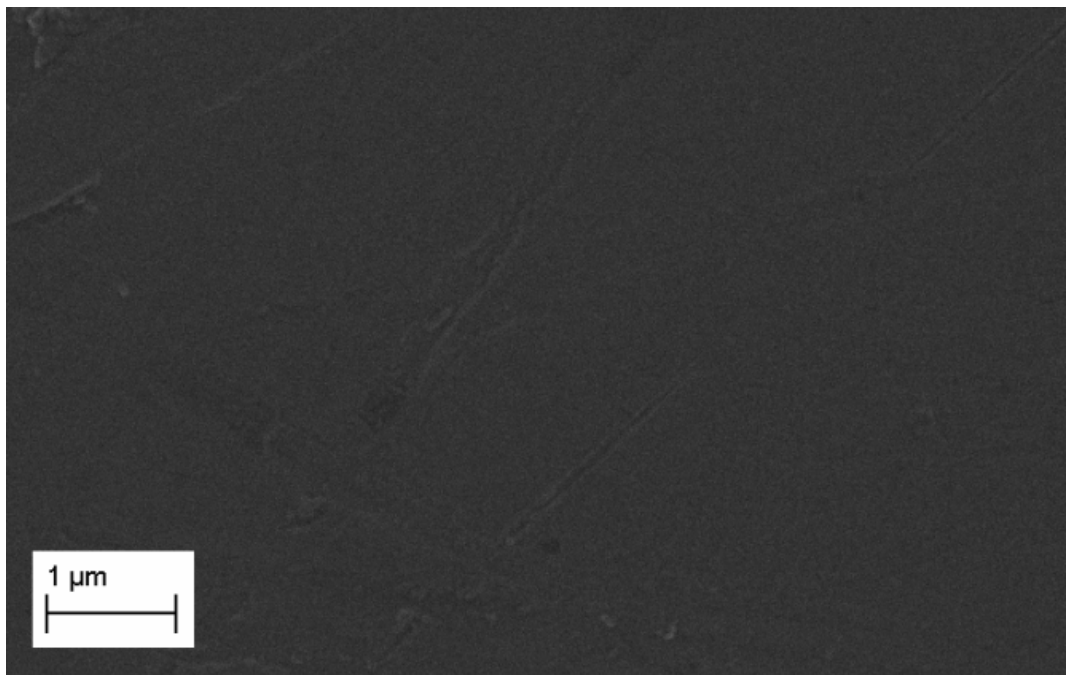


**Figure 7-2.** Scanning electron micrograph of outside the wear scar of steel plates after tribological testing using pure dodecane (0wt% particles) as a lubricating oil.

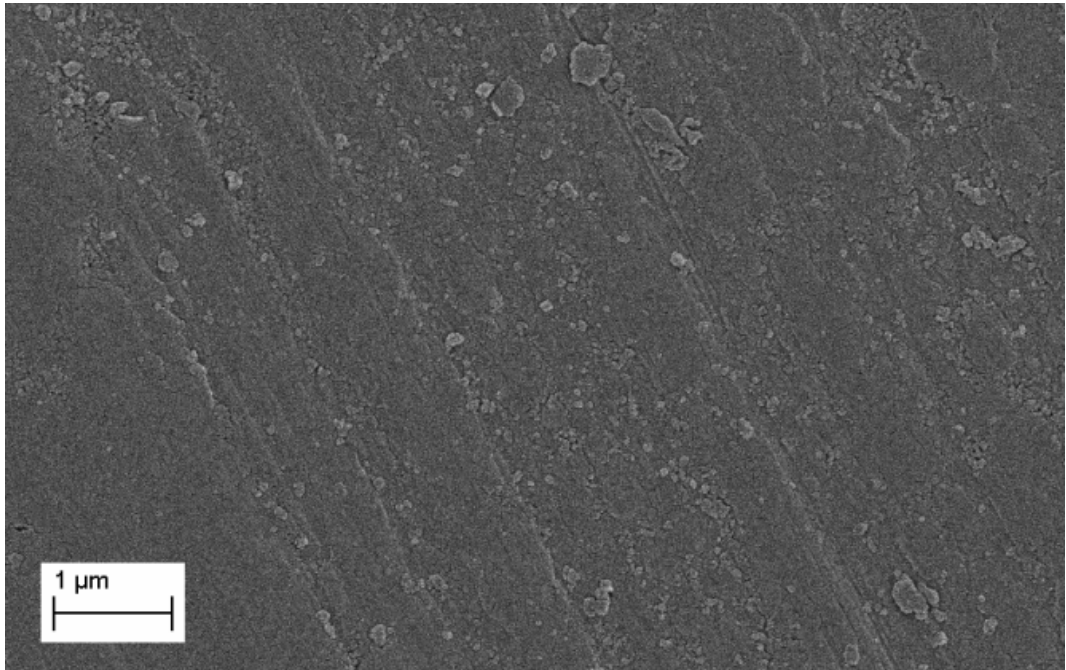


**Figure 7-3.** Scanning electron micrograph of inside the wear scar of steel plates after tribological testing using pure dodecane (0wt% particles) as a lubricating oil.

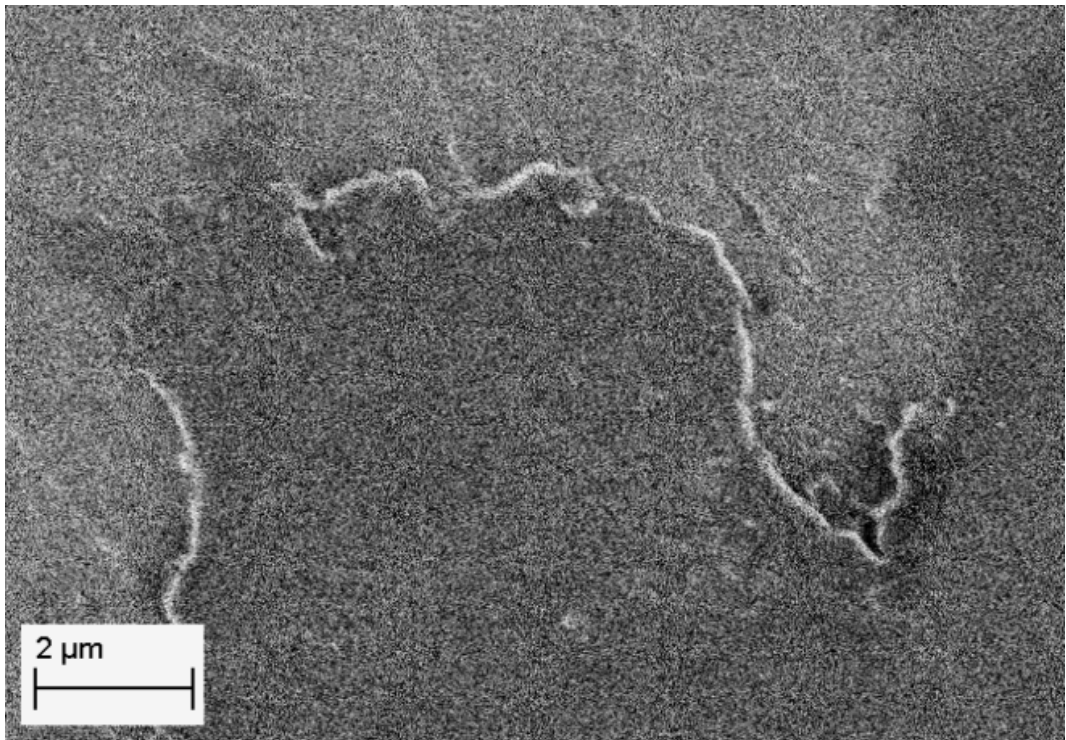


**Figure 7-4.** Scanning electron micrographs of inside the wear scar after tribological testing using dodecane containing 1.5wt% solid PMMA particles.

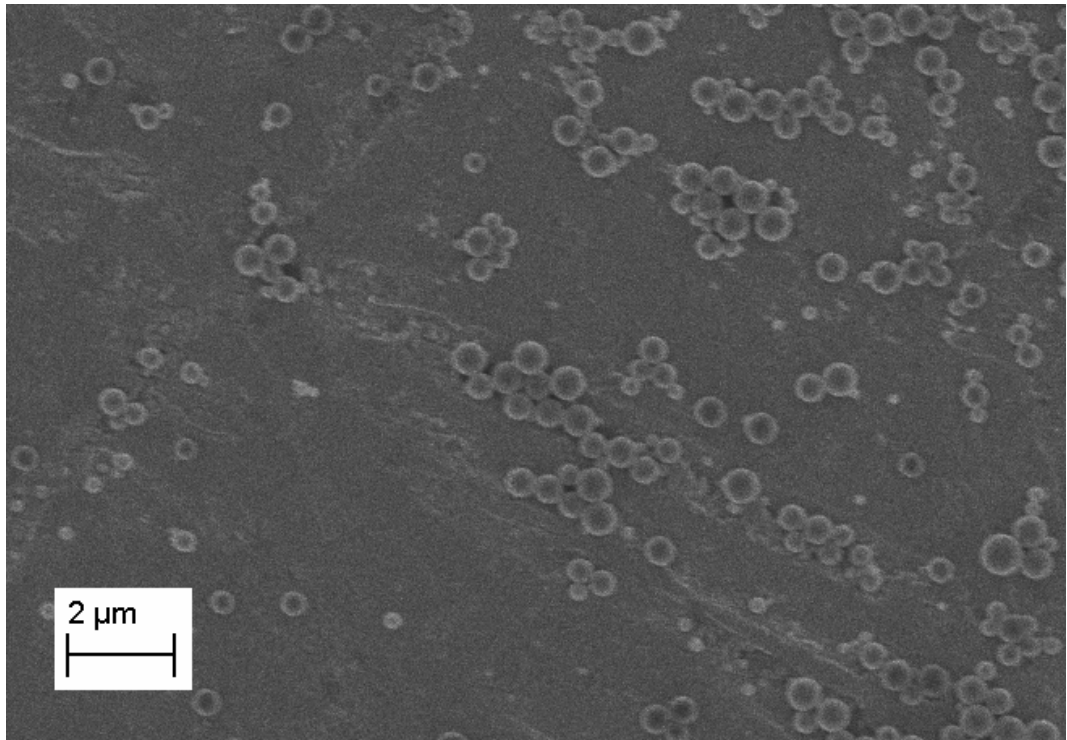


**Figure 7-5.** Scanning electron micrographs of outside the wear scar after tribological testing using dodecane containing 1.5wt% solid PMMA particles.

When 3.5wt% solid particles are tested a complete tribofilm forms, this is seen by the disappearance of the polishing marks on the surface of the sample, and no particles can be seen in the wear scar. This suggests that asperities on the surface have been completely smoothed out by particles which have become trapped and then broken in the contact and smoothed to produce a flat PMMA tribofilm.

When increasing the particle concentration up to 14wt%, a complete PMMA tribofilm can be seen inside the wear scar and can be confirmed by systematic damaging of the surface using the electron beam in SEM analysis. Outside of the wear scar intact particles can be found across the surface (**Figures 7-6 and Figure 7-7**) but once again no damage can be caused to the surface by the electron beam as no polymer tribofilm has formed here.

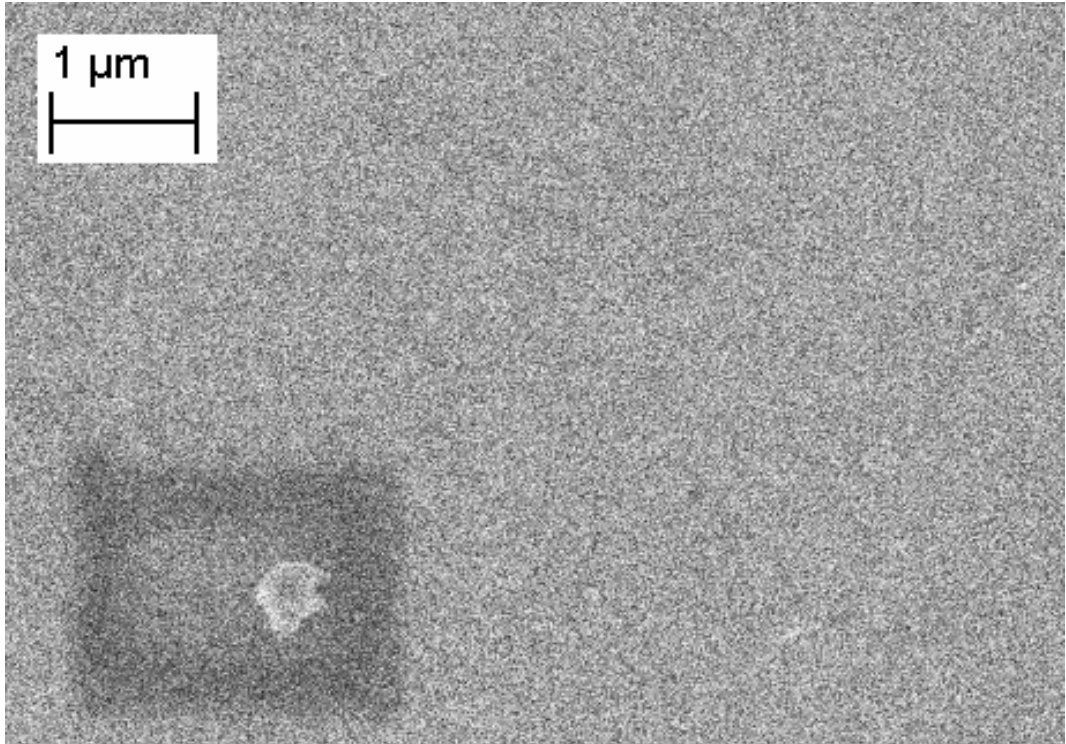


**Figure 7-6.** Scanning electron micrographs of steel plates used in tribological testing inside the wear scar (14wt% solid particles), polymer tribofilm can be damaged by the electron beam.

Wear debris can be seen mixed with intact particles closer to the wear scar. This suggests wear of the plate occurs before the formation of a polymer tribofilm (**Figure 7-8**), further testing would need to be carried out in order to determine whether this is indeed the case. The drop in friction coefficient at higher particle concentration may therefore be due to the formation of a PMMA film working alongside a further friction reducing mechanism deriving from these intact particles.

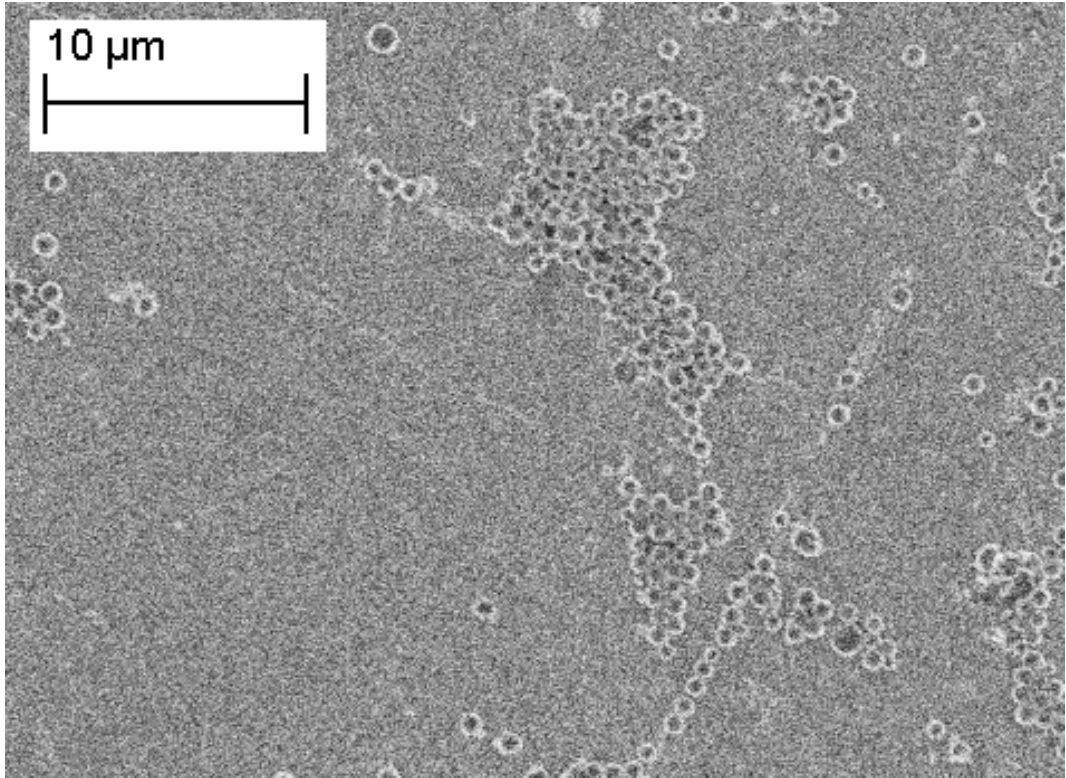


**Figure 7-7.** Scanning electron micrographs of steel plates used in tribological testing outside of the wear scar (14wt% particles), some particles remain on the surface but no polymer tribofilm can be seen. Plates are rinsed with hexane and dried at 40°C for one week before testing by SEM.

Many theories have been suggested as to the mechanism taking place at higher concentrations of particles, all of which focus on the physical separation of the two sliding surfaces due to the action of the particles [104, 113, 184].

A number of studies of metallic nanoparticles suggest that a rolling mechanism may be taking place alongside film formation [106], however this is unlikely to be the case here as polymer particles will not have sufficient strength to support the load applied.

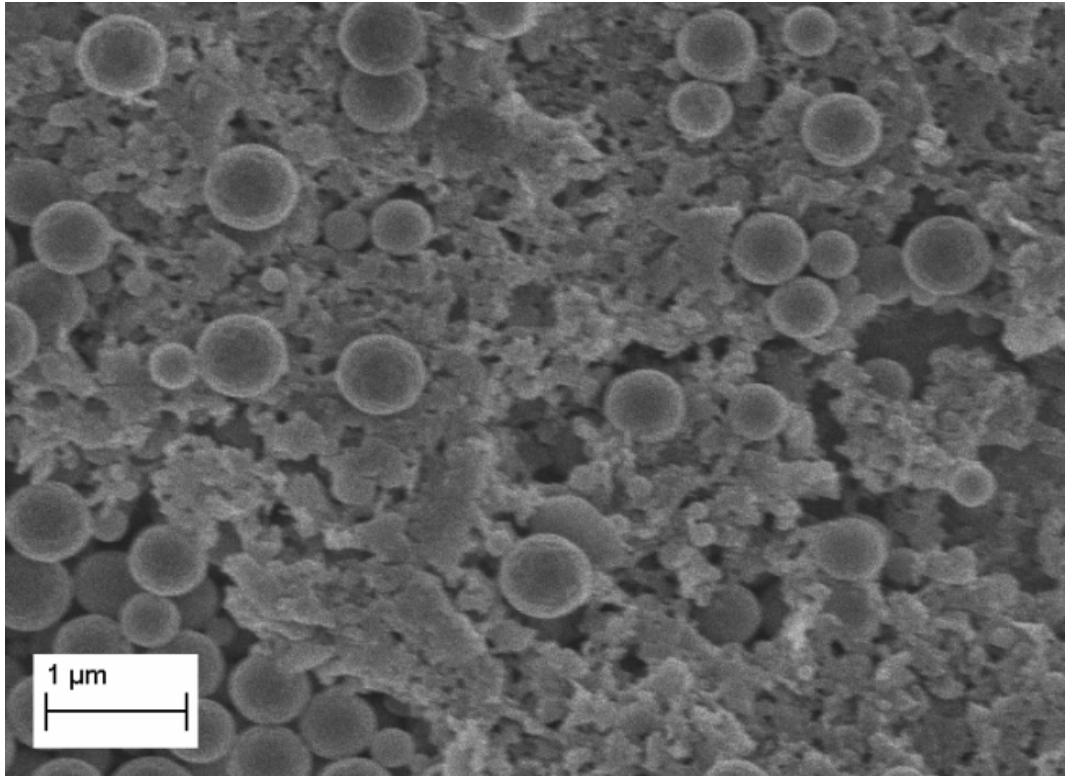


**Figure 7-8.** Scanning electron micrograph of steel plates after tribological testing. Intact PMMA particles and wear debris found outside the wear scar.

### 7.3.2 Formation of polymer tribofilm

In all cases the addition of particles reduced both the friction coefficient and measured wear volume when compared to both pure dodecane (0wt% particles) and dodecane fully saturated with FM (0wt% particles). SEM analysis has confirmed the formation of a polymer tribofilm within the wear scar. Similar mechanisms were suggested, but not proven, for ZDDP coated metallic core nanoparticles by Li *et al.* [191] and also by Hu *et al.* [104] for lanthanum borate.

A schematic of the proposed action of the particles in the contact is shown in **Figure 7-9** below.

**Section 6.4.1** shows that reduction of friction is linked to the amount of FM encapsulated within the core of the particle being tested; those particles with higher concentrations of FM encapsulated within the core exhibited the greatest decrease in friction. This suggests that the delivery method of FM into the dodecane continuous

phase may be dominated by the bursting of particles which can quickly deliver the FM to exactly where and when it is needed within the contact.

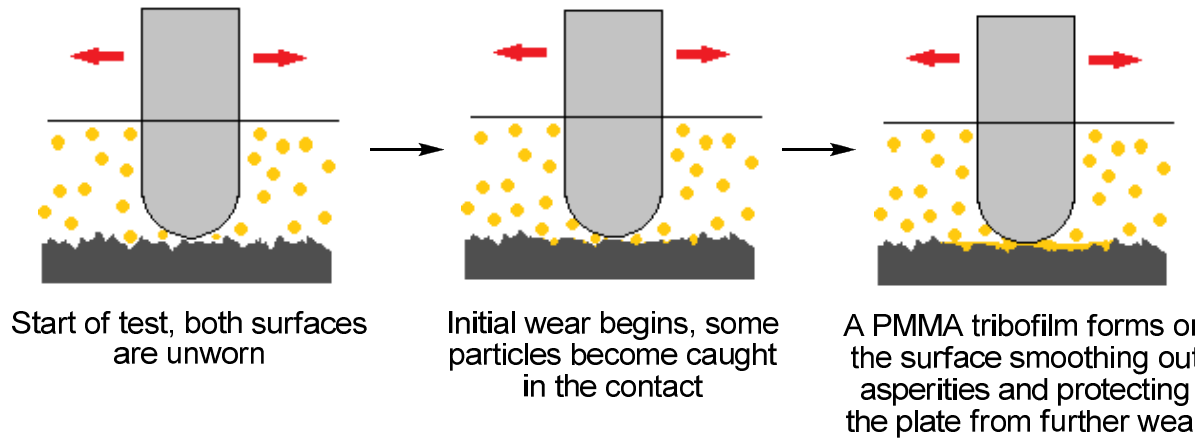


**Figure 7-9.** Proposed mechanism of friction and wear reduction in samples containing solid particles.

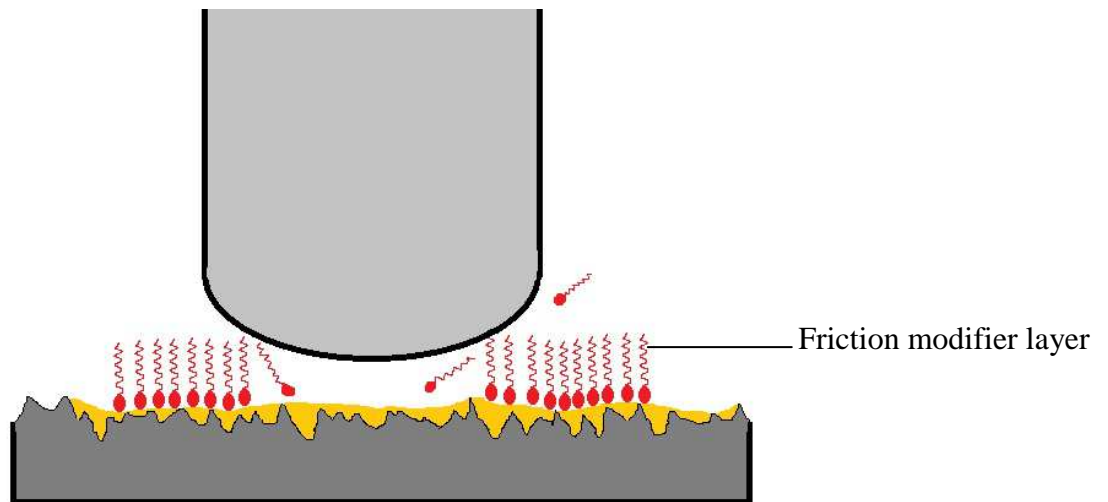


**Figure 7-10.** Proposed mechanism of friction and wear reduction in samples containing FM-loaded particles. It should be noted that polymer tribofilm is likely to form on both surfaces as is the FM layer.

In samples containing encapsulated FM this PMMA tribofilm acts alongside the action of the FM itself. The FM self assembles a tribolayer on the surface through hydrogen bonding with the polymer film. Other FM molecules will align head to head and tail to tail, dependent on the polarities of the uppermost layer of FM, to form a protective multilayer characteristic of organic FMs. This multilayer, which acts as a sacrificial layer, is removed by the action of the pin moving across the surface of the plate, resulting in free FM in the dodecane continuous phase. This FM then adheres onto the surface to reform the tribolayer which was removed, shown in **Figure 7-10**.

## **Chapter 8. Conclusions**

### **8.1 Concluding remarks**

This study has detailed work to synthesise and optimise poly(methyl methacrylate) particles, produced *via* a dispersion polymerisation in a non-aqueous continuous phase, and which with the addition of a co-solvent can be used to encapsulate an organic friction modifier within a liquid core. Tribological testing of these particles has been carried out to determine what affect the addition of these particles to a model oil, in this case dodecane, has on the lubricating properties of that oil.

It has been shown that solid PMMA particles can be synthesised with control over the final particle size and polydispersity. This can be achieved by altering the concentrations of the various components of the initial polymerisation mixture used during polymerisation. Increasing the monomer (MMA) concentration in the initial polymerisation mixture increases the size of PMMA particles produced. Increasing the stabiliser (PDMS-MA) concentration leads to a decrease in particle size. Increasing the initiator (AIBN) concentration also increases final particle size, although the size change measured is less dramatic than when altering monomer or stabiliser concentrations. The smallest particles were produced by combining the effect of decreasing monomer concentration and increasing stabiliser concentration. The particle yield can be increased, without altering the final particle size, by scaling the initial polymerisation mixture to contain more monomer while keeping the ratio of monomer to stabiliser constant.

Particles with a polymer shell-liquid core morphology have been produced by the addition of co-solvent to the dispersion polymerisation mixture. Changing the ratio of continuous phase to co-solvent can also control particle size however this has some limitations due to the wall thickness of the particles produced.

An organic friction modifier, believed to be stearamide, has been encapsulated within the core of polymer particles by ensuring that the FM is preferentially soluble in the core rather than in the continuous phase. Using a co-solvent in which the FM is highly soluble gives the potential to increase the concentration of FM within the particles, and in the oil, dramatically. Currently, formulated engine oils contain about 0.3wt% of FM, this can be increased to at least 1 wt% by the addition of these particles.

Particles have been synthesised which have the ability to act as an ‘additive reservoir’, complementary to the amount of FM conventionally blended into the finished engine oil, and thus keeping an equilibrium between the two environments.

A method of monitoring the release of FM from unbroken particles by HPLC has been developed. Samples for this testing were obtained by centrifugation, removal of supernatant liquid and then redispersing the particles in fresh dodecane. This has shown that 85-88% of the FM added in the polymerisation stage is present in the particle system after the removal of unreacted monomer and excess stabiliser. It was found that 15 minutes was sufficient to saturate the fresh dodecane with FM indicating that the particles can sufficiently keep the concentration of FM within the dodecane topped up efficiently. The concentration of FM soluble in dodecane was found to increase in the presence of particles; the cause of this needs further clarification but, due to issues surrounding solubility, was determined to be outside the scope of this project.

The effects of particle concentration, particle size, particle morphology and concentration of encapsulated FM have all been investigated in this study. It has been found that adding particles, either solid PMMA, PMMA with a methanol core or PMMA with a methanol core containing encapsulated FM, can decrease the friction coefficient below that of pure dodecane and in some cases can even decrease the friction coefficient below those measured for dodecane which has been saturated with FM *via* traditional blending methods. It has also been found that the addition of particles, any type, can reduce the measured wear volumes when compared with pure dodecane or the dodecane fully saturated with FM. The effects of friction and wear reduction can be seen with the addition of only 1.5wt% concentration of particles. This suggests that the delivery method of the FM may be dominated by the

bursting of particles and the quick delivery of FM to where and when it is needed rather than the slow leeching of FM from the particles over time as was the initial hypothesis.

A mechanism for friction and wear reduction has been proposed by analysis of the steel plates which had been used in tribological testing by using SEM. When exposed to an electron beam, such as that in scanning electron microscopy, PMMA will cross-link and become damaged. This phenomenon has been used to confirm the presence of a polymer tribofilm inside the wear scar. This damage cannot be caused outside the wear scar indicating that the tribofilm is only formed by particles being broken as they enter into the contact and therefore the polymer tribofilm cannot be formed outside of the wear scar.

## **8.2 Suggestions for future work**

In the process of this study some observations, which were deemed outside the scope of the project, have been made and require further investigate to explain them fully.

The concentration of FM measured in dodecane during the FM release study was higher than should be soluble in dodecane by traditional blending. This may be due to some limited solubility of methanol in dodecane. All data tables and literature has stated the two are completely immiscible and over the course of this project it has not been possibly to develop a method to test this. One possible method investigated involves removing the desiccant from a standard desiccator and replacing it with methanol. A beaker of dodecane would then be left in this 'weticator' for a week. This process has previously use by Infineum to add methanol to base oil; after a month concentration of methanol was then measured using IR and UV spectroscopy.

Ideally, a full evaluation of the proposed friction and wear reduction mechanism should also be carried out. This includes, but is not limited to;

- A determination of the lowest particle concentration required in an oil in order to reduce friction and wear.
- Determinating when wear occurs in tribological testing.
- Studying particles in different testing conditions.

An investigation of the lowest particle concentration which can be added to dodecane to produce the desired decrease in friction and wear below measurements seen for pure dodecane. It has been found that only 1.5wt% particle concentration (with or without FM encapsulated) will decrease the friction and wear dramatically but even lower concentrations should be investigated in order to find the optimum concentration of particles to use. As previously stated one of the desired criteria asked for by Lubrizol was that particles produced should not alter the current look of fully formulated engine oils. The use of lower particle concentrations will reduce visibility of particles in the oil improving the overall appearance of the oil.

Determining whether wear occurs on the plate before or after the formation of a polymer tribofilm. It may be the case that the tribofilm forms then acts as a sacrificial layer to protect the steel substrate from wear. Alternatively wear of the plate may occur first and this is filled in with the polymer which then limits further wear. Interferometry of the surface after testing could be carried out without removal of the tribofilm then repeated after removal of the polymer from the surface. The presence or absence of a wear scar after removing the tribofilm would indicate at what point in testing wear a tribofilm is formed.

Testing of particles at different conditions to determine the optimum test conditions for this system and what limitations and complications arise from the addition of polymer particles into an engine oil. Current testing is carried out at 80°C in order to keep the PMMA under its glass transition temperature; this is below the operating temperature of most engines and it is possible that particles may operate differently if full engine testing was carried out. Testing of a range of operating temperatures is possible with a TE77 tribometer. Carrying out testing of this variable could be used to assess the suitability of particles in different systems. Examining the effect of using different loading or frequency would also allow the optimum running conditions of these particles in an engine. There are a wide range of tribometers available which simulate the many varied types of tribological contacts present in

any mechanical system. This is another area which could be investigated to determine the correct application in which the particles produced in this project could be used. Particle composition, concentration and FM loading concentration were all investigated in this project and the data collected here will be able to guide the conditions used in future testing.

Tribological testing was carried out in this project over a two hour time period. Longer tests should be carried out to determine the fate of the polymer particles and FM over time. SEM imaging of plates after TE77 testing showed that, at higher concentrations, some polymer particles remain intact after this time period. Carrying out testing at longer periods would allow an analysis of whether all particles eventually become consumed by the system or whether some remain intact and continue acting as an 'additive reservoir'.

Particles synthesised in this project have been able to release FM from unbroken particles into fresh dodecane in as little as 15 minutes. This is another aspect of which could be investigated and optimised dependant upon the system the particles are to be used in. The testing carried out in this thesis shows that the particles are capable of reducing friction and wear below that possible when pure dodecane is used as a lubricating oil. If so desired the particles could be tuned to act purely *via* the 'additive reservoir' mechanism by altering the synthesis and therefore morphology of the particles. The creating of particles with thicker walls may retard the leeching of FM from within the core into the depleted outer continuous phase. Alternatively crosslinking of polymer chains in the particles may be used to achieve the same effect. It should be noted that changing the morphology of the particles in this way may alter the degree of polymer tribofilm formation which occurs during testing. Again the testing presented in this project should be used to guide as to how future testing should be carried out.

Particles have been optimised to encapsulate an organic friction modifier and testing has been carried out to determine the effects of these particles on the lubricating action of dodecane. It may be the case that the method of increasing additive concentration presented here is better suited to different additives, or different polymers or in tribological testing of the lubricating action of dodecane with different substrates. Each of these could lead to a new test matrix surrounding

each of these variables now that the effect of particle size, concentration, morphology and additive loading have been determined.

## Appendix A

- Antioxidants, as the name suggests, inhibit oxidation from occurring within the oil [192]. Oxidation is defined as the loss of one or more electrons from a chemical species and will take place more readily in high temperature, oxygen rich conditions, such as those found in an engine, resulting in the formation of acids. These acids can cause corrosion of metallic surfaces of engine components leading to the decreased performance of the engine. As well as increasing the overall acidity of the oil these acids can go on to react with other species that may be within the oil and can lead to an increase the oil viscosity. Antioxidants can prevent the effects of oxidation from occurring by either,
  - reacting with the oxidising agent so oxidation cannot occur or
  - reacting with the products to form less reactive compounds.

Antioxidants are commonly either organometallic based or organic, oil soluble chemicals, these are typically phenol or amine based. Example antioxidant structures are shown in **Figure A-1**.

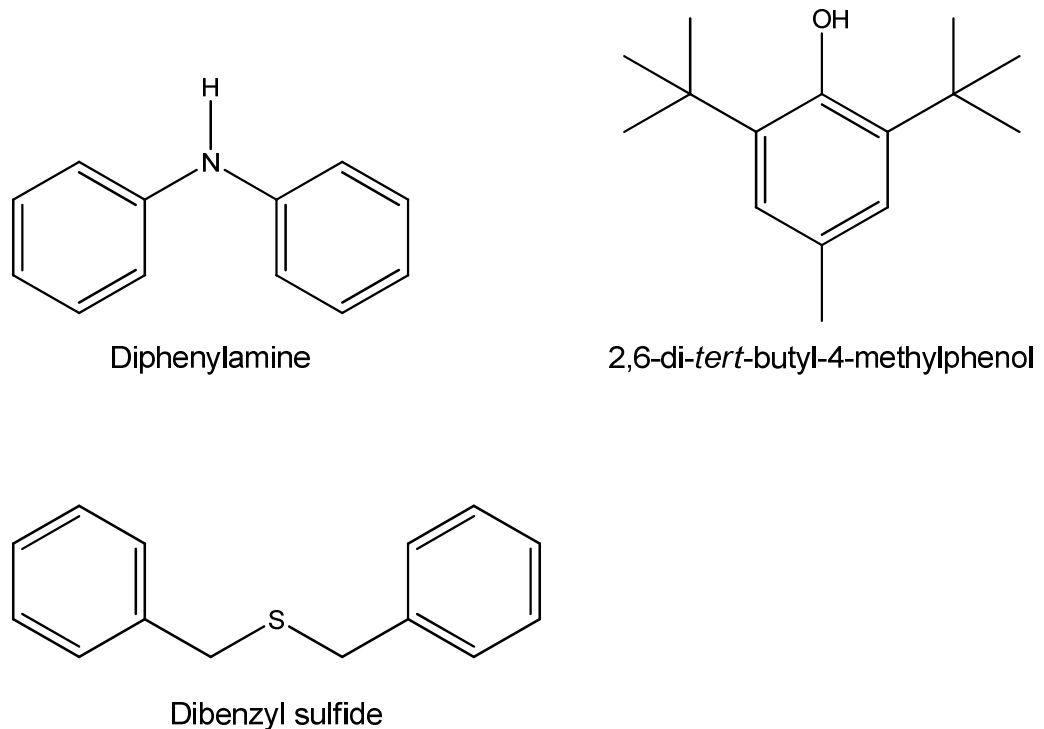


**Figure A-1.** Common examples of antioxidant additives used in engine oil formations.

- The pour point of an oil is measured as 3°C above the temperature at which the oil will stop flowing [48]. Pour point depressants are added to lubricants in order to lower the temperature of the pour point and allow the lubricant to flow at lower temperatures. At low temperatures wax crystals can form in an oil and once they form these crystals will then assemble in an end to end arrangement which creates crystalline sheets in the oil. Pour point depressants are polymers which can react at the growing edge of the wax crystals preventing the formation of these wax crystals at too low a temperature. In doing this they allow the formation of small wax crystals but sterically hinder the formation of larger wax crystals which would inhibit the flow of the oil. Without the addition of pour point depressants wax crystals over 100µm have been recorded. Pour point depressants tend to have a comb polymer like structure, with side chains of differing length; longer side chains are capable of reacting with the wax and shorter side chains control the degree of these reactions [193].
- Antiwear (AW) additives work under low to moderate loads and ambient temperatures to reduce wear by forming a surface tribolayer on asperities. A tribolayer is defined as the layer formed by the action of a sliding contact. This type of additive is often closely linked to extreme pressure (EP) additives. As the name suggests EP additives operate under more severe load, speed and temperature conditions than AW additives. EPs therefore have to be able to prevent more serious types of surface damage than AW additives [188, 194]. In some cases additives can perform as an AW or EP additive dependent on the conditions they are under at the time. Examples of this type of additive include tricresyl phosphate and zinc dialkyldithiophosphate as shown in **Figure A-2**.

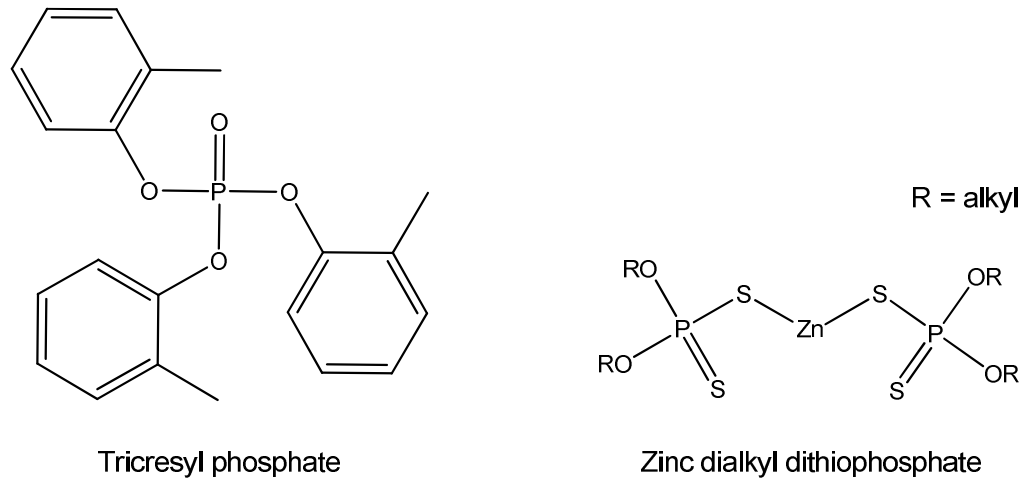


**Figure A-2.** Example antiwear/extreme pressure additives.

- During routine movements of the engine, the lubricating oil will be agitated and as a result of this gas will become dissolved in the oil, and this gas can lead to the production of a foam. The gases in the foams can cause oxidation of the oil producing harmful species and increasing oil viscosity, and they can also cause incomplete lubricant films to form between surfaces. To prevent foams from forming and the problems associated with this foam formation anti-foaming agents are added to the oil [195]. Surfactants are commonly used as anti-foaming agents in order to decrease the surface tension between the oil/gas interface and thus causing any bubbles formed to burst.
- Detergents work in two ways; they neutralize any undesirable chemical species present within the oil, such as acids and ketones, to form inorganic salts, they then go on to act as a surfactant, suspending these salts in the oil, preventing the deposition of salts on surfaces [196, 197] as shown in **Figure A-3**. The generic formulae for detergent molecules are given in **Figure A-4**.

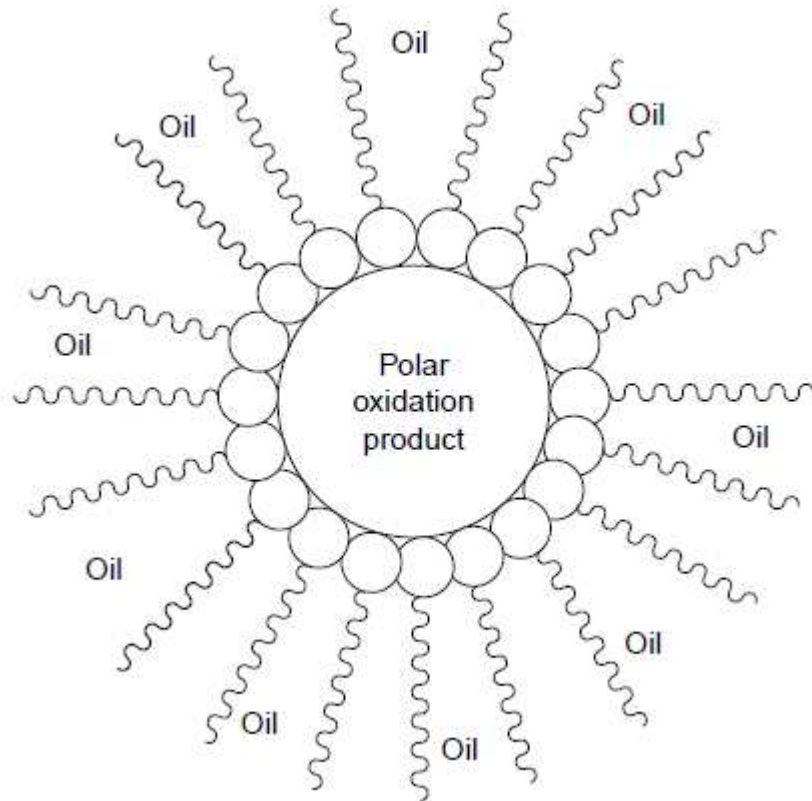
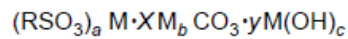
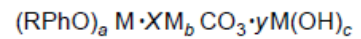


**Figure A-3.** Micellar action of detergents to suspend unwanted chemical species found in oil [196].



Basic sulfonate



Basic phenate



Basic carboxylate

$a$  and  $c = 1$  and  $b = 2$ , if the metal  $M$  is monovalent;  $a$  and  $c = 2$  and  $b = 1$ , if the metal  $M$  is divalent

**Figure A-4.** Generic structures of detergents molecules [196].

- Dispersants play a similar key role to those of detergents in oils. The addition of dispersants ensures that surfaces remain deposit free by keeping foreign particles in the oil such as sludge, dirt and wear particles in suspension. Dispersants and detergents differ by their chemical nature. While dispersants have a higher molecular weight than detergents, they do not have the capability to neutralise acidic species in the way detergents do and unlike detergents they contain no metallic species [196].

- Viscosity index improvers are added to ensure that the viscosity of oil will remain the same at high temperatures as it does at low temperatures. At higher temperatures, such as those which can be found in engines, the viscosity of oil will decrease; this can lead to an incomplete lubricant film between the surface and their asperities, which in turn will lead to an increase in wear. Viscosity index improvers tend to be straight chain, high molecular weight polymers such as poly(methacrylate) or copolymers, for example olefin copolymer, both of which are shown in **Figure A-5**, however recently star polymers have also been used [198].

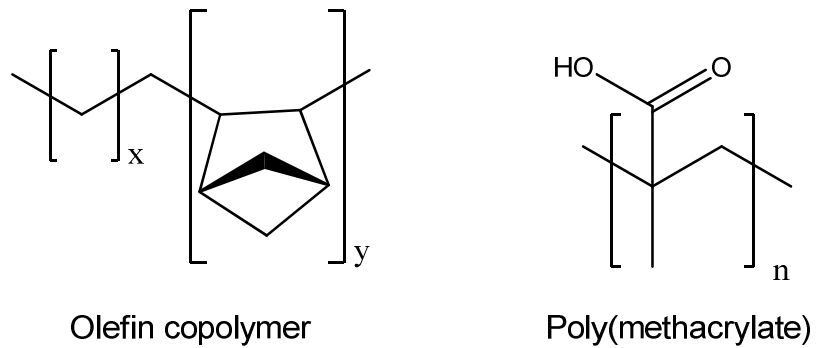


**Figure A-5.** Examples of viscosity index improvers.

## Appendix B

From the known amount of MMA and methanol added to the reaction vessel at the start of the synthesis.

$$\textit{Volume MMA} + \textit{Volume MeOH} = \textit{Total volume of all particles}$$

Using the particle diameter, measured by DLS, it is possible to work out the radius of one particle.

$$\frac{\textit{Diameter}}{2} = \textit{Radius}$$

This can then be used to work out the volume of one particle.

$$\frac{4}{3}\pi r^3 = \textit{Volume of 1 particle}$$

We now know the total volume of all the particles and the total volume of a single particle and so can now work out the total number of polymer particles in the system.

$$\frac{\textit{Total volume of all particles}}{\textit{Volume of 1 particle}} = \textit{Number of particles}$$

It is now possible to calculate the volume of methanol which should be found in the core of one particle.

$$\frac{\textit{Volume of MeOH}}{\textit{Number of particles}} = \textit{Volume of MeOH in 1 particle}$$

From this it is possible to calculate the radius of the methanol core of the particle.

$$\text{Radius of MeOH core in 1 particle} = \sqrt[3]{\frac{\text{Volume of MeOH in 1 particle}}{\frac{4}{3}\pi}}$$

The difference between the radius of the methanol core and the radius of the measured particle will be the theoretical thickness of the PMMA shell.

$$\begin{aligned} \text{Radius of 1 particle} - \text{Radius of the MeOH core of 1 particle} \\ = \text{Theoretical shell thickness} \end{aligned}$$

## Appendix C

Rheological data is presented here demonstrating the role of the particles used in this project on the viscosity of dodecane. Viscosity testing was carried out using a Malvern Kinexus Pro running the Malvern rSpace software. Pure dodecane and dodecane with particles which have a methanol core at 14wt% particles concentration were tested. In liquids containing particles viscosity varies with the concentration of particles in suspension and the size of those particles. In samples containing larger particles or high concentrations of particles there will be a greater number of interactions between the particles and this will therefore increase the viscosity of the liquid. Particles chosen for this testing were 1600nm in diameter; these were the largest particles used in TE77 testing. In demonstrating that particles of this size have no effect on the viscosity of the pure dodecane it can be confirmed that the particles used in this project do not alter the viscosity and therefore the lubrication regime under which the samples are being tested. The particle concentrations chosen in these rheometry tests were chosen as the highest and lowest particles concentrations which were tested using the TE77. Showing that the particles concentration is also not sufficiently high to alter the recorded viscosity of the dodecane.

Samples were tested at a constant temperature of 80°C, the same temperature as TE77 testing which was chosen to be below the glass transition temperature of the PMMA polymer, at differing shear rates. This is shown on the below in **Figure C-1**.

It can be seen that pure dodecane and the dodecane containing particles showed very little difference in viscosity and were within error of each other. The samples of dodecane containing particles were at the highest concentration and the largest particles tested in tribological testing. Knowing the behaviour of particles and how they can alter the viscosity of a liquid, dependant on size and concentration of the particles used, it can be concluded that the samples containing smaller particles and those samples containing lower concentrations should not alter dodecane viscosity.

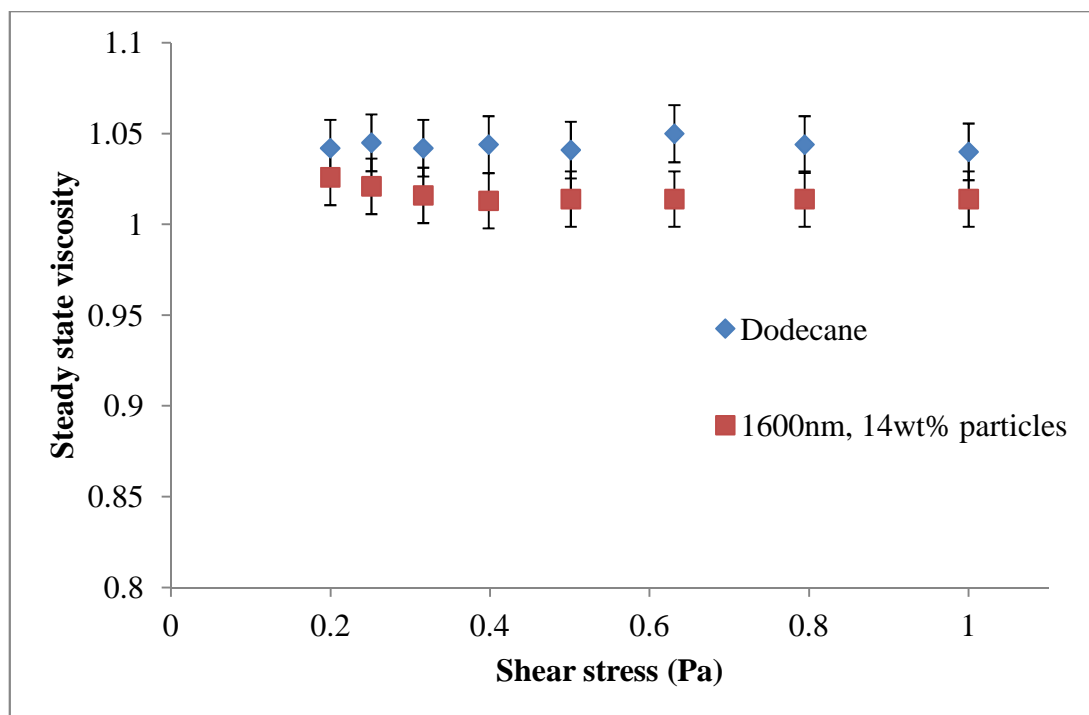


**Figure C-1.** Steady state viscosity at different shear stresses (Pa) at 80°C. Pure dodecane (blue ♦), dodecane containing 1600nm particles with a methanol core (red ■).

1. Taylor, C.M., *Automobile engine tribology design considerations for efficiency and durability*. Wear, 1998. **221**(1): p. 1-8.
2. Priest, M. and C.M. Taylor, *Automobile engine tribology approaching the surface*. Wear, 2000. **241**(2): p. 193-203.
3. Holmberg, K., P. Andersson, and A. Erdemir, *Global energy consumption due to friction in passenger cars*. Tribology International, 2012. **47**(0): p. 221-234.
4. Pinkus, O. and D.F. Wilcock, *Strategy for energy conservation through tribology*. Lubrication Engineering, 1977. **34**(11): p. 599-610.
5. Tung, S.C. and M.L. McMillan, *Automotive tribology overview of current advances and challenges for the future*. Tribology International, 2004. **37**(7): p. 517-536.
6. Haque, T., A. Morina, and A. Neville, *Influence of friction modifier and antiwear additives on the tribological performance of a non-hydrogenated DLC coating*. Surface and Coatings Technology, 2010. **204**(24): p. 4001-4011.
7. Komvopoulos, K., G. Pennecot, E.S. Yamaguchi, and S.W. Yeh, *Antiwear properties of blends containing mixtures of zinc dialkyl dithiophosphate and different detergents*. Tribology Transactions, 2008. **52**(1): p. 73-85.
8. Bearchell, C.A., D.M. Heyes, D.J. Moreton, and S.E. Taylor, *Overbased detergent particles: Experimental and molecular modelling studies*. Physical Chemistry Chemical Physics, 2001. **3**: p. 4774-4783.
9. Vipper, A.B., W. Bartz, A.K. Karaulov, O.A. Mischuk, and M.Y. Lukinyuk, *Antifriction action of lubricant additives*. Lubrication Science, 1995. **7**(3): p. 247-259.
10. Spikes, H.A., *Additive-additive and additive-surface interactions in lubrication*. Lubrication Science, 1989. **2**(1): p. 3-23.
11. Unnikrishnan, R., M.C. Jain, A.K. Harinarayan, and A.K. Mehta, *Additive-additive interaction: an XPS study of the effect of ZDDP on the AW/EP characteristics of molybdenum based additives*. Wear, 2002. **252**(3-4): p. 240-249.

12. Sarin, R., D.K. Tuli, A.S. Verma, M.M. Rai, and A.K. Bhatnagar, *Additive-additive interactions: Search for synergistic FM-EP-AW composition*. *Wear*, 1994. **174**(1-2): p. 93-102.
13. Ramakumar, S.S.V., A.M. Rao, and S.P. Srivastava, *Studies on additive-additive interactions: Formulation of crankcase oils towards rationalization*. *Wear*, 1992. **156**(1): p. 101-120.
14. Sarpal, A.S., J. Christopher, S. Mukherjee, M.B. Patel, and G.S. Kapur, *Study of additive-additive interactions in a lubricant system by NMR, ESCA, and thermal techniques*. *Lubrication Science*, 2005. **17**(3): p. 319-345.
15. UNION, T.E.P.A.T.C.O.T.E., *Regulation (EC) No 715/2007 of the European Parliament and of the Council*, in *715/2007/EC C.o.t.E.U*. European Parliament, Editor 2007, THE EUROPEAN PARLIAMENT AND THE COUNCIL OF THE EUROPEAN UNION.
16. Yamamoto, K., M. Nakamura, H. Yane, and H. Yamashita, *Simulation on catalytic reaction in diesel particulate filter*. *Catalysis Today*, 2010. **153**(3-4): p. 118-124.
17. Zheng, M., G.T. Reader, and J.G. Hawley, *Diesel engine exhaust gas recirculation—a review on advanced and novel concepts*. *Energy Conversion and Management*, 2004. **45**(6): p. 883-900.
18. Arshady, R., *Microcapsules for food*. *Journal of Microencapsulation*, 1993. **10**(4): p. 413-435.
19. Freiberg, S. and X.X. Zhu, *Polymer microspheres for controlled drug release*. *International Journal of Pharmaceutics*, 2004. **282**(1-2): p. 1-18.
20. Nelson, G., *Application of microencapsulation in textiles*. *International Journal of Pharmaceutics*, 2002. **242**(1-2): p. 55-62.
21. Yow, H.N. and A.F. Routh, *Formation of liquid core-polymer shell microcapsules*. *Soft Matter*, 2006. **2**(11): p. 940-949.
22. Jost, H.P. and Great Britain Ministry of Technology, *Committee on Tribology Report, 1966-67*. 1968: H.M. Stationery Office.
23. Sousanis, J. *World Vehicle Population Tops 1 Billion Units*. 2011 15.8.2014 [cited 2014 30.7.2014]; Available from: [http://wardsauto.com/ar/world\\_vehicle\\_population\\_110815](http://wardsauto.com/ar/world_vehicle_population_110815).
24. Bhushan, B., *Principles and applications of tribology*. 2013: John Wiley & Sons.

25. Pollock, H., *Fundamentals of friction*. Vol. 220. 1992: Springer.
26. Dowson, D., *A tribological day*. Proceedings of the Institution of Mechanical Engineers, Part J: Journal of Engineering Tribology, 2009. **223**(3): p. 261-273.
27. Khurshudov, A. and R.J. Waltman, *Tribology challenges of modern magnetic hard disk drives*. Wear, 2001. **251**(1–12): p. 1124-1132.
28. Tan, A.H. and S. Wei Cheng, *A novel textured design for hard disk tribology improvement*. Tribology International, 2006. **39**(6): p. 506-511.
29. Adams, M.J., S.A. Johnson, P. Lefèvre, V. Lévesque, V. Hayward, T. André, and J.-L. Thonnard, *Finger pad friction and its role in grip and touch*. Journal of The Royal Society Interface, 2013. **10**(80): p. 20120467.
30. Gorshkov, Y.V., S.V. Evdokimov, and V.S. Kombalov, *A device for wear resistance tests of artificial heart valves*. Proceedings of the Institution of Mechanical Engineers, Part H: Journal of Engineering in Medicine, 1992. **206**(3): p. 169-173.
31. Rennie, A.C., P.L. Dickrell, and W.G. Sawyer, *Friction coefficient of soft contact lenses: measurements and modeling*. Tribology Letters, 2005. **18**(4): p. 499-504.
32. Yan, Y., A. Neville, D. Dowson, S. Williams, and J. Fisher, *Effect of metallic nanoparticles on the biotribocorrosion behaviour of metal-on-metal hip prostheses*. Wear, 2009. **267**(5–8): p. 683-688.
33. Bhushan, B., G. Wei, and P. Haddad, *Friction and wear studies of human hair and skin*. Wear, 2005. **259**(7–12): p. 1012-1021.
34. Lewis, R., M.J. Carré, and S.E. Tomlinson, *Skin friction at the interface between hands and sports equipment*. Procedia Engineering, 2014. **72**(0): p. 611-617.
35. Polidori, G., R. Taïar, S. Fohanno, T.H. Mai, and A. Lodini, *Skin-friction drag analysis from the forced convection modeling in simplified underwater swimming*. Journal of Biomechanics, 2006. **39**(13): p. 2535-2541.
36. Roberts, E.W., *Space tribology: its role in spacecraft mechanisms*. Journal of Physics D: Applied Physics, 2012. **45**(50): p. 503001.
37. Kopeliovich, D. *Bearings In Internal Combustion Engines*. 2010 2012 [cited 2014 18.02.2014]; Available from:

[http://www.substech.com/dokuwiki/doku.php?id=bearings\\_in\\_internal\\_combustion\\_engines](http://www.substech.com/dokuwiki/doku.php?id=bearings_in_internal_combustion_engines).

38. Stezi, A.Z., *Fluid Film Lubrication*. 2nd ed. 2010, Cambridge: Cambridge University Press.
39. Coles, J.M., D.P. Chang, and S. Zauscher, *Molecular mechanisms of aqueous boundary lubrication by mucinous glycoproteins*. *Current Opinion in Colloid & Interface Science*, 2010. **15**(6): p. 406-416.
40. Tomizawa, H. and T.E. Fischer, *Friction and wear of silicon nitride and silicon carbide in water: Hydrodynamic lubrication at low sliding speed obtained by tribochemical wear*. *A S L E Transactions*, 1987. **30**(1): p. 41-46.
41. Tomimoto, M., K. Mizuhara, and T. Yamamoto, *Effect of particles on lubricated friction - theoretical analysis of friction caused by particles in journal bearing*. *Tribology Transactions*, 2002. **45**(1): p. 47-54.
42. Mizuhara, K., M. Tomimoto, and T. Yamamoto, *Effect of particles on lubricated friction*. *Tribology Transactions*, 2000. **43**(1): p. 51-56.
43. Hamrock, B.J., B. Jacobson, and S.R. Schmid, *Fundamentals of machine elements*. 1999, USA: The McGraw-Hill Companies.
44. Gates, R.S. and S.M. Hsu, *Silicon nitride boundary lubrication: Effect of sulfonate, phenate and salicylate compounds*. *Tribology Transactions*, 2000. **43**(2): p. 269-274.
45. Hsu, S.M., *Molecular basis of lubrication*. *Tribology International*, 2004. **37**(7): p. 553-559.
46. Winer, W.O., *Molybdenum disulfide as a lubricant: A review of the fundamental knowledge*. *Wear*, 1967. **10**(6): p. 422-452.
47. Toyo Drilube Co. Ltd. *DRILUBE® products containing molybdenum disulfide*. 1999 [September 2014]; Available from: [http://www.drilube.co.jp/english/common/img/product/img\\_molybdenum.jpg](http://www.drilube.co.jp/english/common/img/product/img_molybdenum.jpg).
48. Crawford, J., A. Psaila, and S.T. Orszulik, *Miscellaneous additives and vegetable oils*, in *Chemistry and Technology of Lubricants*, R.M. Mortier, M.F. Fox, and S.T. Orszulik, Editors. 1997, Blackie Academic & Professional: Suffolk.

49. Vipper, A.B., V.L. Lashkhi, R.M. Matveevskii, I.A. Buyanovskii, V.V. Kulagin, and A.I. Natchuk, *Friction modifiers as antifriction additives for motor oils*. Chemistry and Technology of Fuels and Oils, 1981. **17**(1): p. 36-39.
50. Castle, R.C. and C.H. Bovington, *The behaviour of friction modifiers under boundary and mixed EHD conditions*. Lubrication Science, 2003. **15**(3): p. 253-263.
51. Landry-Coltrain, C.J., B.K. Coltrain, and M.J. Corrigan, *Simultaneous coatings of stearamide lubricant layer*, 2000, Google Patents.
52. Kenbeck, D. and T.F. Bunemann, *Organic friction modifiers*, in *Lubricant Additives Chemistry and Applications*, L.R. Rudnick, Editor. 2009, CRC Press: Florida. p. 195-209.
53. Shin, H.S., Y.M. Jung, T.Y. Oh, T. Chang, S.B. Kim, D.H. Lee, and I. Noda, *Glass transition temperature and conformational changes of poly(methyl methacrylate) thin films determined by a two-dimensional map representation of temperature-dependent reflection-absorption FTIR spectra*. Langmuir, 2002. **18**(15): p. 5953-5958.
54. Graham, J., H. Spikes, and S. Korcek, *The friction reducing properties of molybdenum dialkyldithiocarbamate additives: Part I: Factors influencing friction reduction*. Tribology Transactions, 2001. **44**(4): p. 626-636.
55. Neville, A., A. Morina, T. Haque, and M. Voong, *Compatibility between tribological surfaces and lubricant additives. How friction and wear reduction can be controlled by surface/lube synergies*. Tribology International, 2007. **40**(10-12): p. 1680-1695.
56. Abd-Alla, G.H., *Using exhaust gas recirculation in internal combustion engines: A review*. Energy Conversion and Management, 2002. **43**(8): p. 1027-1042.
57. Koebel, M., M. Elsener, and M. Kleemann, *Urea-SCR: a promising technique to reduce NO<sub>x</sub> emissions from automotive diesel engines*. Catalysis Today, 2000. **59**(3-4): p. 335-345.
58. Eichelbaum, M., R.J. Farrauto, and M.J. Castaldi, *The impact of urea on the performance of metal exchanged zeolites for the selective catalytic reduction of NO<sub>x</sub>: Part I. Pyrolysis and hydrolysis of urea over zeolite catalysts*. Applied Catalysis B: Environmental, 2010. **97**(1-2): p. 90-97.

59. Castrol Limited. *Euro 4 and Euro 5 Legislation*. 2004 [cited 2012 6.7.2012]; Available from: <http://www.castrol.com/castrol/extendedsectiongenericarticle.do?categoryId=9034603&contentId=7064146>.
60. Lovell, P.A. and M.S. El-Aasser, *Emulsion Polymerization and Emulsion Polymers*. 1997: Wiley.
61. Housecroft, C.E. and E.C. Constable, *Chemistry*. 3rd ed. 2006, Essex: Pearson Education Limited.
62. Gavrilović, I., K. Mitchell, A.D. Brailsford, D.A. Cowan, A.T. Kicman, and R.J. Ansell, *A molecularly imprinted receptor for separation of testosterone and epitestosterone, based on a steroidal cross-linker*. *Steroids*, 2011. **76**(5): p. 478-483.
63. Arshady, R., *Suspension, emulsion, and dispersion polymerization: A methodological survey*. *Colloid and Polymer Science*, 1992. **270**(8): p. 717-732.
64. Jahanzad, F., S. Sajjadi, M. Yianneskis, and B.W. Brooks, *In situ mass-suspension polymerisation*. *Chemical Engineering Science*, 2008. **63**(17): p. 4412-4417.
65. Sánchez-Silva, L., J.F. Rodríguez, A. Romero, A.M. Borreguero, M. Carmona, and P. Sánchez, *Microencapsulation of PCMs with a styrene-methyl methacrylate copolymer shell by suspension-like polymerisation*. *Chemical Engineering Journal*, 2010. **157**(1): p. 216-222.
66. Sánchez, L., P. Sánchez, M. Carmona, A. de Lucas, and J.F. Rodríguez, *Influence of operation conditions on the microencapsulation of PCMs by means of suspension-like polymerization*. *Colloid and Polymer Science*, 2008. **286**(8-9): p. 1019-1027.
67. Sánchez, L., P. Sánchez, A. de Lucas, M. Carmona, and J. Rodríguez, *Microencapsulation of PCMs with a polystyrene shell*. *Colloid and Polymer Science*, 2007. **285**(12): p. 1377-1385.
68. Duguet, E., M. Abboud, F. Morvan, P. Maheu, and M. Fontanille, *PMMA encapsulation of alumina particles through aqueous suspension polymerisation processes*. *Macromolecular Symposia*, 2000. **151**(1): p. 365-370.

69. Dubey, R., *Microencapsulation Technology and Applications*. 2009. Vol. 59. 2009.
70. Supsakulchai, A., G. Ma, M. Nagai, and S. Omi, *Preparation of uniform titanium dioxide (TiO<sub>2</sub>) polystyrene-based composite particles using the glass membrane emulsification process with a subsequent suspension polymerization*. *Journal of microencapsulation*, 2003. **20**(1): p. 1-18.
71. Sundberg, D.C., A.P. Casassa, J. Pantazopoulos, M.R. Muscato, B. Kronberg, and J. Berg, *Morphology development of polymeric microparticles in aqueous dispersions. I. Thermodynamic considerations*. *Journal of Applied Polymer Science*, 1990. **41**(7-8): p. 1425-1442.
72. Ma, G.H., Z.G. Su, S. Omi, D. Sundberg, and J. Stubbs, *Microencapsulation of oil with poly(styrene-*N,N*-dimethylaminoethyl methacrylate) by SPG emulsification technique: Effects of conversion and composition of oil phase*. *Journal of Colloid and Interface Science*, 2003. **266**(2): p. 282-294.
73. Müller, K., M. Klapper, and K. Müllen, *Synthesis of conjugated polymer nanoparticles in non-aqueous emulsions*. *Macromolecular Rapid Communications*, 2006. **27**(8): p. 586-593.
74. Riess, G., *Micellization of block copolymers*. *Progress in Polymer Science*, 2003. **28**(7): p. 1107-1170.
75. Hecht, L.L., C. Wagner, K. Landfester, and H.P. Schuchmann, *Surfactant concentration regime in miniemulsion polymerization for the formation of MMA nanodroplets by high-pressure homogenization*. *Langmuir*, 2011. **27**(6): p. 2279-2285.
76. Okubo, M., F.J. Schork, Y. Luo, W. Smulders, J. Russum, A. Butt<sup>Ã©</sup>, and K. Fontenot, *Miniemulsion polymerization*, in *Polymer Particles*. 2005, Springer Berlin Heidelberg. p. 129-255.
77. Durand, A. and E. Marie, *Macromolecular surfactants for miniemulsion polymerization*. *Advances in Colloid and Interface Science*, 2009. **150**(2): p. 90-105.
78. Tiarks, F., K. Landfester, and M. Antonietti, *Preparation of polymeric nanocapsules by miniemulsion polymerization*. *Langmuir*, 2001. **17**(3): p. 908-918.

79. Landfester, K., *Miniemulsion polymerization and the structure of polymer and hybrid nanoparticles*. Angewandte Chemie International Edition, 2009. **48**(25): p. 4488-4507.
80. Weiss, C.K. and K. Landfester, *Miniemulsion polymerization as a means to encapsulate organic and inorganic materials*, in *Hybrid Latex Particles*. 2010, Springer. p. 185-236.
81. Landfester, K., *Polyreactions in miniemulsions*. Macromolecular Rapid Communications, 2001. **22**(12): p. 896-936.
82. Haga, Y., T. Watanabe, and R. Yosomiya, *Encapsulating polymerization of titanium dioxide*. Die Angewandte Makromolekulare Chemie, 1991. **189**(1): p. 23-34.
83. Quaroni, L. and G. Chumanov, *Preparation of polymer-coated functionalized silver nanoparticles*. Journal of the American Chemical Society, 1999. **121**(45): p. 10642-10643.
84. Kim, S.Y., K. Lee, H. Jung, S.E. Shim, and S. Choe, *Effect of polyurethane-based macromonomers in the dispersion polymerization of styrene*. Journal of Applied Polymer Science, 2008. **109**(4): p. 2656-2664.
85. Klein, S.M., V.N. Manoharan, D.J. Pine, and F.F. Lange, *Preparation of monodisperse PMMA microspheres in nonpolar solvents by dispersion polymerization with a macromonomeric stabilizer*. Colloid and Polymer Science, 2003. **282**(1): p. 7-13.
86. Harris, H.V. and S.J. Holder, *Octadecyl acrylate based block and random copolymers prepared by ATRP as comb-like stabilizers for colloidal micro-particle one-step synthesis in organic solvents*. Polymer, 2006. **47**(16): p. 5701-5706.
87. Roberts, G.S., R. Sanchez, R. Kemp, T. Wood, and P. Bartlett, *Electrostatic charging of nonpolar colloids by reverse micelles*. Langmuir, 2008. **24**(13): p. 6530-6541.
88. Okubo, M., S. Kawaguchi, and K. Ito, *Dispersion polymerization*, in *Polymer Particles*. 2005, Springer Berlin Heidelberg. p. 299-328.
89. Shim, S.E., H. Jung, K. Lee, J.M. Lee, and S. Choe, *Dispersion polymerization of methyl methacrylate with a novel bifunctional polyurethane macromonomer as a reactive stabilizer*. Journal of Colloid and Interface Science, 2004. **279**(2): p. 464-470.

90. Ma, Y. and W. Yang, *Nonaqueous dispersion polymerization of styrene in methanol with the ionomer block copolymer poly[(4-methylstyrene)-co-(4-vinyltriethylbenzyl ammonium bromide)]-b-polyisobutene as a stabilizer*. Journal of Polymer Science Part A: Polymer Chemistry, 2004. **42**(11): p. 2678-2685.
91. Richez, A.P., H.N. Yow, S. Biggs, and O.J. Cayre, *Dispersion polymerisation in non polar solvent: Evolution towards emerging applications*. 2013.
92. Dawkins, J.V. and G. Taylor, *Nonaqueous polystyrene dispersions: Radical dispersion polymerization in the presence of AB block copolymers of polystyrene and poly(dimethyl siloxane)*. European Polymer Journal, 1979. **15**(5): p. 453-457.
93. Wu, Y.Y., W.C. Tsui, and T.C. Liu, *Experimental analysis of tribological properties of lubricating oils with nanoparticle additives*. Wear, 2007. **262**(7-8): p. 819-825.
94. Rapoport, L., Y. Feldman, M. Homyonfer, H. Cohen, J. Sloan, J.L. Hutchison, and R. Tenne, *Inorganic fullerene-like material as additives to lubricants: structure - function relationship*. Wear, 1999. **225-229**, Part 2(0): p. 975-982.
95. Hirech, K., S. Payan, G. Carnelle, L. Brujes, and J. Legrand, *Microencapsulation of an insecticide by interfacial polymerisation*. Powder Technology, 2003. **130**(1-3): p. 324-330.
96. Onder, E., N. Sarier, and E. Cimen, *Encapsulation of phase change materials by complex coacervation to improve thermal performances of woven fabrics*. Thermochemica Acta, 2008. **467**(1-2): p. 63-72.
97. Desobry, S.A., F.M. Netto, and T.P. Labuza, *Comparison of spray-drying, drum-drying and freeze-drying for  $\beta$ -carotene encapsulation and preservation*. Journal of Food Science, 1997. **62**(6): p. 1158-1162.
98. Lindstrom, R.S., A.A. Massucco, M.F. van Buren, and T. Williamson, *Cast material with encapsulated lubricant*, 1993, Google Patents.
99. Guo, Q.B., K.T. Lau, B.F. Zheng, M.Z. Rong, and M.Q. Zhang, *Imparting ultra-low friction and wear rate to epoxy by the incorporation of microencapsulated lubricant*. Macromolecular Materials and Engineering, 2009. **294**(1): p. 20-24.

100. Guo, Q.B., K.T. Lau, M.Z. Rong, and M.Q. Zhang, *Optimization of tribological and mechanical properties of epoxy through hybrid filling*. *Wear*, 2010. **269**(1-2): p. 13-20.
101. Capelli, A.J., *Bearing material with microencapsulated lubricant*, 1976, Google Patents.
102. Zhou, J., Z. Wu, Z. Zhang, W. Liu, and Q. Xue, *Tribological behavior and lubricating mechanism of Cu nanoparticles in oil*. *Tribology Letters*, 2000. **8**(4): p. 213-218.
103. Sunqing, Q., D. Junxiu, and C. Guoxu, *Tribological properties of CeF<sub>3</sub> nanoparticles as additives in lubricating oils*. *Wear*, 1999. **230**(1): p. 35-38.
104. Hu, Z.S., J.X. Dong, G.X. Chen, and J.Z. He, *Preparation and tribological properties of nanoparticle lanthanum borate*. *Wear*, 2000. **243**(1-2): p. 43-47.
105. Hernández Battez, A., R. González, J.L. Viesca, J.E. Fernández, J.M. Díaz Fernández, A. Machado, R. Chou, and J. Riba, *CuO, ZrO<sub>2</sub> and ZnO nanoparticles as antiwear additive in oil lubricants*. *Wear*, 2008. **265**(3-4): p. 422-428.
106. Kao, M.J. and C.R. Lin, *Evaluating the role of spherical titanium oxide nanoparticles in reducing friction between two pieces of cast iron*. *Journal of Alloys and Compounds*, 2009. **483**(1): p. 456-459.
107. Rapoport, L., A. Moshkovich, V. Perfilyev, A. Laikhtman, I. Lapsker, L. Yadgarov, R. Rosentsveig, and R. Tenne, *High lubricity of re-doped fullerene-like MoS<sub>2</sub> nanoparticles*. *Tribology Letters*, 2012. **45**(2): p. 257-264.
108. Liu, G., X. Li, B. Qin, D. Xing, Y. Guo, and R. Fan, *Investigation of the mending effect and mechanism of copper nano-particles on a tribologically stressed surface*. *Tribology Letters*, 2004. **17**(4): p. 961-966.
109. Yadgarov, L., V. Petrone, R. Rosentsveig, Y. Feldman, R. Tenne, and A. Senatore, *Tribological studies of rhenium doped fullerene-like MoS<sub>2</sub> nanoparticles in boundary, mixed and elasto-hydrodynamic lubrication conditions*. *Wear*, 2013. **297**(1-2): p. 1103-1110.
110. Luo, T., X. Wei, H. Zhao, G. Cai, and X. Zheng, *Tribology properties of Al<sub>2</sub>O<sub>3</sub>/TiO<sub>2</sub> nanocomposites as lubricant additives*. *Ceramics International*, 2014. **40**(7, Part A): p. 10103-10109.

111. Lee, J., S. Cho, Y. Hwang, C. Lee, and S. Kim, *Enhancement of lubrication properties of nano-oil by controlling the amount of fullerene nanoparticle additives*. Tribology Letters, 2007. **28**(2): p. 203-208.
112. Rabaso, P., F. Ville, F. Dassenoy, M. Diaby, P. Afanasiev, J. Cavoret, B. Vacher, and T. Le Mogne, *Boundary lubrication: Influence of the size and structure of inorganic fullerene-like MoS<sub>2</sub> nanoparticles on friction and wear reduction*. Wear, 2014. **320**(0): p. 161-178.
113. Peng, D.-X., C.-H. Chen, Y. Kang, Y.-P. Chang, and S.-Y. Chang, *Size effects of SiO<sub>2</sub> nanoparticles as oil additives on tribology of lubricant*. Industrial Lubrication and Tribology, 2010. **62**(2): p. 111-120.
114. Qiu, S., Z. Zhou, J. Dong, and G. Chen, *Preparation of Ni nanoparticles and evaluation of their tribological performance as potential additives in oils*. Journal of Tribology, 2001. **123**(3): p. 441-443.
115. Sunqing, Q., D. Junxiu, and C. Guoxu, *A review of ultrafine particles as antiwear additives and friction modifiers in lubricating oils*. Lubrication Science, 1999. **11**(3): p. 217-226.
116. Chinas-Castillo, F. and H.A. Spikes, *Mechanism of action of colloidal solid dispersions*. Transactions of the ASME, 2003. **125**: p. 552-557.
117. Kao, M.J. and C.R. Lin, *Evaluating the role of spherical titanium oxide nanoparticles in reducing friction between two pieces of cast iron*. Journal of Alloys and Compounds, 2009. **483**(1-2): p. 456-459.
118. Meng, F.M., Y.Y. Zhang, Y.Z. Hu, and H. Wang, *Numerical study of influences of hard particles in lubricant on tribological performances of the piston ring*. Proceedings of the Institution of Mechanical Engineers, Part C: Journal of Mechanical Engineering Science, 2007. **221**(3): p. 361-372.
119. Liu, W., Z. Zhang, S. Chen, and Q. Xue, *The research and application of colloids as lubricants*. Journal of Dispersion Science and Technology, 2000. **21**(4): p. 469-490.
120. Leshchinsky, V., R. Popovitz-Biro, K. Gartsman, R. Rosentsveig, Y. Rosenberg, R. Tenne, and L. Rapoport, *Behavior of solid lubricant nanoparticles under compression*. Journal of Materials Science, 2004. **39**(13): p. 4119-4129.
121. Loginova, T.P., Y.A. Kabachii, S.N. Sidorov, D.N. Zhironov, P.M. Valetsky, M.G. Ezernitskaya, L.V. Dybrovina, T.P. Bragina, O.L. Lependina, B. Stein,

- and L.M. Bronstein, *Molybdenum sulfide nanoparticles in block copolymer micelles: Synthesis and tribological properties*. Chemistry of Materials, 2004. **16**(12): p. 2369-2378.
122. Bakunin, V.N., A.Y. Suslov, G.N. Kuzmina, and O.P. Parenago, *Synthesis and application of inorganic nanoparticles as lubricant components - A review*. Journal of nanoparticle research, 2004. **6**: p. 273-284.
123. Greenberg, R., G. Halperin, I. Etsion, and R. Tenne, *The effect of WS<sub>2</sub> nanoparticles on friction reduction in various lubrication regimes*. Tribology Letters, 2004. **17**(2): p. 179-186.
124. Nishio, T., *Self-lubricating nanoparticles: Self-organization into 3D-superlattices during a fast drying process*. Chem. Commun, 2010.
125. Einstein, A., *Investigations on the theory of, the Brownian motion*. 1st ed. 1956, United States of America: Dover Publications, INC.
126. Harada, Y., *Dynamics and dynamic light-scattering properties of brownian particles under laser radiation pressure*. Journal of Pure and Applied Optics. Journals of the European Optical Society Part A, 1998. **7**(5).
127. Malvern, *Zetasizer User Manual*. 2004.
128. Atkins, P.W., *Physical Chemistry*. 5th ed. 1994, Somerset: Oxford University Press.
129. Sarkar, S.L., X. Aimin, and D. Jana, *Scanning Electron Microscopy, X-Ray Microanalysis of Concretes*, in *Handbook of Analytical Techniques in Concrete Science and Technology*, V.S.R.J.J. Beaudoin, Editor. 2001, William Andrew Publishing/Noyes: Norwich, N.Y., USA.
130. Goldstein, J.I., D.E. Newbury, P. Echlin, D.C. Joy, C. Fiori, and E. Lifshin, *Scanning electron microscopy and X-ray microanalysis. A text for biologists, materials scientists, and geologists*. 1981.
131. Atteberry, J. *How scanning electron microscopes work* 2009 [1st August 2011]; Available from: <http://science.howstuffworks.com/scanning-electron-microscope.htm>.
132. Hu, W., T. Orlova, and G.H. Bernstein, *Technique for preparation of precise wafer cross sections and applications to electron beam lithography of poly(methylmethacrylate) resist*. Journal of Vacuum Science & Technology B, 2002. **20**(6): p. 3085-3088.

133. Loxley, A. and B. Vincent, *Preparation of poly(methylmethacrylate) microcapsules with liquid cores*. Journal of Colloid and Interface Science, 1998. **208**(1): p. 49-62.
134. Campbell, D., R.A. Pethrick, and J.R. White, *Scanning Electron Microscopy*, in *Polymer Characterization Physical Techniques*, D. Campbell, R.A. Pethrick, and J.R. White, Editors. 2000, Stanley Thornes: Cheltenham.
135. Rondot, S., O. Jbara, S. Fakhfakh, R. Belkorissat, and J.M. Patat, *Effect of surface mechanical finishes on charging ability of electron irradiated PMMA in a scanning electron microscope*. Nuclear Instruments and Methods in Physics Research Section B: Beam Interactions with Materials and Atoms, 2011. **269**(19): p. 2117-2123.
136. Fakhfakh, S., O. Jbara, S. Rondot, A. Hadjadj, and Z. Fakhfakh, *Experimental characterisation of charge distribution and transport in electron irradiated PMMA*. Journal of Non-Crystalline Solids, 2012. **358**(8): p. 1157-1164.
137. Azonano. *Transmission electron microscope - A basic look how TEMs work*. 2006 [cited 2013 December 10th 2013]; Available from: [http://www.azonano.com/article.aspx?ArticleID=1723#\\_How\\_TEMs\\_Work](http://www.azonano.com/article.aspx?ArticleID=1723#_How_TEMs_Work).
138. Wang, S., X. Wang, and Z. Zhang, *Preparation of polystyrene particles with narrow particle size distribution by  $\gamma$ -ray initiated miniemulsion polymerization stabilized by polymeric surfactant*. European Polymer Journal, 2007. **43**(1): p. 178-184.
139. Almgren, M., K. Edwards, and G. Karlsson, *Cryo transmission electron microscopy of liposomes and related structures*. Colloids and Surfaces A: Physicochemical and Engineering Aspects, 2000. **174**(1-2): p. 3-21.
140. Mortensen, K. and Y. Talmon, *Cryo-TEM and SANS microstructural study of pluronic polymer solutions*. Macromolecules, 1995. **28**(26): p. 8829-8834.
141. Adrian, M., J. Dubochet, J. Lepault, and A.W. McDowell, *Cryo-electron microscopy of viruses*. Nature, 1984. **308**(5954): p. 32-36.
142. Barrett Group. *Nanotechnology: A Brief Overview*. July 2012 11th July 2012 [cited December 2013; Available from: <http://barrett-group.mcgill.ca/tutorials/nanotechnology/nano02.htm>.
143. Campbell, D., R.A. Pethrick, and J.R. White, *Vibrational spectroscopy: Infra-red and raman spectroscopy*, in *Polymer Characterization Physical*

- Techniques*, D. Campbell, R.A. Pethrick, and J.R. White, Editors. 2000, Stanley Thornes: Cheltenham.
144. Perkin Elmer Inc. *FTIR Spectroscopy: Attenuated Total Reflectance (ATR)*. 28th July 2008 4th March 2011]; Available from: [http://shop.perkinelmer.com/content/TechnicalInfo/TCH\\_FTIRATR.pdf](http://shop.perkinelmer.com/content/TechnicalInfo/TCH_FTIRATR.pdf).
145. Farajzadeh, M.A., M. Ebrahimi, A. Ranji, E. Feyz, V. Bejani, and A.A. Matin, *HPLC and GC methods for determination of lubricants and their evaluation in analysis of real samples of polyethylene*. *Microchimica Acta*, 2006. **153**(1-2): p. 73-78.
146. Marquez-Ruiz, G. and M.C. Dobarganes, *High performance size-exclusion chromatography for lipid analysis in organic media*. 2006. **Chapter 9**: p. 205-238.
147. Waters. *How Does High Performance Liquid Chromatography Work?* 2014 [cited 2014; Available from: [http://www.waters.com/webassets/cms/category/media/other\\_images/primer\\_e\\_lcsystem.jpg](http://www.waters.com/webassets/cms/category/media/other_images/primer_e_lcsystem.jpg).
148. Perez Delgado, Y., K. Bonny, P. De Baets, P.D. Neis, O. Malek, J. Vleugels, and B. Lauwers, *Impact of wire-EDM on dry sliding friction and wear of WC-based and ZrO<sub>2</sub>-based composites*. *Wear*, 2011. **271**(9-10): p. 1951-1961.
149. Li, B., *The Theory and Practice of Interferometry with WYKO NT8000 Optical Profiler*, 2006.
150. Leach, R., L. Brown, X. Jiang, R. Blunt, M. Conroy, and D. Mauger, *Guide for the Measurement of Smooth Surface Topography using Coherence Scanning Interferometry*. A National Measurement Good Practice Guide. Vol. 108. 2008: National Physical Laboratory.
151. Hariharan, P., *Basics of Interferometry*. Electronics & Electrical. 2007: Academic Press. 1.
152. Petzing, J., J. Coupland, and R. Leach, *The Measurement of Rough Surface Topography using Coherence Scanning Interferometry*. Vol. 116. 2010: National Physical Laboratory.
153. Wypych, G., *PMMA polymethylmethacrylate*, in *Handbook of Polymers*, G. Wypych, Editor. 2012, Elsevier: Oxford. p. 450-454.

154. Shen, S., E.D. Sudol, and M.S. El-Aasser, *Control of particle size in dispersion polymerization of methyl methacrylate*. Journal of Polymer Science Part A: Polymer Chemistry, 1993. **31**(6): p. 1393-1402.
155. Barrett, K.E.J., *Dispersion polymerisation in organic media*. British Polymer Journal, 1973. **5**(4): p. 259-271.
156. Tai, H., W. Wang, R. Martin, J. Liu, E. Lester, P. Licence, H.M. Woods, and S.M. Howdle, *Polymerization of vinylidene fluoride in supercritical carbon dioxide: Effects of poly(dimethylsiloxane) macromonomer on molecular weight and morphology of poly(vinylidene fluoride)*. Macromolecules, 2005. **38**(2): p. 355-363.
157. Jiang, S., E. David Sudol, V.L. Dimonie, and M.S. El-Aasser, *Dispersion polymerization of methyl methacrylate: Effect of stabilizer concentration*. Journal of Applied Polymer Science, 2008. **107**(4): p. 2453-2458.
158. Lee, J., J.U. Ha, S. Choe, C.-S. Lee, and S.E. Shim, *Synthesis of highly monodisperse polystyrene microspheres via dispersion polymerization using an amphoteric initiator*. Journal of Colloid and Interface Science, 2006. **298**(2): p. 663-671.
159. Moad, G., D.H. Solomon, S.R. Johns, and R.I. Willing, *Fate of the initiator in the azobisisobutyronitrile-initiated polymerization of styrene*. Macromolecules, 1984. **17**(5): p. 1094-1099.
160. Horák, D., N. Semenyuk, and F. Lednický, *Effect of the reaction parameters on the particle size in the dispersion polymerization of 2-hydroxyethyl and glycidyl methacrylate in the presence of a ferrofluid*. Journal of Polymer Science Part A: Polymer Chemistry, 2003. **41**(12): p. 1848-1863.
161. Awan, M.A., V.L. Dimonie, and M.S. El-Aasser, *Anionic dispersion polymerization of styrene. II. Mechanism of particle formation*. Journal of Polymer Science Part A: Polymer Chemistry, 1996. **34**(13): p. 2651-2664.
162. Steward, P.A. *Fick's Laws of Diffusion*. 1998 [cited 2013; Available from: <http://www.initium.demon.co.uk/fick.htm>].
163. Okubo, M., J. Izumi, T. Hosotani, and T. Yamashita, *Production of micron-sized monodispersed core/shell polymethyl methacrylate/polystyrene particles by seeded dispersion polymerization*. Colloid and Polymer Science, 1997. **275**(8): p. 797-801.

164. Williams, D.B. and C.B. Carter, *Transmission Electron Microscopy A Textbook for Materials Science*. Vol. Basics I. 1996, New York: Plenum Press.
165. Sigma Aldrich, *Safety Data Sheet*.
166. Antipov, A.A., G.B. Sukhorukov, E. Donath, and H. Möhwald, *Sustained release properties of polyelectrolyte multilayer capsules*. The Journal of Physical Chemistry B, 2001. **105**(12): p. 2281-2284.
167. Dong, Z., Y. Ma, K. Hayat, C. Jia, S. Xia, and X. Zhang, *Morphology and release profile of microcapsules encapsulating peppermint oil by complex coacervation*. Journal of Food Engineering, 2011. **104**(3): p. 455-460.
168. Scott, A.W., B.M. Tyler, B.C. Masi, U.M. Upadhyay, Y.R. Patta, R. Grossman, L. Basaldella, R.S. Langer, H. Brem, and M.J. Cima, *Intracranial microcapsule drug delivery device for the treatment of an experimental gliosarcoma model*. Biomaterials, 2011. **32**(10): p. 2532-2539.
169. Datta, S.S., A. Abbaspourrad, E. Amstad, J. Fan, S.-H. Kim, M. Romanowsky, H.C. Shum, B. Sun, A.S. Utada, M. Windbergs, S. Zhou, and D.A. Weitz, *25th anniversary article: Double emulsion templated solid microcapsules: Mechanics and controlled release*. Advanced Materials, 2014. **26**(14): p. 2205-2218.
170. Dowding, P.J., R. Atkin, B. Vincent, and P. Bouillot, *Oil core-polymer shell microcapsules prepared by internal phase separation from emulsion droplets. I. Characterization and release rates for microcapsules with polystyrene shells*. Langmuir, 2004. **20**(26): p. 11374-11379.
171. Qiu, X., S. Leporatti, E. Donath, and H. Möhwald, *Studies on the drug release properties of polysaccharide multilayers encapsulated ibuprofen microparticles*. Langmuir, 2001. **17**(17): p. 5375-5380.
172. Rapoport, L., O. Nepomnyashchy, A. Verdyan, R. Popovitz-Biro, Y. Volovik, B. Ittah, and R. Tenne, *Polymer nanocomposites with fullerene-like solid lubricant*. Advanced Engineering Materials, 2004. **6**(1-2): p. 44-48.
173. Bailey, B.C. and M. Yoda, *An aqueous low-viscosity density- and refractive index-matched suspension system*. Experiments in Fluids, 2003. **35**(1): p. 1-3.
174. Coelho, J.F.J., J. Gois, A.C. Fonseca, R.A. Carvalho, A.V. Popov, V. Percec, and M.H. Gil, *Synthesis of poly(2-methoxyethyl acrylate) by single electron*

- transfer—Degenerative transfer living radical polymerization catalyzed by Na<sub>2</sub>S<sub>2</sub>O<sub>4</sub> in water.* Journal of Polymer Science Part A: Polymer Chemistry, 2009. **47**(17): p. 4454-4463.
175. Hirzinger, B., M. Helmstedt, and J. Stejskal, *Light scattering studies on core-shell systems: determination of size parameters of sterically stabilized poly(methylmethacrylate) dispersions.* Polymer, 2000. **41**(8): p. 2883-2891.
176. Mrkvičková, L., B. Porsch, and L.O. Sundelöf, *Study of poly(methyl methacrylate) stereocomplexes by size exclusion chromatography and dynamic light scattering.* Macromolecules, 1999. **32**(4): p. 1189-1193.
177. Sauls, F.C. and R.J. Michael, *A demonstration of refractive index matching using isopropyl alcohol and MgF<sub>2</sub>.* Journal of Chemical Education, 2006. **83**(8): p. 1170.
178. Underwood, S.M. and W. Meigen, *Refractive index variation in nonaqueous sterically stabilized copolymer particles.* Colloid and Polymer Science, 1996. **274**(11): p. 1072-1080.
179. Yousif, M.Y., D.W. Holdsworth, and T.L. Poepping. *Deriving a blood-mimicking fluid for particle image velocimetry in sylgard-184 vascular models.* in *Engineering in Medicine and Biology Society, 2009. EMBC 2009. Annual International Conference of the IEEE.* 2009.
180. Yuan, Y.C., *Self healing in polymers and polymer composites. Concepts, realization and outlook: A review.* Express Polymer Letters, 2008. **2**(4): p. 238-250.
181. Rule, J.D., N.R. Sottos, and S.R. White, *Effect of microcapsule size on the performance of self-healing polymers.* Polymer, 2007. **48**(12): p. 3520-3529.
182. Blaiszik, B.J., N.R. Sottos, and S.R. White, *Nanocapsules for self-healing materials.* Composites Science and Technology, 2008. **68**(3-4): p. 978-986.
183. Wu, D.Y., S. Meure, and D. Solomon, *Self-healing polymeric materials: A review of recent developments.* Progress in Polymer Science, 2008. **33**(5): p. 479-522.
184. Chen, S. and W. Liu, *Oleic acid capped PbS nanoparticles: Synthesis, characterization and tribological properties.* Materials Chemistry and Physics, 2006. **98**(1): p. 183-189.
185. Goto, M. and F. Honda, *Film-thickness effect of Ag lubricant layer in the nano-region.* Wear, 2004. **256**(11-12): p. 1062-1071.

186. Radice, S. and S. Mischler, *Effect of electrochemical and mechanical parameters on the lubrication behaviour of Al<sub>2</sub>O<sub>3</sub> nanoparticles in aqueous suspensions*. *Wear*, 2006. **261**(9): p. 1032-1041.
187. Bartz, W.J., *Some investigations on the influence of particle size on the lubricating effectiveness of molybdenum disulfide*. *A S L E Transactions*, 1972. **15**(3): p. 207-215.
188. Liu, W., Z. Zhang, S. Chen, and Q. Xue, *The research and application of colloid as lubricants*. *Journal of Dispersion Science and Technology*, 2000. **21**(4): p. 469-490.
189. Kumar, A., R. Schmid, S. Wilson, and R.D. William, *Particle behavior in two-phased lubrication*. *Wear*, 1997. **206**(1-2): p. 130-135.
190. Jiao, D., S. Zheng, Y. Wang, R. Guan, and B. Cao, *The tribology properties of alumina/silica composite nanoparticles as lubricant additives*. *Applied Surface Science*, 2011. **257**(13): p. 5720-5725.
191. Li, B., X. Wang, W. Liu, and Q. Xue, *Tribochemistry and antiwear mechanism of organic-inorganic nanoparticles as lubricant additives*. *Tribology Letters*, 2006. **22**(1): p. 79-84.
192. Dong, J. and C.A. Migdal, *Antioxidants*, in *Lubricant Additives Chemistry and Applications*, L.R. Rudnick, Editor. 2009, CRC Press: Florida. p. 1-27.
193. Kinker, B.G., *Polymethacrylate viscosity modifiers and pour point depressants*, in *Lubricant Additives Chemistry and Applications*, L.R. Rudnick, Editor. 2009, CRC Press: Florida.
194. Farng, F.O., *Antiwear Additives and Extreme Pressure Additives*, in *Lubricant Additives Chemistry and Applications*, L.R. Rudnick, Editor. 2009, CRC Press: Florida.
195. von Phul, S.A. and L. Stern. *Antifoam, What Is It? How Does It Work?* 2005 [cited 2011 2.6.2011]; Available from: [http://www.d-foam.com/files/Antifoam\\_What\\_Is\\_It.pdf](http://www.d-foam.com/files/Antifoam_What_Is_It.pdf).
196. Rizvi, S.Q.A., *Detergents*, in *Lubricant Additives Chemistry and Applications*, L.R. Rudnick, Editor. 2009, CRC Press: Florida.
197. O'Connor, S.P., J. Crawford, and C. Cane, *Overbased lubricant detergents – a comparative study*. *Lubrication Science*, 1994. **6**(4): p. 297-325.

198. The Lubrizol Corporation. *Breakthrough VM Technology for High Viscosity Index (VI) Lubricants*. Unknown [cited 2014 18.2.2014]; Available from: <http://www.lubrizol.com/ViscosityModifiers/Asteric/default.html>.